

# **Synthesis, crystallization and aggregation of supramolecular precision polymers**

## **Dissertation**

zur Erlangung des  
Doktorgrades der Naturwissenschaften (Dr. rer. Nat.)

Der

Naturwissenschaftlichen Fakultät II

Chemie, Physik und Mathematik

der Martin-Luther-Universität  
Halle-Wittenberg,

vorgelegt

von Frau Sophie Reimann  
geb. am 05.06.1989 in Luckau

Gutachter

1. Prof. Dr. Wolfgang H. Binder
2. Prof. Dr. Bert Klumperman

Verteidigung: 11.04.2019

Halle (Saale), 25.10.2018

## **Danksagung**

An dieser Stelle möchte ich mich bei Herrn Prof. Dr. Wolfgang Binder für die Bereitstellung des interessanten Themas und die freundliche Unterstützung sowie die stete Diskussionsbereitschaft während der Durchführung dieser Dissertation bedanken.

Weiterhin möchte ich mich bei allen aktuellen und ehemaligen Mitgliedern der Arbeitsgruppe Binder für das angenehme Arbeitsklima und die gute Zusammenarbeit bedanken. Mein ganz besonderer Dank gilt hierbei Susanne Tanner und Julia Weichhold für die Bereitstellung von Chemikalien und Arbeitsmaterialien, die Aufnahme sämtlicher GPC-, IR-, ESI- und MALDI-ToF-MS Messungen, sowie die permanente seelische und moralische Unterstützung. Ein riesiges Dankeschön geht auch an Anke Hassi für die Unterstützung bei jeglichen administrativen Angelegenheiten und ihre Hilfe und aufmunternden Worte bei kleinen und großen Problemchen. Weiterhin möchte ich mich bei meinem langjährigen Studien- und Laborkollegen Steve Neumann, der mir stets mit Rat und Tat zur Seite stand, für die sehr gute und amüsante Zusammenarbeit bedanken.

Für die Aufnahme zahlreicher NMR-Spektren danke ich dem Team um Herrn Dr. Dieter Ströhl. Des Weiteren möchte ich mich bei der Arbeitsgruppe von Prof. Beiner, besonders bei Varun Danke, für die Aufnahme der WAXS Messungen und die Hilfe bei der Auswertung bedanken.

Abschließend möchte ich mich herzlich bei meiner Familie und meinen Freunden für die entgegengebrachte Unterstützung während meines bisherigen Studiums und die ständige Motivation während des Anfertigens dieser Arbeit bedanken.

All denen, die zum Gelingen dieser Arbeit beigetragen haben und nicht erwähnt wurden sei ebenso herzlich gedankt.

## Abstract

In the scope of this thesis precision polymers bearing 2,6-diaminopyridine (DAP), urea or TEMPO moieties were synthesized via acyclic diene metathesis (ADMET) polymerization and characterized to determine the influence of various internal constraints on the crystallization of polyethylene analogues. These introduced functional moieties are able to interact with each other via hydrogen bonding and/or  $\pi$ - $\pi$ -stacking and serve as conformational constraint on the polymer chain as they are planar and rotation is restricted.

Via chemical synthesis the designed symmetrical monomers containing unprotected and *N*-benzyl or *N*-methyl protected DAP, urea or TEMPO moieties were prepared followed by bulk polymerizations using different Grubbs' type and Umicore catalysts. Subsequent hydrogenation using *p*-toluenesulfonyl hydrazide yielded the fully saturated polymers with molecular weights ranging from 1100 g/mol up to 18300 g/mol. Successful conversion and the purity of the resulting compounds were proven via <sup>1</sup>H- and <sup>13</sup>C-NMR and IR spectroscopy, GPC as well as ESI and MALDI ToF MS.

The thermal properties of all polymers were investigated via DSC analysis proving hindered crystallization in all *N*-benzyl protected DAP containing polymers, compensated by an increasing methylene spacer length. The *N*-methyl protected DAP containing polymers show semi-crystallinity and melting temperatures above the  $T_m$  of pure ADMET polyethylene ( $T_m = 134$  °C), explainable by enhanced thermal stability due to hydrogen bonds, also observed for the urea containing polymers.

Furthermore, the crystallization behavior was examined via WAXS analysis, observing a lamellar morphology for all precision polymers. Investigations on the saturated DAP containing polymers with *N*-methyl protection group indicate the formation of a mixture of orthorhombic and triclinic crystal structures. Based on DSC results and the calculated lamellar crystal thicknesses a partial incorporation of the functional groups into the crystalline lamella and their parallel arrangement can be assumed. For the unprotected DAP and urea containing polymers a triclinic crystal structure is proposed.

Moreover, the behavior of the saturated, *N*-methyl protected DAP containing polymers in solution was analyzed via DLS measurements proving the formation of single-chain polymer nanoparticles and bigger aggregates, whose sizes are independent from the methylene spacer length. Changing the polarity leads either to the unfolding of the polymer chain or precipitation.

Finally, the saturated *N*-methyl protected DAP containing polymer with a methylene spacer length of  $x = 20$  was separated via preparative GPC to determine the influence of polydispersity on the melting and crystallization behavior. WAXS and DSC measurements of the individual fractions indicate similar properties as the precursor polymer.

## Kurzdarstellung

Im Rahmen dieser Arbeit wurden Präzisionspolymere mit 2,6-Diaminopyridin (DAP), Harnstoff oder TEMPO Funktionalitäten über die acyclische Dienmetathese (ADMET) Polymerisation hergestellt und anschließend kristallographisch analysiert um den Einfluss unterschiedlicher interner Zwänge auf die Kristallisation von Polyethylen Analoga zu untersuchen. Diese Gruppen sind in der Lage über Wasserstoffbrücken und/oder  $\pi$ - $\pi$ -Wechselwirkungen miteinander zu interagieren und üben einen konformativen Zwang auf die Polymerkette aus, da sie planar und nicht frei rotierbar sind.

Über mehrstufige Synthesen wurden symmetrische Monomere, welche sowohl ungeschützte als auch *N*-benzyl oder *N*-methyl geschützte DAP, Harnstoff oder TEMPO Funktionalitäten enthalten, synthetisiert und anschließend in Massepolymerisationen unter Zuhilfenahme von Grubbs' und Umicore Katalysatoren umgesetzt. Durch die anschließende Hydrierung mit *p*-Toluolsulfonylhydrazid wurden vollständig gesättigte Polymere mit Molekulargewichten von 1100 g/mol bis 18300 g/mol erhalten. Die erfolgreiche Umsetzung und die Reinheit der erhaltenen Substanzen wurden mittels  $^1\text{H}$ - und  $^{13}\text{C}$ -NMR Spektroskopie, IR Spektroskopie, GPC sowie ESI und MALDI ToF MS nachgewiesen.

Die thermischen Eigenschaften aller Polymere wurden mittels DSC analysiert und zeigen eine gehinderte Kristallisation in allen Benzyl-geschützten DAP Polymeren, welche durch einen größeren Abstand zwischen den Defekten ausgeglichen werden kann. Die Methyl-geschützten DAP Polymere zeigen semikristallines Verhalten sowie Schmelztemperaturen, welche über der von reinem Polyethylen ( $T_m = 134\text{ °C}$ ) liegen, erklärbar durch das Auftreten von Wasserstoffbrücken. Ein ähnliches Verhalten wird auch für die harnstoffhaltigen Polymere beobachtet.

Mit Hilfe von WAXS Experimenten konnte für alle Polymere eine lamellare Morphologie nachgewiesen werden. Die Untersuchung der gesättigten, Methyl-geschützten DAP Polymere weist auf eine Mischung von orthorhombischen und triklinen Kristallstrukturen hin. Basierend auf den DSC Ergebnissen und den Dicken der Kristalllamellen kann davon ausgegangen werden, dass die Defekte zumindest partiell in die kristalline Phase eingeschlossen werden, in der sie eine parallele Anordnung einnehmen. Für die ungeschützten DAP und harnstoffhaltigen Polymere wird eine trikline Kristallstruktur angenommen.

Untersuchungen der *N*-methyl geschützten DAP Polymere in Lösung mittels DLS Messungen zeigen das Auftreten von Nanopartikeln, bestehend aus einer Polymerkette und größeren Aggregaten. Die Änderung der Polarität des Lösungsmittels führen entweder zur Entfaltung der Kette oder zum Ausfällen des Präzisionspolymers.

Zuletzt wurde der Einfluss der Polydispersität auf das Schmelz- und Kristallisationsverhalten eines *N*-methyl geschützten DAP Polymers mittels präparativer GPC untersucht, wobei die einzelnen Fraktionen ähnliche Eigenschaften wie die des Ausgangspolymers zeigen.

## Table of Contents

|  |    |
|--|----|
| Danksagung.....  | 1  |
| Abstract .....   | 2  |
| Kurzdarstellung .....  | 3  |
| List of abbreviations .....  | 7  |
| 1. Introduction .....  | 11 |
| 1.1 Precision polymers .....   | 11 |
| 1.1.1 Synthesis of natural polypeptides - biological precision polymers..... | 12 |
| 1.1.2 Synthesis of non-natural polypeptides/polypeptoids .....               | 14 |
| 1.1.3 Synthesis of non-natural/artificial precision polymers .....           | 15 |
| 1.1.3.1 Chain-growth polymerizations .....                                   | 16 |
| 1.1.3.2 Step-growth polymerizations .....                                    | 17 |
| 1.1.4 Properties and applications of precision polymers .....                | 21 |
| 1.1.4.1 Biological precision polymers.....                                   | 21 |
| 1.1.4.2 Artificial precision polymers.....                                   | 21 |
| 1.2 Polymer crystallization .....  | 22 |
| 1.2.1 Thermodynamic considerations .....                                     | 23 |
| 1.2.2 Primary nucleation .....   | 24 |
| 1.2.3 Secondary nucleation .....   | 26 |
| 1.2.3.1 Hofmann-Lauritzen theory .....                                       | 27 |
| 1.3 Crystallization under confinements .....                                 | 29 |
| 1.3.1 External confinements .....  | 29 |
| 1.3.2 Internal confinements.....   | 31 |
| 1.3.2.1 Side-chain defects .....   | 31 |
| 1.3.2.2 In-chain defects .....   | 38 |
| 1.3.2.3 Determination of defect inclusion or exclusion .....                 | 41 |
| 2. Aim of the thesis .....   | 43 |
| 2.1 Motivation/Aim .....   | 43 |
| 2.2 Concept.....   | 44 |
| 3. Results and Discussion.....   | 46 |
| 3.1 Monomer synthesis.....   | 46 |
| 3.1.1. Synthesis of the diaminopyridine containing monomers.....             | 46 |
| 3.1.2 Synthesis of the urea containing monomer .....                         | 47 |
| 3.1.3 Synthesis of the TEMPO containing monomer .....                        | 48 |
| 3.1.4 Protection of Acid-M-9.....  | 49 |
| 3.2 ADMET polymerization.....  | 50 |
| 3.3 Hydrogenation .....  | 53 |
| 3.4 Post-functionalization of Acid-sP-20 ( <b>16</b> ).....                  | 56 |
| 3.5 Thermal analysis.....  | 57 |
| 3.6 Structural analysis.....   | 60 |

|   |     |
|---|-----|
| 3.6.1 WAXS analysis of the saturated <i>N</i> -methyl protected DAP containing polymers<br>( <b>14d-f</b> ).....                              | 60  |
| 3.6.2 Impact of different supramolecular interactions on the crystal structure.....   | 61  |
| 3.7 DLS analysis.....   | 64  |
| 3.8 Fractionation of the <i>N</i> -methyl protected DAP containing polymer ( <b>14f</b> ) via<br>preparative GPC and subsequent analysis..... | 66  |
| 4. Experimental Part.....   | 71  |
| 4.1 Materials.....  | 71  |
| 4.2 Instrumentation.....  | 71  |
| 4.3 Monomer synthesis.....  | 74  |
| 4.3.1 Synthesis of the diaminopyridine containing monomers ( <b>1a-c</b> ).....   | 74  |
| 4.3.2 Protection of the amide moieties.....   | 76  |
| 4.3.3 Synthesis of the urea containing monomer.....   | 79  |
| 4.3.3.1 Synthesis of undec-10-enamide ( <b>3</b> ).....   | 79  |
| 4.3.3.2 Synthesis of undec-10-en-1-amine ( <b>4</b> ).....  | 80  |
| 4.3.3.3 Synthesis of 1,3-diundec-10-en-1-ylurea (Urea-M-9) ( <b>5</b> ).....  | 80  |
| 4.3.4 Synthesis of the TEMPO containing monomer.....  | 81  |
| 4.3.4.1 Synthesis of diethyl-2,2-di(undec-10-en-1-yl)malonate ( <b>6</b> ).....   | 81  |
| 4.3.4.2 Synthesis of 2,2-di(undec-10-en-1-yl)malonic acid ( <b>7</b> ).....   | 82  |
| 4.3.4.3 Synthesis of 2-(undec-10-en-1-yl)tridec-12-enoic acid (Acid-M-9) ( <b>8</b> ).....  | 82  |
| 4.3.4.4 Synthesis of TEMPO-M-9 ( <b>9</b> ).....  | 83  |
| 4.3.5 Protection of Acid-M-9.....   | 84  |
| 4.4 ADMET-Polymerization.....   | 85  |
| 4.5 Hydrogenation.....  | 91  |
| 4.6 Post-functionalization of Acid-sP-20.....   | 95  |
| 4.6.1 Chlorination of Acid-sP-20.....   | 95  |
| 4.6.2 Synthesis of TEMPO-sP-20 ( <b>18</b> ).....   | 95  |
| 5. Summary.....   | 96  |
| 6. References.....  | 100 |
| 7. Appendix.....  | 121 |
| 7.1 IR- and NMR spectra and ESI ToF MS of the DAP containing monomers ( <b>1a-c</b> ).....  | 121 |
| 7.2 NMR spectra and ESI ToF MS of the <i>N</i> -methyl protected DAP containing<br>monomers ( <b>2a-c</b> ).....                              | 124 |
| 7.3 NMR spectra and ESI ToF MS of the <i>N</i> -benzyl protected DAP containing<br>monomers ( <b>2d-f</b> ).....                              | 127 |
| 7.4 NMR spectra and ESI ToF MS of undec-10-enamide ( <b>3</b> ).....  | 129 |
| 7.5 NMR spectra and ESI ToF MS of undec-10-en-1-amine ( <b>4</b> ).....   | 130 |
| 7.6 NMR spectra and ESI ToF MS of 1,3-diundec-10-en-1-ylurea (Urea-M-9) ( <b>5</b> ).....   | 131 |
| 7.7 NMR spectra of diethyl-2,2-di(undec-10-en-1-yl)malonate ( <b>6</b> ).....   | 132 |
| 7.8 NMR spectra and ESI ToF MS of 2-(undec-10-en-1-yl)tridec-12-enoic acid<br>(Acid-M-9) ( <b>8</b> ).....                                    | 133 |

|  |     |
|--|-----|
| 7.9 NMR spectra and ESI ToF MS of Acid-M-Ee-9 ( <b>10</b> ) .....  | 134 |
| 7.10 IR spectra of the unsaturated DAP containing polymers ( <b>11a-c</b> ).....   | 135 |
| 7.11 NMR spectra and MALDI ToF MS of the unsaturated <i>N</i> -methyl protected<br>DAP containing polymers ( <b>11d-f</b> ) .....            | 135 |
| 7.12 NMR spectra of the unsaturated <i>N</i> -benzyl protected DAP containing polymers<br>( <b>11g-i</b> ) .....                             | 137 |
| 7.13 NMR spectra of Acid-uP-20 ( <b>13</b> ) .....   | 138 |
| 7.14 IR spectra of the saturated DAP containing polymers ( <b>14a-c</b> ).....   | 139 |
| 7.15 NMR spectra and MALDI ToF MS of the saturated <i>N</i> -methyl protected DAP<br>containing polymers ( <b>14d-f</b> ) .....              | 139 |
| 7.16 NMR spectra and MALDI ToF MS of the saturated <i>N</i> -benzyl protected DAP<br>containing polymers ( <b>14g-i</b> ) .....              | 142 |
| 7.17 IR spectra of Urea-M-9 ( <b>5</b> ), Urea-uP-20 ( <b>12</b> ) and Urea-sP-20 ( <b>15</b> ).....   | 143 |
| 7.18 NMR spectra of Acid-sP-20 ( <b>16</b> ).....  | 143 |
| 7.19 DSC analysis of the <i>N</i> -unprotected DAP containing monomers and polymers<br>( <b>1a-c</b> , <b>11a-c</b> and <b>14a-c</b> ) ..... | 144 |
| 7.20 DSC analysis of the <i>N</i> -protected DAP containing polymers ( <b>11d-i</b> and <b>14d-i</b> ).....                                  | 145 |
| 7.21 DSC analysis of the urea containing polymers ( <b>12</b> and <b>15</b> ) .....  | 148 |
| 8. Curriculum Vitae .....  | 149 |
| 9. Eigenständigkeitserklärung .....  | 152 |

## List of abbreviations

|                   |  |
|-------------------|--|
| 4-Amino TEMPO     | 4-amino-2,2,6,6-tetramethyl-1-piperidinyloxy radical   |
| ADMET             | acyclic diene metathesis   |
| ATRP              | atom transfer radical polymerization   |
| CCl <sub>4</sub>  | carbon tetrachloride   |
| CuAAC             | copper(I)-catalyzed alkyne-azide cycloaddition   |
| DAP               | diaminopyridine  |
| DCM               | dichloromethane  |
| DCTB              | <i>trans</i> -2-[3-(4- <i>tert</i> -butylphenyl)-2-methyl-2-propenylidene]<br>malononitrile  |
| DIPEA             | <i>N,N</i> -diisopropylethylamine  |
| DKP               | diketopiperazine   |
| DLS               | dynamic light scattering   |
| DMF               | <i>N,N</i> -dimethylformamid   |
| DNA               | deoxyribonucleic acid  |
| DSC               | differential scanning calorimetry  |
| EA                | ethyl acetate  |
| ED                | entropy-driven   |
| EDC-HCl           | <i>N</i> -(3-dimethylaminopropyl)- <i>N'</i> -ethylcarbodiimide hydrochloride  |
| EPR               | electron paramagnetic resonance  |
| ESI               | electrospray ionization  |
| Et <sub>2</sub> O | diethyl ether  |
| EtOH              | ethanol  |
| FTIR              | Fourier-transform infrared spectroscopy  |
| FWHM              | full width at half maximum   |
| G1                | Grubbs' 1 <sup>st</sup> generation catalyst - benzylidene<br>bis(tricyclohexylphosphine)dichlororuthenium                                |
| GH1               | Grubbs-Hoveyda 1 <sup>st</sup> generation catalyst - dichloro-<br>(2-isopropoxyphenylmethylene)(tricyclohexylphosphine)<br>ruthenium(II) |
| GPC               | gel permeation chromatography  |
| HDPE              | high-density polyethylene  |



|                  |   |
|------------------|---|
| HPLC             | high-performance liquid chromatography            |
| IR               | infrared  |
| s                | strong  |
| m                | middle  |
| w                | weak  |
| LCB              | long-chain branching                              |
| LLDPE            | linear low-density polyethylene                   |
| MALDI            | matrix-assisted laser desorption/ionization       |
| MeOH             | methanol  |
| $M_n$            | number average molar mass                         |
| mRNA             | messenger ribonucleic acid                        |
| MS               | mass spectrometry                                 |
| $M_w$            | weight average molar mass                         |
| NCA              | <i>N</i> -carboxyanhydride                        |
| NHC              | <i>N</i> -heterocyclic carbene                    |
| NMR              | nuclear magnetic resonance spectroscopy           |
| NNCA             | <i>N</i> -substituted- <i>N</i> -carboxyanhydride |
| PCR              | polymerase chain reaction                         |
| PCy <sub>3</sub> | tricyclohexylphosphine                            |
| PDI              | polydispersity index ( $PDI = M_w/M_n$ )          |
| PE               | polyethylene                                      |
| PNA              | peptide nucleic acid                              |
| PPh <sub>3</sub> | triphenylphosphine                                |
| RI               | refractive index                                  |
| RNA              | ribonucleic acid                                  |
| ROP              | ring-opening polymerization                       |
| ROMP             | ring-opening metathesis polymerization            |
| rRNA             | ribosomal ribonucleic acid                        |
| SAXS             | small-angle X-ray scattering                      |
| SCB              | short-chain branching                             |
| SCNP             | single-chain polymer nanoparticle                 |
| SSA              | successive self-nucleation and annealing          |
| TBD              | triazabicyclo[4.4.0]dec-5-ene                     |

|                     |  |
|---------------------|--|
| TEG                 | tetraethylene glycol                         |
| TEM                 | transmission electron microscopy             |
| TEMPO               | 2,2,6,6-tetramethyl-1-piperidinyloxy radical |
| TES                 | thiol-ene step-growth                        |
| TFA                 | trifluoroacetic acid                         |
| T <sub>c</sub>      | crystallization temperature                  |
| T <sub>g</sub>      | glass transition temperature                 |
| T <sub>m</sub>      | melting temperature                          |
| THF                 | tetrahydrofuran                              |
| TLC                 | thin-layer chromatography                    |
| ToF                 | time of flight                               |
| tRNA                | transfer ribonucleic acid                    |
| TsNHNH <sub>2</sub> | <i>p</i> -toluenesulfonyl hydrazide          |
| U1                  | umicore M1 catalyst                          |
| WAXS                | wide-angle X-ray scattering                  |

Parts of the results and discussion as well as of the experimental part were already published in “*Synthesis and Crystallization of Precision Polymers with Repetitive Folding Elements*” (Reimann, S.; Baumeister, U.; Binder, W. H. *Macromol. Chem. Phys.* **2014**, *215*, 1963. <http://dx.doi.org/10.1002/macp.201400183>), in “*Synthesis of supramolecular precision polymers: Crystallization under conformational constraints*” (Reimann, S.; Danke, V.; Beiner, M.; Binder, W. H. *J. Polym. Sci.* **2017**, *55*, 3736. <http://dx.doi.org/10.1002/pola.28759>) and in “*Structure formation in nanophase-separated systems with lamellar morphology: Comb-like vs. linear precision polymers*” (Danke, V.; Gupta, G.; Reimann, S.; Binder, W. H.; Beiner, M. *Eur. Polym. J.* **2018**, *103*, 116. <https://doi.org/10.1016/j.eurpolymj.2018.03.041>) and were in parts reprinted and adapted with permission from John Wiley and Sons (Copyright 2014 & 2017)

# 1. Introduction

## 1.1 Precision polymers

Nature has always been one of the greatest archetype for scientists. Biomacromolecules own an awesome repertoire of interesting functions such as molecular recognition, information storage or catalysis<sup>1-3</sup>, which could up to now not be observed for synthetic macromolecules. First, biomacromolecules exhibit an accurately defined primary structure, whereby the single amino acid monomers are precisely placed in a defined sequence, enabling the storage of information.<sup>4</sup> Triggered by the supramolecular interactions, more specifically hydrogen bonds exerted by the building blocks, biomacromolecules are able to assemble into secondary structures like  $\alpha$ -helices or  $\beta$ -sheets and -turns.<sup>4</sup> These folded chains finally organize into superstructures yielding tertiary and quaternary structures, whereby proteins gain the ability to catalyze numerous processes.<sup>4</sup> The formation of these complex structures is schematically shown in Figure 1.

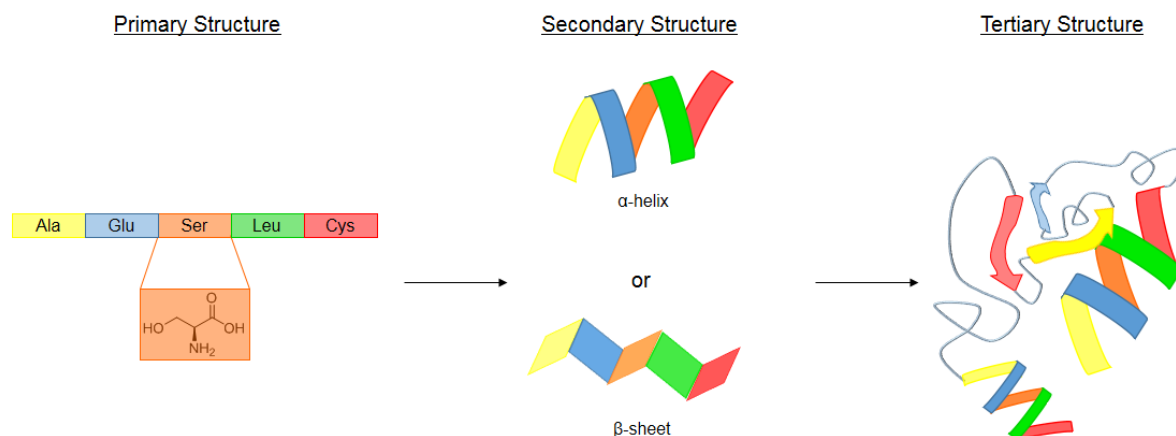


**Figure 1:** Schematic representation of the primary, secondary and tertiary structure of biomacromolecules.<sup>5</sup>

Considering, that nature offers all of its astonishing features on the basis of just 21 amino acids, it is barely imaginable what scientist could create with an infinite number of synthetic monomers.

Polymers exhibiting a defined primary structure just like biomacromolecules are called precision polymers whereat it can be distinguished between sequence-controlled and sequence-defined polymers.<sup>3</sup> Sequence-controlled polymers show a more or less controlled order of monomers in the polymer chain, whereby macromolecules differing in length and composition are obtained<sup>3</sup>, including for example, block copolymers, as well as alternating, periodic or gradient copolymers.<sup>1,3</sup> In contrast, sequence-defined polymers are uniform macromolecules in which the order of monomers in the polymer backbone is perfectly defined just as in biopolymers or foldamers.<sup>3</sup> To introduce such a precision into a monomer sequence different synthetic strategies based on biological and synthetic approaches can be used.

### 1.1.1 Synthesis of natural polypeptides - biological precision polymers

Deoxyribonucleic acid (DNA), ribonucleic acid (RNA) and proteins are probably the best-known and most important representatives of biological precision polymers. These biomacromolecules are produced in the human organism through replication, transcription and translation processes.<sup>6,7</sup>

Replication is a natural process in which DNA is duplicated before each cell division (mitosis). Therefore, the DNA double strand is unwound and the helicase dissolves the hydrogen bonds between the complementary nucleobases leading to the splitting into two single strands. Primers are synthesized at which ends the DNA polymerase starts to attach complementary bases onto the single strands resulting in the formation of two new identical DNA double helices.<sup>6</sup> During transcription transfer RNA (tRNA), messenger RNA (mRNA) and ribosomal RNA (rRNA) are synthesized with the help of a DNA template. The addition of RNA polymerase to the DNA double strand leads to its unwinding followed by the attachment of complementary ribonucleotides, whereby DNA is transcribed into RNA.<sup>7</sup>

Thus, the prepared mRNA can be used for protein synthesis in the ribosomes via translation. Each base triplet (codon) in the mRNA strand encodes a special amino acid, which is transported to the ribosome with the help of tRNA, where it is linked to the adjacent amino acid via peptide coupling forming step by step the coded protein.<sup>7</sup>

It is also possible to synthesize such polypeptides artificially by different methods, which are explained below.

#### *DNA Templating*

In the simplest case polypeptides are synthesized using DNA templates in processes that proceed analogously to replication and transcription by connecting nucleic acids and their analogues with each other.<sup>1,8,9</sup> Therefore, nucleotides are linked via Watson-Crick base pairing to the corresponding template, followed by their subsequent polymerization initiated by DNA/RNA polymerases<sup>1,10-14</sup> as schematically shown in Figure 2.

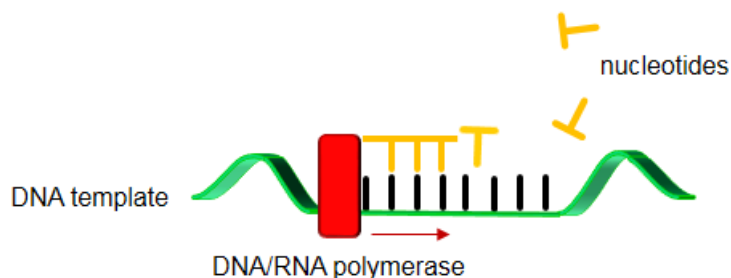


**Figure 2:** Schematic representation of the synthesis of biological precision polymers using DNA templates.<sup>15</sup>

Orgel and coworkers were also able to present systems, which do not require the use of enzymes, broadening the scope of application of this method.<sup>16,17</sup> Nevertheless, this method is not particularly efficient as the synthesis of the templates is very time-consuming and the desired precision polymers are obtained in very poor yields due to the strong adhesion of the synthesized oligomers to the template.<sup>1</sup>

### Templating via the polymerase chain reaction

The synthesis of polypeptides can also be realized by enzyme catalyzed methods like the polymerase chain reaction (PCR).<sup>1,18</sup> Here, a DNA template is initially denatured at high temperatures to break the hydrogen bonds between the complementary strands followed by the addition of a primer, which accumulates to the single DNA-strand. Finally a DNA-polymerase is added, enabling the attachment of complementary bases and thus the replication of the template<sup>18,19</sup>, which is schematically shown in Figure 3. With the help of the temperature-resistant polymerases nowadays natural as well as non-natural monomers can be polymerized into well-defined sequences.<sup>1,18,20-22</sup> However the PCR still constitutes a laborious process.<sup>1,19</sup>

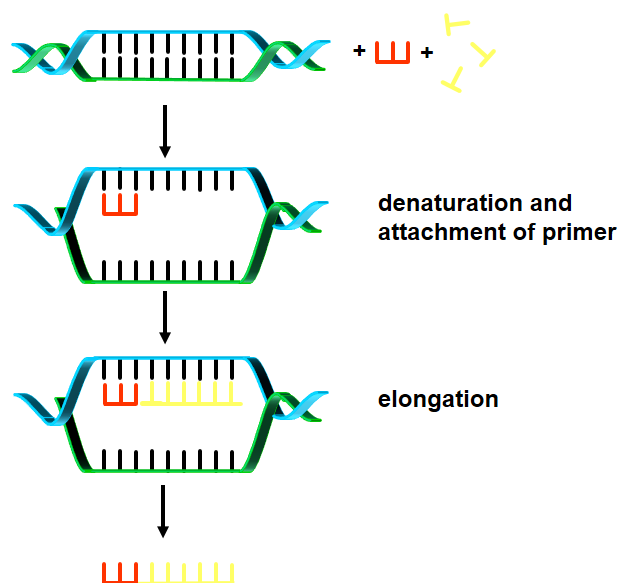


**Figure 3:** Schematic representation of the synthesis of sequence-controlled polymers using the polymerase chain reaction.<sup>1</sup>

### Protein Engineering

Protein Engineering represents the most known and widespread biological method for the synthesis of sequence-defined polymers.<sup>1,8,23</sup> For this purpose an artificial gene is being inserted into plasmid DNA, which is further incorporated into a host system (e.g. *E. coli*), where the synthesis of the targeted protein takes place, followed by its extraction and purification.<sup>1,8,19,23-26</sup>

### Merrifield synthesis

The solid-phase synthesis, pioneered by Merrifield in 1963<sup>27</sup>, represents a well-known and highly optimized method for peptide synthesis.<sup>28</sup> Here, individual amino acids are linked with each other one after one, leading to a high sequence control.<sup>1</sup> A filterable polystyrene bead (also known as Merrifield resin) serves as solid support to which a *N*-protected amino acid is bound via its *C*-terminus. After successful conversion the protection group is removed, enabling the linkage with the next *N*-protected amino acid via peptide coupling.<sup>2,4,19,28,29</sup> The process of solid-phase synthesis is schematically shown in Figure 4. Due to the attachment to the solid phase, the growing oligomer can be purified easily after each coupling step via filtration

allowing the facilitated removal of undesired side products.<sup>1,4,19</sup> This process can also be carried out automatically in special peptide synthesizers, leading to a significant decrease in reaction times.<sup>1</sup> Unfortunately, the scope of application is limited to the synthesis of oligopeptides, consisting of two to fifty monomer units.<sup>2,19,29</sup>

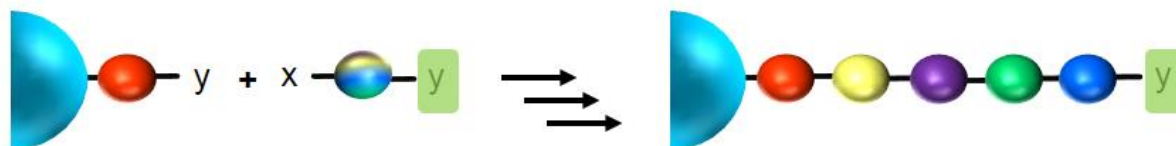


**Figure 4:** Schematic representation of the synthesis of sequence-controlled polymers via templated multi-step-growth polymerization, whereby the letters x and y represent different functional groups. The green square represents a protection group. Figure reproduced and adapted from reference<sup>2</sup> with permission from the Royal Society of Chemistry.

### 1.1.2 Synthesis of non-natural polypeptides/polypeptoids

#### *Artificial ribosomes*

As sequence controlled polymers are synthesized in natural transcription processes it is conceivable that artificial ribosomes are capable of equal performances. A relatively new biological attempt to synthesize such artificial systems is based on rotaxanes, which resemble ribosomes like a molecular machine.<sup>1,8</sup> Here, a thiol-modified ring moves along an axis on which amino acids are deposited and couples them on by one creating a sequence-controlled polymer chain.<sup>1,8,30,31</sup>

#### *Solid-phase synthesis*

Natural monomers can also be linked to non-natural polypeptides or polypeptoids using the modified Merrifield synthesis. To avoid time-consuming protection and deprotection steps two different monomers (xx and yy) can be used instead of one bifunctional (xy) building block.<sup>1</sup> The successful synthesis of poly(amidoamines)<sup>32,33</sup> as well as [oligo(*N*-substituted glycines)]<sup>34</sup> and other polypeptoids<sup>35-37</sup> prove the applicability of this method.

#### *Ring-opening polymerization*

Non-natural polypeptides and polypeptoids can be synthesized not only by biological but also by chemical methods. Therefore, the appropriate amino acids are converted into *N*-carboxyanhydrides (NCAs) or *N*-substituted-*N*-carboxyanhydrides (NNCAs) (for the synthesis of polypeptoids) via Fuchs-Farthing method using triphosgene, followed by ring-opening polymerization (ROP) to yield linear precision polymers.<sup>38-41</sup> This polymerization can be combined with the approach of solid-phase synthesis by binding the initiator to an insoluble support as demonstrated by Luxenhofer and coworkers,<sup>42</sup> whereby sequence-controlled polymers can be prepared via one after one attachment. Obviously, this is not a generally valid method for the synthesis of precision polymers as it is currently limited to the use of *N*-substituted glycine *N*-carboxyanhydrides as monomers.

### 1.1.3 Synthesis of non-natural/artificial precision polymers

Deviating from natural monomers to artificial building blocks allows the preparation of precision polymers via biological approaches as well as chemical syntheses.

#### *Templating*

Just like biological precision polymers, synthetic ones can also be synthesized with the help of DNA templates by attaching monomers to the end of single DNA strands. Via interaction of two complementary strands the monomers are located in close proximity to each other, which allows them to be linked by chemical means. After removing the “empty” strand, a new one bearing another monomer can be added leading to the formation of a sequence controlled polymer via one after one attachment as schematically shown in Figure 5.

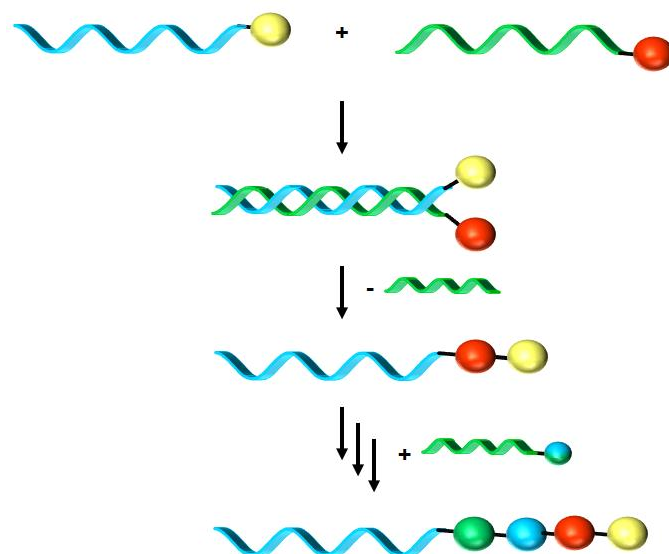


**Figure 5:** Schematic representation of the synthesis of sequence-controlled polymers using DNA templates. Figure reproduced and adapted from reference<sup>14</sup> with permission from The Royal Society of Chemistry.

Another possibility is to bind the monomers to peptide nucleic acid (PNA) adapters, which are able to recognize different base codons on the DNA template and to complementary interact with them<sup>43</sup> as shown schematically in Figure 6. Here again the monomers are brought into close proximity to each other enabling their linkage using different chemical reactions.

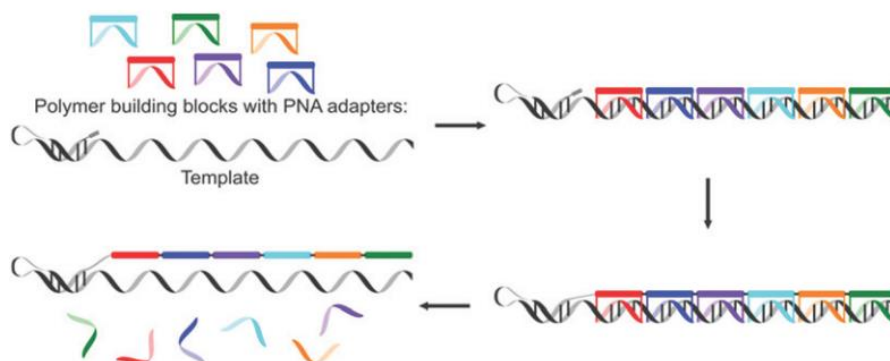


**Figure 6:** Schematic representation of precision polymer synthesis using DNA templates and PNA adapters. Figure reprinted with permission from reference<sup>9</sup>-Published by the Royal Society of Chemistry.



Apart from DNA also synthetic macromolecules like poly(sarcosine)<sup>44</sup> or poly(2-vinylpyridine)<sup>45,46</sup> can be used as templates. The template is able to interact only with certain monomers via supramolecular interactions, leading to the preferential incorporation into the growing polymer chain.

### *Solid-phase synthesis - iterative chemistry*

Artificial precision polymers can also be synthesized using the modified Merrifield synthesis. This is referred to as solid-phase iterative chemistry<sup>8,47,48</sup>, which is basically a multi-step-growth polymerization.<sup>1,2,4</sup> Here again a bifunctional monomer with one temporarily protected functional group is tethered via labile covalent bond to a support (mostly a cross-linked polymer bead).<sup>2,4,29</sup> Afterwards the protection group is removed enabling the reaction with the next monomer.

Via one after one attachment the monomer sequence can be perfectly controlled and the attachment to the polymer bead allows the purification of the growing oligomer by filtration after each coupling step, whereby undesired side products are easily removed as schematically shown in Figure 4.<sup>1,4,19</sup> Using this method up to now several sequence-controlled polymers including oligoesters<sup>49</sup>, oligoureas<sup>50</sup>, oligocarbamates<sup>51</sup> and others<sup>52-54</sup> could be prepared. Unfortunately, the deprotection steps are very time-consuming and the scope of application is limited to the synthesis of oligomers.<sup>2,29</sup>

### 1.1.3.1 Chain-growth polymerizations

Chain-growth polymerizations provide an opportunity for the synthesis of sequence-controlled polymers (see Figure 7).

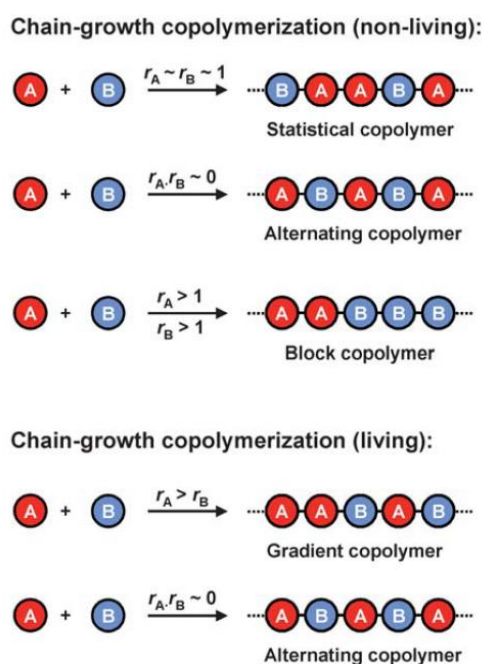


**Figure 7:** Possible polymer sequences obtained via chain-growth polymerizations. Figure reproduced and adapted from reference<sup>2</sup> with permission from the Royal Society of Chemistry.

In the simplest case two monomers can be copolymerized by the means of radical or ionic polymerizations<sup>8,55,56</sup>, which usually leads to the generation of a statistical copolymer.<sup>2</sup> However, if two monomers with appropriate copolymerization parameters are used, the synthesis of either block copolymers ( $r_i > 1$ ) or alternating copolymers ( $r_i = 0$ ), in which the monomer sequence within the polymer chain is exactly defined, is possible.<sup>2</sup> The radical copolymerization of styrene (electron-donor) with malic anhydride (electron-acceptor) represents one example for the synthesis of a perfectly alternating copolymer.<sup>1,2,57,58</sup>

### *Kinetic control*

This alternating behavior can be reinforced by using kinetically controlled processes as shown for the atom transfer radical polymerization (ATRP) of styrene and *N*-substituted maleimides.<sup>1,2,59-61</sup> Here, the maleimides are added to the polymerization mixture at defined times, according to a strict polymerization protocol, whereby they are incorporated into narrow regions into the polystyrene chain, as the cross propagation is favored to the homopolymerization of the styrene.<sup>1,2,4,59-61</sup>

The co-polymerization of *exo*- and *endo*-norborene via ring-opening metathesis polymerization (ROMP)<sup>62,63</sup> as well as the cationic terpolymerization of oxiranes, ketones and vinyl ethers<sup>64</sup> are further examples for the synthesis of precision polymers under the aspect of kinetic control. However, these techniques do not lead to perfectly sequence-defined polymers, but demonstrate the proof of concept.<sup>4</sup>

### *Monomer reactivity*

Further increase in sequence-control can be accomplished by decreasing the reactivity of the monomers gradually, achieving a single monomer insertion. So far, there is no known general approach to reduce reactivity, but at least some examples have already been given. Thus, the addition of hydroiodic acid to the cationic polymerization of vinyl ethers or styrene leads to the formation of inactive iodo-species, which are reactivated by the addition of  $ZnI_2$  in the presence of the next monomer.<sup>2,65,66</sup>

### **1.1.3.2 Step-growth polymerizations**

Among the chain-growth reactions it is also possible to synthesize precision polymers via step-growth polymerizations. An elementary example represents the reaction of monomers bearing two different functional end groups (see Figure 8).<sup>2</sup> In order that no statistical copolymer is being generated, one of the functionalities must be provided with a protection group, which has to be removed before the respective reaction. To circumvent these effortful protection and deprotection steps one can refer to monomers bearing the same functionality at both reactive ends.<sup>2</sup>

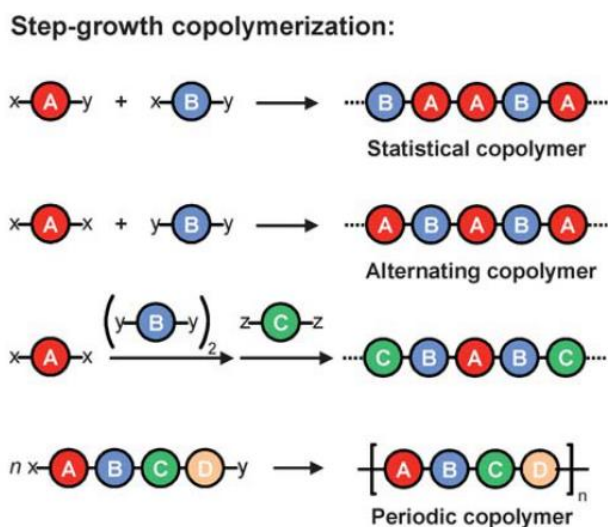


**Figure 8:** Schematic representation of the synthesis of sequence-controlled polymers via step-growth co-polymerizations, whereby the letters x, y and z represent different functional groups. Figure reproduced and adapted from reference<sup>2</sup> with permission from the Royal Society of Chemistry.

At this point particularly the ADMET polymerization, which is used since 1991 by Wagener and coworkers<sup>67</sup> for the synthesis of precision polymers will be explained in more detail, as this kind of polymerization was applied in this doctoral thesis.

#### *Acyclic diene metathesis polymerization*

The acyclic diene metathesis polymerization is a polyaddition or rather a polycondensation reaction and is characterized by a stepwise growth of the polymer chain<sup>68</sup>. The formation of high molecular weight polymers via dimers, tetramers and so on can only be achieved at high monomer conversions of about 99%<sup>69-71</sup> as described by the simplified Carothers equation<sup>72</sup> (eq. 1), which can be applied if only one kind of monomer is being used.

$$\bar{X}_n = \frac{1}{1 - p} \quad (1)$$

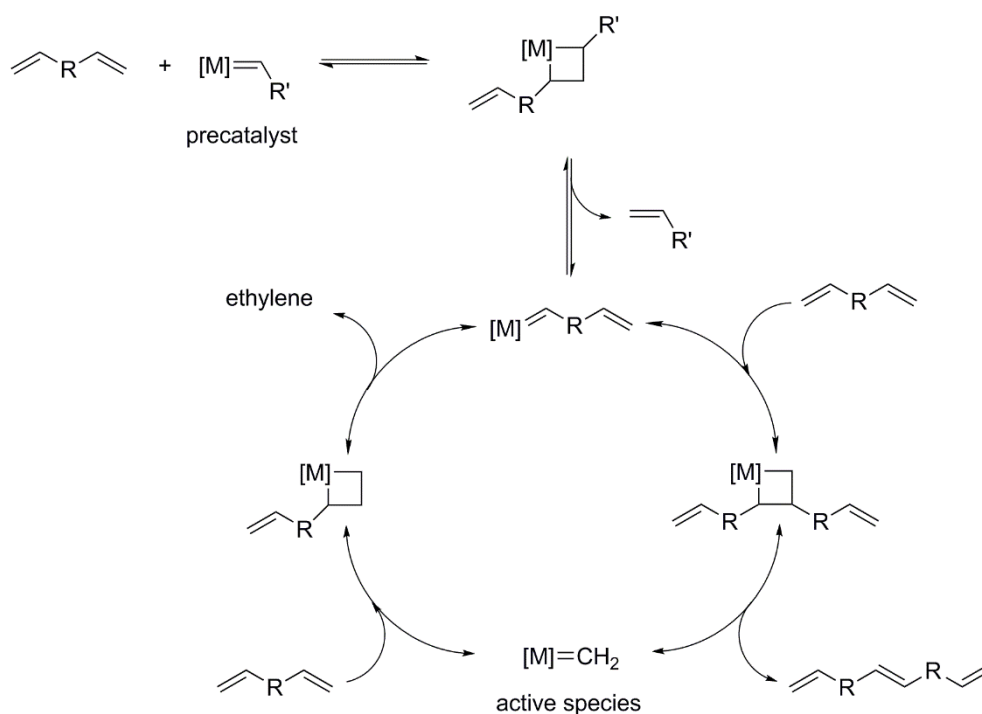
where  $\bar{X}_n$  represents the degree of polymerization and p is the conversion.

Symmetric  $\alpha,\omega$ -dienes serve as monomers, which are reacted with an appropriate metathesis catalyst to produce polymers exhibiting the same functionality and symmetry as found in the monomer<sup>68,73</sup>. The starting materials should possess a high purity to prevent side reactions and poisoning of the catalyst. Monomers, which are able to form 5-, 6- or 7-membered rings should be avoided to eliminate the possibility of cyclization during the polymerization via intramolecular backbiting.<sup>74,75</sup> Schrock and Grubbs' carbenoid catalysts are used to catalyze the polymerization reaction.<sup>70</sup> Schrock's molybdenum containing catalyst shows very high activity in olefin metathesis but their application is limited due to their sensitivity towards air, moisture and polar functional moieties<sup>68,69,76-79</sup>. Therefore, predominantly ruthenium based Grubbs' catalysts are used, which are more stable and more tolerant towards functional groups<sup>68</sup> due to their late transition metal center combined with tricyclohexylphosphine (PCy<sub>3</sub>) ligands.<sup>68</sup> The use of *N*-heterocyclic carbene (NHC) ligands in the Grubbs' 2<sup>nd</sup> generation catalyst leads to an

increase in activity<sup>68,80-82</sup> as these ligands stabilize the mono(phosphine) intermediates, which constitute the actual active species in metathesis polymerization.<sup>70,83-85</sup> Grubbs'-Hoveyda catalysts are even more stable due to the exchange of the PCy<sub>3</sub> ligands with aromatic ethers causing long catalyst life times, whereby high molecular weight polymers can be obtained in high yields.<sup>70,86</sup>

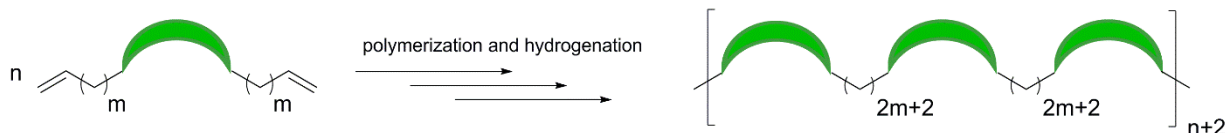
The polymerization takes place via metal-carbene mechanism<sup>68,69,71,73,75,87</sup> as shown in Scheme 1, which was first proposed by Chauvin in 1971.<sup>88</sup>

The reaction of an olefin with a precatalyst via 2+2 cycloaddition leads to the formation of a metallocyclobutane intermediate, which is converted via 2+2 cycloreversion into an  $\alpha$ -substituted metal-alkylidene species. The reaction with another monomer produces a dimer and a metal-methylidene, the actual active species, via an  $\alpha,\beta$ -substituted metallocyclobutane intermediate<sup>68</sup>. Hence, the catalytic cycle proceeds under formation of ethylene as side product, which has to be removed from the reaction to drive the polymerization forward by shifting the equilibrium towards the products and to avoid back reactions.<sup>68,75</sup> The internal double bonds in the polymer backbone created via ADMET polymerization can be removed by subsequent hydrogenation.



**Scheme 1:** Mechanism of the acyclic diene metathesis polymerization. <sup>73,87,89</sup>

The length of the alkenyl chain of the symmetric monomer precisely defines the distance between the functional groups in the final polymer (see Scheme 2) enabling the synthesis of sequence-defined precision polyolefins.



**Scheme 2:** The distance between two functional groups is precisely determined by the symmetric monomer.

As mentioned previously cyclization can occur as side reactions, which can be suppressed by the choice of appropriate monomers and their use in high concentrations as is the case in bulk polymerizations.<sup>70,75</sup> By application of Grubbs' 2<sup>nd</sup> generation catalysts isomerization reactions can appear<sup>90</sup>, that will be suppressed by the addition of tin(II) chloride and bromide salts<sup>91</sup>, 2,6-dichloro-1,4-benzoquinone<sup>92</sup> or phenyl phosphoric acid.<sup>93</sup>

By means of the ADMET polymerization up to now a great variety of polyethylene-like polymers were synthesized<sup>94-106</sup> allowing the investigation of polymer crystallization influenced by defects. This topic is discussed further in chapter 1.3.2.

### *Ring-opening metathesis polymerization*

Diversely substituted cyclic olefins can be converted into linear, sequence-specific copolymers using the ring-opening metathesis polymerization (ROMP) (see Figure 9). This reaction proceeds analogously to the olefin metathesis via metallocyclobutane intermediates and can be catalyzed by Grubbs' catalysts like the ADMET polymerization. This method can also be used to increase the number of different monomers per sequence by polymerizing macrocycles<sup>8</sup>, bearing the desired segments.<sup>107</sup>



**Figure 9:** Synthesis of sequence-controlled polymers using ROMP. Figure reproduced from reference<sup>107</sup> with permission from the American Chemical Society.

These macrocycles can be created using the relay-ring closing metathesis polymerization presented by Park and coworkers, whereby long-chain sequences are cyclized with an alkene-alkyne trigger.<sup>107,108</sup> To compensate the missing ring strain in such large cyclic structures the entropy-driven ring-opening metathesis polymerization (ED-ROMP) can be applied.<sup>4,109</sup>

### *Other step-growth polymerizations*

Further possibilities to synthesize precision polymers via step-growth polymerizations were presented by Du Prez, Lutz or Han, using “click” chemistry as for example the copper(I)-mediated alkyne-azide cycloaddition (CuAAC)<sup>110-112</sup> or thiol-ene couplings<sup>113,114</sup>.<sup>8</sup>

Equally, the Passerini three-component reaction, whereby isocyanides, aldehydes and carboxylic acids<sup>115</sup> are combined to a sequence-defined polymer accounts to the step-growth polymerizations.<sup>4,8</sup>

Furthermore the thiol-ene step-growth (TES) polymerization is suited for the synthesis of sequence-controlled polymers. This polymerization is initiated photochemically by organic substances and produces precision polymers with an already saturated backbone. Due to its high tolerance towards air and functional groups precision polymers containing thioethers and sulfoniums could be synthesized<sup>116-122</sup>.

## **1.1.4 Properties and applications of precision polymers**

### **1.1.4.1 Biological precision polymers**

Some precision polymers like foldamers or single-chain nanoparticles (SCNP) are able to adopt folded secondary structures, whereby they gain the opportunity to mimic properties and functions of globular proteins, as for example most importantly the catalysis based on enzymes.<sup>4</sup> A lot of enzymes catalyze processes with the help of metals, which are located in hydrophobic pockets formed by secondary interactions.<sup>4</sup> Some groups already prepared synthetic enzymes (enzyme-mimics) on the basis of SCNPs. Thus, polystyrene chains, bearing triarylphosphine ligands in exactly defined intervals, can bind Pd(II), forming a catalytically active SCNP.<sup>123</sup> A similar behavior was observed by acetoacetoxy based polymers, synthesized by Sanchez, after the addition of Cu(II).<sup>124</sup> Equally, artificial [Fe-Fe] hydrogenase as well as heme model mimics could already be prepared.<sup>125</sup>

Polymer hydrogel nanoparticles based on polyamides exhibit chaperone-like behavior and thus could prevent misfolding of proteins.<sup>126</sup> Poly-NIPAM was proven to bind and neutralize toxins, whereby the use of precision polymers as synthetic antibodies can also be taken into account.<sup>127</sup>

### **1.1.4.2 Artificial precision polymers**

Based on the possibility to define the primary structure of precision polymers monomer by monomer they are suited for use in the area of information storage.<sup>29,128</sup> Thus, documents can be written in binary code by synthesizing a copolymer consisting of two monomers being defined as either “0” or “1” bit.<sup>128</sup> Of course also codes containing more than two monomers, allowing the storage of huge data volumes on short polymer sequences, are imaginable.<sup>29</sup> This possible application was already successfully tested by Lutz and coworkers on sequence-defined polyphosphates, which were synthesized based on two different phosphoramidite monomers.<sup>29</sup> As the synthesis of this precision polymer is very complex due to numerous deprotection processes also polymerization approaches without protection chemistry were pursued.<sup>29</sup> Thus, sequence-defined oligo(triazole amides)<sup>129</sup>, oligo(alkoxyamine amides)<sup>130</sup>, oligourethanes<sup>128</sup> as well as oligocarbamates<sup>51</sup>, containing encoded messages, could be synthesized via iterative chemistry. Reading these codes can be enabled by tandem mass spectrometry<sup>1,3,29,131</sup>, whereby the polymer is firstly characterized by ESI ToF MS resulting in a polydisperse spectrum, the so-called 1<sup>st</sup> dimension fingerprint. The subsequent analysis of each single peak via MS/MS reveals the 2<sup>nd</sup> dimension fingerprint enabling the decoding of the sequence.<sup>128</sup>

Also nanopore sequencing can be used to decode such messages.<sup>131</sup> Therefore, a nanopore is embedded into a lipid bilayer, followed by applying an electric voltage, which induces a certain channel current in the pore.<sup>131</sup> If now the precision polymer is driven through the protein pore a blockade in the channel current is induced, whereby the blockage amplitude is characteristic for each monomer unit allowing the decryption of the sequence.<sup>3,29,131</sup>

Precision polymers can store huge amounts of information with low space requirement and are in addition long-term stable, whereby their use as molecular barcodes or anti-counterfeiting agents can be taken into consideration.<sup>128</sup>

## 1.2 Polymer crystallization

Although, the crystallization of polymers was an essential part of numerous studies during the past decades this process is not elucidated completely until now. Since the first X-ray diffraction experiments on polymers, which were conducted during the 1920s, an endless number of scientific papers and reviews concerning various polymer crystallization theories and extensions of such were published.<sup>132-141</sup>

In general it can be considered, that all polymers exhibiting a regular and symmetric structure are capable to crystallize.<sup>142</sup> Thus, unbranched polymers with an all-*trans* conformation are most likely to adopt a regular packing, which is one prerequisite for the formation of crystals. The most prominent example therefore is surely polyethylene, whereof already in 1957 first single crystals could be synthesized and analyzed by several groups.<sup>141,143-145</sup>

If the polymers do contain side chains or other substituents they should be arranged regularly along the polymer backbone as for example in isotactic or syndiotactic polypropylene.<sup>146,147</sup> Nevertheless, also a multitude of atactic polymers are able to undergo crystallization.<sup>148-150</sup> In addition the side chains or substituents should be of small size as otherwise the polymer chains cannot arrange themselves close enough to each other. Intramolecular interactions between the substituents can lead to a stabilization of the formed crystal.

It remains supplementary to mention that polymers never crystallize completely as their long molecular chains form entangled, random coils in the melt,<sup>151</sup> wherefore the alignment of the chains to form a single crystal would only be possible under extreme high pressure or stretching.<sup>152,153</sup> Furthermore, the polymer chain forms loops when exiting and re-entering the crystallite and can even participate in different nuclei.<sup>154</sup> Hence, every crystallite contains crystalline and amorphous parts, which is why polymers are regarded as semi-crystalline.

In the following chapters the process of polymer crystallization as well as basic theories and concepts should be outlined in a simple, but detailed manner.

Under which conditions the crystallization of polymers proceeds is described by thermodynamics, which will be explained briefly in the next chapter.

### 1.2.1 Thermodynamic considerations

In order that processes take place spontaneously the change of the free energy, which is given by the Gibbs-Helmholtz-equation (eq. 2) must exhibit negative values.

$$\Delta G = \Delta H - T\Delta S \quad (2)$$

where  $\Delta G$  is the change in Gibbs free energy,  $\Delta H$  is the change in enthalpy,  $T$  is the absolute temperature and  $\Delta S$  represents the change in entropy.

Figure 10 illustrates the relationship between the temperature and the Gibbs free energy of solids and liquids.

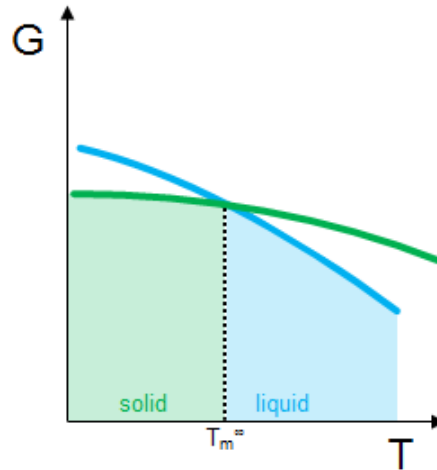


**Figure 10:** Graphical depiction of the relationship between Gibbs free energy and temperature.<sup>155</sup>

As a crystal exhibits a lower free energy than its corresponding liquid below the equilibrium melting point (see Figure 10) the phase transformation (crystal formation) proceeds spontaneously under constant pressure. If the crystalline and the amorphous/liquid phase are existent in equilibrium to each other the change of free energy equals zero, happening at the so called equilibrium melting temperature, which can be calculated with the equation given below

$$T_m^\infty = \frac{\Delta H_f}{\Delta S_f} = \frac{H_l - H_s}{S_l - S_s} \quad (3)$$

The process of crystallization is a first-order transition,<sup>151</sup> which means that the first derivations of the free energy with respect to pressure or temperature (see eq. 4 and 5) show a step change at the point of phase transformation<sup>155</sup>, which is illustrated in Figure 11.

$$\Delta G = Vdp - SdT \quad (4)$$

$$\left(\frac{\partial G}{\partial p}\right)_T dp = V \quad \text{and} \quad \left(\frac{\partial G}{\partial T}\right)_p dT = -S \quad (5)$$



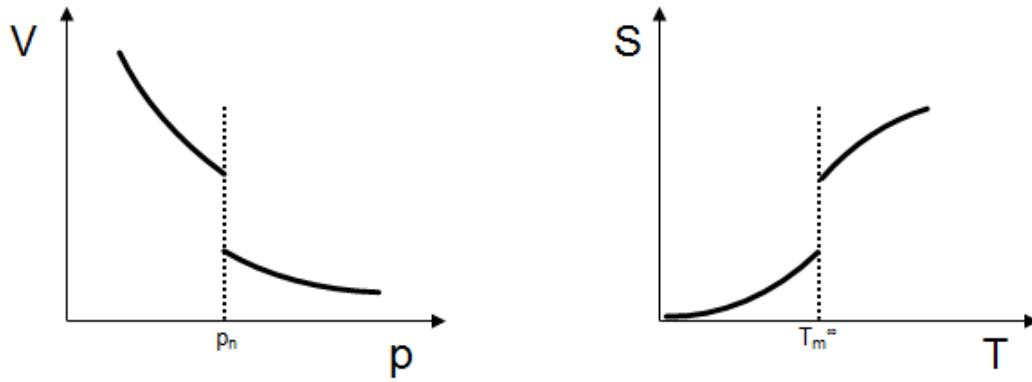


**Figure 11:** Curve progression of the first derivations of the free energy with respect to pressure or temperature for a first-order transition.<sup>156</sup>

### 1.2.2 Primary nucleation

Every polymer crystallization starts with the formation of a crystalline nucleus via random fluctuations in density or order due to Brownian motion in the polymer melt. This process is called primary nucleation and takes place at a certain crystallization temperature, which lies below the melting temperature of the polymer.<sup>154</sup> This temperature range is called supercooling and can be defined as follows

$$\Delta T = T_m - T_c \quad (6)$$

where  $T_m$  represents the melting temperature and  $T_c$  the crystallization temperature.<sup>151</sup>

Primary nucleation events can be divided into homogenous and heterogeneous nucleations, describing the formation of the nucleus, as well as thermal and athermal nucleations, indicating whether the nucleation event is temperature dependent or not. If the formation of nuclei is caused just by random fluctuations, which happens predominantly at high supercoolings, this is called a homogeneous nucleation.<sup>157</sup> This process is temperature dependent and thus can be classified as thermal nucleation leading to different sized crystallites as the nuclei starts to grow independent from each other. In contrast heterogeneous nucleation takes place if nucleation starts on pre-existing surfaces like dust particles, catalysts or the walls of the reaction vessel. This kind of nucleation can be referred to as thermal or athermal, the latter implying the formation of comparable sized crystals, as they start growing at approximately the same time.<sup>155,158</sup> Wunderlich introduced another possibility for the primary nucleation, the so called “self-nucleation“, occurring if single crystals survive the melting process and serve as nuclei during polymer crystallization.<sup>159,160</sup>

Figure 12 schematically shows the relationship between the free energy and the size of a given nucleus.

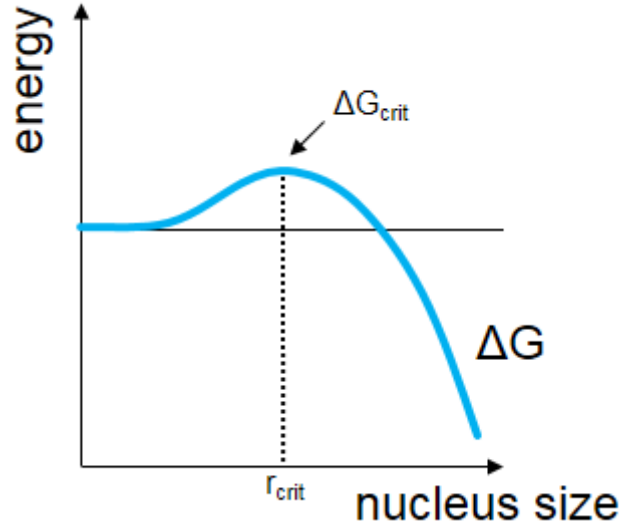


**Figure 12:** Schematic description of the relationship between the energy and the size of a given nucleus.

To obtain a stable nuclei the change in free energy of the nucleation process (calculation for a spherical nucleus with radius 'r' given in eq. 7) must be negative.

$$\Delta G = \frac{4}{3}\pi r^3 \Delta g_f + 4\pi r^2 \sigma \quad (7)$$

where  $\Delta g_f$  represents the difference in free energy of fusion per unit volume of the crystal and  $\sigma$  the surface free energy. If the nucleus exhibits a size below the critical nucleus size ( $r < r_{crit}$ ) the surface free energy prevails and  $\Delta G$  adopts positive values, meaning that the seed decomposes under energy gain. The change in free energy only takes on negative values if the nucleus exceeds the critical nucleus size ( $r > r_{crit}$ ) leading to the formation of a stable crystallite. The inflection of the curve represents the critical nucleus size, which can be calculated as shown in equation (8), at which the system is in equilibrium ( $\Delta G = 0$ ).<sup>141</sup>

$$r_{crit} = \frac{2\sigma}{\Delta g_f} \quad (8)$$

Therefore, at this point the change in free energy can be determined by the following equation<sup>155,161-163</sup>

$$\Delta G = \frac{16\pi\sigma^3}{3\Delta g_f^2} \quad (9)$$

Afterwards, the crystal is growing, whereby a lamella is formed, whose thickness determines the melting temperature. The Gibbs-Thomson equation<sup>164</sup> (eq. 10) describes the indirect proportionality of these parameter to each other.

$$T_m = T_m^0 \left( 1 - \frac{2\sigma_e}{\Delta H_m} \frac{1}{l} \right) \quad (10)$$

where  $T_m^0$  represents the equilibrium melting point,  $\sigma_e$  the surface free energy of the lamella,  $l$  the lamella crystal thickness and  $\Delta H_m$  the heat of fusion.<sup>164</sup>

### 1.2.3 Secondary nucleation

After the formation of the first nuclei the crystallite will grow further by depositing new stems on the previously formed surfaces. How the crystal growth proceeds exactly can be explained by two different models. The “fringed micelle“ model was postulated by Hermann, Gerngross and Abitz in 1930.<sup>165,166</sup> This model assumes that parts of the polymer chains disentangle, align and form bundled crystalline stems within an amorphous surrounding as depicted in Figure 13.

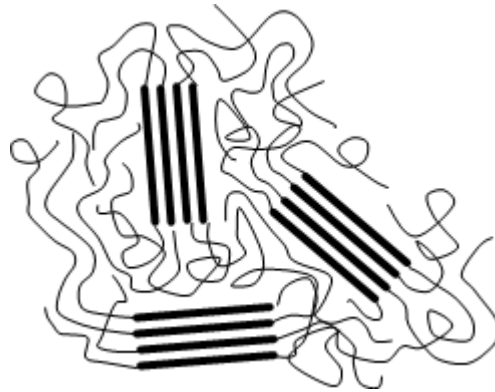


**Figure 13:** Schematic picture of the fringed micelle model.<sup>141,167</sup>

These crystallites could act as cross-linkers whereby the polymer shows properties of reinforced rubbers as well as the elasticity and low density of polyethylenes could be explained assuming this model. Nevertheless, the formation of such fiber-like crystallites seems to be very difficult just via thermal fluctuations and the occurrence of spherulites in optical microscopy cannot be explained using the fringed micelle model.<sup>141,151</sup>

Due to the inconsistencies and further experiments and calculations<sup>168</sup> this theory was replaced with the so called “folded chain” model, which was mentioned for the first time by Storks in 1938.<sup>169</sup> He assumed, that the polymer chain must fold back and forth in the polymer crystals due to its length, which exceeds the size of one crystal lamella. Twenty years later this theory was confirmed by Keller and other groups via crystallographic analysis of polyethylene single crystals and is generally accepted until today.<sup>143-145,170,171</sup> Although, the adoption of a folded conformation seems to be energetically adverse, it is surely the most logical option. In solution a completely extended polymer chain would exhibit the largest possible surface and thus, the minimal conformational entropy. Via folding into a lamella this chain adopts the smallest possible conformation and is consequently in a thermodynamic stable state, which was also demonstrated by different experiments.<sup>141,172-177</sup> Equally, in the melt thermodynamic and kinetic factors suggest the adoption of a folded conformation than the formation of an extended chain crystal as estimated by several research groups.<sup>141,178-180</sup>

The mechanism of chain folding can be described with different models, which are summarized in Figure 14.

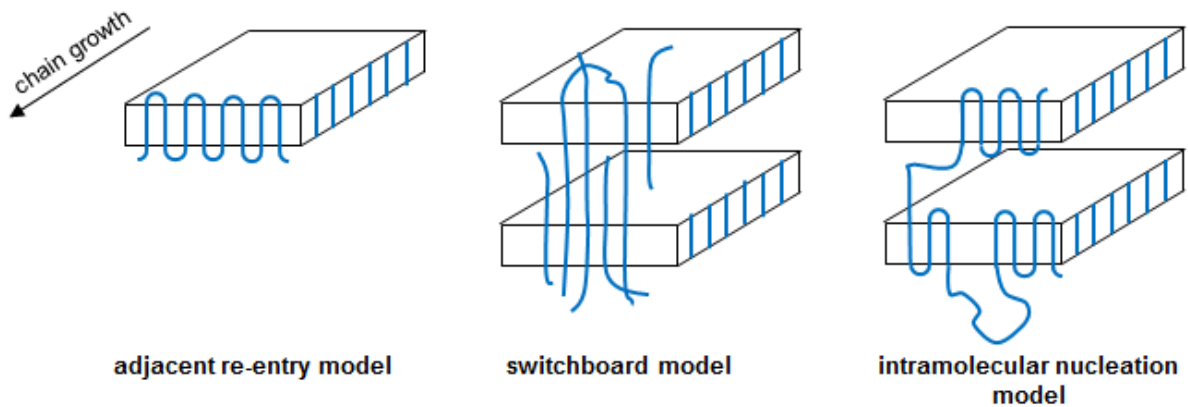


**Figure 14:** Different mechanisms of chain folding: adjacent re-entry model, switchboard model and intramolecular nucleation model.<sup>141,151</sup>

Firstly, one polymer chain can exit and re-enter just one single crystallite, whereby only small amorphous regions will be formed at the end of the lamella. This adjacent re-entry model was postulated by Hoffman and colleagues in 1979.<sup>181</sup> Another assumption is the switchboard model from Flory, which implies the participation of one polymer chain in different lamella acting as tie molecule or the non-adjacent re-entry into the crystallite leading to the formation of amorphous loops.<sup>168</sup> The intramolecular nucleation model represents a revision of the switchboard model, which includes the possibility of adjacent re-entries.<sup>141,182,183</sup>

Now that these basic details have been clarified, the next chapter will focus on the description of the most popular secondary nucleation theory. This theory is of kinetic nature, whereby the difference in free energy between the amorphous and crystalline state below the equilibrium melting temperature acts as driving force.<sup>141</sup>

### 1.2.3.1 Hofmann-Lauritzen theory

The Hofmann-Lauritzen theory, which was first presented in 1960 by John Hofmann and John Lauritzen is probably the most known and widespread secondary nucleation theory.<sup>133,161,184,185</sup>

This theory involves simplifications and assumptions to impart the mechanism of polymer crystal growth and corresponding kinetics vividly. A graphical description of the theory is shown in Figure 15.

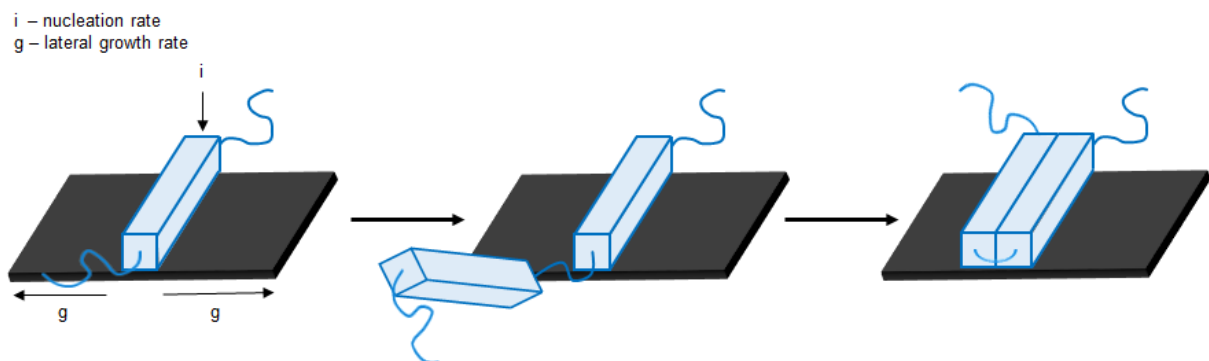


**Figure 15:** Graphical representation of the Hofmann-Lauritzen theory, whereby  $i$  stands for the nucleation rate and  $g$  for the lateral growth rate.<sup>141</sup>

For the sake of simplicity a single stem with a smooth surface, which was formed during primary nucleation via random fluctuation was assumed to serve as critical nucleus. Subsequently, further stems, one at a time, are being deposit on the existing growth front until a new surface is formed on which the next nucleation event can take place.<sup>141,151,155,186</sup> The crystal growth rate can be estimated and its calculation depends on the chosen crystallization temperature and thus the corresponding growth regime (see Figure 16).

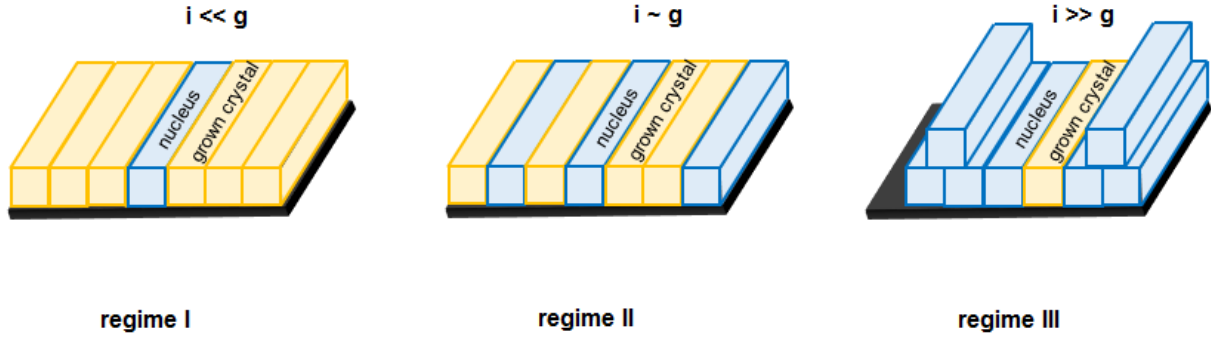


**Figure 16:** Illustration of the three different growth regimes during secondary nucleation.<sup>142,155,186</sup>

Considering only a small supercooling (see eq. 6), meaning a crystallization temperature close to the melting temperature, the system will be located in regime I,<sup>161,185,187,188</sup> where the nucleation proceeds much slower than the lateral spreading. In other words, after the formation of the nucleus the next stems will be deposit very quickly until a new smooth surface is formed on which the next nucleation event can take place. Hence, the growth rate is limited by the nucleation rate and can be calculated with the equation given below

$$G_I = ibL_p \quad (11)$$

where  $i$  is the surface nucleation rate,  $b$  is the thickness of on molecular chain stem and  $L_p$  is called the “persistence length”.<sup>141,186</sup>

If the crystallization temperature is located below the melting temperature, nucleation rate equals the lateral spreading rate, resulting in the existence of more than one nucleus at the same time. If a new nucleus can be formed before the previous layer is filled completely the system is located in regime II<sup>185,187,189</sup> and the corresponding growth rate can be calculated as follows

$$G_{II} = b\sqrt{ig} \quad (12)$$

where  $g$  stands for the lateral growth rate.<sup>141,186</sup>

Regime III<sup>185,190</sup> is characterized by a very high supercooling, where the nucleation proceeds much faster than the lateral spreading. Thus, so many nucleation events take place at the same time that the lateral spreading rate becomes physically irrelevant and the growth rate is calculated as for regime I with the following equation

$$G_{III} = ibL_p \quad (13)$$

With the help of these considerations the lamellar crystal thickness as well as the crystal growth kinetics can be predicted.<sup>141,186</sup>

As mentioned previously this theory contains certain simplifications as for example assuming the critical nucleus to be a complete crystal stem. Therefore, this model was revised by Frank and Tosi in 1961<sup>191</sup> who described that the crystal growth proceeds by addition of single subunits, one at a time. These units are subjected to fluctuations meaning, that in each step a unit can either be attached or removed from the growing stem along the vertical direction as shown in Figure 17. Therefore, the polymer chain can only fold to start a new lamella if the length of attached subunits equals the lamellar crystal thickness. This process is also called “fine grained model”.

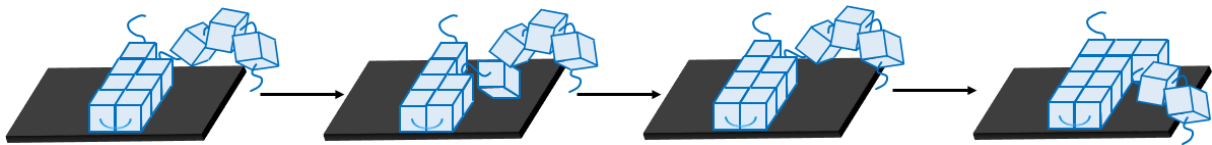


**Figure 17:** Graphical description of the fine grained model.<sup>141</sup>

Furthermore, this model was expanded by Jean-Jacques Point who assumed that chain folding can happen at each step during crystal growth even if the lamellar crystal thickness is not reached yet.<sup>192,193</sup> However, the crystal can only grow further if this defect is removed and the following units are attached in direction of the lamellar thickness. Figure 18 represents this hypothesis graphically.

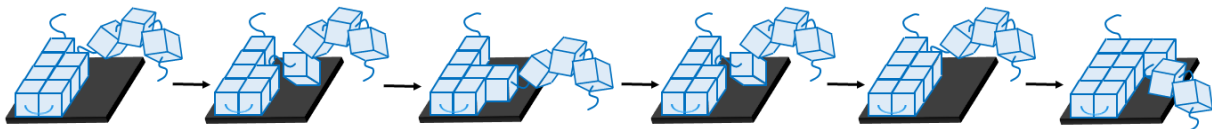


**Figure 18:** Schematic representation of the modified Hoffman-Lauritzen theory postulated by Point.<sup>141</sup>

## 1.3 Crystallization under confinements

### 1.3.1 External confinements

The crystallization process as well as the resulting crystal structure of polymers can be influenced by different constraints, which can either be exerted from the “outside” (e.g. geometrical confinement) or the “inside” (incorporation of defects into the polymer chain) on the polymeric system.

Restricting the space in the size range of micrometers to nanometers, similar to the size of lamellar crystals, represents the simplest variant to exert an external constraint onto the polymer. Therefore, the bulk polymer is divided into smaller fractions, which are also termed as microdomains.<sup>194</sup>

One example for such microdomains are polymer droplets. The polymer to be examined is spin-coated onto a non-interacting, immiscible support, followed by heating the sample above the melting point of the polymer, leading to dewetting and the formation of polymer droplets.<sup>195-197</sup> Furthermore these droplets can also be prepared via inkjet printing<sup>198</sup>, aqueous dispersions or

mini-emulsion polymerizations.<sup>199,200</sup> As the nucleation mechanism is changing from heterogeneous to homogeneous, assuming that no impurities are contained in the droplets, the crystallization takes place at lower temperatures compared to the bulk polymer.<sup>194</sup> The nucleation is initiated by either fluctuations due to Brownian motion or the surface on which the droplet is located, leading to a dependence on the roughness of the surface, meaning the smoother the surface, the lower the crystallization temperature.<sup>196</sup> Equally, the crystallization behavior is influenced by the volume and the thickness of the polymer droplet. Whereas droplets with a thickness of 2-3 nm mostly contain only one nucleus, resulting in a slow crystal growth, thicker droplets (3.5-5 nm) promote the formation of several nuclei leading to enhanced growth rates.<sup>194,197</sup>

Another possibility to restrict the space is the formation of thin polymer films, whereby not only the nucleation and the crystal growth but also the orientation of the crystallites is influenced as the crystallization is confined to just one dimension.<sup>194</sup> The glass transition as well as the crystallization temperature conform to the particular position of the polymer chain within the film. Chains in contact to the surface are restricted in mobility thus exhibiting higher glass transition temperatures and along with the highest nucleation rate higher crystallization temperatures are ensued.<sup>194</sup> The crystallites can be oriented parallel to the substrate in the case of films thicker than 100 nm. Decreasing the film thickness leads to the parallel or perpendicular arrangement of the crystalline lamella.<sup>194,201</sup>

In solution some polymers, predominantly amphiphilic compounds, form crystallizable nanoparticles or micelles.<sup>194</sup> One of the most widely studied examples is polyethylene, forming nanoparticles in diluted solutions consisting of exactly one polymer chain.<sup>173,194,202</sup> During crystallization this chain arranges into one single crystalline lamella, which is surrounded by amorphous material at both ends. This nanoparticle, colloquially called “nanohamburger”, exhibits an enormously low crystallization temperature, indicating a homogeneous nucleation.<sup>173</sup> Both, the crystallization behavior and the crystal structure are influenced by the molecular weight of the polymer and the chosen solvent.<sup>194,202</sup>

The insertion of polymers into inorganic and organic materials represents another possibility of an external confinement.<sup>194</sup> Thus, great attention was paid to the investigation of polymer crystallization in anodic aluminum oxide nanopores.<sup>203,204</sup> In these pores predominantly surface nucleation takes place and the crystallization as well as the melting temperature are directly proportional to the pore diameter. The crystallites will be oriented parallel to the pore axis if the pore exhibits a small diameter, whereas the lamella in pores with bigger diameters will be arranged perpendicular.<sup>204</sup>

Blending two immiscible polymers leads to the dispersion of the crystallizable compound (provided that it is added in small amounts) in a polymeric matrix.<sup>194</sup> The crystallization temperature now depends on the number of impurities contained in the single polymer droplets. No or only few impurities in the dispersed material cause homogeneous or surface nucleation taking place at very low crystallization temperatures.<sup>194</sup> If the amount of impurities lies in the same order of magnitude as the amount of microdomains, each nucleation event is triggered by a different heterogeneity, leading to the occurrence of fractionated crystallization.<sup>194</sup>

Block copolymers represent a special form of polymer blends, whereby the final morphology of the crystal is determined by the segregation strength between the two blocks as well as by the order-disorder transition temperature, the glass transition of the amorphous part and the crystallization temperature of the crystallizable polymer.<sup>194,205,206</sup> Based on the Flory-Huggins interaction parameter and the volume fractions of the polymers different morphologies (cubic, lamellar, etc.) can be adopted by the block copolymer. Depending on the above mentioned parameters this morphology is either preserved during crystallization or disrupted due to breakout crystallization leading to the formation of a crystalline lamella, which is surrounded by amorphous material.<sup>194</sup>

### 1.3.2 Internal confinements

By exertion of internal confinements on the crystallization behavior and the resultant crystal structure via incorporation of defects into the polymer chain a material with tuned properties can be produced. Popular examples are linear low-density polyethylene (LLDPE), high-density polyethylene (HDPE) etc., which obtain their enhanced thermal and mechanical properties via short-chain (SCB) or long-chain branching (LCB). Due to their industrial importance it is necessary to understand the structure-property relationship of these materials<sup>207</sup>. Unfortunately, their crystallization behavior as well as the final morphologies could not be elucidated completely up to now as X-ray diffraction measurements and other methods for structural investigation show no clear signals due to the random distribution of the defects within the polymer backbone.<sup>89</sup> Here, the ADMET polymerization, which was already dealt with in chapter 1.1.3.2, represented a revolution. Thus, polyethylene with a wide variety of exactly placed side-chains could be synthesized and used to improve the comprehension of the structure-property relationship. In contrast to their random analogues these precision polymers exhibit higher crystallinities due to highly ordered systems, leading to enhanced thermal properties, whereby they are characterized by narrower and sharper melting endotherms at lower temperatures in DSC<sup>68</sup>. Furthermore, they show a narrower lamellar thickness distribution.

#### 1.3.2.1 Side-chain defects

##### *Alkyl branches*

The probably simplest precision polymers contain a methyl side chain in defined distances along the polymer backbone. Placing this group on every 5<sup>th</sup> or 7<sup>th</sup> carbon yields totally amorphous polymers<sup>208</sup>. Extending the methylene spacer length between these defects to at least eight carbon atoms leads to the formation of hexagonal crystals<sup>209</sup>, which feature a typical initial stage during the crystallization of polyethylene. In pure polyethylene the chains slide past each other after the formation of a metastable hexagonal mesophase devolving into an all-*trans* configuration until the equilibrium lamellar crystal thickness is reached followed by the transformation into a stable orthorhombic phase<sup>207,210-212</sup>. As this structure is not formed here the inclusion of the methyl groups into the crystalline phase can be assumed causing the



disturbance of the unit cell. If the methyl group is placed on every 15<sup>th</sup> carbon, it is also included and a triclinic crystal structure is formed in which the alkyl chains between the defects adopt a hexagonal sublattice.<sup>89,102,213</sup> Equally, the defect is included if it is placed on every 21<sup>st</sup> carbon and the appropriate polymer exhibits a monoclinic structure.<sup>102,213,214</sup> A schematic depiction of the crystal structure with included methyl defects is shown in Figure 21. Even if the methylene spacer length is expanded to 38 carbon atoms the methyl group is continuously included in the crystalline phase. A particular feature here is the formation of two different crystal structures, a dominant orthorhombic phase and a metastable monoclinic one. This example shows, that the reduction of branch frequency leads to less disturbance of the unit cell<sup>102</sup>, whereby the orthorhombic phase of polyethylene is preserved, accompanying only with an expansion of the unit cell. Figure 19 schematically shows the crystal structures adopted by methyl-branched polyethylene in dependence of the methylene spacer length.

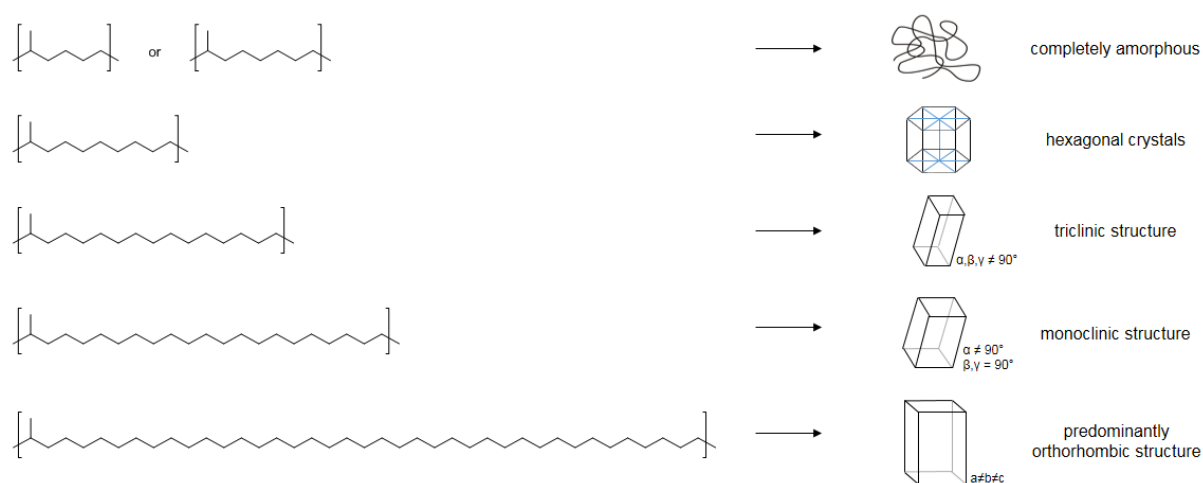


**Figure 19:** Formation of different crystal structures of methyl-branched polyethylene in dependence of the methylene spacer length.

Expanding this defect to a gem-dimethyl group and placing it on every 9<sup>th</sup> carbon atom leads to a complete amorphous polymer due to the increased space requirement of the defect.<sup>71,102</sup> Only the placement on every 15<sup>th</sup> or 21<sup>st</sup> carbon ensures the formation of a semi-crystalline structure exhibiting a polymorphic character.<sup>71,102,214</sup> Continuing the analog series, an ethyl group is the next examined defect. Placing it on every 9<sup>th</sup> carbon the appropriate polymer as well is completely amorphous<sup>102</sup> and shows only semi-crystalline behavior after the methylene spacer length is expanded to 14 carbon atoms.<sup>71,215</sup> This polymer exhibits a bimodal melting behavior in the DSC, indicating the partial inclusion of the ethyl group into the crystal. Thus some crystallites contain ethyl groups and some not, resulting in polymorphism.<sup>71</sup> Of course, the final morphology of the crystal also depends on the crystallization temperature, which is explicitly demonstrated by the precision polymer bearing an ethyl group on every 21<sup>st</sup> backbone carbon as schematically shown in Figure 20.<sup>102,212,214-218</sup> Crystallizing this polymer at 5-8 °C very small crystalline lamella are formed, expelling the defect into the amorphous region. Increasing the temperature to 10-15 °C leads to the formation of a hexagonal mesophase, which can thin or thicken, resulting in the inclusion of none or one ethyl group, whereby lamella with two different thicknesses are obtained.<sup>212,214-216</sup> The inclusion of exactly one ethyl group per

crystalline lamella is reached at a crystallization temperature of 17 °C. At elevated crystallization temperatures between 21 °C and 28 °C no hexagonal phase is formed anymore as it is destabilized due to the inclusion of two defects per lamella, resulting in the formation of triclinic spherulites.<sup>207,212,214-216</sup>

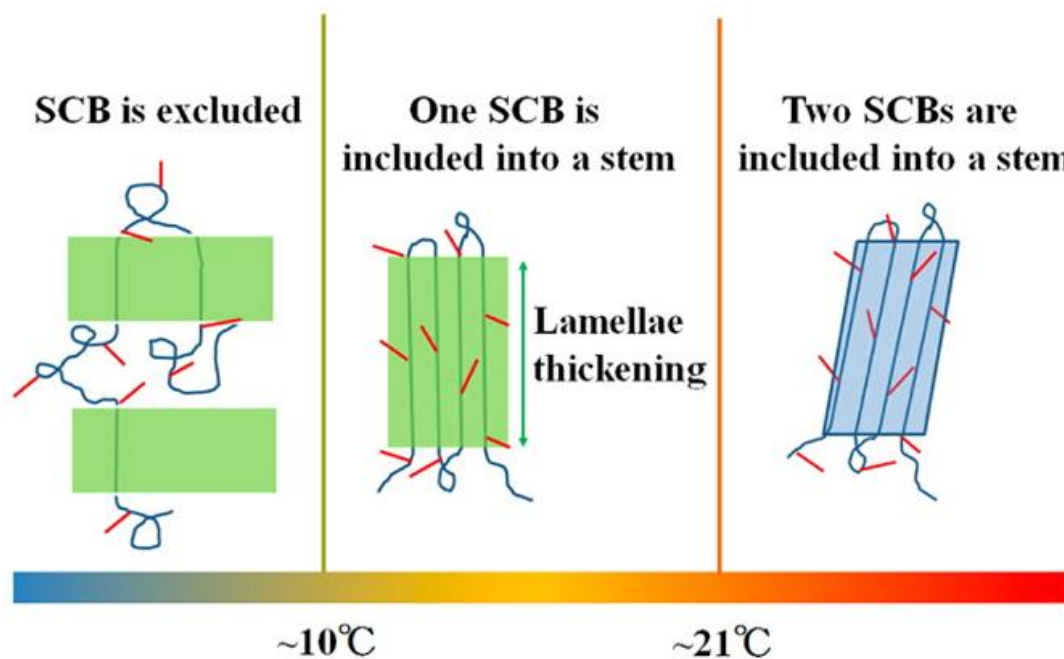


**Figure 20:** Schematic model of branch inclusion in precision polyethylene bearing an ethyl group on every 21<sup>st</sup> carbon at various crystallization temperatures. Reprinted with permission from reference<sup>212</sup>. Copyright 2013, American Chemical Society.

Placing this ethyl group on every 39<sup>th</sup> carbon atom leads to the exclusion of the defect from the crystalline phase, as the polymer chain between the defects shows a sufficient long run length to pack into a crystallite, expelling the side group into the fold and thus the amorphous phase. Further series of studies focused on the examination of the relationship between crystal structure and increasing defect size.<sup>219,220</sup> Thus, precision polymers bearing branches of various lengths (ranging from methyl to pentadecyl groups<sup>220</sup>) and size (*iso*-propyl, *sec*-butyl, *tert*-butyl, cyclohexyl and adamantyl groups<sup>219</sup>) as defects on every 21<sup>st</sup> carbon were synthesized. It was found, that all polymers with defects exceeding the size of an ethyl group exhibit similar melting temperatures and wide-angle X-ray scattering (WAXS) patterns<sup>89,219,220</sup>, indicative of an exclusion of the defect from the crystalline phase. Same behavior is observed at a methylene spacer length of 38 carbons, just that here also the ethyl group is excluded from the crystalline phase.<sup>220</sup> The melting temperatures of these polymers lie much closer together and the crystallographic analysis indicates a mixture of a predominantly orthorhombic and a small amount of monoclinic crystals. This is due to the fact, that the excluded groups agglomerate at the folding surface of the crystal, leading to a packing problem, which causes a shear of the unit cell, whereby a metastable phase is formed.<sup>219-221</sup>

This impact vanishes with a methylene spacer length of 74 carbon atoms as demonstrated for precision polymers bearing a butyl group on every 75<sup>th</sup> carbon. Here, the polymer shows a perfect orthorhombic unit cell comparable to pure ADMET polyethylene<sup>207,222</sup>. Another specialty occurs if the length of the branch exceeds the length of ten carbon atoms enabling the

defect to co-crystallize observed for precision polyethylene with a heneicosanyl branch on every 15<sup>th</sup> or 19<sup>th</sup> backbone carbon.<sup>223,224</sup> These polymers exhibit narrower melting profiles and higher melting temperatures compared to their butyl branched analogues. Both polymers crystallize in a hexagonal phase and show two melting points in the DSC, indicative of two lamella with different thicknesses.<sup>223</sup> Transmission electron microscopy (TEM) reveals the existence of thin lamella if the methylene spacer length accounts to 15 carbons and thick lamella for the polymer with defects on every 19<sup>th</sup> carbon. In the case of the thin lamella the side chains crystallize separately from the backbone, whereas the thick lamella are formed due to the co-crystallization of backbone and branches.<sup>223</sup> The side chain crystallization occurs if the branch exceeds the size of the methylene spacer length, whereas the co-crystallization dominates if the branch exhibits the same size as the spacer.<sup>223</sup>

Even amphiphilic branches, consisting of tetraethylene glycol (TEG) as hydrophilic part and a pyrene, hexyl or tetradecyl group as hydrophobic part can be included as defect into the polymer backbone as proven by Wagener and coworkers.<sup>217</sup> These polymers behave contrary to the trend of other ADMET polymers, showing that increasing the size of the hydrophobic part has a tremendous influence on the polymer morphology.<sup>71,217</sup> Using pyrene as graft end-group excludes the defects from the crystalline phase followed by their aggregation in the amorphous interphase. Amphiphilic branches containing hexyl groups as hydrophobic part are also expelled from the crystal but co-crystallize, leading to the formation of two separate crystalline regions, indicated by two different melting endotherms in the DSC. Expanding the hydrophobic part results in the inclusion of the defect into the crystalline phase, where it co-crystallizes together with the backbone resulting in only one melting endotherm.<sup>71,217</sup>

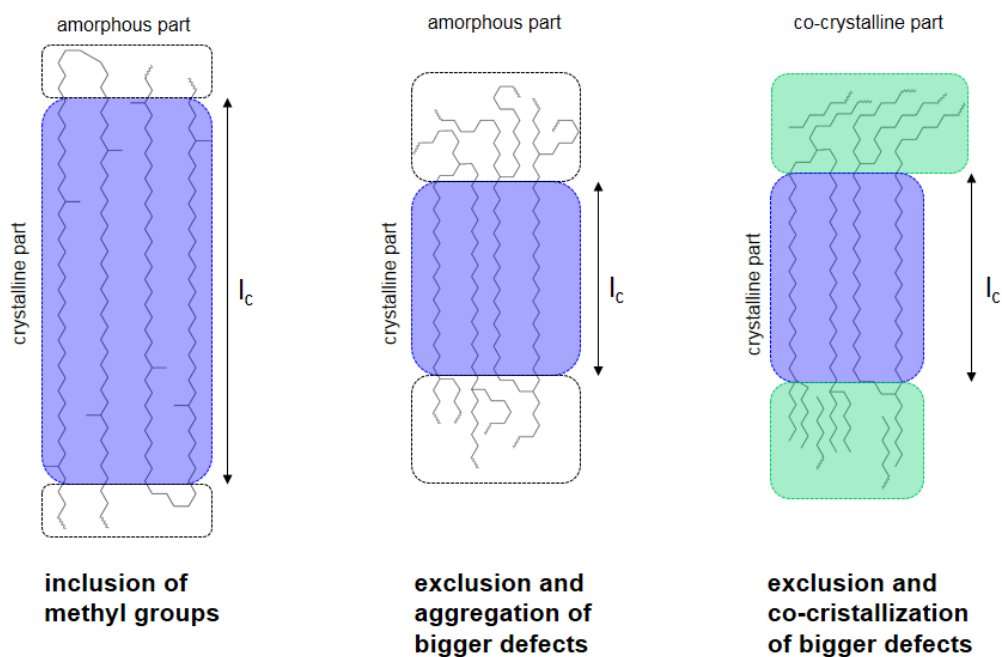


**Figure 21:** Graphic depiction of the crystallization behavior of precision polymers bearing different sized alkyl branch defects.

In summary it can be said that the crystal structure of polyethylene is significantly influenced by the introduction of alkyl branches to exactly defined points within the polymer backbone.

Placing the branches on every 7<sup>th</sup> carbon or less results in completely amorphous polymers as the defects disrupt the order in the polyethylene unit cell<sup>68</sup>. Increasing the methylene spacer length leads to the formation of semi-crystalline crystal structures, whereby small defects as methyl or ethyl groups can be included into the crystalline phase. Bigger defects are excluded from the crystal and expelled to the amorphous phase where they can agglomerate or even co-crystallize causing a packing problem in the crystal lattice (see Figure 21). These polymers exhibit approximately similar melting points, whereby a lower branch frequency leads to increasing melting temperatures and melting enthalpies. Amphiphilic branches, where an increase of branch size results in the inclusion of the defect in the crystalline phase, occur as exceptions.

### *Halogen atoms*

Since small alkyl groups can be included into the crystalline phase as mentioned earlier there is a hypothesis that also other sterically not demanding groups can be incorporated into the crystal. This assumption could be proven with the help of precision polymers bearing precisely placed halogens (fluorine, chlorine and bromine) along the polymer backbone.<sup>68,225</sup> These precision halogenated polyolefins also follow the trend of increasing melting temperature as well as melting enthalpy with decreasing defect size and branch frequency.<sup>225-227</sup> The incorporation of fluorine atoms into the crystalline phase of polyethylene lead, due to the small defect size, to the minimal expansion of the unit cell, whereby the orthorhombic crystal structure is not disturbed that much<sup>68,71,225,226,228</sup>. Replacing fluorine by chlorine also lead to defect inclusion, but also to a decrease of melting temperature and the change from orthorhombic to triclinic crystal structure<sup>68</sup>, due to the increase in space requirement.<sup>71,223,225-227,229,230</sup> Which morphology is being developed strongly depends on the crystallization temperature and the size of the first formed nucleus. Cooling the polymer melt rapidly leads to the formation of a nucleus, whose critical stem length is shorter than the alkyl chain between the defects.<sup>230</sup>

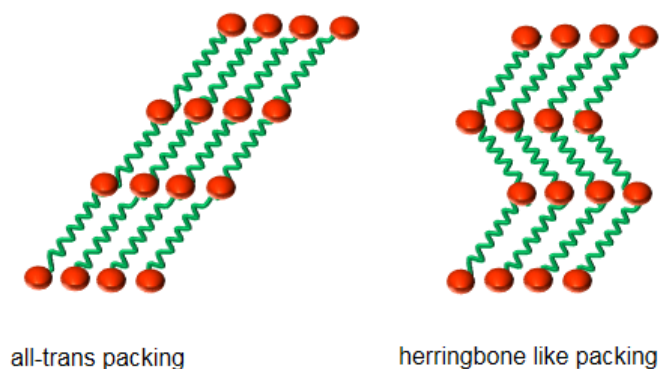


**Figure 22:** Schematic representation of the crystal morphologies adopted by precision halogenated polyolefins. Figure reprinted and adapted with permission from reference<sup>230</sup>. Copyright 2014, American Chemical Society.

Thus, the crystal grows by stacking the backbone via van-der-Waals interactions, prevailing between the methylene units, leading to the formation of an *all-trans* morphology as visualized in Figure 22.<sup>225</sup> Using slow cooling rates result in a critical stem length which is the same size

or bigger than the methylene spacer length, whereby the chlorine atoms are being packed densely leading to the formation of a herringbone-like structure with the defects located in the kinks of the chain as shown in Figure 22.<sup>230</sup> In both cases a layered chlorine distribution can be observed, whereby the respective polymers exhibit lamellar morphologies.<sup>225,230</sup> The inclusion of the defect as well as the triclinic crystal structure is being preserved when using the sterically more demanding bromine atom<sup>68</sup> causing only a decrease in melting temperature and melting enthalpy.<sup>71,226,231</sup> Based on the crystallization temperature here as well several different crystalline modifications can be observed. Fast cooling of the polymer melt leads to an all-*trans* conformation of the polymer chains in which the bromine atoms are packed in layers, but shifted in height to the adjacent chain.<sup>225,231</sup> At room temperature this conformation is converted fast to the next modification also exhibiting a fully extended all-*trans* conformation in which the bromine atoms of adjacent chains are arranged at the same height.<sup>231</sup> However, cooling the polymer melt slowly results in the formation of a herringbone-like structure, comparable to the structure of chlorine substituted polyethylenes, whereby the bromine atoms are located in the kinks of the polymer chain as visualized in Figure 22. These modifications can be irreversibly transformed into each other by heating or stretching.<sup>225,231</sup>

### *Supramolecular defects*

It is also interesting to find out how the morphology of polyethylene is changed, if the defects are able to interact with each other via supramolecular interactions. Incorporating a hydroxyl group into the polymer backbone serves as simplest example for a supramolecular defect. This group, regardless of the methylene spacer length, is excluded from the crystalline phase and forms a channel-like hydrogen bonding network stabilizing the amorphous phase as shown in Figure 23, resulting in high polymer melting temperatures in the region of about 100 °C<sup>73,232</sup>. Due to the exclusion of the functional group from the crystalline phase, the orthorhombic crystal structure of polyethylene is preserved.

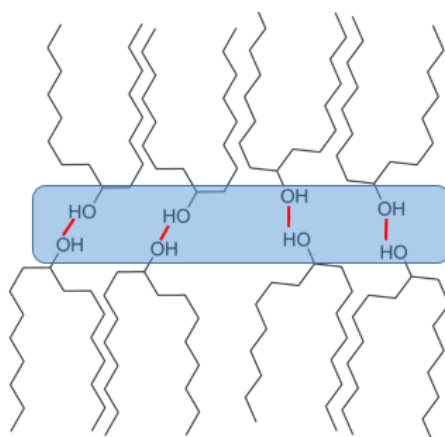


**Figure 23:** Hydrogen channels formed by precision polymer bearing precisely placed hydroxyl groups.

A similar behavior is observed for precision polymers, bearing a carboxylic acid group on every 21<sup>st</sup> carbon. These defects are also excluded from the orthorhombic crystal lattice<sup>89</sup> and form dimers<sup>71,207</sup>, that are arranged perpendicular to the polymer chain<sup>99</sup>, via hydrogen bonding in the amorphous phase resulting in acid-rich layers between the crystal lamella observable via X-

ray diffraction.<sup>87,99,233</sup> Increasing the acid content also increases the number of hydrogen bonds and the interactions between the groups become so strong that they act as physical crosslinks, which restrict the mobility of the polymer chains<sup>207</sup>, whereby the formation a crystal lamella is hindered resulting in completely amorphous polymers<sup>71,220</sup>. The interactions between two acid moieties are so strong, that they even persist above the melting temperature of the polymer<sup>89</sup>. In solution the precision polymers with polar defects form self-stabilized nanocrystals in which the functional groups are located at the upper and lower surface of the crystalline lamella and their lamella thickness is dictated by the length of the methylene spacer<sup>99,172</sup> as schematically shown in Figure 24.

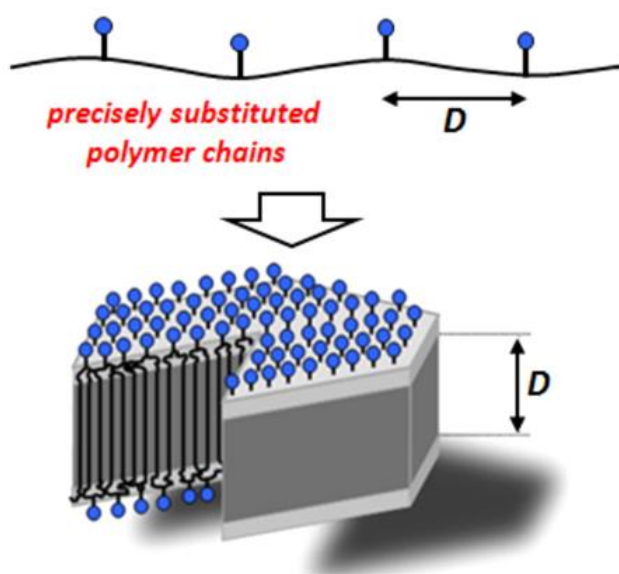


**Figure 24:** Schematic representation of carboxy-substituted precision polyethylene forming self-stabilized nanocrystals in solution. Reprinted with permission from reference<sup>172</sup>. Copyright 2013, American Chemical Society.

By addition of metal salts these precision polymers can be converted into precision ionomers, which self-assemble into ionic clusters<sup>89,207,234</sup> via electrostatic interactions resulting in the adoption of a cubic lattice<sup>233-236</sup>. Here again the methylene spacer length influences the ability to form crystals as shown for 1-methylimidazolium bromide containing precision polymers, which exhibit completely amorphous polymers if the ion content is too high.<sup>237</sup>

Increasing the number of hydrogen bonds per monomer unit by using phosphonic<sup>100,238,239</sup> or sulfonic<sup>240,241</sup> acids, which are also excluded from the crystalline phase<sup>71</sup>, result in the formation of acid-rich layers between the crystal lamella, which are oriented perpendicular to the polymer chain. The final morphology is still influenced by the crystallization of polyethylene, whereby the big aggregates consisting of acid groups are located at the surface of the crystalline lamella and induce packing problems in the crystal lattice.<sup>71,100,239</sup>

However, not only hydrogen bonding but also other supramolecular interactions like  $\pi$ - $\pi$ -stacking can have an influence on the morphology of polyethylene as observed for boronic acids<sup>242</sup> and phenyl rings incorporated as defects into precision polymers. The sterically demanding rings cause an extreme melting point depression and the formation of two melting

endotherms, whereby one of these endotherms can be traced back to the aggregates, which are formed by stacking of the defects via  $\pi$ - $\pi$ -interactions in the amorphous part.<sup>243</sup>

### 1.3.2.2 In-chain defects

Besides the possibility to introduce functionalities in precision polyethylene via side chains it is also possible to include the functional group directly into the polymer backbone. In this area not that much research as in the case of side-chain functionalities was carried out up to now, but nevertheless first results, which allow conclusions on the relationship between defect size or structure, respectively and the polymer morphology, could be achieved.

#### *Polar defects*

Initially, precision polymers bearing polar defects like polyacetals, polyketones, polycarbonates and polyesters were analyzed.<sup>244-246</sup> These defects disrupt the crystal structure of polyethylene thus causing decreased melting temperatures and crystallinities, whereby the melting point is still higher compared to precision polymers with side-chain defects due to strong polarities.<sup>244,245</sup> Polyacetals with a small acetal content exhibit an orthorhombic crystal structure with defects included into the crystalline lamella. By increasing the defect concentration heterogeneous crystalline morphologies are formed due to the *gauche* conformation of the defect (induced by the anomeric effect), which is incompatible with the all-*trans* conformation of polyethylene.<sup>246</sup> The use of ketone-defects has hardly any influence on the crystal structure and melting temperature of polyethylene<sup>247</sup>, as these are, due to their size (similar to a methyl group), incorporated into the crystal resulting in an orthorhombic crystal lattice.<sup>245</sup> Polycarbonates as well as polyesters are also included into the crystalline phase creating polar layers via dipol-dipol interactions<sup>244</sup>, which reduce the disturbing effect on the crystallization of polyethylene. The more polar these groups are the better they form these layers and thus less disturb the orthorhombic crystal structure.<sup>244,245</sup> Therefore, in contrast to polyesters more nonpolar polycarbonates show lower melting temperatures.

Also initial examinations on precision polymers with sterically demanding oxidized phosphorous functionalities, which can be found in polyphosphoesters<sup>248,249</sup> (e.g. polyphosphonates<sup>250-252</sup> or polyphosphoamidates<sup>253,254</sup>), were carried out. Up to now it can be declared that, no matter how these defects are linked to the polymer chain, they are excluded from the crystalline phase and self-assemble into clusters via dipol-dipol interactions.<sup>164</sup> A layer-like morphology is formed, whereby crystalline lamella alternate with cluster containing layers (as visualized in Figure 25), the latter disturbing the packing of the crystal resulting in a pseudo-hexagonal crystal structure.<sup>164,250</sup> The melting temperatures of these precision polymers decrease with both increasing number of defects and increased steric demand of substituents (e.g. phenyl rings).<sup>164,248</sup> A similar behavior is observed for oxidized sulphur functionalities like sulfites<sup>255</sup> or sulfonate esters<sup>256</sup>. Here as well, clusters that are segregated from the crystalline phase are formed due to polar interactions, causing the disturbance of the methylene sequence, whereby a mixture of monoclinic and orthorhombic crystal structures is obtained.<sup>255</sup> Precision polymers bearing sulfone defects occupy a special position as they are the only polymers

exhibiting melting temperatures higher than that of pure ADMET polyethylene.<sup>257</sup> Contrary to the trend for precision polymers synthesized via ADMET polymerization, their melting temperatures and melting enthalpies increase with increasing defect concentration. It is assumed, that this behavior can be ascribed to the small size and the geometry of the SO<sub>2</sub> group, which is comparable to that of a CH<sub>2</sub> group.<sup>257</sup> Furthermore, these moieties are able to form hydrogen bonds with adjacent chains increasing the thermal stability of these polymers. Nevertheless, the defects disrupt the formation of an orthorhombic crystal structure resulting in polymorphism.<sup>257</sup>

### Supramolecular defects

Moreover, also hydrogen bonding motifs like amides<sup>258</sup> or amino acids<sup>259</sup> can be incorporated into the polymer backbone. Precision polymers bearing on average between one and fifty amide groups per 1000 methylene units occupy a special position between polyethylene and commercial polyamides. Usually, polyamides possess a high temperature stability due to hydrogen bonds between adjacent polymer chains. By reducing the amide content drastically, these polyamides adopt a polyethylene-like orthorhombic crystal structure, whose melting temperatures lie below those of pure ADMET polyethylene.<sup>258</sup> With increasing amide content the hydrogen bonding dominates the van-der-Waals interactions of the hydrocarbon chains<sup>73</sup>, whereby the crystal lattice of polyethylene is disturbed and no orthorhombic structure can be formed anymore.<sup>258</sup> The incorporation of polar amino acids (e.g. glutamic acid or aspartic acid) into the polymer backbone also yields semi-crystalline polymers with either included or excluded defects, leading to the formation of a mixture of orthorhombic and monoclinic crystal structures.<sup>259</sup>

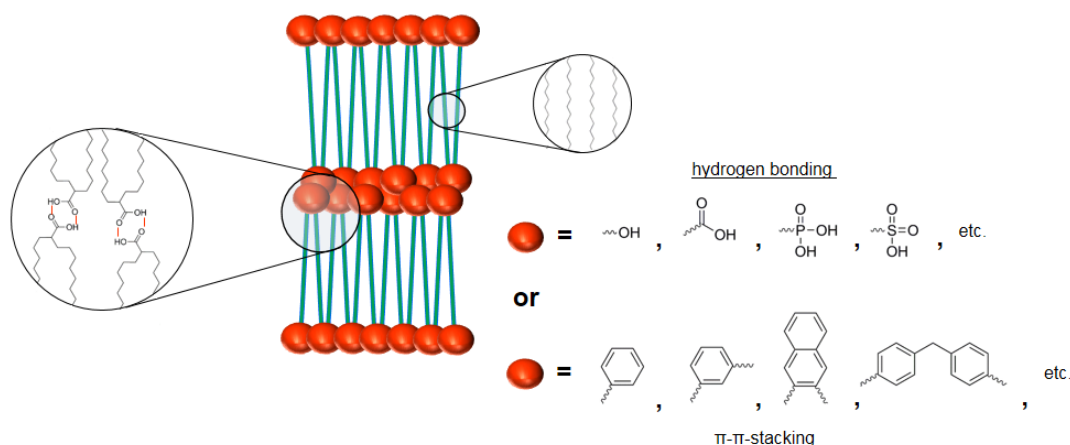


**Figure 25:** Schematic representation of the formation of defect-rich layers between crystal lamella due to dipole-dipole or supramolecular interactions exerted by different excluded defects.

Also polymers bearing aliphatic or aromatic ring defects could already be synthesized and analyzed.<sup>260</sup> Aliphatic cycles, e.g. cyclohexylene, exhibit a non-planar, flexible structure and can be present as *cis*- or *trans*-isomer.<sup>261</sup> Defects possessing a *cis*-conformation lead to the formation of kinks in the polymer chain and are being excluded from the orthorhombic crystalline phase during the crystallization, whereas *trans*-isomers are included into the crystalline phase due to their suitable conformation, leading to a mixture of orthorhombic and



other coexisting crystal structures.<sup>260,261</sup> If the defect consists of two cycles (e.g. a 4,4'-bicyclohexandioxy group) it can adopt three different conformations, namely *trans-trans*, *cis-trans* or *cis-cis*, whereby only the structurally favorable *trans-trans* conformation will be included into the crystal forming a disrupted orthorhombic structure, also observed for precision polymers bearing two cycles that are linked via an unsubstituted methylene bridge.<sup>260</sup> Placing methyl or phenyl substituents on the methylene bridge leads to the exclusion of the defects due to the increased steric demand followed by their agglomeration in the amorphous phase, whereby they disrupt the packing of the alkyl sequences resulting in a triclinic crystal structure.<sup>260</sup>

Conversely, aromatic rings possess, due to their double bonds, a planar, rigid structure, which can hinder the crystallization of the polymer via  $\pi$ - $\pi$ -stacking<sup>262</sup>, if the distance between the defects is too small (less than eight methylene units)<sup>75</sup>, resulting in cluster formation.<sup>262</sup> Increasing the methylene spacer length produces semi-crystalline polymers with melting points lower than that of pure ADMET polyethylene in which the inclusion or exclusion of the defects from the crystalline phase is dictated by the disubstitution position of the ring as schematically shown in Figure 26.<sup>263</sup> *Ortho*-substituted aromatic rings exhibit an appropriate conformation for mimicking a chain fold, whereby they are excluded into the amorphous phase where they form stacks via  $\pi$ - $\pi$ -interactions (see Figure 25 for schematic representation) and a disturbed orthorhombic crystal structure becomes visible.<sup>263</sup> Defects with *para*-substitution are included into the crystal due to their conformation and the orthorhombic crystal structure of polyethylene is not altered significantly.<sup>263</sup> In the case of *meta*-substituted aromatic rings there is the possibility that the defects are either included or excluded, whereby a mixture of orthorhombic and triclinic crystals is obtained. The expansion of these defects to naphthylene units shows the same dependence on the disubstitution position.<sup>263</sup> As in the case of aliphatic bicyclic defects also the aromatic analogues are incorporated into the crystal under formation of an orthorhombic structure, if no substituents are present on the methylene bridge.<sup>260,264</sup>

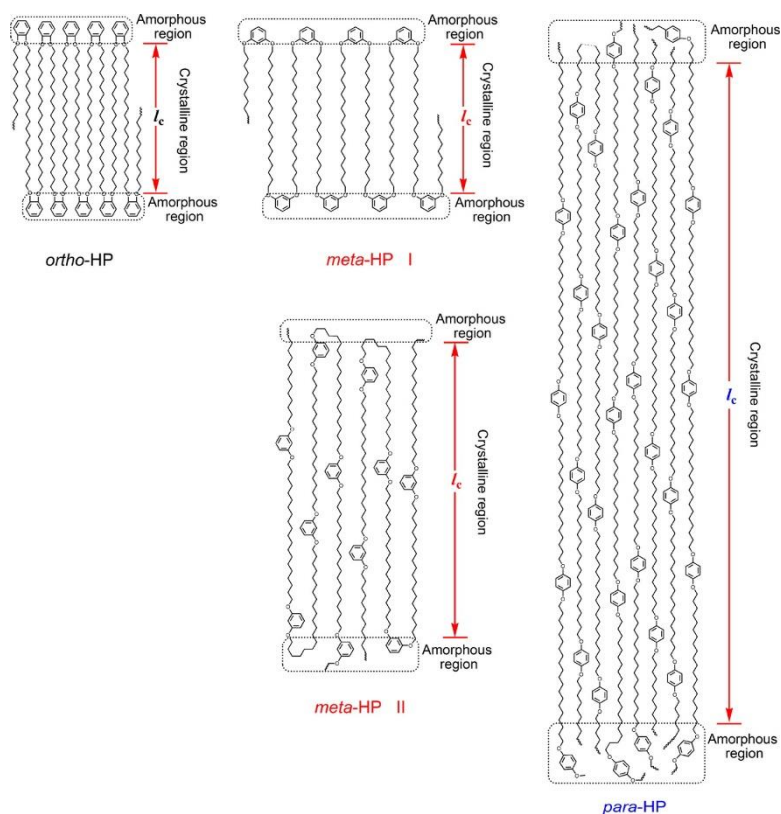


**Figure 26:** Schematic representation of the inclusion or exclusion of arylene ether defects depending on their disubstitution position. Reprinted with permission from reference<sup>263</sup>. Copyright 2016, American Chemical Society.

In summary it can be concluded, that the functional group, existent as branch defect, will be excluded from the crystalline phase when exceeding a certain size (propyl group at a methylene spacer length of 20 carbons<sup>207,213</sup> and ethyl group at a length of 38 carbon atoms<sup>220</sup>), whereby the polymer chain will be preferentially folded at the location of the defect. The side chains, regardless if they are alkyl branches or supramolecular defects exhibiting hydrogen bonding or  $\pi$ - $\pi$ -stacking, can form aggregates or co-crystallize causing a disturbance of the crystal structure<sup>220,222</sup>. If the defect is located directly in the polymer chain the concentration determines the crystallizability of the polymers and its size as well as its conformation designate the inclusion or exclusion. A defect with an appropriate geometry can even function as a fold in the polymer chain and thus be expelled to the amorphous phase (e.g. *ortho*-substituted arylene ethers<sup>263</sup>). Excluded defects can agglomerate in the amorphous phase via dipole-dipole interactions, hydrogen bonds or  $\pi$ - $\pi$ -stacking as visualized in Figure 25 and thus exert a disturbing effect on the crystallization behavior of polyethylene.

### 1.3.2.3 Determination of defect inclusion or exclusion

#### *Differential scanning calorimetry*

To determine if a defect is being included or excluded different methods can be used. If a polymer synthesized via ADMET polymerization exhibits a melting endotherm in the DSC only in its saturated state, it can be assumed that the crystallizability was enabled just by the removal of the impeding double bonds, meaning that the defects have no influence on the formation of crystals and thus will probably be located segregated in the amorphous phase. The occurrence

of cold crystallizations and melt-recrystallizations point to a complicated and slow crystal growth indicative of the inclusion of defects, which disrupt the order in the forming crystal.<sup>263</sup> Another method based on DSC measurements is the so-called successive self-nucleation and annealing (SSA)<sup>265-268</sup> by which more precise predictions about the crystal structure can be made. Here, a polymer is subjected to a thermal protocol with exactly defined variables resulting in its thermal, but not physical fractionation.<sup>265,267</sup> Due to alternating application of self-nucleation and annealing steps the polymer is separated into fractions containing different numbers of defects<sup>265,266</sup>, whereby the fraction exhibiting the highest melting temperature can be assigned to defect-free crystals. If the defects are excluded from the crystalline phase all crystalline lamella exhibit the same length and composition, whereby no fractionation occurs after carrying out the SSA protocol.

#### *Nuclear magnetic resonance*

Furthermore, the distribution of defects in the amorphous and crystalline phase can be determined by the means of solid state <sup>13</sup>C-NMR measurements. If the distribution in both phases is the same as demonstrated for chlorine and bromine atoms in precision polymers<sup>227</sup>, the defects are most likely included into the crystal.

#### *X-ray diffraction*

Also the lamellar crystal thickness determined via X-ray diffraction or TEM measurements can provide information about the location of defects. If the crystal thickness exceeds the length of the methylene spacer the defects are included in the crystalline phase. An exclusion of defects into the adjoining amorphous phase is existent if the lamellar crystal thickness exhibits the same size as the length of the alkyl chain between the defects.<sup>263</sup>

## 2. Aim of the thesis

### 2.1 Motivation/Aim

The aim of this thesis was the synthesis of precision polymers bearing artificial folding elements, which are repetitively located within a polyethylene chain. These folding elements should exert a conformational constraint on the polymer backbone due to their planar geometry and hindered rotation. Furthermore, these groups are able to interact via supramolecular interactions such as hydrogen bonding and/or  $\pi$ - $\pi$ -stacking, which is schematically shown in Figure 27. The supramolecular moieties were expected to induce a molecular order and organize into superstructures via self-assembly, interfering or competing with the crystallization of the polymer backbone.

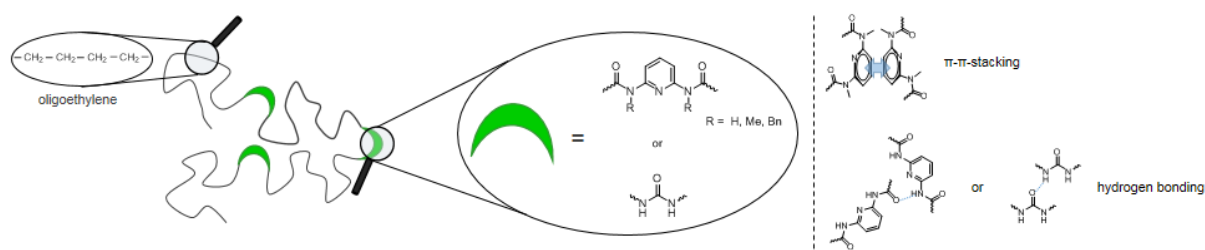


**Figure 27:** Schematic structure of the precision polyolefin containing artificial folding elements and corresponding supramolecular interactions exerted by the functional moieties.

The complete structural elucidation of the polymers will be followed by their crystallographic analysis to study the structure formation of the self-assembled system in the melt.

Thereby, it should be evaluated if the formation of crystallites can be observed or whether the polymer will be amorphous. Whether and to what extent the supramolecular interactions affect the crystallization behavior and the final crystal structure of the precision polymers will be examined as well. Furthermore, it should be determined if the functional moieties will be incorporated into the crystalline lamella or be excluded from the crystal lattice into the interstitial space. In case the supramolecular groups will be incorporated it will also be investigated if the moieties adopt an ordered substructure or whether they will just be irregularly placed in the crystal. These proposed possible structural arrangements are summarized in Figure 28.

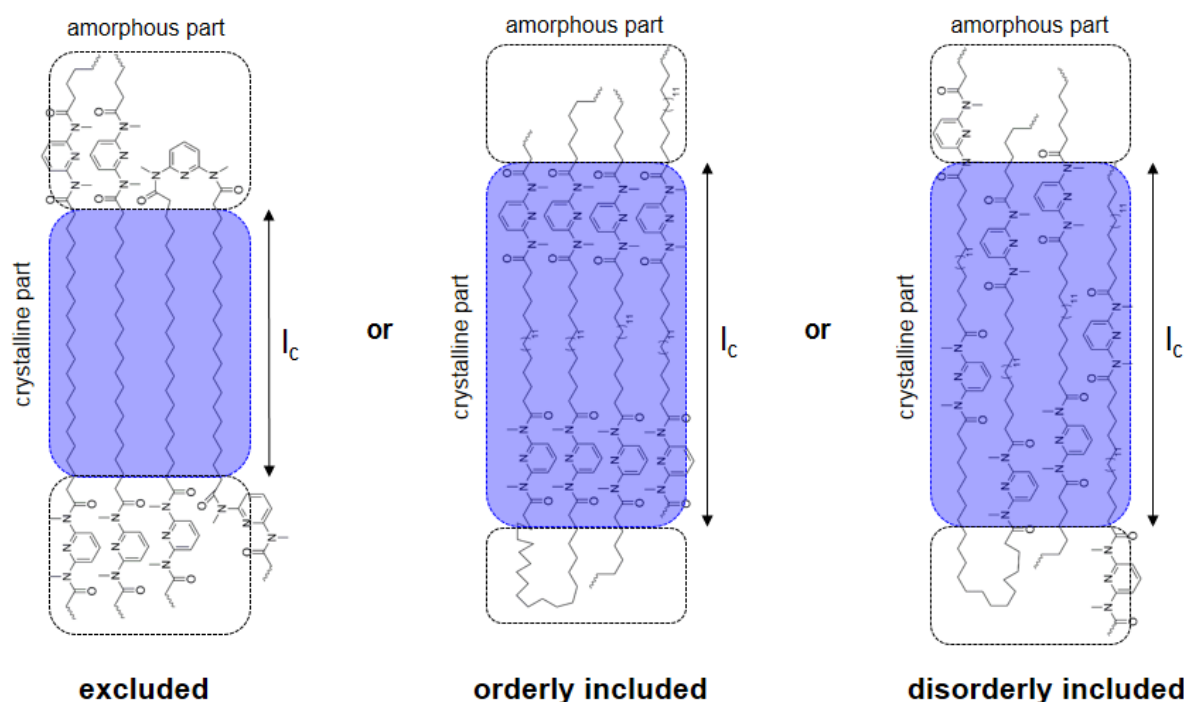


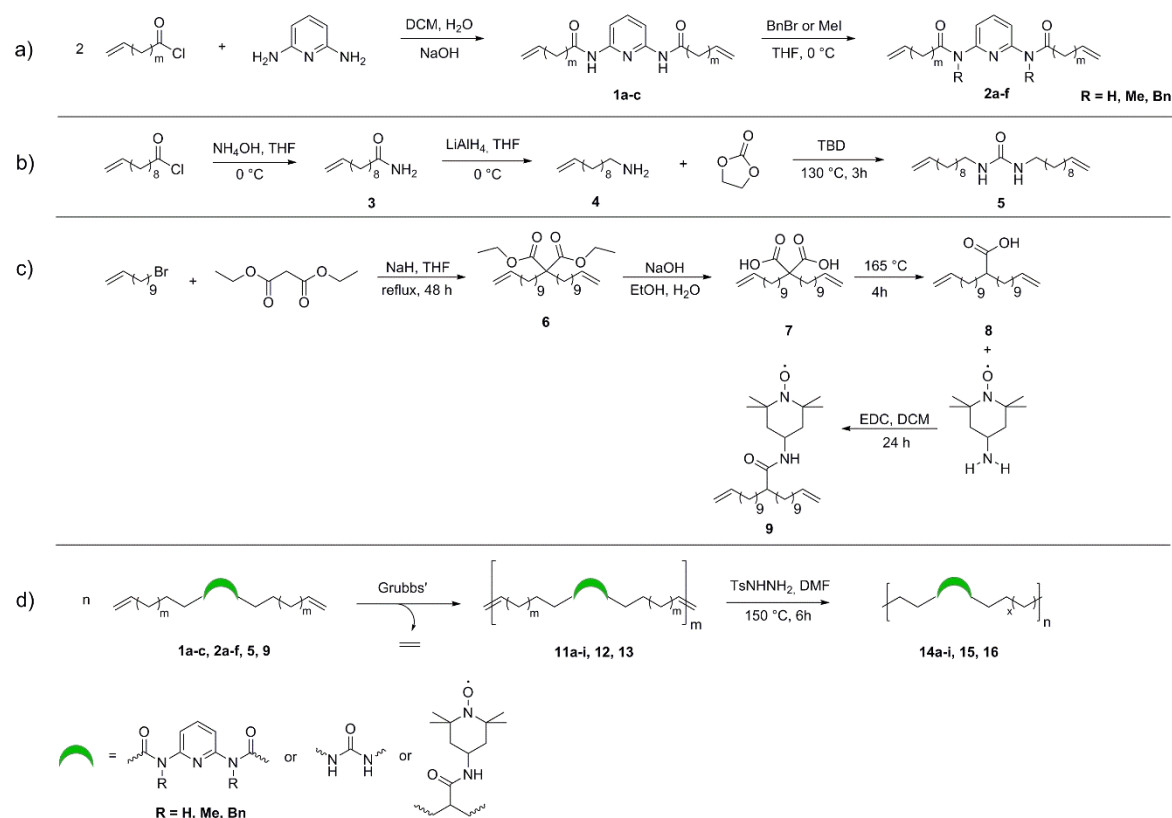
**Figure 28:** Proposed possible structural arrangements of the supramolecular moieties within the crystalline polymer backbone here using the diaminopyridine moiety as example.

Furthermore, the behavior in solution of the precision polymers synthesized within this thesis will be determined to investigate the structure formation via self-assembly under the influence of concentration and the polarity of the chosen solvent.

## 2.2 Concept

In order to ensure the precise placement of the functional groups along the polymer chain the polymerization should be accomplished via acyclic diene metathesis polymerization. 2,6-Diaminopyridine (DAP) and urea moieties should be incorporated into the polyethylene backbone via specially designed symmetrical monomers. These elements were chosen as they are planar and able to act as fold-inducing element and to interact with each other via hydrogen bonding and/or  $\pi$ - $\pi$ -stacking. Starting from 2,6-diaminopyridine and alkenoic acid chlorides with variable methylene spacer length ( $m = 7, 8$  and  $9$ ) the DAP containing monomers should be synthesized using a Schotten-Baumann reaction. To sustain the solubility of the products during and after polymerization the amide moieties had to be protected using methyl iodide or benzyl bromide respectively. The synthesis of the urea containing polymer should be accomplished by the reaction of undec-9-enoyl chloride with ammonium hydroxide, followed by the reduction with  $\text{LiAlH}_4$  and subsequent conversion with ethylene carbonate under use of TBD without any solvents to yield the final product. Additionally, a TEMPO containing monomer was synthesized via reaction of 11-bromo-1-undecene with diethyl malonate, followed by hydrolysis, decarboxylation and further conversion with 4-amino TEMPO to enable the investigation of structure formation in solution via EPR spectroscopy. Polymerization of the monomers should be carried out using different Grubbs' type and

Umicore catalysts followed by subsequent hydrogenation with *p*-toluenesulfonylhydrazide. The reaction pathway is shown in Scheme 3.



**Scheme 3:** Synthetic route for the a) preparation of unprotected and protected DAP containing monomers (**1a-c**, **2a-f**), b) the preparation of the urea containing monomer (**5**), c) the preparation of the TEMPO containing monomer (**9**) and d) the ADMET polymerization and subsequent hydrogenation.

After the complete structural characterization via gel permeation chromatography, NMR and IR spectroscopy as well as mass spectrometry (ESI and MALDI) the crystal structure of the precision polymers had to be analyzed using DSC investigations and scattering experiments (WAXS).

The structure formation via self-assembly in solution should be investigated in different solvents at various concentrations by the means of dynamic light scattering (DLS) analysis and transmission electron microscopy (TEM) measurements.

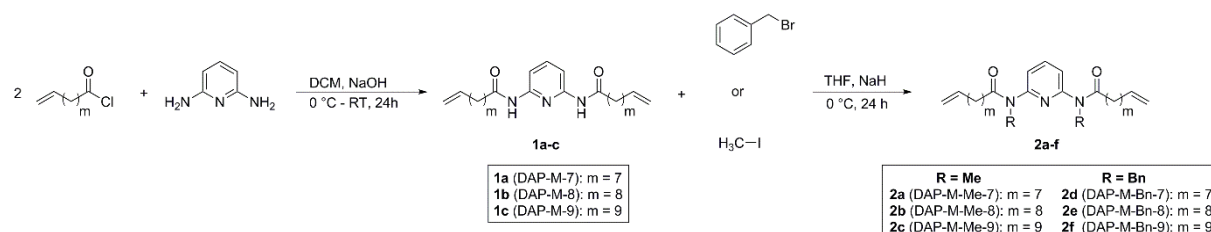
### 3. Results and Discussion

Parts of the results and discussion as well as of the experimental part were already published in “*Synthesis and Crystallization of Precision Polymers with Repetitive Folding Elements*” (Reimann, S.; Baumeister, U.; Binder, W. H. *Macromol. Chem. Phys.* **2014**, *215*, 1963. <http://dx.doi.org/10.1002/macp.201400183>)<sup>269</sup>, in “*Synthesis of supramolecular precision polymers: Crystallization under conformational constraints*” (Reimann, S.; Danke, V.; Beiner, M.; Binder, W. H. *J. Polym. Sci.* **2017**, *55*, 3736. <http://dx.doi.org/10.1002/pola.28759>)<sup>270</sup> and in “*Structure formation in nanophase-separated systems with lamellar morphology: Comb-like vs. linear precision polymers*” (Danke, V.; Gupta, G.; Reimann, S.; Binder, W. H.; Beiner, M. *Eur. Polym. J.* **2018**, *103*, 116. <https://doi.org/10.1016/j.eurpolymj.2018.03.041>)<sup>271</sup> and were in parts reprinted and adapted with permission from John Wiley and Sons (Copyright 2014 & 2017).

#### 3.1 Monomer synthesis

##### 3.1.1. Synthesis of the diaminopyridine containing monomers

The synthesis of the DAP containing monomers with varying alkyl chain lengths was accomplished as reported previously<sup>269,270,272</sup> using a biphasic Schotten-Baumann reaction. Therefore, 9-decenoic acid, 10-undecenoic acid or 11-dodecenoic acid (synthesized via Grignard reaction)<sup>98,272</sup> were converted into the appropriate acid chloride using oxalyl chloride<sup>273,274</sup> followed by the conversion with 2,6-diaminopyridine in a H<sub>2</sub>O/DCM emulsion (see Scheme 4).

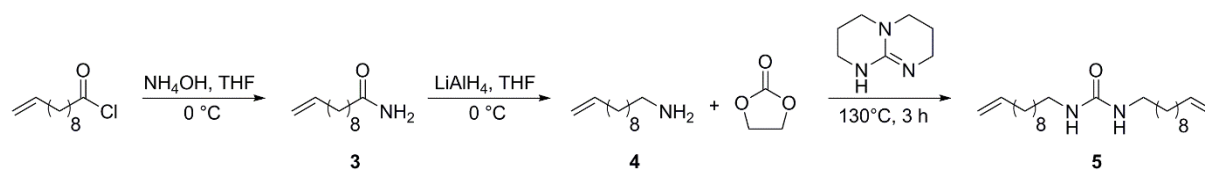


**Scheme 4:** Synthesis of the unprotected and protected DAP containing monomers (**1a-c** and **2a-f**).

The amide functionalities were protected with methyl or benzyl groups to maintain the solubility of the products during and after polymerization (see Scheme 4). The protection was accomplished by deprotonation of the monomers (**1a-c**) with sodium hydride in THF at 0 °C, followed by the conversion with either methyl iodide or benzyl bromide for 24 h.<sup>269,270,275</sup> All compounds were analyzed via <sup>1</sup>H- and <sup>13</sup>C-NMR spectroscopy as well as ESI ToF MS and the corresponding spectra are shown in Figures A 1-A 16. A triplet at ~7.88 ppm, which can be assigned to the aromatic proton H<sub>a</sub> and the signals of the allylic endgroups H<sub>l/m</sub>, H<sub>m/n</sub> and H<sub>n/o</sub> (5.95-5.68 and 5.11-4.84 ppm) in the <sup>1</sup>H-NMR are characteristic for all samples. The ratio of these resonances of 1:2 or 1:4 respectively proves the formation of the bivalent products. In the case of the *N*-protected monomers the signals at 3.36 ppm (CH<sub>3</sub>-group, see Figure 32 and Figure

A 7) and ~5.01 ppm ( $CH_2$ -group, see Figure A 12), which are present in a ratio of 1:6 or 1:4 according to the aromatic proton  $H_a$ , demonstrate the elimination of all free amide moieties.

### 3.1.2 Synthesis of the urea containing monomer



**Scheme 5:** Synthesis of the urea containing monomer (**5**).

The synthesis of the urea containing monomer was accomplished via a three-step-synthesis according to literature<sup>270,274</sup> as shown in Scheme 5. In the first step the reaction of 10-undecenyl chloride with ammonium hydroxide at 0 °C yielded undec-10-enamide (**3**) as white solid. Complete conversion was proven by the shift of the carbonyl resonance ( $C_a$ ) from 174.1 ppm to 175.9 ppm and the shift of the signal assigned to the adjacent  $CH_2$  group ( $C_b$ ) from 46.9 ppm to 36.1 ppm in the  $^{13}C$ -NMR spectrum (see Figure 29, top). Compound **3** was subsequently converted into undec-10-en-1-amine (**4**) via reduction with  $LiAlH_4$  in dry THF at 0 °C. The disappearance of the carbonyl resonance as well as the shift of  $C_b$  from 36.1 ppm to 33.9 ppm indicate complete conversion. Furthermore, the new signal at 42.4 ppm can be assigned to the  $CH_2$  group adjacent to the amine functionality (see Figure 29, middle). Afterwards, the final product, Urea-M-9 (**5**), was obtained by the reaction of the amine **4** with ethylene carbonate at 130 °C using TBD as organocatalyst.

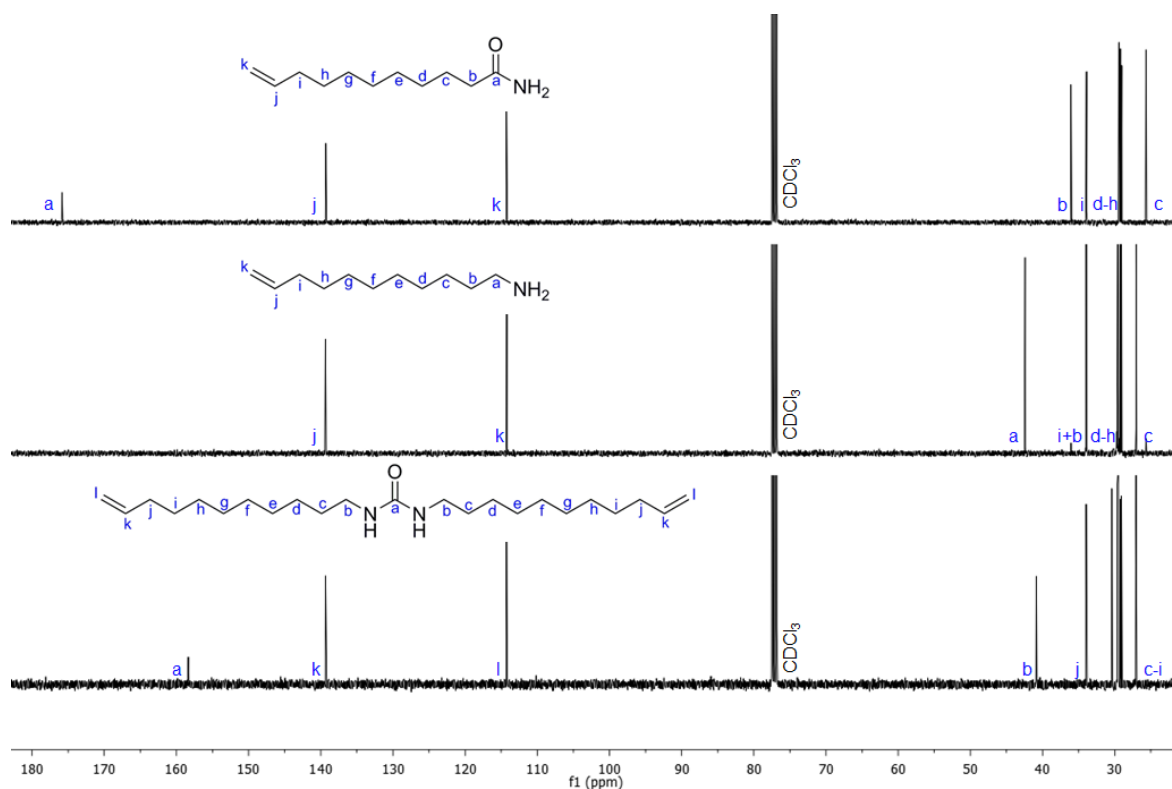
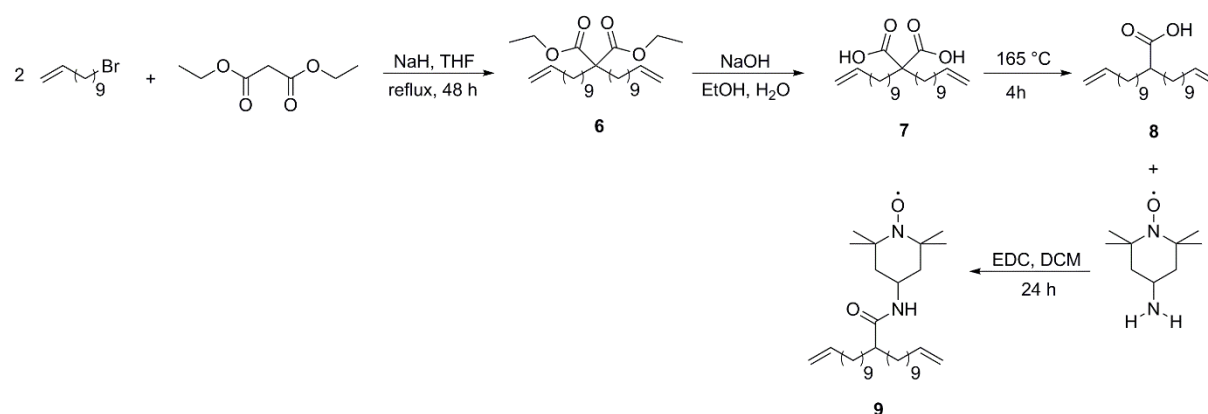


**Figure 29:** Comparison of the  $^{13}C$ -NMR spectra of undec-10-enamide (**3**) (top), undec-10-en-1-amine (**4**) (middle) and Urea-M-9 (**5**) (bottom).



The purity of the intermediate products (**3** and **4**) and the urea containing monomer (**5**) were proven via  $^1\text{H}$ - and  $^{13}\text{C}$ -NMR spectroscopy and ESI ToF MS, which are shown in Figures A 17-A 22. Successful conversion into the symmetrical urea was proven by the signal at 158.3 ppm, which can be clearly assigned to the carbonyl group ( $\text{C}_a$ ) as well as the resonances belonging to the terminal olefin bonds at 139.3 ppm and 114.3 ppm in the  $^{13}\text{C}$ -NMR (see Figure 29, bottom) and at 5.88-5.74 ppm and 5.06-4.88 ppm in the  $^1\text{H}$ -NMR spectrum (see A 21, top).

### 3.1.3 Synthesis of the TEMPO containing monomer



**Scheme 6:** Synthesis of the TEMPO containing monomer (**9**).

The synthesis of the TEMPO containing monomer was accomplished via several steps according to literature.<sup>276-279</sup> The reaction scheme is shown in Scheme 6. Firstly, diethyl malonate was deprotonated using sodium hydride in THF followed by addition of 11-bromo-1-undecene and heating under reflux conditions to yield diethyl 2,2-di(undec-10-en-1-yl)malonate (**6**) as pale yellow liquid. The disappearance of the signal at 3.36 ppm in the  $^1\text{H}$ -NMR as well as the shift of the resonances belonging to the carbonyl (shift from 166.8 ppm to 172.1 ppm) and the central C-atom ( $\text{C}_a$ , shift from 41.4 ppm to 57.7 ppm) prove the complete conversion. Afterwards, compound **6** was hydrolyzed by heating under reflux conditions with sodium hydroxide in a 1:1 mixture of ethanol and water and subsequent acidification with concentrated hydrochloric acid, whereby a color change from orange to yellow indicated the successful reaction. Removal of the solvent yielded crude 2,2-di(undec-10-en-1-yl)malonic acid (**7**), which was used without further purification. Decarboxylation of compound **7** was accomplished by stirring at 165 °C for 4 h,<sup>277</sup> whereby 2-(undec-10-en-1-yl)tridec-12-enoic acid (Acid-M-9, **8**) was obtained. The disappearance of the signals at 4.19-4.13 ppm in the  $^1\text{H}$ -NMR and at 61.0 ppm in the  $^{13}\text{C}$ -NMR and the new signal at ~2.34 ppm in the  $^1\text{H}$ -NMR spectrum, which can be assigned to the central  $\text{CH}$  group ( $\text{H}_a$ ), indicate the complete conversion. Additionally, the shift of the carbonyl resonance from 172.1 ppm to 182.5 ppm and the shift of the resonance, belonging to the central C-atom from 57.7 ppm to 45.6 ppm also prove the successful reaction. Attempts to accomplish the decarboxylation of compound **7** via addition of 1,1'-carbonyldiimidazole<sup>276</sup> or via microwave-assisted conversion of the di-acid with poly-4-vinylpyridine<sup>280</sup> turned out to be not successful. The intermediate products **6** and **8** were analyzed with  $^1\text{H}$ -NMR and  $^{13}\text{C}$ -NMR spectroscopy as well as ESI ToF MS and the

corresponding spectra are shown in Figures A 23-A 25. In a final step Acid-M-9 (**8**) was reacted with 4-amino TEMPO in DCM using EDC-HCl as coupling agent to obtain the desired product TEMPO-M-9 (**9**).

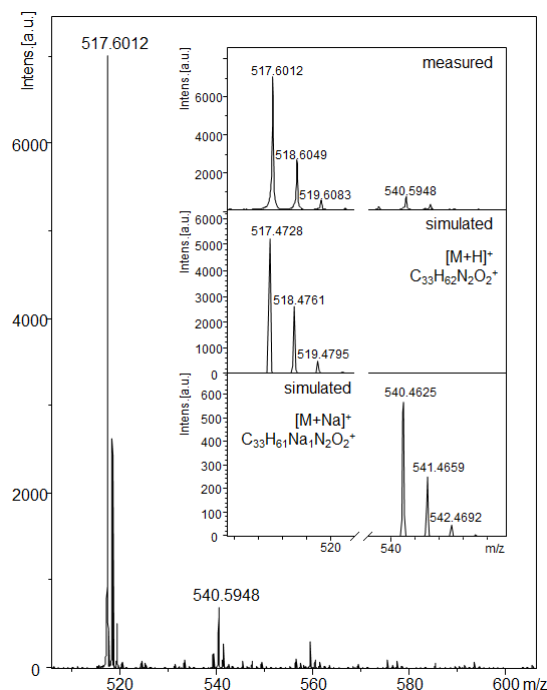
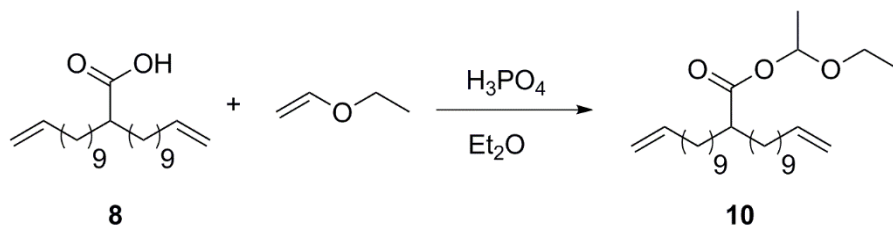


**Figure 30:** ESI ToF MS analysis of TEMPO-M-9 (**9**).

The successful conversion was proven by the appearance of two signals in the ESI ToF MS (see Figure 30). The first signal at 517.6012 g/mol was assigned to the protonated species without counterion ( $[M+H]^+$ ,  $C_{33}H_{62}N_2O_2^+$ ), which fits with its simulation of 517.4728 g/mol (error: 248 ppm). The second signal at 540.5948 g/mol was identified as the sodium adduct ( $[M+Na]^+$ ,  $C_{33}H_{61}Na_1N_2O_2^+$ ), whereby the simulation of 540.4625 g/mol (error: 247 ppm) fits with the observed peaks.

### 3.1.4 Protection of Acid-M-9



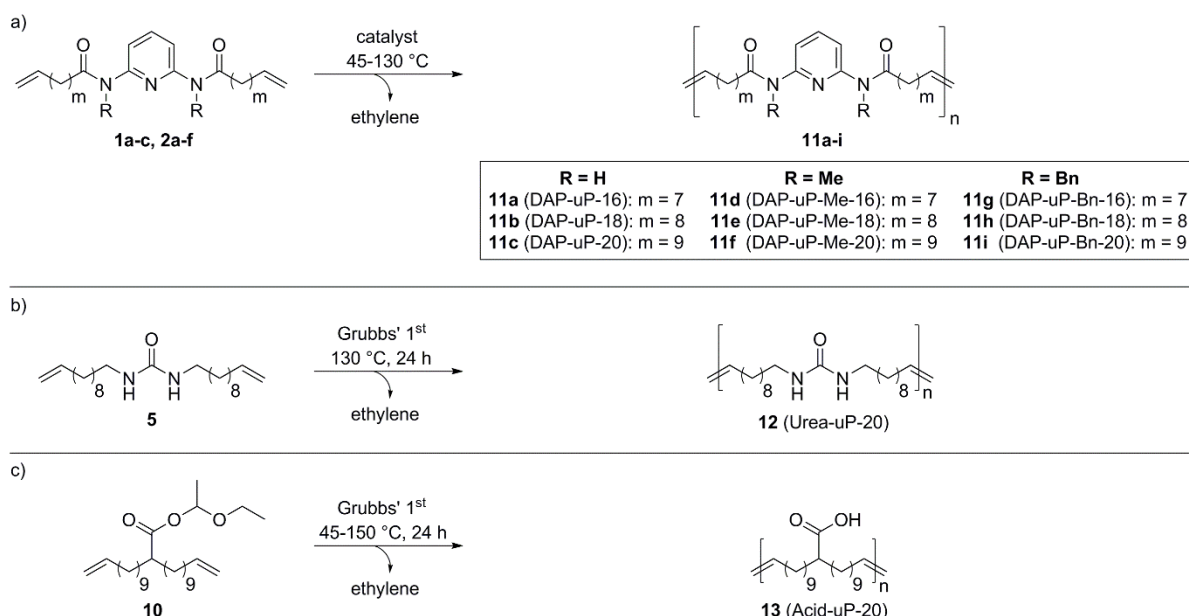
**Scheme 7:** Synthesis of Acid-M-Ee-9 (**10**).

Before polymerizing the monomer Acid-M-9 (**8**) the acid functionality has to be protected to sustain the activity of the used catalyst. Therefore, Acid-M-9 (**8**) was dissolved in diethyl ether and an excess of ethyl vinyl ether as well as a catalytic amount of phosphoric acid were added. After stirring the reaction mixture at room temperature for three days Acid-M-Ee-9 (**10**) was obtained as colorless liquid. The purity of the compound was proven via  $^1H$ -NMR and  $^{13}C$ -NMR spectroscopy and ESI ToF MS, which are shown in Figures A 26 and A 27. All

resonances could be assigned and especially the new signals at  $\sim 5.95$  ppm ( $H_n$ ) and 3.73-3.51 ppm ( $H_p$ ) in the  $^1\text{H-NMR}$  and at 96.1 ppm ( $C_n$ ) and 64.7 ppm ( $C_p$ ) in the  $^{13}\text{C-NMR}$  spectrum indicate the introduction of the protection group.

### 3.2 ADMET polymerization

The polymerizations were carried out analogous to literature<sup>68,75,224,281</sup> and previous investigations<sup>269,270,272</sup> under a dry, inert atmosphere of nitrogen as bulk polymerization as the used monomers (**1a-c**, **2a-f**, **5** and **10**) are either viscous liquids or present in the molten state at the chosen polymerization temperature. After degassing the monomers via freeze-thaw cycle the appropriate catalyst was added and the mixtures were stirred at 40-150 °C for 24-144 h at reduced pressure to remove generated ethylene. After the evolution of ethylene stopped and the magnetic stir bar was unable to move due to increased viscosity the crude polymer was dissolved in THF and precipitated into MeOH. The synthetic route for the preparation of the unsaturated polymers **11a-i**, **12** and **13** is shown in Scheme 8.



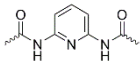
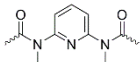
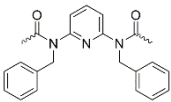
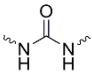
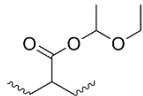
**Scheme 8:** ADMET-polymerization of the a) unprotected and protected DAP containing monomers (**1a-c**, **2a-f**), b) urea containing monomer (**5**) and c) acid containing monomer (**10**).

Initially, different types of catalysts were tested, whereby the use of the Grubbs' 2<sup>nd</sup> and 3<sup>rd</sup> generation and the Umicore M1 catalyst only produced either oligomers or polymers in a very low yield (see Table 7, entries 6, 7 and 9). Thus, the Grubbs' 1<sup>st</sup> generation and Grubbs' Hoveyda 1<sup>st</sup> generation catalyst were chosen to determine the ideal molar ratio between the monomer and the catalyst testing ratios from 50:1 to 1000:1 (Table 9, entries 3-7). As there was no obvious difference in the obtained molecular weights, a ratio of 250:1 was chosen for the following polymerizations as described in literature<sup>68</sup>. The polymerization temperature was set to 65 °C (130 °C for monomers **1a-c** and **9**) and was increased stepwise up to 85 °C to counteract the increase in viscosity and sustain a thorough mixing. After the complete consumption of the monomer, which was determined by the disappearance of the corresponding signal in TLC, the

evolution of ethylene stopped and the polymerization was quenched by opening the Schlenk tube.

Selected polymerization results and conditions are presented in Table 1.

**Table 1:** Experimental details for the synthesis of the *N*-protected DAP containing polymers (**11d-i**) and the acid containing polymer (**13**) and corresponding molecular weight data.

| functional moiety   | polymer <sup>a)</sup> | catalyst | T [°C] | M <sub>n</sub> <sup>b)</sup> (GPC) [g/mol] | PDI | M <sub>n</sub> <sup>c)</sup> (NMR) [g/mol] | yield <sup>d)</sup> [%] |
|---|-----------------------|----------|--------|--|-----|--|-------------------------|
|    | <b>11a</b>            | G1       | 130    |  |     |  | 41                      |
|   | <b>11b</b>            | G1       | 130    | e)   | e)  | e)   | 58                      |
|   | <b>11c</b>            | G1       | 130    |  |     |  | 54                      |
|    | <b>11d</b>            | GH1      | 65-85  | 4250                                       | 1.6 | 20520                                      | 98                      |
|   | <b>11e</b>            | GH1      | 65-85  | 3640                                       | 1.6 | 5222                                       | 97                      |
|   | <b>11f</b>            | GH1      | 65-85  | 8980                                       | 1.8 | 8661                                       | 83                      |
|    | <b>11g</b>            | GH1      | 65-85  | 2720                                       | 2.2 | 7211                                       | 85                      |
|   | <b>11h</b>            | GH1      | 65-85  | 4370                                       | 2.1 | 32225                                      | 65                      |
|   | <b>11i</b>            | GH1      | 65-85  | 9890                                       | 2.1 | 20305                                      | 62                      |
|   | <b>12</b>             | G1       | 130    | e)   | e)  | e)   | 64                      |
|  | <b>13</b>             | G1       | 65-85  | 16270                                      | 2.1 | 76681                                      | 96                      |

<sup>a)</sup> polymerizations were carried out for 24 h; <sup>b)</sup> determined by GPC analysis in HPLC-grade THF using polystyrene calibration; <sup>c)</sup> calculated from the ratio of signals assigned to the terminal olefins at 5.91-5.64 ppm as well as 5.10-4.78 ppm and the signals of the newly formed internal double bond at 5.47-5.12 ppm in the <sup>1</sup>H-NMR spectrum; <sup>d)</sup> isolated yields after purification; <sup>e)</sup> determination of the molecular weight and the PDI was not possible due to insolubility in any tested solvent.

The polymers **11a-c** and **12** were synthesized using Grubbs' 1<sup>st</sup> generation catalyst, which was added in a monomer-catalyst ratio of 250:1. The polymerizations were carried out at 130 °C for 24 h and yielded products that were insoluble in any tested solvent, presumably caused by hydrogen bonding, allowing no analysis via GPC or NMR spectroscopy. Attempts to polymerize the TEMPO containing monomer (**9**) using Grubbs' 1<sup>st</sup>, Grubbs' 3<sup>rd</sup> or Grubbs' Hoveyda 1<sup>st</sup> generation catalyst did not produce any polymer at all, wherefore the preparation via post functionalization of Acid-sP-20 (**16**) was chosen.

The values for the molecular weights determined by GPC and NMR analysis are very different, although the deviations do not follow a specific trend. This could be due to the fact that the determination of the molecular weight via GPC is a relative method. The determined retention times of the DAP, urea and acid containing polymers are calibrated to a polystyrene standard, showing a different hydrodynamic radius. Therefore, the determined values are only a rough estimation of the molecular weight. More precise results could be obtained with the help of a light scattering detector including the Mark-Houwink parameters of the polymers. Due to the inaccuracy of these measurements also no reliable PDI values are obtained.

The successful conversion to the unsaturated polymers (**11d-i** and **13**) was proven by the occurrence of the olefinic signals in the  $^1\text{H-NMR}$  and  $^{13}\text{C-NMR}$  spectrum at 5.47-5.12 ppm and 131.3-130.0 ppm, respectively (see Figure 32 (middle) and Figures A 29,A 30 and A 33-A 35), which can be assigned to the newly formed internal double bonds.<sup>248,257,282</sup> As the termination of the polymerization was conducted without a special quenching agent, the resonances belonging to the terminal double bonds can be found at 5.91-5.64 ppm and 5.10-4.78 ppm in the  $^1\text{H-NMR}$  spectrum allowing the calculation of the molecular weight and the *cis/trans* ratio, which turned out to be approximately 30 % *cis* and 70 % *trans* for all of the polymers. The MALDI ToF MS spectrum of DAP-uP-Me-18 (**11e**) is shown in Figure 31, displaying one series with a mass distribution from 1300 to 4900 g/mol and a maximum at 2200 g/mol.

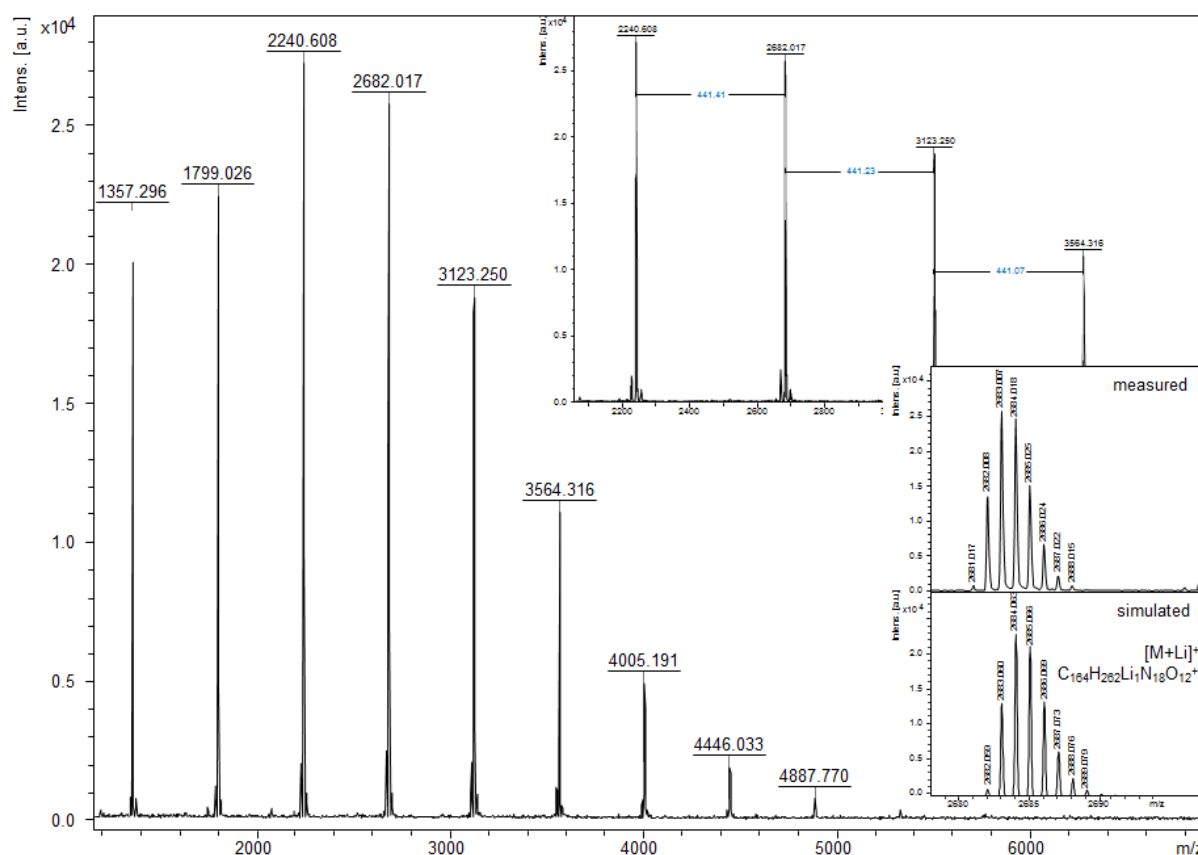
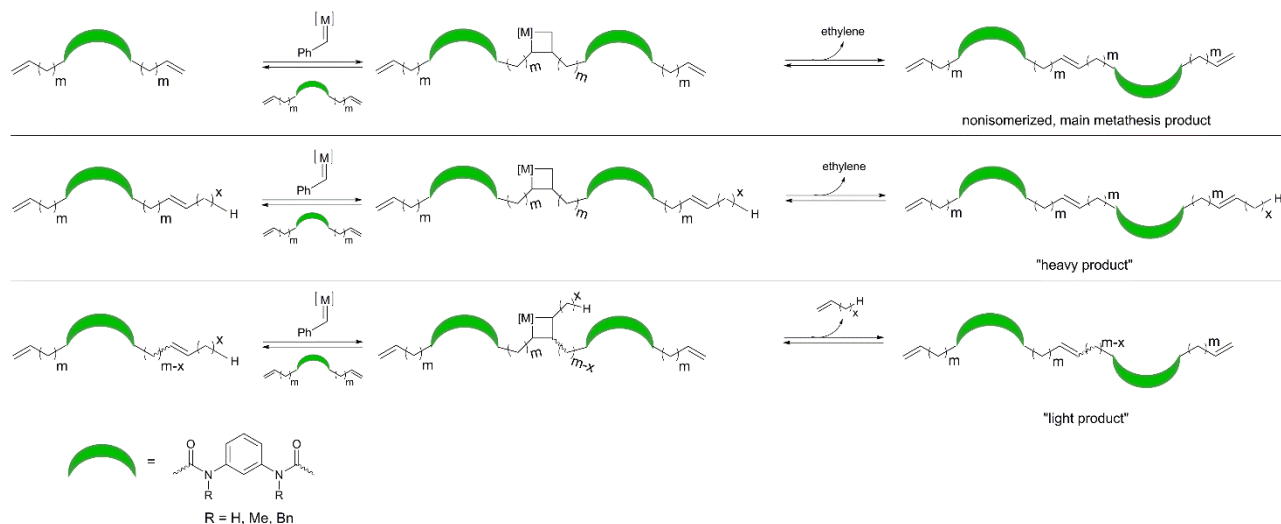


**Figure 31:** MALDI ToF MS analysis of DAP-uP-Me-18 (**11e**).

The distance between two peaks is 441 Da, reflecting the mass of the repetitive DAP unit. The shown series can be identified as the Li adduct ( $[\text{M}+\text{Li}]^+$ ), whereby the simulation of 2682.059 g/mol is in good agreement with the measured value of 2681.017 g/mol (error: 390 ppm). The polymers **11d** and **11f** were also analyzed via MALDI ToF MS and the corresponding spectra are shown in Figures A 31 and A 32. Zooming into the mass spectrum reveals that every polymeric peak consists of a bunch of peaks separated by 14 Da, a phenomenon, which occurs due to isomerization effects during olefin metathesis also observed for precision polyethylene bearing amino acid functionalities.<sup>283</sup> These additional peaks can be assigned to the non-isomerized, main metathesis products as well as the “heavy” and “light” products, whose formation is shown in Scheme 9.<sup>284</sup> The light products are generated if the

monomer is isomerized, i.e. when the position of the double bond is shifted. Thus, during metathesis not ethylene but propylene, butylene etc. is released, whereby the isomerized monomer exhibits a smaller mass than originally. If the isomerization of the monomer is followed by a non-productive metathesis, monomers with a mass higher than originally are formed, leading to the generation of heavy products.



**Scheme 9:** Formation of the different isomerization products during ADMET polymerization.<sup>284</sup>

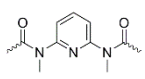
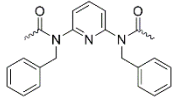
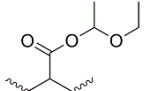
Attempts to suppress isomerization via addition of tin(II) chloride and bromide salts<sup>91</sup>, 2,6-dichloro-1,4-benzoquinone<sup>92</sup> or phenyl phosphoric acid<sup>93</sup> during the polymerization (see Table 8, entry 3-6) were not successful or did not even produce polymer.

The polymerization progress of the unprotected polymers (**11a-c** and **12**) was monitored via IR spectroscopy since they could not be analyzed via NMR spectroscopy or GPC analysis due to their insolubility. The decrease of the signals at  $\sim 911$  and  $\sim 991$   $\text{cm}^{-1}$  belonging to the C-H out-of-plane deformation vibration of the vinylic end groups of the monomers as well as the appearance of the signal at  $\sim 963$   $\text{cm}^{-1}$ , which can be assigned to C-H out-of-plane vibration of the newly formed internal C=C double bonds prove a successful conversion (see the corresponding IR spectra in Figure 33 and Figures A 6, A 28 and A 44).<sup>219</sup>

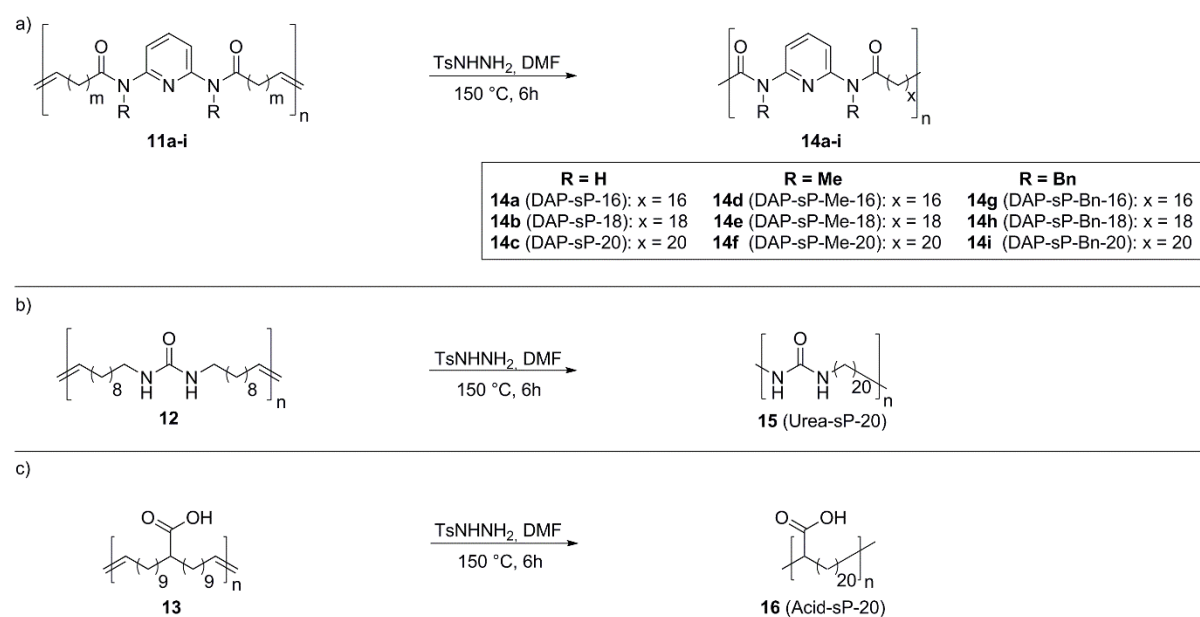
### 3.3 Hydrogenation

Hydrogenation of the polymers was accomplished by the reaction with *p*-toulenesulfonylhydrazide (TsNHNH<sub>2</sub>) and *N,N*-diisopropylethylamine (DIPEA) in DMF at 150 °C for 6 h – conditions well known to enable a complete hydrogenation.<sup>217,263,269,270,282,285</sup> The reaction pathway is shown in Scheme 10 and selected results are listed in Table 2.

**Table 2:** Molecular weight data of the *N*-protected DAP containing polymers (**14g-i**) and the acid containing polymer (**16**).

| functional moiety   | polymer    | M <sub>n</sub> <sup>a)</sup> (GPC)<br>[g/mol] | PDI | M <sub>n</sub> <sup>b)</sup> (NMR)<br>[g/mol] | yield <sup>c)</sup><br>[%] |
|---|------------|---|-----|---|----------------------------|
|  | <b>14d</b> | 3880  | 1.4 | 2909  | 73                         |
|   | <b>14e</b> | 3140  | 1.6 | 3407  | 92                         |
|   | <b>14f</b> | 6380  | 1.8 | 8344  | 99                         |
|  | <b>14g</b> | 4430  | 1.6 | 8204  | 68                         |
|   | <b>14h</b> | 7460  | 1.4 | 8634  | 33                         |
|   | <b>14i</b> | 10000   | 1.9 | 5278  | 53                         |
|  | <b>16</b>  | 18250   | 1.9 | 5606  | 48                         |

<sup>a)</sup> determined by GPC analysis in HPLC-grade THF using polystyrene calibration; <sup>b)</sup> calculated from the ratio of signals assigned to the terminal methyl groups at 0.95-0.76 ppm and the signal of the aromatic unit at 7.75-7.60 ppm (for the DAP containing polymers **14d-i**) or the signal assigned to the proton next to the carboxylic acid functionality at 2.26-2.15 ppm (for the acid containing polymer **16**) in the <sup>1</sup>H-NMR spectrum; <sup>c)</sup> isolated yields after purification.

**Scheme 10:** Synthesis of the saturated a) DAP containing polymers (**14a-i**), b) urea containing polymer (**15**) and c) acid containing polymer (**16**).

The disappearance of all olefinic signals (from 5.91 to 4.78 ppm) and the formation of terminal methyl groups, which signals can be seen at ~0.86 ppm in the <sup>1</sup>H-NMR spectra (see Figure 32 and Figures A 37, A 42 and A 45) prove the complete conversion to the saturated polymers. Completion of the hydrogenation of the unprotected polymers (**11a-c** and **12**) was proven via IR spectroscopy by the disappearance of the absorption band at ~963 cm<sup>-1</sup> (see Figure 33 and Figures A 36 and A 44).

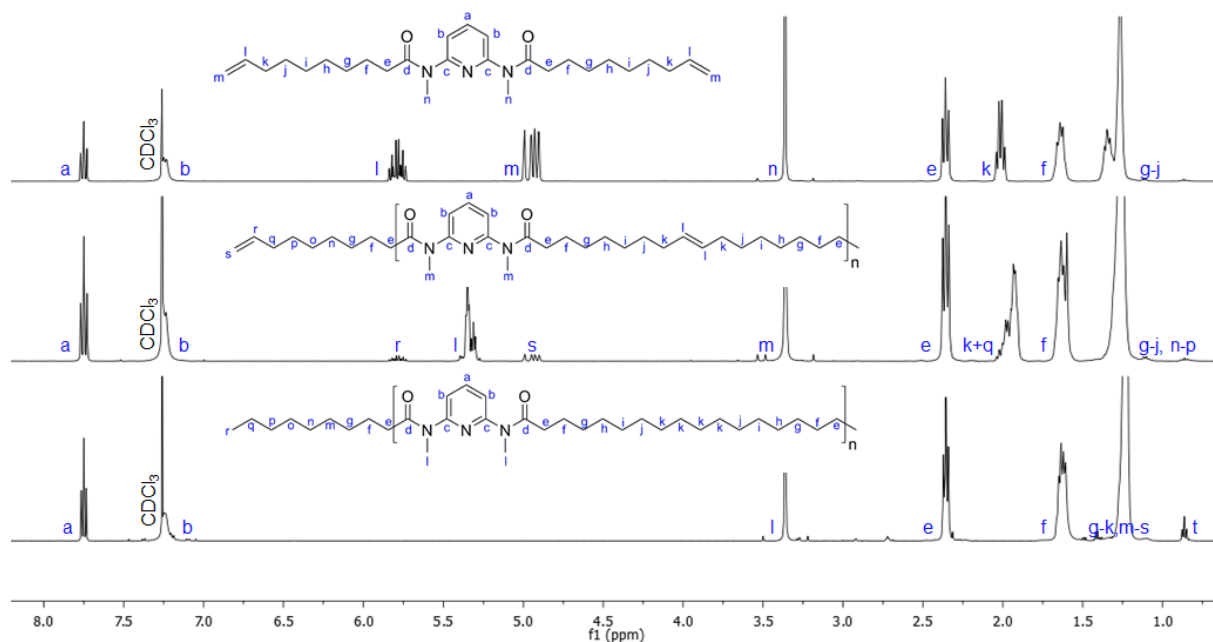


**Figure 32:** Comparison of the  $^1\text{H}$ -NMR spectra of DAP-M-Me-7 (**2a**) (top), DAP-uP-Me-16 (**11d**) (middle) and DAP-sP-Me-16 (**14d**) (bottom).

Additionally, the *N*-methyl protected polymers (**14d-f**) were analyzed via MALDI ToF MS, showing one to three different series with a mass distribution from 1300 to 5100 g/mol (see Figures A 39-A 41). The main series can be assigned to the  $\text{Li}^+$  adduct of the linear polymers, while the other series indicate the polymer fragmentation due to the relatively high laser energy used during MALDI measurement. The distance between two peaks accounts from  $\sim 415$  Da to  $\sim 471$  Da, reflecting the mass of the corresponding repetitive DAP unit.

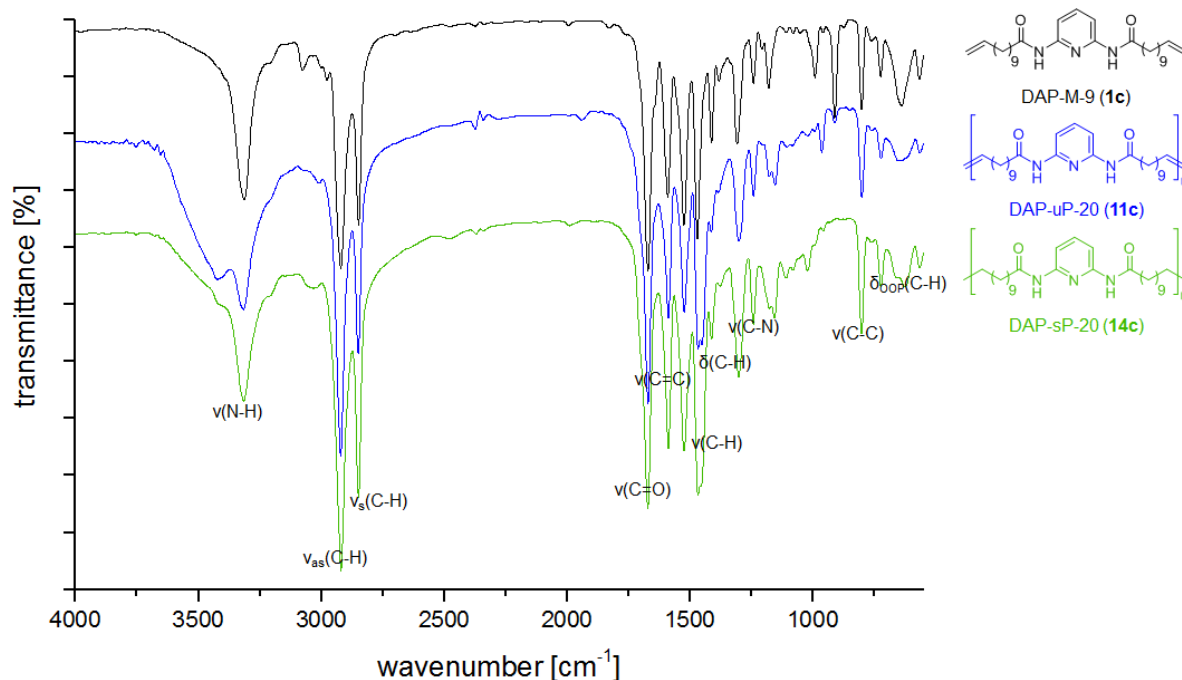


**Figure 33:** Comparison of the IR spectra of DAP-M-9 (**1c**) (top), DAP-uP-20 (**11c**) (middle) and DAP-sP-20 (**14c**) (bottom).



### 3.4 Post-functionalization of Acid-sP-20 (16)

As the direct polymerization of the TEMPO containing monomer (**9**) using Grubbs' 1<sup>st</sup>, Grubbs' 3<sup>rd</sup> or Grubbs' Hoveyda 1<sup>st</sup> generation catalyst did not succeed, attempts were made to introduce the functional group via post-functionalization of Acid-sP-20 (**16**).

Therefore, the acid functionalized polymer was converted into the appropriate acid chloride by reaction with triphenylphosphine in carbon tetrachloride, which was used without further purification. In the next step 4-amino TEMPO, DIPEA and pyridine were added and the mixture was heated to 80 °C for 6 h. Excessive 4-amino TEMPO was removed by purification via neutral alumina column yielding TEMPO-sP-20 (**18**) as orange solid. Complete conversion and purity of the polymer should be determined via MALDI ToF MS and the corresponding spectrum is shown in Figure 34.

Although, several matrices and salts as well as different methods were tested, the ionization of TEMPO-sP-20 (**18**) turned out to be very difficult. Thus, only signals with a low intensity and at small molecular weights could be obtained. The mass spectrum is displaying one series with a mass distribution from 1778 to 3244 g/mol and a maximum at 2267 g/mol, whereby the distance between two peaks accounts to 489 Da. This distance does not reflect the expected mass of the repetitive unit, which ought to be 491 Da without any counter ion.

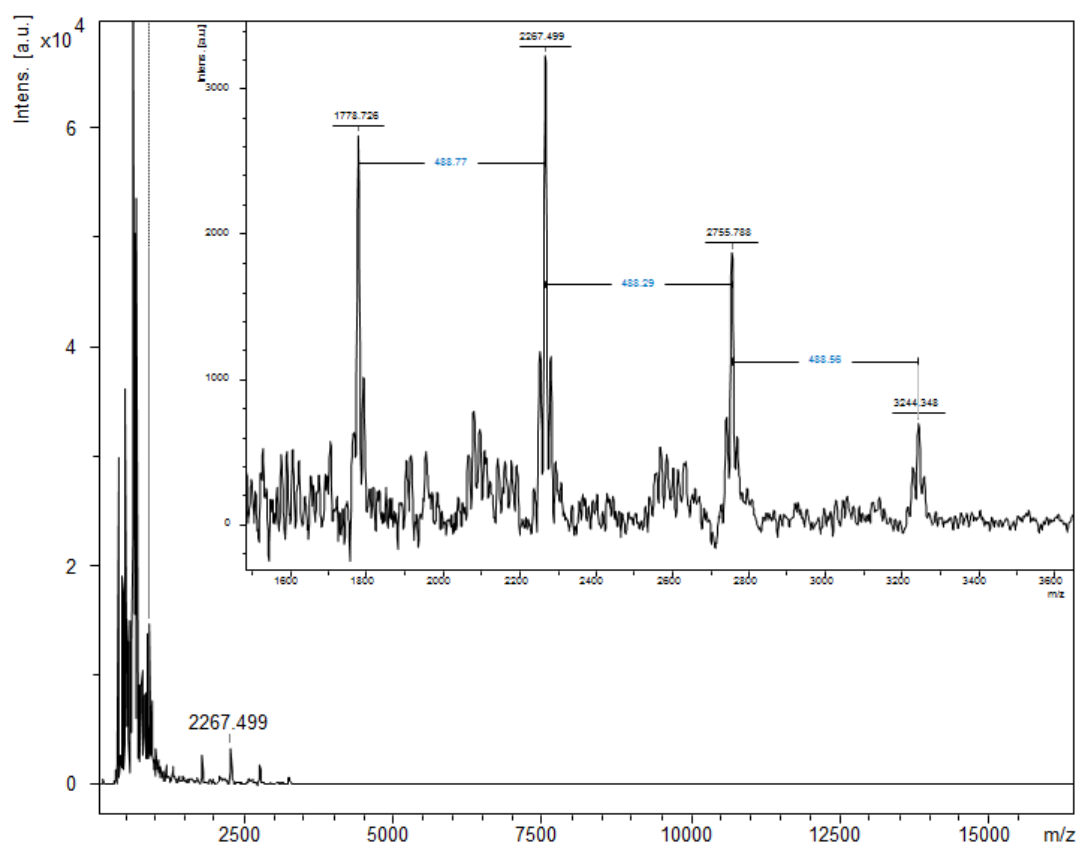


**Figure 34:** MALDI ToF MS spectrum of TEMPO-sP-20 (**18**).

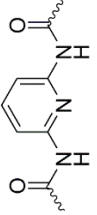
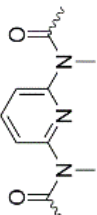
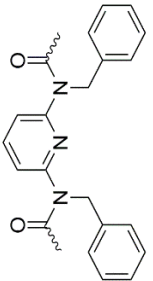
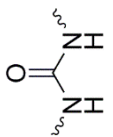
Assuming an incomplete hydrogenation of the acid functionalized polymer (**16**) and subsequent reaction with the 4-amino TEMPO could explain the deviation of 2 Da if the unsaturated

TEMPO containing polymer can be ionized better than the saturated one. Nevertheless, the successful synthesis of the desired, saturated TEMPO containing product cannot be proven.

### 3.5 Thermal analysis

The thermal properties of all synthesized polymers was investigated via DSC measurements and selected thermograms and thermal data are shown in Figure 35 and Figure 36 and Table 3.

**Table 3:** Thermal properties of the DAP (**11a-i**) and urea (**12** and **15**) containing polymers.

| functional moiety   | polymer    | T <sub>g</sub> [°C] | T <sub>m</sub> [°C] | T <sub>c</sub> [°C] | ΔH <sub>m</sub> <sup>0</sup> [J/g] | ΔT <sup>a)</sup> [°C] | X <sub>c</sub> <sup>b)</sup> [%] |
|---|------------|---------------------|---------------------|---------------------|------------------------------------|-----------------------|----------------------------------|
|   | <b>11a</b> | -                   | 123.1<br>133.5      | 108.3               | 63.01                              | 25.2                  | 28                               |
|    | <b>11b</b> | -                   | 137.6               | 118.7               | 66.17                              | 18.9                  | 28                               |
|   | <b>11c</b> | 54.7                | 123.3               | 96.0                | 43.50                              | 27.3                  | 18                               |
|   | <b>14a</b> | -                   | 167.7               | 140.5               | 71.99                              | 27.2                  | 32                               |
|   | <b>14b</b> | -                   | 153.4<br>167.8      | 138.8               | 52.40                              | 29.0                  | 21<br>23                         |
|   | <b>14c</b> | -                   | 142.1<br>154.8      | 128.7               | 57.07                              | 26.1                  | 23                               |
|   |            | <b>11d</b>          | -16.8               | -                   | -                                  | -                     | -                                |
|  | <b>11e</b> | -21.7               | 60.2                | -                   | 41.62                              | -                     | 18                               |
|   | <b>11f</b> | -14.6               | 71.7                | 1.2                 | 42.79                              | 70.5                  | 17                               |
|   | <b>14d</b> | -                   | 88.2                | 39.6                | 67.08                              | 48.6                  | 30                               |
|   | <b>14e</b> | -                   | 87.4                | 44.8                | 76.36                              | 42.6                  | 33                               |
|   | <b>14f</b> | -                   | 96.3                | 63.4                | 42.51                              | 32.9                  | 17                               |
|   |            | <b>11g</b>          | -7.7                | -                   | -                                  | -                     | -                                |
|  | <b>11h</b> | -10.1               | -                   | -                   | -                                  | -                     | -                                |
|   | <b>11i</b> | -8.6                | -                   | -                   | -                                  | -                     | -                                |
|   | <b>14g</b> | -8.0                | -                   | -                   | -                                  | -                     | -                                |
|   | <b>14h</b> | -2.2                | -                   | -                   | -                                  | -                     | -                                |
|   | <b>14i</b> | -                   | 15.0                | 9.3                 | 34.49                              | 5.7                   | 14                               |
|   |            | <b>12</b>           | -                   | 104.5<br>131.0      | 120.5                              | 93.25                 | 10.5                             |
|  | <b>15</b>  | -                   | 107.2<br>124.8      | 94.6                | 57.28                              | 30.2                  | 23                               |

<sup>a)</sup> ΔT = T<sub>m</sub> - T<sub>c</sub>, <sup>b)</sup> calculated via equation (14).

Nearly all *N*-benzyl protected polymers are amorphous, displaying glass transition temperatures in the range of -10 to -2 °C (see Figures A 51-A 53). Only the saturated polymer with the longest methylene spacer length (**14i**) shows a small melting point at 15 °C. With the corresponding

enthalpy of fusion the crystallinity of the sample can be calculated using the equation given below

$$X_c = \frac{\Delta H_m}{\Delta H_m^0} \times 100 \quad (14)$$

where  $\Delta H_m^0$  is the enthalpy of fusion of the corresponding alkene [hexadecane:  $\Delta H_m^0 = 225.146$  J/g used for polymers with a methylene spacer length of  $x = 16$  (**14a**, **14d** and **14g**), octadecane:  $\Delta H_m^0 = 232.269$  J/g used for polymers with  $x = 18$  (**14b**, **14e** and **14h**) or eicosane<sup>286</sup>  $\Delta H_m^0 = 247.3$  J/g<sup>287</sup> used for polymers with  $x = 20$  (**14c**, **14f**, **14i**, **12** and **15**) with 100 % crystallinity. At an enthalpy of fusion of 34.49 J/g a crystallinity of 14 % can be calculated for DAP-uP-Bn-20 (**14i**). The low or even missing crystal character of the *N*-benzyl protected polymers (**11g-i** and **14g-i**) can be explained by the size of the protection group, which is sterically demanding and thus cannot be incorporated into the crystal lamella, unless the chain length between the functional groups is big enough to enable the formation of crystals.<sup>282</sup> If the *N*-benzyl group is replaced by a methyl protection group only the unsaturated polymer with the shortest methylene spacer length (**11d**) is still amorphous showing a glass transition at  $-16.8$  °C (see Figure A 49, black curve). All the other *N*-methyl protected polymers (**11e-f** and **14d-f**) are crystalline, showing melting temperatures ranging from 60 to 96 °C (see Figure 35, A 49 and A 50, which are below the  $T_m$  of pure ADMET PE.

Upon hydrogenation the melting temperatures increase by  $\sim 30$  °C (see Figure 35 and A 46-A 50) due to removal of the steric hindrance caused by the *cis/trans* isomerism of the double bond, which prevents a tight packing of the adjacent polymer chains, also observed for other precision polymers.<sup>263</sup>

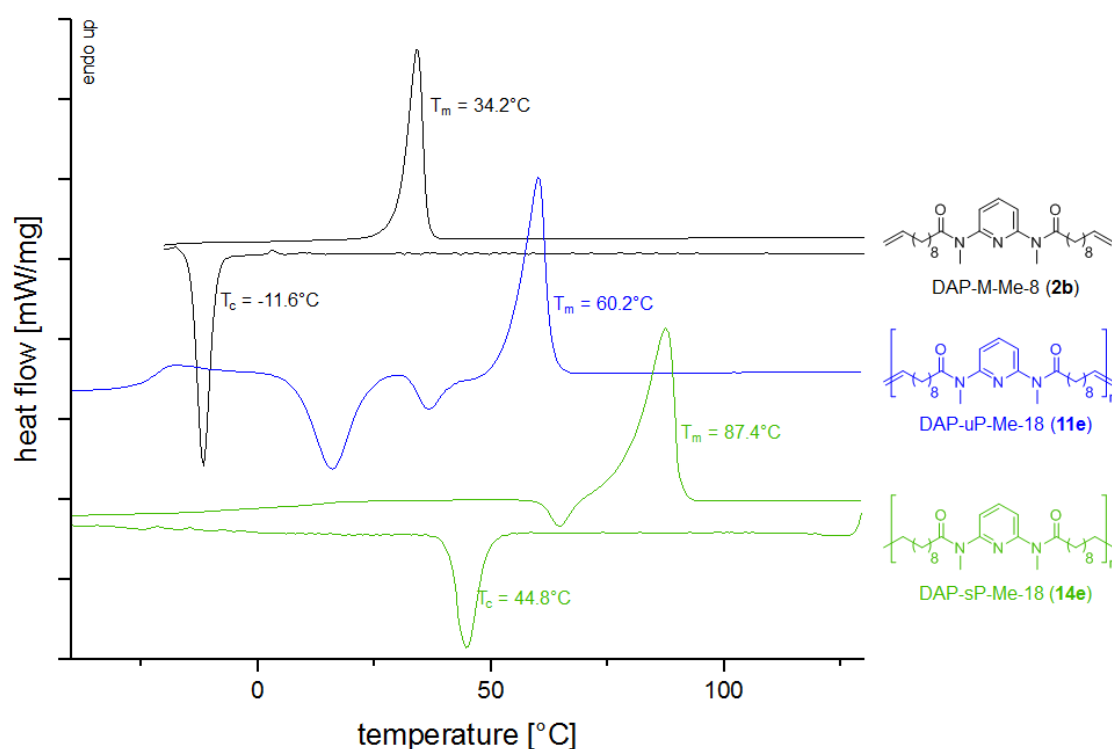


**Figure 35:** DSC thermograms of DAP-M-Me-8 (**2b**), DAP-uP-Me-18 (**11e**) and DAP-sP-Me-18 (**14e**).

The comparison of the polymers with different methylene spacer lengths (**11d-f** and **14d-f**) shows an increase in the melting temperatures with increasing spacer size (see Table 3) as the percentage of defects is decreasing. Another characteristic for all unsaturated and saturated *N*-methyl protected polymers (**11d-f** and **14d-f**) is the so called cold crystallization observable in every melting endotherm (see Figure 35, A 49 and A 50), implying a non-completed crystallization during the cooling process typically observed for polymers with slow crystallization rate. This, in conjunction with the high supercooling, can be interpreted as an at least partial incorporation of the functional moieties into the crystalline lamella, similar to observations for other precision polymers.<sup>98,263,288</sup>

The polymers without protection group (**11a-c**, **12**, **14a-c** and **15**) exhibit increased melting temperatures ( from 104 °C up to 167 °C, see Figure 36, A 46-A 48 and A 54), some even higher than the  $T_m$  of pure ADMET polyethylene ( $T_m = 134$  °C).<sup>102,219,220,222</sup> The enhanced thermal stability can be explained by the formation of hydrogen bonds between adjacent DAP or urea moieties, comparable to diketopiperazine (DKP) or sulfone functionalized polyethylenes.<sup>257,289</sup>

Based on the decreased supercooling ( $\Delta T = 10 - 30$  °C) a facilitated inclusion of the functional moieties into the crystalline lamella can be considered. All saturated polymers without protection group (**14a-c** and **15**) exhibit two melting endotherms (in the case of **14c** even a melting-recrystallization), indicating the formation of different polymorphs, also observed for polyethylene bearing *para*-phenylene ether groups along the polymer backbone.<sup>263</sup>

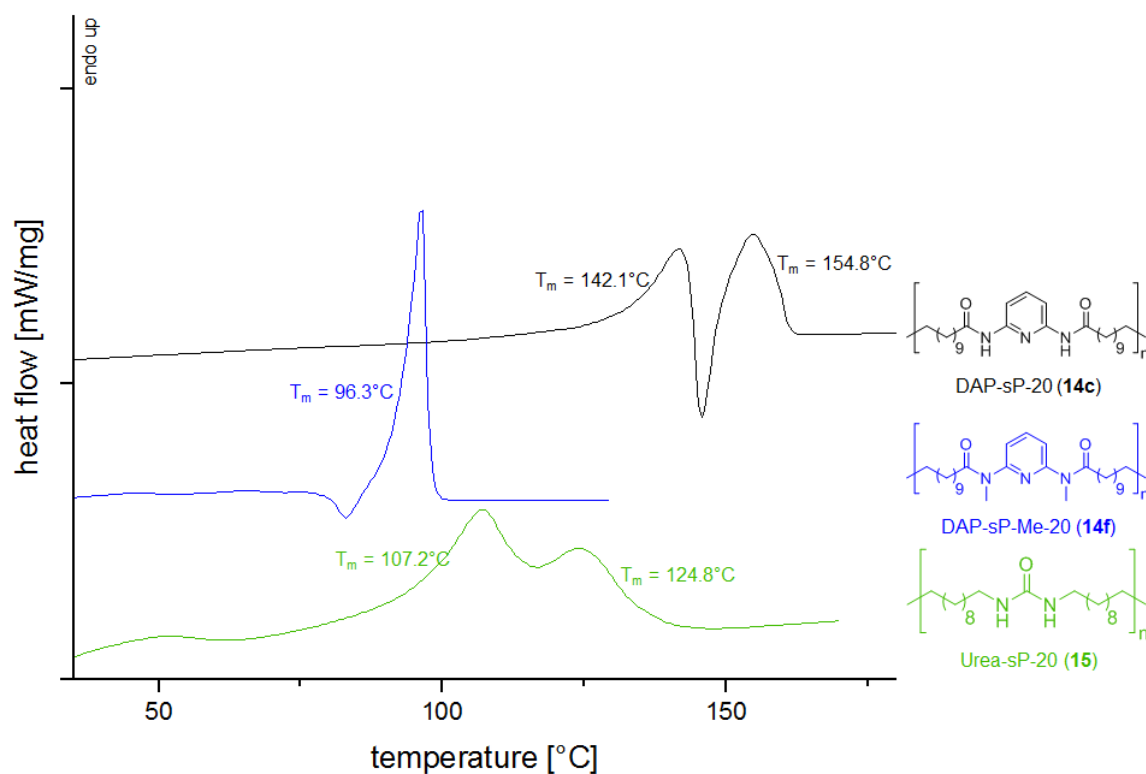


**Figure 36:** Comparison of the DSC thermograms of DAP-sP-20 (**14c**), DAP-sP-Me-20 (**14f**) and Urea-sP-20 (**15**).

### 3.6 Structural analysis

#### 3.6.1 WAXS analysis of the saturated *N*-methyl protected DAP containing polymers (14d-f)

To understand the influence of the functional group and different methylene spacer lengths on the crystallization of the precision polymers, the saturated DAP containing polymers with methyl protection group (14d-f) were studied via wide angle X-ray scattering (WAXS) and the corresponding diffraction patterns are displayed in Figure 37.

All diffractograms show a signal in the range of  $2.4 < q < 2.8 \text{ nm}^{-1}$ , which is shifting systematically to higher  $q$  values (corresponding to lower distances according to Bragg's law  $d_{hkl} = 2\pi/q_{hkl}$ ) with decreasing methylene spacer lengths. Thus, these signals can be assigned to the (001) reflection indicating the distance between two DAP moieties along the polymer chain. The second order peak (002) visible at  $4.8 < q < 5.6 \text{ nm}^{-1}$  indicates a lamellar morphology, which was also observed for sulfone functionalized precision polyethylene.<sup>257</sup> All polymers exhibit a peak at  $8.9 \text{ nm}^{-1}$ , which shows no dependence on the methylene spacer length, thus representing the periodicity along one of the two lateral directions. These signals can be assigned to the (100) reflex indicating the distance between two DAP moieties of adjacent polymer chains. For the corresponding second order peak (200) distances of 0.35-0.36 nm can be calculated, representing the expected  $\pi$ - $\pi$ -stacking between the DAP units, which are in a good accordance to the literature values of 0.33-0.38 nm.<sup>290</sup> Therefore, the DAP moieties of adjacent polymer chains are assumed to show a parallel arrangement.<sup>270</sup>

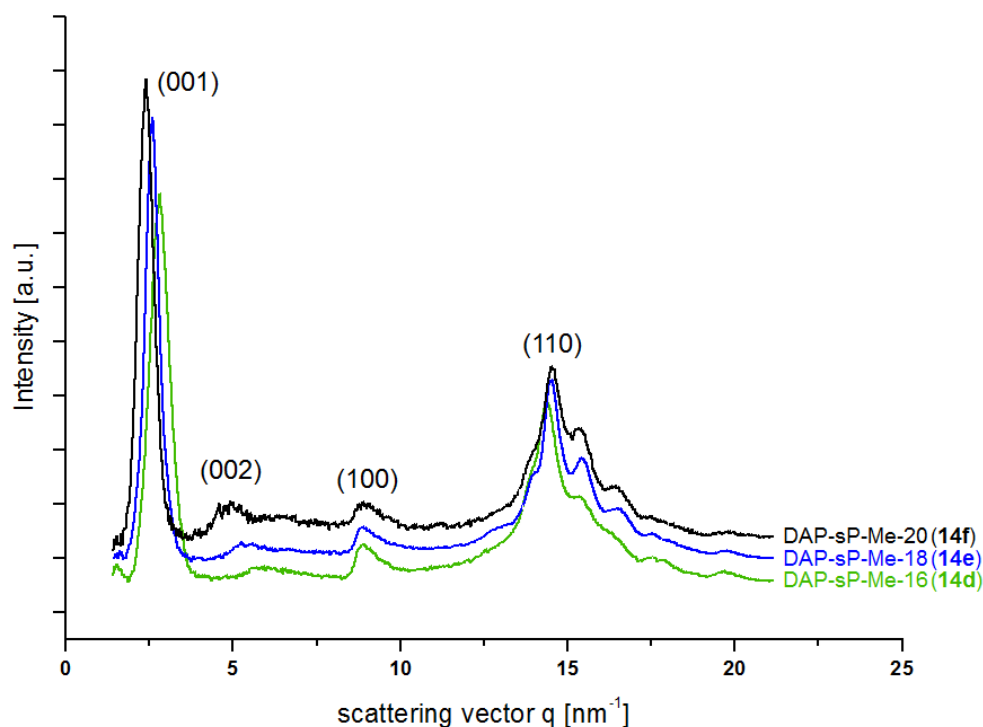


**Figure 37:** X-ray diffraction pattern of the saturated, *N*-methyl protected DAP containing polymers (14d-f).

The broad signal at  $14 \leq q \leq 16 \text{ nm}^{-1}$  in the wide angle range shows also no dependence on the methylene spacer length and is corresponding to the (110) reflection of an orthorhombic PE crystal.<sup>222</sup> Based on the (001) reflections the lamellar spacing  $d_{001}$  can be calculated to give

values of 2.24 nm for  $x = 16$  (**14d**), 2.44 nm for  $x = 18$  (**14e**) and 2.64 nm for  $x = 20$  (**14f**), which show a linear dependence when plotted against the number of methylene units  $x$ . Extrapolating these values to  $x = 0$  results in an intercept of about 6.3 Å, which corresponds to the size of the DAP layer in the lamellar structure and matches the theoretically calculated value for the size of a DAP group of 6.7 Å (structure simulated with Avogadro: an open-source molecular builder and visualization tool. Version 1.2.0<sup>291</sup>) very well. A slope of 1 Å per CH<sub>2</sub> unit is observed for saturated, *N*-methyl protected DAP containing polymers (**14d-f**), which is less than the ideal slope of 1.25 Å per CH<sub>2</sub> expected for fully extended and interdigitated methylene sequences in the all-*trans* state without tilting, meaning that the polymer chain is either not fully extended or does not show an overall all-*trans* conformation.

### 3.6.2 Impact of different supramolecular interactions on the crystal structure

WAXS measurements of the unprotected (**14c**) and protected (**14f**) DAP containing polymers as well as the urea containing polymer (**15**) were conducted after annealing the samples at 40 °C to compare the influence of different supramolecular interactions on the crystal structure. The corresponding diffraction patterns are shown in Figure 38. Upon annealing the saturated *N*-methyl protected DAP containing polymer (**14f**) shows a better resolved diffraction pattern. The appearance of additional peaks in the wide angle range indicates the formation of a mixture of orthorhombic and triclinic crystal structures, also observed for precision polymers containing *meta*-substituted phenylenes.<sup>263</sup>

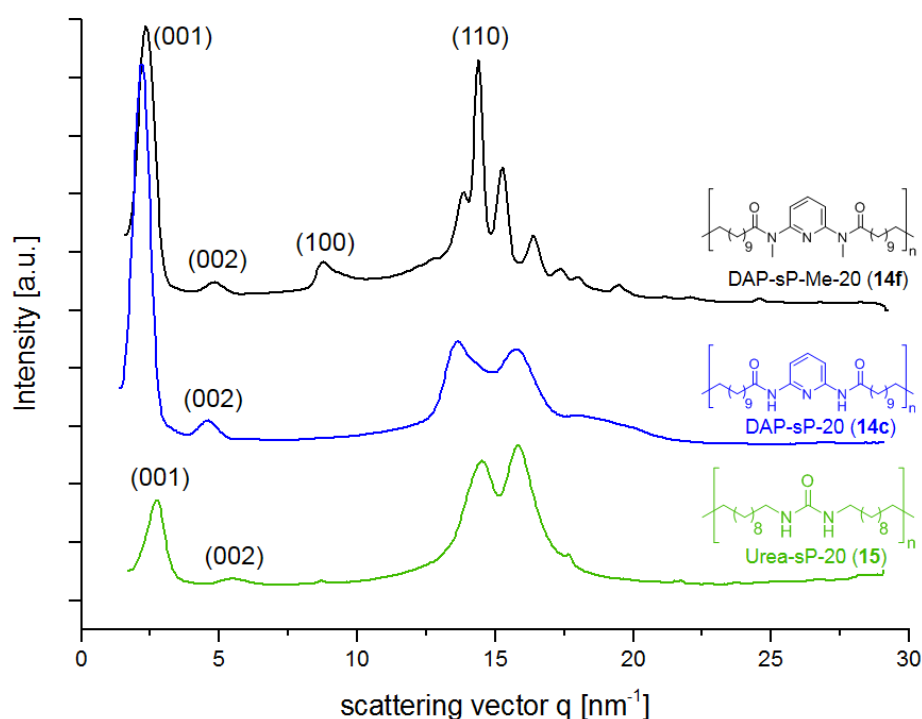


**Figure 38:** X-ray diffraction patterns of the annealed unprotected (**14c**) (blue), and protected (**14f**) (black) DAP containing polymers and the urea containing polymer (**15**) (green).

By assigning the reflexes to the corresponding planes of an orthorhombic crystal cell (for **14d-f**) the calculation of the unit cell parameters, listed in Table 4, was possible using the equations<sup>263</sup> given below

$$a = d_{(100)} \quad (15)$$

$$b = \sqrt{a^2 d_{(110)}^2 / (a^2 - d_{(110)}^2)} \quad (16)$$

where  $d_{(100)}$  and  $d_{(110)}$  are the distances of the (100) and (110) crystalline planes, which can be calculated from the Bragg equation

$$2d \sin \theta = n\lambda \quad (17)$$

where  $\theta$  is a Bragg angle of the relevant reflection and  $\lambda = 0.154$  nm is the wavelength of the used Cu-K $\alpha$  radiation.

**Table 4:** Unit cell parameters and lamellar crystal thicknesses of the saturated DAP containing polymers with methyl protection group (**14d-f**).

| polymer | $a$ [nm] | $b$ [nm] | $c$ [nm] | $l_c$ [nm] |
|---------|----------|----------|----------|------------|
| 14d     | 0.71     | 0.55     | 2.24     | 8.42       |
| 14e     | 0.71     | 0.55     | 2.44     | 12.11      |
| 14f     | 0.71     | 0.54     | 2.64     | 9.65       |

The comparison of these parameters with those of orthorhombic PE ( $a = 0.74$  nm,  $b = 0.49$  nm)<sup>220,292</sup> shows no big change in the  $a$ -direction but a certain dilation of the unit cell in the direction of the  $b$ -axis<sup>270</sup>, concluding the at least partial inclusion of the functional group into the crystalline region. The assumed structure of the unit cell is visualized in Figure 39a. The X-ray diffraction pattern of the unprotected DAP containing polymer **14c** (see Figure 38, blue curve) also features two peaks in the low angle range, representing the distance in the  $c$ -direction and can be assigned to the (001) and (002) reflex, indicating the preservation of the lamellar morphology.<sup>270</sup> Remarkable here is the disappearance of the signal at  $8.9$  nm<sup>-1</sup>, which indicates that the DAP units are not arranged parallel to each other anymore<sup>270</sup>, explainable by the shift of the polymer chains in either  $a$ - or  $c$ -direction or by tilting. The increase in the lamellar spacing  $d_{001}$  to  $2.92$  nm (compared to the protected polymer **14f**,  $d_{001} = 2.64$  nm) supports this hypothesis. Furthermore, a change in the wide angle range can be observed, where now the two signals at  $13.7$  nm<sup>-1</sup> and  $15.8$  nm<sup>-1</sup> are dominating, which could be assigned to the (100) and (010) planes of the triclinic crystal structure of PE, also reported for branched precision PE<sup>219,226,229</sup> Possibly, changing the supramolecular interactions from  $\pi$ - $\pi$ -stacking to hydrogen bonding leads to the change from the orthorhombic to the triclinic crystal structure. In this triclinic unit cell the DAP units would be arranged ladder-like in the direction of the  $b$ -axis (visualization in Figure 39b), which is in good agreement with the arrangement observed in low-molecular weight DAP containing compounds.<sup>293</sup> However, since only a few broad

signals are observable, which could superimpose other reflexes, no clear statement but an assumption regarding the crystal structure can be made.

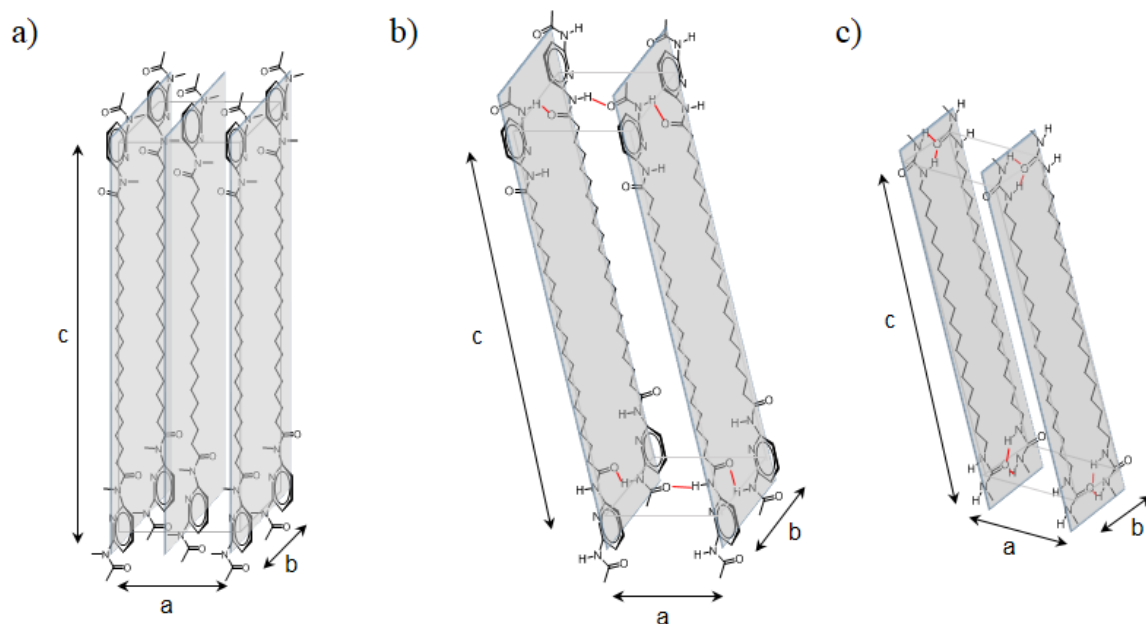


**Figure 39:** Estimated unit cell structures of the a) *N*-methyl protected DAP containing polymer (**14f**), b) the unprotected DAP containing polymer (**14c**) and c) the urea containing polymer (**15**).

The polymer containing a urea moiety (**15**) shows nearly the same diffraction pattern (see Figure 38, green curve) as the DAP containing polymer without protection group (**14c**). The signals at  $2.7 \text{ nm}^{-1}$  and  $5.4 \text{ nm}^{-1}$  in the small angle range represent the (001) and (002) plane, thus implying a lamellar morphology, which was also observed in low-molecular weight urea containing compounds interacting via hydrogen bonding<sup>294, 270</sup>. The signals representing the (100) and (010) planes can be observed at  $14.5 \text{ nm}^{-1}$  and  $15.8 \text{ nm}^{-1}$ , respectively. Shifting of the peaks in the small angle region as well as of the (100) peak to higher  $q$ -values compared to the DAP containing polymers indicate the contraction of the unit cell, which is logic due to the decreased defect size. Since here too only a few broad signals are observable, as in the case of the unprotected DAP containing polymer (**14c**), just an assumption regarding the crystal structure can be made and the estimated structure is visualized in Figure 39c.

Another indication for the at least partial inclusion of the functional groups into the crystalline lamella (beside the dilation of the unit cell) is the lamellar thickness, which was calculated with the help of the Scherrer equation given below<sup>270</sup>

$$l_c = \frac{K \cdot \lambda}{\Delta(2\theta) \cdot \cos \theta_{hkl}} \quad (18)$$

where  $\Delta(2\theta)$  is the full peak width at half maximum height (FWHM),  $K \sim 1$  is the dimensionless Scherrer constant,  $\lambda = 0.154 \text{ nm}$  is the wavelength of the used Cu- $K_\alpha$  radiation, and  $\theta_{hkl}$  is a Bragg angle of the relevant reflection.<sup>270</sup>



If the functional group would be excluded from the crystal, the lamellar crystal thickness would be equivalent to the length of the corresponding CH<sub>2</sub>-chain. Assuming an all-*trans* geometry a length of 1.88 nm for the C<sub>16</sub>-chain, 2.13 nm for C<sub>18</sub> and 2.38 nm for C<sub>20</sub> would be expected. All of the calculated values for the lamellar crystal thickness, which range between 8.42 nm and 12.11 nm (see Table 4) exceeded these values, which further hints toward the inclusion of 3-5 functional groups into one crystal lamella.<sup>270</sup>

### 3.7 DLS analysis

Precision polymers bearing supramolecular, complementary recognition groups (i.e. diaminopyridine-thymine or cyanuric acid-Hamilton wedge)<sup>295,296</sup> at preselected points within the polymer backbone tend to fold themselves into well-defined three-dimensional architectures in highly diluted solutions ( $c < 1$  mM) forming so-called single-chain polymer nanoparticles (SCNPs) via intramolecular coupling.<sup>297</sup>

Thus, the saturated, *N*-methyl protected DAP containing polymers (**14d-f**) were analyzed via DLS measurements to determine their self-assembly behavior in solution. Initially, the self-assembly of the polymers was explored in two different solvents, CHCl<sub>3</sub> and THF, at a concentration of 2 mg/mL and the particle formation was observed for 3 h. The results are displayed in Figure 40.

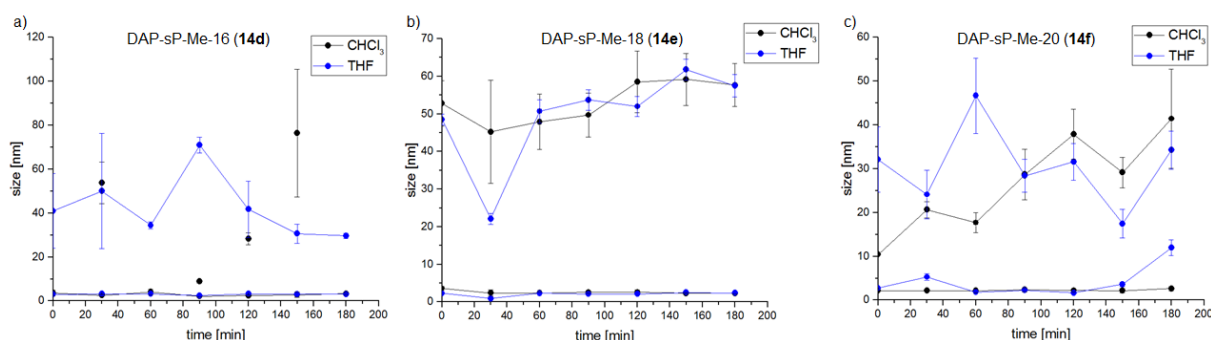


**Figure 40:** Time-dependent DLS measurements of a) DAP-sP-Me-16 (**14d**), b) DAP-sP-Me-18 (**14e**) and c) DAP-sP-Me-20 (**14f**) at 2 mg/mL in CHCl<sub>3</sub> (black) or THF (blue).

All polymers show the formation of small and intermediate particles with sizes ranging from 2-4 nm or 40-60 nm, respectively, which are not changing significantly with the time. Also the methylene spacer lengths as well as the choice of solvent does seem to have no influence on the particle size. Afterwards the concentration dependence in CHCl<sub>3</sub> was determined, whereby concentrations ranging from 0.001 mg/mL to 5 mg/mL were used and the results are shown in Figure 41.

Especially at the lowest concentration of 0.001 mg/mL all polymers show the formation of small particles with a size of 2-4 nm. These particles are assumed to consist of a single-polymer chain, also observed for other precision polymers under diluted ( $\sim 10^{-5}$  to  $10^{-6}$  M) conditions.<sup>295,298-300</sup> Possibly, so-called single-chain polymer nanoparticles are formed through intramolecular chain collapse, triggered by a non-covalent crosslinking via  $\pi$ - $\pi$ -stacking of the DAP units, comparable to observations for other supramolecular precision polymers bearing

anthracene<sup>301</sup> or phenyl and 2,3,4,5,6-pentafluorophenyl<sup>302</sup> moieties. The size of 2-4 nm also matches the size range for SCNPs given in literature.<sup>300,303</sup> At concentrations higher than 0.001 mg/mL bigger particles (40-60 nm) appear, which are aggregations of more than one polymer chain formed by intermolecular interactions. The self-assembly of DAP-sP-Me-20 (**14f**) into SCNPs at  $c = 0.001$  mg/mL and into aggregates at  $c > 1$  mM was also proven via TEM measurements and the corresponding images are shown in Figure 41d and e.

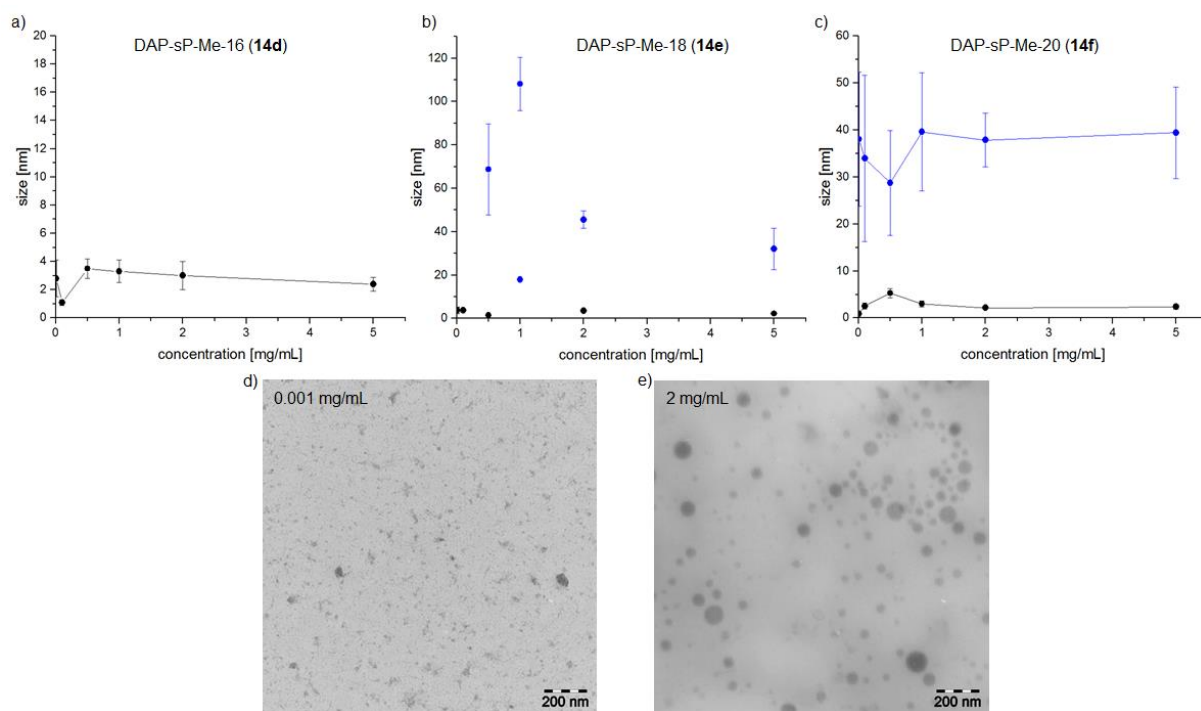


**Figure 41:** Concentration-dependent DLS measurements of a) DAP-sP-Me-16 (**14d**), b) DAP-sP-Me-18 (**14e**) and c) DAP-sP-Me-20 (**14f**) in  $\text{CHCl}_3$  as well as TEM images of DAP-sP-Me-20 (**14e**) at d) 0.001 mg/mL and e) 2 mg/mL.

Furthermore, different portions of methanol or hexane were added to the solutions to test the dependence of polarity on the particle size and the results are visualized in Figure 42. Decreasing the polarity by addition of hexane seem to have no significant influence on the particle size measured by DLS, but a look at the corresponding TEM image (see Figure 42c) indicates a change in structure. The former round particles (see Figure 41e) transformed into a thread-like network, whereby the single strings could be identified as the extended polymer chains. Due to the good solubility of the oligoethylene chains in hexane the polymer-solvent interactions exceed the polymer-polymer attraction forces leading to a complete solvation of the chain segments and thus the adoption of an unfolded conformation. Conversely, increasing the polarity by the addition of methanol leads to an increase in particle size up to  $\sim 200$  nm, as soon as the methanol content exceeds 25 vol%, followed by the precipitation of the polymers DAP-sP-Me-16 (**14d**) and DAP-sP-Me-18 (**14e**).

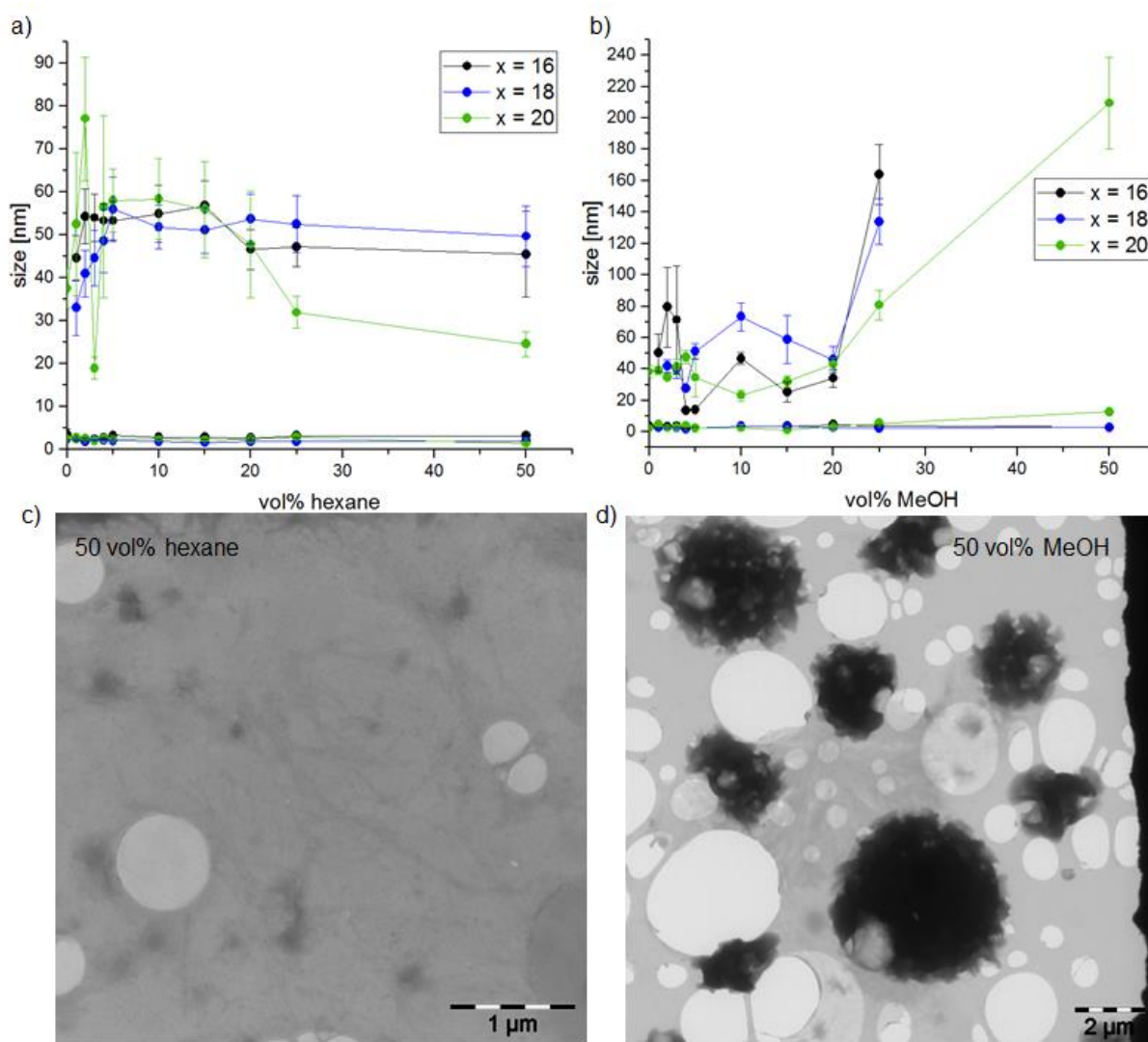


**Figure 42:** Change of the particle size with increasing a) hexane or b) methanol content as well as TEM images of DAP-sP-Me-20 (**14f**) in c) CHCl<sub>3</sub>:hexane (50:50) and d) CHCl<sub>3</sub>:methanol (50:50).

By increasing the methanol content to 50 vol% or higher also DAP-sP-Me-20 (**14f**) starts to precipitate and the corresponding TEM image (Figure 42d) shows the formation of big aggregates with sizes up to several micrometers.

### 3.8 Fractionation of the *N*-methyl protected DAP containing polymer (**14f**) via preparative GPC and subsequent analysis

Due to the synthesis of all polymers via ADMET polymerization (non-living polycondensation) they exhibit broad polydispersity indices ranging from 1.4 to 2.4. To determine how much the polydispersity influences the melting and crystallization behavior the saturated *N*-methyl protected DAP containing polymer with a methylene spacer length of 20 (**14f**) was fractionated via preparative GPC using THF as solvent and the corresponding fractionation pattern is shown in Figure 43.

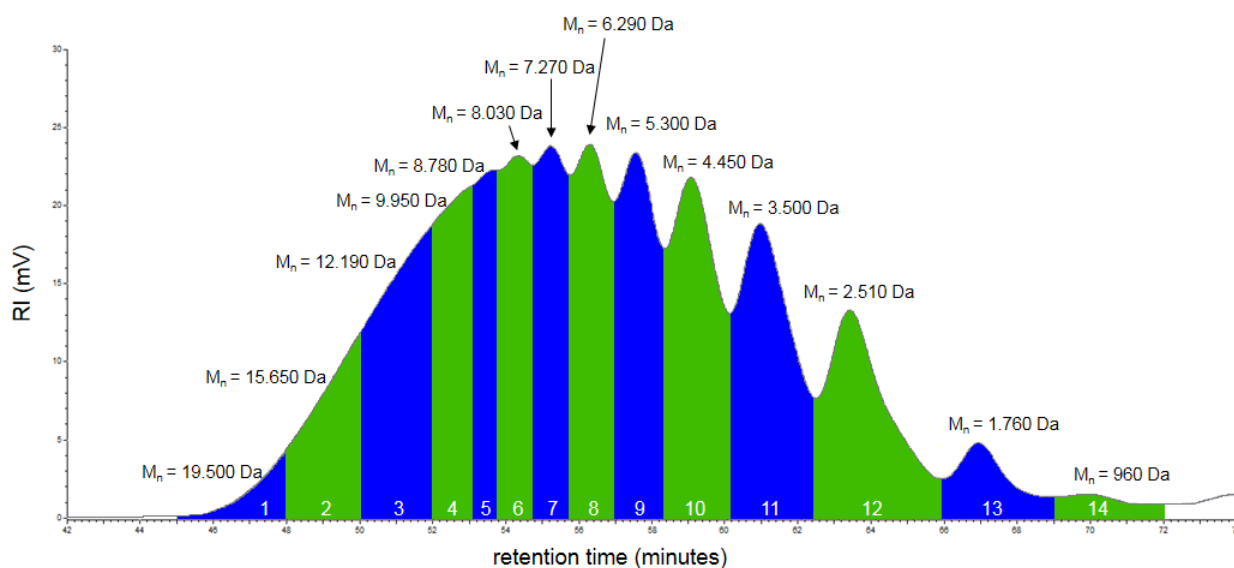


**Figure 43:** GPC trace of the fractionation of DAP-sP-Me-20 (**14f**) via preparative GPC.

The polymer was separated into 14 different fractions, which were dried under high vacuum before determining the molecular weights via GPC and MALDI ToF MS analysis and the corresponding spectra are shown in Figure 44 and Figure 45.

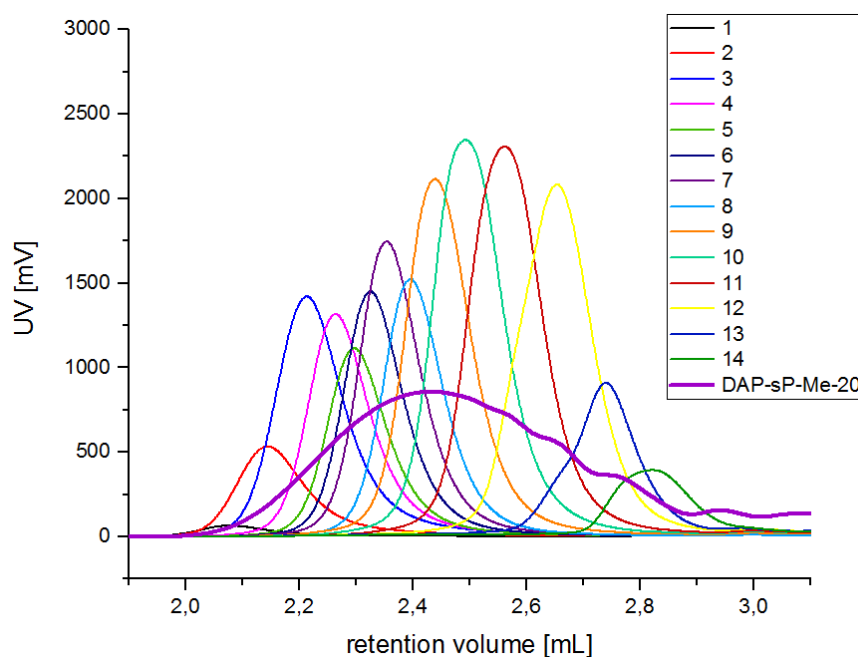


**Figure 44:** GPC traces of the individual fractions of DAP-sP-Me-20 (**14f**).

The GPC traces show monomodal distributions and shift to higher retention volumes with increasing fraction number as expected. Starting from a polymer with a molecular weight of 6380 g/mol and a PDI of 1.8 fractions with molar masses ranging from 19500 g/mol to 960 g/mol and PDIs of about 1.1 were obtained. The molecular weight data for all fractions are listed in Table 5.

MALDI ToF MS spectra were recorded using DCTB as matrix and LiTFA as salt. Here as well the molecular weight is decreasing with increasing fraction number, whereby MALDI ToF MS shows smaller values compared to GPC results, explainable by the hampered vaporization and detection of heavier polymer species. For each fraction two series can be observed, whereby the distance between two peaks of each series accounts 471 Da, reflecting the mass of the repetitive DAP unit.

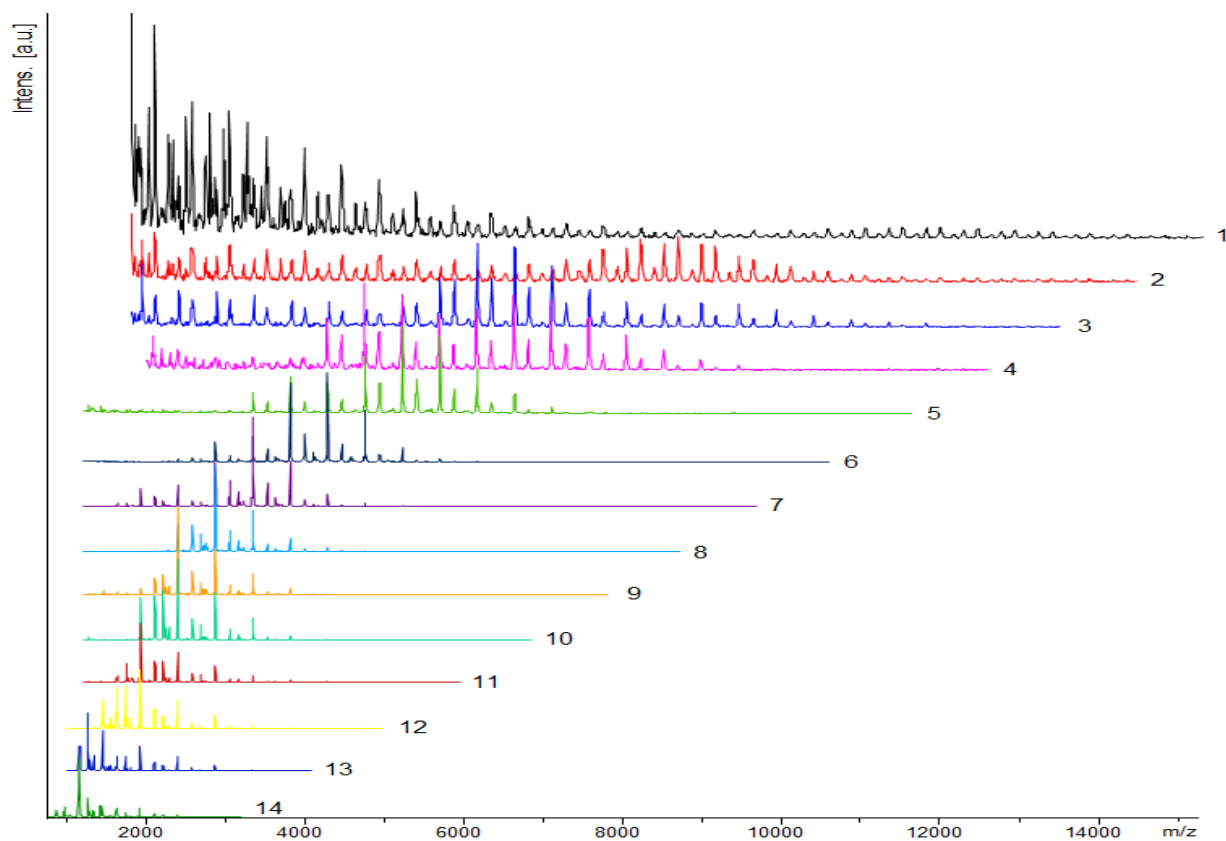


**Figure 45:** MALDI ToF MS analysis of the individual fractions of DAP-sP-Me-20 (**14f**).

The main series can be assigned to the respective Li adducts ( $[M+Li]^+$ ) and matches the simulations very well.

**Table 5:** Molecular weight data and thermal properties of the different fractions achieved by the fractionation of DAP-sP-Me-20 (**14f**).

| fraction | $M_n$ [g/mol] | PDI | $T_m$ [°C] | $\Delta H_m^0$ [kJ/mol] | $X_c$ <sup>a)</sup> [%] |
|----------|---------------|-----|------------|-------------------------|-------------------------|
| 1        | 19500         | 1.3 | -          | -                       | -                       |
| 2        | 15650         | 1.2 | 54.6       | 26.45                   | 1                       |
| 3        | 12190         | 1.1 | 56.7       | 70.70                   | 2                       |
| 4        | 9950          | 1.1 | 55.3       | 29.95                   | 1                       |
| 5        | 8780          | 1.1 | 51.4       | 17.91                   | 1                       |
| 6        | 8030          | 1.1 | 54.5       | 46.57                   | 2                       |
| 7        | 7270          | 1.1 | 53.7       | 27.55                   | 1                       |
| 8        | 6290          | 1.1 | 52.9       | 23.21                   | 1                       |
| 9        | 5300          | 1.1 | 56.5       | 82.31                   | 6                       |
| 10       | 4450          | 1.1 | 52.5       | 42.99                   | 4                       |
| 11       | 3500          | 1.1 | 46.0       | 9.98                    | 1                       |
| 12       | 2510          | 1.1 | 37.7       | 4.54                    | 1                       |
| 13       | 1760          | 1.1 | -          | -                       | -                       |
| 14       | 960           | 1.6 | -          | -                       | -                       |

<sup>a)</sup> calculated via equation (14).

Thermal behavior of the individual fractions was determined via DSC measurements and the corresponding data are listed in Table 5. Nearly all fractions exhibit melting points ranging from 51 °C to 56 °C (thermograms are shown in Figure A 55) and crystallinities of 1-6 %. Fractions 1, 13 and 14 could not be characterized due to the lack of substance. Because of the decreasing molecular weight of fractions 11 and 12 the melting temperatures are also decreasing to 46 °C and 37.7 °C, respectively.

Furthermore, WAXS measurements were performed for the fractions with molecular weights of approximately 12000, 7000 and 3000 g/mol (fractions 3, 7 and 12) and the corresponding diffraction patterns, which are displayed in Figure 46, resemble the pattern of the precursor polymer (cf. Figure 38, black curve). Although, the signals become broader with decreasing molecular weight due to the elevation of the amorphous fraction, an orthorhombic crystal structure can be assumed. The signals at  $2.1 < q < 2.3 \text{ nm}^{-1}$  and  $4.3 < q < 4.8 \text{ nm}^{-1}$  can be assigned to the (001) reflection and the corresponding second order peak (002), indicating a lamellar morphology. Additionally, the (100) and (110) reflections are visible at  $q \sim 8.8 \text{ nm}^{-1}$  and  $q \sim 14.5 \text{ nm}^{-1}$ . The corresponding unit cell parameters as well as the lamellar crystal thicknesses were calculated according to equations (15), (16) and (18) and are listed in Table 6.

**Table 6:** Unit cell parameters ( $a$ ,  $b$  and  $c$ ) and lamellar crystal thicknesses ( $l_c$ ) of the fractions 3, 7 and 12 achieved by the fractionation of DAP-sP-Me-20 (**14f**).

| fraction | $a$ [nm] | $b$ [nm] | $c$ [nm] | $l_c$ [nm] |
|----------|----------|----------|----------|------------|
| 3        | 0.71     | 0.54     | 2.75     | 12.15      |
| 7        | 0.72     | 0.54     | 2.75     | 11.55      |
| 12       | 0.71     | 0.54     | 2.94     | 13.66      |

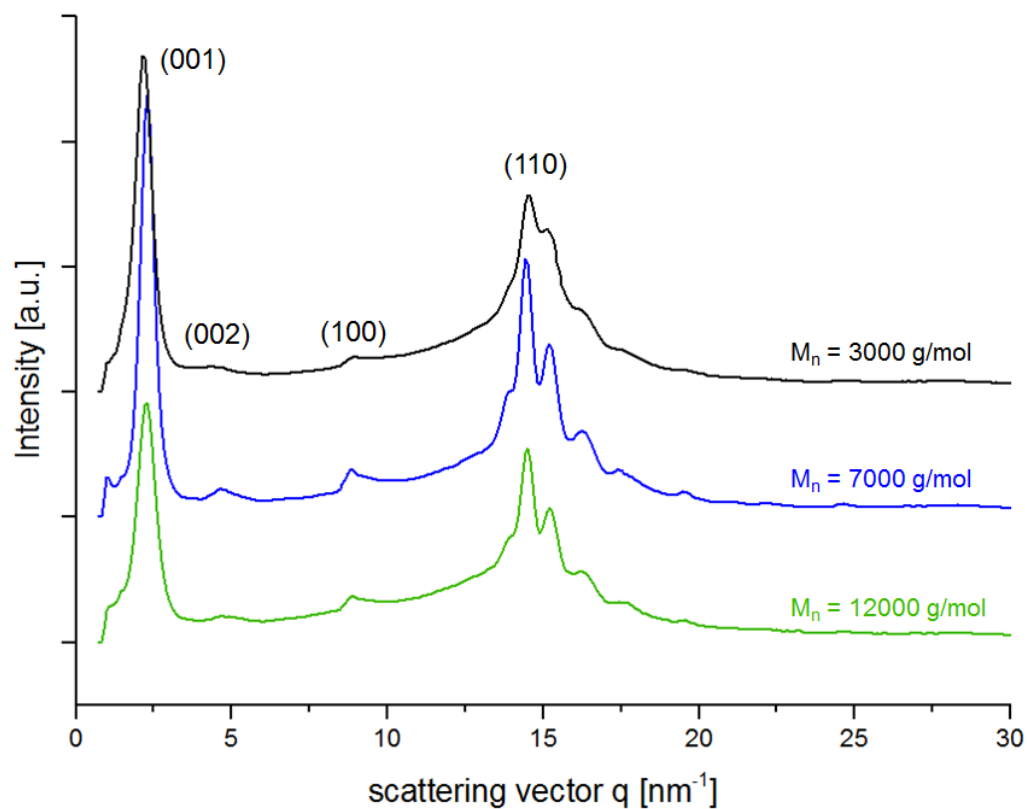


**Figure 46:** X-ray diffraction patterns of the fractions 3 (green), 7 (blue) and 12 (black).

## 4. Experimental Part

### 4.1 Materials

2,6-Diaminopyridine (98 %), 9-decenoic acid (90 %), 10-undecenoic acid (99 %), 11-bromo-1-undecene (95 %), methyl iodide (99 %), sodium hydride (60 % dispersion in mineral oil), lithium aluminum hydride (95 %), ethylene carbonate (98 %), triazabicyclo[4.4.0]dec-5-ene, sodium bicarbonate, ethyl vinyl ether (98 %), phosphoric acid (85 %), Grubbs' 1<sup>st</sup>, 2<sup>nd</sup> and 3<sup>rd</sup> generation catalyst, Grubbs' Hoveyda 1<sup>st</sup> generation catalyst, phenyl phosphoric acid, poly-(4-vinylpyridin) (average  $M_w \sim 60000$  g/mol), *p*-toluenesulfonyl hydrazide (99 %), *N,N*-diisopropylethylamine (99 %) and carbon tetrachloride (99 %) were purchased from Sigma Aldrich. Magnesium sulfate (99 %), 1-ethyl-3-(3-dimethylaminopropyl)carbodiimid (99 %), tin(II) bromide (99.4 %), 2,6-dichloro-1,4-benzoquinone (98 %) and triphenylphosphine were received from Alfa Aesar. Sodium hydroxide and hydrochloric acid were purchased from Grüssing, while diethyl malonate (99 %) and 4-amino-2,2,6,6-tetramethylpiperidine-1-oxyl (97 %) were bought from TCI. Sodium sulfate was received from Carl Roth and benzyl bromide (98 %) from Fluka. The Umicore M1 catalyst was received from Umicore AG. Ammonium hydroxide solution (25 %  $\text{NH}_3$ ) was purchased from VWR and tin(II) chloride was received from Merck. All chemicals were used without further purification if not mentioned otherwise.

Sodium hydride (60 % dispersion in mineral oil) was washed several times with dry THF and stored under an atmosphere of nitrogen before use.

All solvents were purchased in technical grade and were either distilled and/or dried using standard methods. THF was predried over potassium hydroxide and freshly distilled from sodium/benzophenone under an atmosphere of dry nitrogen. DCM was predried over calcium chloride and freshly distilled from calcium hydride before use.  $\text{Et}_2\text{O}$  and toluene were predried over calcium chloride and freshly distilled from sodium/benzophenone under an atmosphere of dry nitrogen.

11-Dodecenoic acid, 9-decenoyl chloride, 10-undecenoyl chloride and 11-dodecenoyl chloride were synthesized according to literatures<sup>98,274</sup> as described in a previous investigation.<sup>272</sup>

### 4.2 Instrumentation

NMR (nuclear magnetic resonance) spectroscopy measurements were conducted on a Varian Gemini 400 ( $^1\text{H}$ -NMR at 400 MHz and  $^{13}\text{C}$ -NMR at 101 MHz) or on a Varian Unity Inova 500 ( $^1\text{H}$ -NMR at 500 MHz and  $^{13}\text{C}$ -NMR at 126 MHz) at 27 °C using  $\text{CDCl}_3$  (Chemotrade, 99.8 Atom%D) and  $\text{THF-d}_8$  (Chemotrade, 99.5 Atom%D) as solvents and tetramethylsilane as internal standard. The coupling constants were given in Hz and the chemical shifts ( $\delta$ ) in ppm and referred to the solvent residue peak [ $\text{CDCl}_3$  7.26 ppm ( $^1\text{H}$ ) and 77.0 ppm ( $^{13}\text{C}$ );  $\text{THF-d}_8$  3.58 and 1.72 ppm ( $^1\text{H}$ ) and 67.2 and 25.3 ppm ( $^{13}\text{C}$ )]. For the interpretation of the spectra MestReNova v. 8.0.0-10524 was used.



Gel permeation chromatography (GPC) measurements were performed on a Viscotek GPCmax VE2001, equipped with a GMH<sub>HR</sub>-N-18055 and a ST-3000 column in THF at 25-30 °C with a sample concentration of 1 mg/mL. The injection volume was 100 µL and the detection was accomplished by refractive index using a VE3580 RI detector or via UV detection (Viscotek, model no. 2600) at 35 °C and a flow rate of 1 mL/min. Polystyrene standards with molecular weights of 1050, 2790, 6040, 13 400 and 29 600 g/mol were used for external calibration.

Preparative gel permeation chromatography was performed on a Hitachi Chromaster System from VWR, equipped with a GPC KF-2002.5 and a GPC KF-LG column from Shodex in THF at 30 °C with a sample concentration of 30 mg/mL. The injection volume was 400 µL and the detection was accomplished by refractive index using a Chromaster HPLC 5450 RI detector at 35 °C and a flow rate of 0.7 mL/min. The fractionation of the sample was accomplished with a Foxy<sup>®</sup> R2 fraction collector from Teledyne ISCO. The processing of the data was carried out using EZChrom Elite Version 3.3.2 SP2 from Agilent.

Electrospray ionization time of flight mass spectrometry (ESI ToF MS) measurements were performed on a Bruker Daltonics Focus microTOF. The sample was dissolved in methanol (HPLC grade, purchased from Sigma-Aldrich) at a concentration of 1 mg/mL without additional salt and directly injected using a flow rate of 180 µL/h. Measurements were performed in the positive mode with an acceleration voltage of 4.5 kV, a transfer line of 190 °C and a scan range of 100-1500 m/z. The processing of the data was carried out using Bruker Daltonics ESI compass 1.3 for MicroTOF (DataAnalysis Version 4.0).

Matrix-assisted laser desorption/ionization mass spectrometry (MALDI ToF MS) measurements were performed on a Bruker Autoflex III System from Bruker Daltonics operating in linear and reflection mode. Ions were formed by laser desorption (smart beam laser at 355, 532, 808 and 1064 ± 5 nm; 3 ns pulse width; up to 2500 Hz repetition rate), accelerated by a voltage of 19-20 kV and detected as positive ions. The matrix *trans*-2-[3-(4-*tert*-butylphenyl)-2-methyl-2-propenylidene]malononitrile (received from Sigma-Aldrich), the salts lithiumtrifluoroacetate and sodiumtrifluoroacetate (purchased from Sigma-Aldrich) as well as the polymer samples were dissolved in THF or methanol with a concentration of 20 mg/mL each. The solutions of the matrix, the polymer and the salt were mixed in a volume ratio of 25:5:1 or 1:1:1 and 1 µL of each mixture was spotted on the MALDI target. A poly(ethylene glycol) monomethyl ether (PEG-OCH<sub>3</sub>) standard (M<sub>n</sub> = 4200 g/mol, M<sub>w</sub>/M<sub>n</sub> = 1.05) was used for external calibration. The interpretation of the data was carried out using flexAnalysis Version 3.4 (build 76) from Bruker.

Fourier-transform infrared (FTIR) spectroscopy was performed as KBr pellet on a Bruker Vertex 70 MIR using Opus 6.5 and OriginPro 2016G for data interpretation.

Differential scanning calorimetry (DSC) measurements were conducted on a NETZSCH DSC 204F1 Phoenix, which was calibrated with indium, tin and zinc. The samples (3-10 mg) were filled into standard aluminum pans with a pierced lid, heated above their melting point and cooled below their crystallization temperature to erase the previous thermal history. Afterwards

the samples were subjected to a thermal program using a heating rate of 10 K/min. The obtained data was processed with NETZSCH Proteus - Thermal Analysis - Version 5.2.1 and OriginPro 2016G.

Initial X-ray diffraction measurements were performed on a glass plate by cooling the samples from the isotropic liquid on a temperature-controlled heating stage. The two-dimensional patterns were recorded by an area detector VÅNTEC500 (Bruker AXS) using Ni-filtered  $\text{CuK}_\alpha$  radiation at a sample-detector distance of 8.95 cm and an exposure time of 30 min.

Further X-ray scattering experiments were conducted in transmission mode using a SAXSLAB laboratory setup (Retro-F), equipped with an AXO microfocus X-ray source with an AXO multilayer X-ray optic (ASTIX) as monochromator for  $\text{CuK}_\alpha$  radiation ( $\lambda = 0.154$  nm). A DECTRIS PILATUS3 R 300K detector was used to record the two-dimensional scattering patterns at various temperatures ( $q = 0.05\text{-}3$  nm<sup>-1</sup>;  $q = 0.25\text{-}7$  nm<sup>-1</sup> and  $q = 1\text{-}29$  nm<sup>-1</sup>). Aluminum discs (2 mm thickness) with a central hole were used as sample holders.

Dynamic light scattering (DLS) experiments were performed in chloroform, tetrahydrofuran or mixtures of these solvents with methanol or hexane at different concentrations on a Viscotek 802. The received data was processed with OmniSIZE Version 3.0.0 292 from Viscotek.

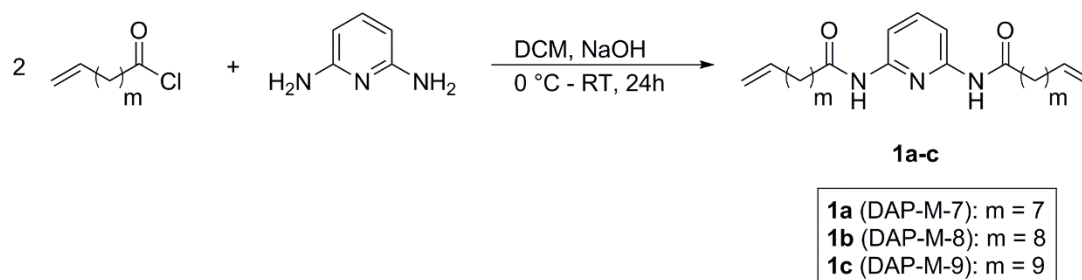
Transmission Electron Microscopy (TEM) measurements were conducted on an EM 900 transmission electron microscope from Carl Zeiss. The samples were dissolved in chloroform or tetrahydrofuran with a concentration of 2 mg/mL and 0.001 mg/mL and 5  $\mu\text{L}$  of these solutions were spread onto a copper grid coated with a carbon film. After one minute the excessive solution was removed with a piece of filter paper. The samples were stained with a uranyl acetate solution (1 % in  $\text{H}_2\text{O}$ ). TEM images were taken using a SSCCD SM-1k-120 camera from TRS.

Thin-layer chromatography (TLC) was carried out on Merck TLC aluminum sheets (silica gel 60 F254). The resulting spots were visualized by UV light (254 nm) or by wetting the sheets with the oxidizing agent “blue stain” and subsequent heating. The stain was prepared by dissolving  $\text{Ce}(\text{SO}_4)_2 \cdot 4\text{H}_2\text{O}$  and  $(\text{NH}_4)_6\text{Mo}_7\text{O}_{24} \cdot 4\text{H}_2\text{O}$  in a mixture of distilled water and concentrated sulfuric acid.

Column chromatography was performed with Kieselgel 60 (230-400 mesh), which was purchased from Merck.

## 4.3 Monomer synthesis

### 4.3.1 Synthesis of the diaminopyridine containing monomers (**1a-c**)



**Scheme 11:** Synthesis of the diaminopyridine monomers with varying alkyl chain lengths (**1a-c**).

All monomers containing the diaminopyridine-moiety were synthesized according to previous investigations,<sup>269,270,272</sup> which were inspired by literature<sup>273</sup> using a Schotten-Baumann reaction. 2,6-Diaminopyridine (4.61 mmol, 0.50 g) and NaOH (9.22 mmol, 0.37 g), dissolved in water, were placed in a one-necked round bottom flask and cooled to 0 °C with the help of an ice-water bath. Furthermore, dec-9-enoyl chloride (10.60 mmol, 2.00 g) was dissolved in DCM and added slowly to the cold mixture over a period of 15 min. After stirring the mixture for 2 h the phases were separated and the organic layer was dried over Na<sub>2</sub>SO<sub>4</sub>, followed by the evaporation of the solvent in vacuum at 45 °C. The crude product was purified via column chromatography (silica gel 60, hexane/EA 8:2) to yield DAP-M-7 (**1a**) as white solid (4.29 mmol, 1.77 g, 93 %). The monomers **1b** and **1c** were synthesized analogously to this procedure with yields ranging from 92-94 %. NMR spectra and ESI ToF MS analyses are shown in Figures A 1-A 6.

#### **1a (DAP-M-7):**

##### <sup>1</sup>H-NMR (400 MHz, CDCl<sub>3</sub>)

$\delta$  = 7.87 (*t*, 1H, <sup>3</sup>*J*<sub>H,H</sub> = 8.3 Hz, *CH*), 7.60 (*d*, 2H, <sup>3</sup>*J*<sub>H,H</sub> = 8.3 Hz, *CH*), 5.91 – 5.68 (*m*, 2H, *CH=CH*<sub>2</sub>), 5.04 – 4.86 (*m*, 4H, *CH*<sub>2</sub>=*CH*), 2.71 (*t*, 4H, <sup>3</sup>*J*<sub>H,H</sub> = 7.5 Hz, *CH*<sub>2</sub>), 2.08 – 1.93 (*m*, 4H, *CH*<sub>2</sub>), 1.83 – 1.70 (*m*, 4H, *CH*<sub>2</sub>), 1.44 – 1.17 (*m*, 16H, *CH*<sub>2</sub>) ppm.

##### <sup>13</sup>C-NMR (101 MHz, CDCl<sub>3</sub>)

$\delta$  = 176.9 (*C=O*), 145.7 (*C*<sub>quart.</sub>), 145.5 (*Ar-C*), 139.1 (*CH=CH*<sub>2</sub>), 114.4 (*CH*<sub>2</sub>=*CH*), 107.9 (*Ar-C*), 37.3 (*CH*<sub>2</sub>), 33.9 (*CH*<sub>2</sub>), 29.3 (*CH*<sub>2</sub>), 29.2 (*CH*<sub>2</sub>), 29.0 (*CH*<sub>2</sub>), 29.0 (*CH*<sub>2</sub>), 24.8 (*CH*<sub>2</sub>) ppm.

##### ESI ToF MS [m/z]

[*M*+Na]<sup>+</sup> C<sub>25</sub>H<sub>39</sub>Na<sub>1</sub>N<sub>3</sub>O<sub>2</sub><sup>+</sup>: calculated 436.2934 g/mol, found 436.3250 g/mol.

##### IR (KBr) [cm<sup>-1</sup>]

3310 (*s*), 2923 (*s*), 2850 (*s*), 1670 (*s*), 1590 (*s*), 1525 (*s*), 1470 (*s*), 1414 (*m*), 1306 (*m*), 1243 (*w*), 1181 (*w*), 993 (*w*), 912 (*m*), 723 (*w*), 635 (*m*).

##### R<sub>f</sub> (TLC) [hexane/EA 8:2]

0.49

**1b (DAP-M-8):**<sup>1</sup>H-NMR (400 MHz, CDCl<sub>3</sub>)

δ = 7.88 (*d*, 2H, <sup>3</sup>J<sub>H,H</sub> = 8.0 Hz, *CH*), 7.69 (*t*, 1H, <sup>3</sup>J<sub>H,H</sub> = 8.1 Hz, *CH*), 7.61 (*s*, 2H, *NH*), 5.95 – 5.69 (*m*, 2H, *CH=CH*<sub>2</sub>), 5.11 – 4.84 (*m*, 4H, *CH*<sub>2</sub>=*CH*), 2.36 (*t*, 4H, <sup>3</sup>J<sub>H,H</sub> = 7.5 Hz, *CH*<sub>2</sub>), 2.10–1.92 (*m*, 4H, *CH*<sub>2</sub>), 1.82 – 1.60 (*m*, 4H, *CH*<sub>2</sub>), 1.47 – 1.16 (*m*, 20H, *CH*<sub>2</sub>) ppm.

<sup>13</sup>C-NMR (101 MHz, CDCl<sub>3</sub>)

δ = 171.7 (*C=O*), 149.4 (*C*<sub>quart.</sub>), 141.1 (*Ar-C*), 139.3 (*CH=CH*<sub>2</sub>), 114.3 (*CH*<sub>2</sub>=*CH*), 109.4 (*Ar-C*), 38.0 (*CH*<sub>2</sub>), 33.9 (*CH*<sub>2</sub>), 29.4 (*CH*<sub>2</sub>), 29.3 (*CH*<sub>2</sub>), 29.2 (*CH*<sub>2</sub>), 29.2 (*CH*<sub>2</sub>), 29.0 (*CH*<sub>2</sub>) 25.4 (*CH*<sub>2</sub>) ppm.

ESI ToF MS [m/z]

[*M*+*Na*]<sup>+</sup> C<sub>27</sub>H<sub>43</sub>Na<sub>1</sub>N<sub>3</sub>O<sub>2</sub><sup>+</sup>: calculated 464.3247 g/mol, found 464.3571 g/mol; [*M*+*K*]<sup>+</sup> C<sub>27</sub>H<sub>43</sub>K<sub>1</sub>N<sub>3</sub>O<sub>2</sub><sup>+</sup>: calculated 480.2987 g/mol, found 480.3307 g/mol.

IR (KBr) [cm<sup>-1</sup>]

3316 (*s*), 2921 (*s*), 2849 (*s*), 1671 (*s*), 1590 (*s*), 1524 (*s*), 1470 (*s*), 1412 (*m*), 1304 (*m*), 1243 (*w*), 1180 (*w*), 991 (*w*), 911 (*m*), 724 (*w*), 636 (*m*).

R<sub>f</sub> (TLC) [hexane/EA 8:2]

0.53

**1c (DAP-M-9):**<sup>1</sup>H-NMR (400 MHz, CDCl<sub>3</sub>)

δ = 7.89 (*d*, 2H, <sup>3</sup>J<sub>H,H</sub> = 8.0 Hz, *CH*), 7.69 (*t*, 1H, <sup>3</sup>J<sub>H,H</sub> = 8.1 Hz, *CH*), 7.56 (*s*, 2H, *NH*), 5.89 – 5.73 (*m*, 2H, *CH=CH*<sub>2</sub>), 5.05 – 4.87 (*m*, 4H, *CH*<sub>2</sub>=*CH*), 2.37 (*t*, 4H, <sup>3</sup>J<sub>H,H</sub> = 7.5 Hz, *CH*<sub>2</sub>), 2.12 – 1.97 (*m*, 4H, *CH*<sub>2</sub>), 1.80 – 1.66 (*m*, 4H, *CH*<sub>2</sub>), 1.46 – 1.18 (*m*, 24H, *CH*<sub>2</sub>) ppm.

<sup>13</sup>C-NMR (101 MHz, CDCl<sub>3</sub>)

δ = 171.7 (*C=O*), 149.5 (*C*<sub>quart.</sub>), 141.1 (*Ar-C*), 139.3 (*CH=CH*<sub>2</sub>), 114.3 (*CH*<sub>2</sub>=*CH*), 109.5 (*Ar-C*), 38.0 (*CH*<sub>2</sub>), 33.9 (*CH*<sub>2</sub>), 29.6 (*CH*<sub>2</sub>), 29.5 (*CH*<sub>2</sub>), 29.5 (*CH*<sub>2</sub>), 29.3 (*CH*<sub>2</sub>), 29.2 (*CH*<sub>2</sub>), 29.1 (*CH*<sub>2</sub>), 25.5 (*CH*<sub>2</sub>) ppm.

ESI ToF MS [m/z]

[*M*+*Na*]<sup>+</sup> C<sub>29</sub>H<sub>47</sub>Na<sub>1</sub>N<sub>3</sub>O<sub>2</sub><sup>+</sup>: calculated 492.3560 g/mol, found 492.3496 g/mol; [*M*+*K*]<sup>+</sup> C<sub>29</sub>H<sub>47</sub>K<sub>1</sub>N<sub>3</sub>O<sub>2</sub><sup>+</sup>: calculated 508.3300 g/mol, found 508.3236 g/mol.

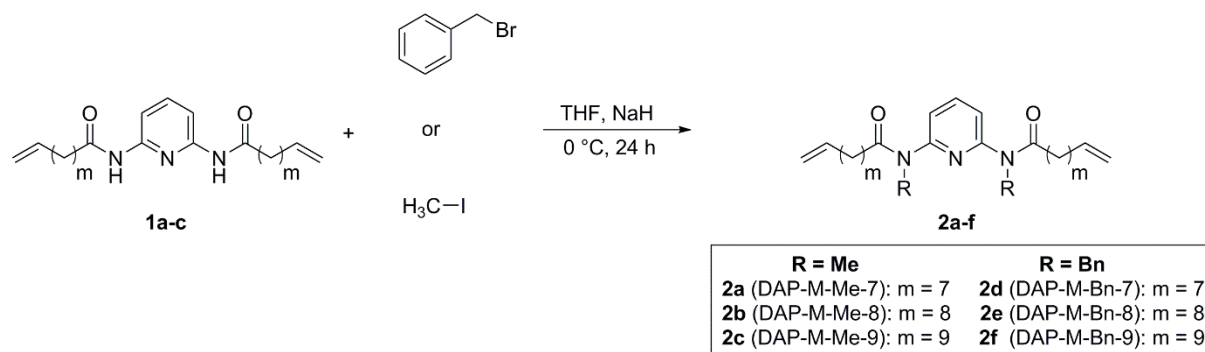
IR (KBr) [cm<sup>-1</sup>]

3314 (*s*), 2921 (*s*), 2849 (*s*), 1671 (*s*), 1590 (*s*), 1524 (*s*), 1470 (*s*), 1412 (*m*), 1308 (*m*), 1242 (*w*), 1180 (*w*), 991 (*w*), 911 (*m*), 724 (*w*), 638 (*m*).

R<sub>f</sub> (TLC) [hexane/EA 8:2]

0.58

### 4.3.2 Protection of the amide moieties



**Scheme 12:** Synthesis of the *N*-methyl or *N*-benzyl-protected diaminopyridine monomers (**2a-f**).

The introduction of the methyl or benzyl protection groups was accomplished according to previous investigations<sup>269,270,272,275</sup> under a dry, inert atmosphere of nitrogen. A two-necked round bottom flask, equipped with a rubber septum and a gas tap was filled with the unprotected monomer **1a** (2.42 mmol, 1.00 g) and methyl iodide (5.80 mmol, 0.36 mL), which were dissolved in dry THF, and cooled to 0 °C. After the portion-wise addition of NaH (5.80 mmol, 0.14 g) the reaction mixture was allowed to stir overnight at room temperature, followed by pouring it carefully into ice water. The reaction mixture was extracted with ethyl acetate and the combined organic layers were washed with water and dried over MgSO<sub>4</sub>. Removal of the solvent in vacuum at 45 °C yielded the crude product, which was further purified via column chromatography (silica gel 60, hexane/EA 8:2) whereby **2a** was obtained as pale yellow oil (1.80 mmol, 0.79 g, 74 %). The protected monomers **2b-f**, were synthesized analogously to this procedure with yields ranging from 69-82 %. Introduction of a benzyl protection group was accomplished by using benzyl bromide instead of methyl iodide. NMR spectra and ESI ToF MS analyses are shown in Figures A 7-A 16.

#### **2a (DAP-M-Me-7):**

##### <sup>1</sup>H-NMR (400 MHz, CDCl<sub>3</sub>)

$\delta$  = 7.75 (*t*, 1H, <sup>3</sup>*J*<sub>H,H</sub> = 7.9 Hz, *CH*), 7.24 (*d*, 2H, <sup>3</sup>*J*<sub>H,H</sub> = 8.4 Hz, *CH*), 5.89 – 5.69 (*m*, 2H, *CH=CH*<sub>2</sub>), 5.05 – 4.86 (*m*, 4H, *CH*<sub>2</sub>=*CH*), 3.36 (*s*, 6H, *CH*<sub>3</sub>), 2.36 (*t*, 4H, <sup>3</sup>*J*<sub>H,H</sub> = 7.6 Hz, *CH*<sub>2</sub>), 2.07 – 1.97 (*m*, 4H, *CH*<sub>2</sub>), 1.71 – 1.59 (*m*, 4H, *CH*<sub>2</sub>), 1.41 – 1.20 (*m*, 16H, *CH*<sub>2</sub>) ppm.

##### <sup>13</sup>C-NMR (101 MHz, CDCl<sub>3</sub>)

$\delta$  = 173.7 (*C=O*), 155.0 (*C*<sub>quart.</sub>), 139.8 (*Ar-C*), 139.2 (*CH=CH*<sub>2</sub>), 117.6 (*Ar-C*), 114.3 (*CH*<sub>2</sub>=*CH*), 35.4 (*CH*<sub>3</sub>), 35.3 (*CH*<sub>2</sub>), 33.9 (*CH*<sub>2</sub>), 29.4 (*CH*<sub>2</sub>), 29.4 (*CH*<sub>2</sub>), 29.1 (*CH*<sub>2</sub>), 29.0 (*CH*<sub>2</sub>), 25.4 (*CH*<sub>2</sub>) ppm.

##### ESI ToF MS [m/z]

[*M*+*Li*]<sup>+</sup> C<sub>27</sub>H<sub>43</sub>Li<sub>1</sub>N<sub>3</sub>O<sub>2</sub><sup>+</sup>: calculated 448.3510 g/mol, found 448.3821 g/mol; [*M*+*Na*]<sup>+</sup> C<sub>27</sub>H<sub>43</sub>Na<sub>1</sub>N<sub>3</sub>O<sub>2</sub><sup>+</sup>: calculated 464.3247 g/mol, found 464.3555 g/mol; [*M*+*K*]<sup>+</sup> C<sub>27</sub>H<sub>43</sub>K<sub>1</sub>N<sub>3</sub>O<sub>2</sub><sup>+</sup>: calculated 480.2987 g/mol, found 480.3294 g/mol.

R<sub>f</sub> (TLC) [hexane/EA 8:2]

0.16

**2b (DAP-M-Me-8):**

<sup>1</sup>H-NMR (400 MHz, CDCl<sub>3</sub>)

δ = 7.74 (*t*, 1H, <sup>3</sup>J<sub>H,H</sub> = 7.9 Hz, *CH*), 7.23 (*d*, 2H, <sup>3</sup>J<sub>H,H</sub> = 7.7 Hz, *CH*), 5.87 – 5.70 (*m*, 2H, *CH=CH*<sub>2</sub>), 5.05 – 4.83 (*m*, 4H, *CH*<sub>2</sub>=*CH*), 3.36 (*s*, 6H, *CH*<sub>3</sub>), 2.35 (*t*, 4H, <sup>3</sup>J<sub>H,H</sub> = 7.6 Hz, *CH*<sub>2</sub>), 2.07 – 1.94 (*m*, 4H, *CH*<sub>2</sub>), 1.63 (*t*, 4H, <sup>3</sup>J<sub>H,H</sub> = 7.4 Hz, *CH*<sub>2</sub>), 1.43 – 1.18 (*m*, 20H, *CH*<sub>2</sub>) ppm.

<sup>13</sup>C-NMR (101 MHz, CDCl<sub>3</sub>)

δ = 173.7 (*C=O*), 155.0 (*C*<sub>quart.</sub>), 139.8 (*Ar-C*), 139.3 (*CH=CH*<sub>2</sub>), 117.6 (*Ar-C*), 114.3 (*CH*<sub>2</sub>=*CH*), 35.3 (*CH*<sub>3</sub>), 35.3 (*CH*<sub>2</sub>), 33.9 (*CH*<sub>2</sub>), 29.5 (*CH*<sub>2</sub>), 29.5 (*CH*<sub>2</sub>), 29.4 (*CH*<sub>2</sub>), 29.2 (*CH*<sub>2</sub>), 29.0 (*CH*<sub>2</sub>), 25.4 (*CH*<sub>2</sub>) ppm.

ESI ToF MS [m/z]

[M+Na]<sup>+</sup> C<sub>29</sub>H<sub>47</sub>Na<sub>1</sub>N<sub>3</sub>O<sub>2</sub><sup>+</sup>: calculated 492.3560 g/mol, found 492.3170 g/mol.

R<sub>f</sub> (TLC) [hexane/EA 8:2]

0.16

**2c (DAP-M-Me-9):**

<sup>1</sup>H-NMR (400 MHz, CDCl<sub>3</sub>)

δ = 7.75 (*t*, 1H, <sup>3</sup>J<sub>H,H</sub> = 7.9 Hz, *CH*), 7.24 (*d*, 2H, <sup>3</sup>J<sub>H,H</sub> = 7.8 Hz, *CH*), 5.88 – 5.72 (*m*, 2H, *CH=CH*<sub>2</sub>), 5.03 – 4.89 (*m*, 4H, *CH*<sub>2</sub>=*CH*), 3.36 (*s*, 6H, *CH*<sub>3</sub>), 2.36 (*t*, 4H, <sup>3</sup>J<sub>H,H</sub> = 7.5 Hz, *CH*<sub>2</sub>), 2.07 – 1.97 (*m*, 4H, *CH*<sub>2</sub>), 1.70-1.58 (*m*, 4H, *CH*<sub>2</sub>), 1.42 – 1.14 (*m*, 24H, *CH*<sub>2</sub>) ppm.

<sup>13</sup>C-NMR (101 MHz, CDCl<sub>3</sub>)

δ = 173.7 (*C=O*), 155.0 (*C*<sub>quart.</sub>), 139.8 (*Ar-C*), 139.3 (*CH=CH*<sub>2</sub>), 117.7 (*Ar-C*), 114.3 (*CH*<sub>2</sub>=*CH*), 35.4 (*CH*<sub>3</sub>), 35.3 (*CH*<sub>2</sub>), 33.9 (*CH*<sub>2</sub>), 29.6 (*CH*<sub>2</sub>), 29.6 (*CH*<sub>2</sub>), 29.5 (*CH*<sub>2</sub>), 29.5 (*CH*<sub>2</sub>), 29.3 (*CH*<sub>2</sub>), 29.1 (*CH*<sub>2</sub>), 25.5 (*CH*<sub>2</sub>) ppm.

ESI ToF MS [m/z]

[M+Na]<sup>+</sup> C<sub>31</sub>H<sub>51</sub>Na<sub>1</sub>N<sub>3</sub>O<sub>2</sub><sup>+</sup>: calculated 520.3873 g/mol, found 520.5881 g/mol.

R<sub>f</sub> (TLC) [hexane/EA 8:2]

0.16

**2d (DAP-M-Bn-7):**

<sup>1</sup>H-NMR (400 MHz, CDCl<sub>3</sub>)

δ = 7.61 (*t*, 1H, <sup>3</sup>J<sub>H,H</sub> = 7.9 Hz, *CH*), 7.26 – 7.14 (*m*, 10H, *CH*), 7.10 (*d*, 2H, <sup>3</sup>J<sub>H,H</sub> = 7.6 Hz, *CH*), 5.92 – 5.69 (*m*, 2H, *CH=CH*<sub>2</sub>), 5.22 – 4.79 (*m*, 8H, *CH*<sub>2</sub> + *CH*<sub>2</sub>=*CH*), 2.24 (*t*, 4H, <sup>3</sup>J<sub>H,H</sub> = 7.3 Hz, *CH*<sub>2</sub>), 2.06 – 1.91 (*m*, 4H, *CH*<sub>2</sub>), 1.67 – 1.53 (*m*, 4H, *CH*<sub>2</sub>), 1.38 – 1.13 (*m*, 16H, *CH*<sub>2</sub>) ppm.

<sup>13</sup>C-NMR (101 MHz, CDCl<sub>3</sub>)

δ = 173.6 (C=O), 154.1 (C<sub>quart.</sub>), 139.7 (CH=CH<sub>2</sub>), 139.2 (Ar-C), 137.6 (C<sub>quart.</sub>), 128.6 (Ar-C), 127.7 (Ar-C), 127.3 (Ar-C), 119.0 (CH<sub>2</sub>=CH), 114.3 (Ar-C), 51.0 (CH<sub>2</sub>), 35.3 (CH<sub>2</sub>), 33.9 (CH<sub>2</sub>), 29.4 (CH<sub>2</sub>), 29.4 (CH<sub>2</sub>), 29.1 (CH<sub>2</sub>), 29.0 (CH<sub>2</sub>), 25.4 (CH<sub>2</sub>) ppm.

ESI ToF MS [m/z]

[M+H]<sup>+</sup> C<sub>39</sub>H<sub>52</sub>N<sub>3</sub>O<sub>2</sub><sup>+</sup>: calculated 594.4054 g/mol, found 594.4369 g/mol; [M+Na]<sup>+</sup> C<sub>39</sub>H<sub>51</sub>Na<sub>1</sub>N<sub>3</sub>O<sub>2</sub><sup>+</sup>: calculated 616.3873 g/mol, found 616.4200 g/mol, [M+K]<sup>+</sup> C<sub>39</sub>H<sub>51</sub>K<sub>1</sub>N<sub>3</sub>O<sub>2</sub><sup>+</sup>: calculated 632.3613 g/mol, 632.3955 g/mol.

R<sub>f</sub> (TLC) [hexane/EA 9:1]

0.62

**2e (DAP-M-Bn-8):**

<sup>1</sup>H-NMR (400 MHz, CDCl<sub>3</sub>)

δ = 7.61 (*t*, 1H, <sup>3</sup>J<sub>H,H</sub> = 7.9 Hz, CH), 7.25 – 7.17 (*m*, 6H, CH), 7.15 – 7.04 (*m*, 6H, CH), 5.86 – 5.74 (*m*, 2H, CH=CH<sub>2</sub>), 5.04 – 4.98 (*m*, 4H, CH<sub>2</sub>), 4.97 – 4.89 (*m*, 4H, CH<sub>2</sub>=CH), 2.24 (*t*, 4H, <sup>3</sup>J<sub>H,H</sub> = 7.4 Hz, CH<sub>2</sub>), 2.02 (*dd*, 4H, <sup>3</sup>J<sub>H,H</sub> = 14.4 Hz, <sup>3</sup>J<sub>H,H</sub> = 6.9 Hz, CH<sub>2</sub>), 1.63 – 1.56 (*m*, 4H, CH<sub>2</sub>), 1.38 – 1.15 (*m*, 20H, CH<sub>2</sub>) ppm.

<sup>13</sup>C-NMR (101 MHz, CDCl<sub>3</sub>)

δ = 173.6 (C=O), 154.1 (C<sub>quart.</sub>), 139.7 (CH=CH<sub>2</sub>), 139.3 (Ar-C), 137.6 (C<sub>quart.</sub>), 128.6 (Ar-C), 127.7 (Ar-C), 127.3 (Ar-C), 119.0 (Ar-C), 114.3 (CH<sub>2</sub>=CH), 51.0 (CH<sub>2</sub>), 35.3 (CH<sub>2</sub>), 33.9 (CH<sub>2</sub>), 29.5 (CH<sub>2</sub>), 29.4 (CH<sub>2</sub>), 29.4 (CH<sub>2</sub>), 29.2 (CH<sub>2</sub>), 29.0 (CH<sub>2</sub>), 25.5 (CH<sub>2</sub>) ppm.

ESI ToF MS [m/z]

[M+Na]<sup>+</sup> C<sub>41</sub>H<sub>55</sub>Na<sub>1</sub>N<sub>3</sub>O<sub>2</sub><sup>+</sup>: calculated 644.4186 g/mol, found 644.4227 g/mol; [M+K]<sup>+</sup> C<sub>41</sub>H<sub>55</sub>K<sub>1</sub>N<sub>3</sub>O<sub>2</sub><sup>+</sup>: calculated 660.3926 g/mol, found 660.3967 g/mol.

R<sub>f</sub> (TLC) [hexane/EA 9:1]

0.63

**2f (DAP-M-Bn-9):**

<sup>1</sup>H-NMR (400 MHz, CDCl<sub>3</sub>)

δ = 7.61 (*t*, 1H, <sup>3</sup>J<sub>H,H</sub> = 7.9 Hz, CH), 7.25 – 7.15 (*m*, 10H, CH), 7.10 (*dd*, 2H, <sup>3</sup>J<sub>H,H</sub> = 7.7 Hz, <sup>3</sup>J<sub>H,H</sub> = 1.9 Hz CH), 5.95 – 5.66 (*m*, 2H, CH=CH<sub>2</sub>), 5.05 – 4.83 (*m*, 8H, CH<sub>2</sub> + CH<sub>2</sub>=CH), 2.24 (*t*, 4H, <sup>3</sup>J<sub>H,H</sub> = 7.5 Hz, CH<sub>2</sub>), 2.11 – 1.92 (*m*, 4H, CH<sub>2</sub>), 1.69 – 1.50 (*m*, 4H, CH<sub>2</sub>), 1.45 – 1.12 (*m*, 24H, CH<sub>2</sub>) ppm.

<sup>13</sup>C-NMR (101 MHz, CDCl<sub>3</sub>)

δ = 173.6 (C=O), 154.1 (C<sub>quart.</sub>), 139.7 (CH=CH<sub>2</sub>), 139.3 (Ar-C), 137.7 (C<sub>quart.</sub>), 128.6 (Ar-C), 127.7 (Ar-C), 127.3 (Ar-C), 119.0 (CH<sub>2</sub>=CH), 114.3 (Ar-C), 51.0 (CH<sub>2</sub>), 35.3 (CH<sub>2</sub>), 33.9 (CH<sub>2</sub>), 29.6 (CH<sub>2</sub>), 29.6 (CH<sub>2</sub>), 29.5 (CH<sub>2</sub>), 29.4 (CH<sub>2</sub>), 29.3 (CH<sub>2</sub>), 29.1 (CH<sub>2</sub>), 25.5 (CH<sub>2</sub>) ppm.

### ESI ToF MS [m/z]

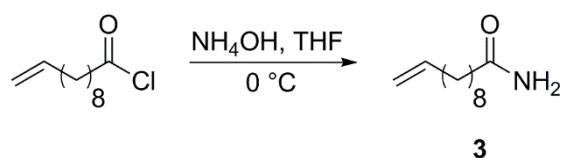
$[M+H]^+$   $C_{43}H_{60}N_3O_2^+$ : calculated 650.4680 g/mol, found 650.4434 g/mol;  $[M+Na]^+$   $C_{43}H_{59}Na_1N_3O_2^+$ : calculated 672.4499 g/mol, found 672.4245 g/mol.

### R<sub>f</sub> (TLC) [hexane/EA 8:2]

0.57

## 4.3.3 Synthesis of the urea containing monomer

### 4.3.3.1 Synthesis of undec-10-enamide (3)



**Scheme 13:** Synthesis of undec-10-enamide (3).

The synthesis was accomplished according to literature.<sup>270,274</sup> A  $NH_4OH$  solution (250 mL, 25 % in  $H_2O$ ) was placed in a two-necked round bottom flask, equipped with a rubber septum and a gas tap, and cooled to 0 °C. Undec-10-enoyl chloride (47.70 mmol, 9.0 g), dissolved in THF (30 mL), was added dropwise and the reaction mixture was allowed to stir overnight. The final product was obtained after filtration and drying in vacuum as a white solid (44.57 mmol, 8.17 g, 93 %). NMR spectra and ESI ToF MS analysis are shown in Figures A 17 and A 18.

### **3 (undec-10-enamide):**

#### $^1H$ -NMR (400 MHz, $CDCl_3$ )

$\delta$  = 5.89 – 5.72 (*m*, 1H,  $CH=CH_2$ ), 5.54 (*d*, 2H,  $NH_2$ ), 5.07 – 4.85 (*m*, 2H,  $CH_2=CH$ ), 2.25 – 2.17 (*m*, 2H,  $CH_2$ ), 2.10 – 1.98 (*m*, 2H,  $CH_2$ ), 1.71 – 1.55 (*m*, 2H,  $CH_2$ ), 1.45 – 1.17 (*m*, 10H,  $CH_2$ ) ppm.

#### $^{13}C$ -NMR (101 MHz, $CDCl_3$ )

$\delta$  = 175.9 ( $C=O$ ), 139.3 ( $CH=CH_2$ ), 114.3 ( $CH_2=CH$ ), 36.1 ( $CH_2$ ), 33.9 ( $CH_2$ ), 29.4 ( $CH_2$ ), 29.4 ( $CH_2$ ), 29.4 ( $CH_2$ ), 29.2 ( $CH_2$ ), 29.0 ( $CH_2$ ), 25.7 ( $CH_2$ ) ppm.

### ESI ToF MS [m/z]

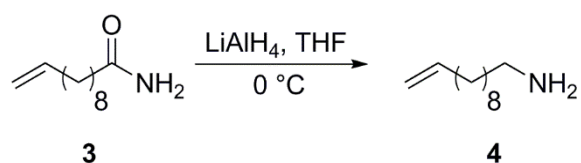
$[M+H]^+$   $C_{11}H_{22}N_1O_1^+$ : calculated 184.1696 g/mol, found 184.1656 g/mol;  $[M+Na]^+$   $C_{11}H_{21}Na_1N_1O_1^+$ : calculated 206.1515 g/mol, found 206.1449 g/mol.

### R<sub>f</sub> (TLC) [DCM/EA 85:15]

0.20



#### 4.3.3.2 Synthesis of undec-10-en-1-amine (4)



Scheme 14: Synthesis of undec-10-en-1-amine (4).

The synthesis was carried out according to literature<sup>270,274</sup> under a dry, inert atmosphere of nitrogen. Undec-10-enamide (**3**) (5.91 mmol, 1 g) was dissolved in dry THF (30 mL), placed in a two-necked round bottom flask, equipped with a rubber septum and a gas tap and cooled to -10 °C. After the careful addition of LiAlH<sub>4</sub> (8.86 mmol, 0.34 g) the reaction mixture was allowed to stir overnight. The reaction was quenched by adding dry Et<sub>2</sub>O (20 mL), H<sub>2</sub>O (1 mL) and then NaOH (2 mL, 10 % in H<sub>2</sub>O). Afterwards, the mixture was filtered and dried over Na<sub>2</sub>SO<sub>4</sub>. The final product was obtained as a white waxy solid (5.06 mmol, 0.79 g, 86 %) after solvent removal in vacuum at 45 °C. NMR spectra and ESI ToF MS analysis are shown in Figures A 19 and A 20.

#### 4 (undec-10-en-1-amine):

##### <sup>1</sup>H-NMR (400 MHz, CDCl<sub>3</sub>)

$\delta$  = 5.89 – 5.71 (*m*, 1H, CH=CH<sub>2</sub>), 5.04 – 4.86 (*m*, 2H, CH<sub>2</sub>=CH), 2.67 (*t*, 2H, <sup>3</sup>J<sub>H,H</sub> = 7.0 Hz, CH<sub>2</sub>), 2.10 – 1.96 (*m*, 2H, CH<sub>2</sub>), 1.48 – 1.22 (*m*, 14H, CH<sub>2</sub>) ppm.

##### <sup>13</sup>C-NMR (101 MHz, CDCl<sub>3</sub>)

$\delta$  = 139.4 (CH=CH<sub>2</sub>), 114.2 (CH<sub>2</sub>=CH), 42.4 (CH<sub>2</sub>), 34.0 (CH<sub>2</sub>), 33.9 (CH<sub>2</sub>), 29.7 (CH<sub>2</sub>), 29.6 (CH<sub>2</sub>), 29.6 (CH<sub>2</sub>), 29.3 (CH<sub>2</sub>), 29.1 (CH<sub>2</sub>), 27.0 (CH<sub>2</sub>) ppm.

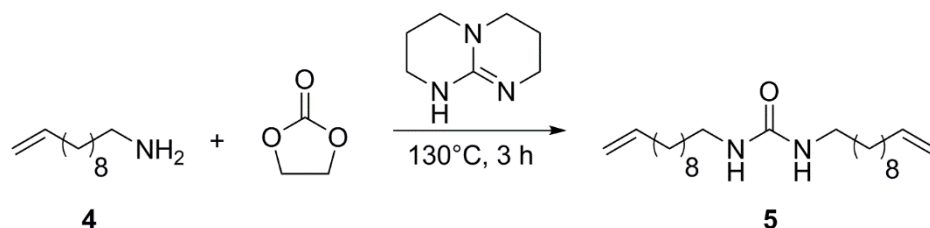
##### ESI ToF MS [m/z]

[M+H]<sup>+</sup> C<sub>11</sub>H<sub>24</sub>N<sub>1</sub><sup>+</sup>: calculated 170.1903 g/mol, found 170.2159 g/mol.

##### R<sub>f</sub> (TLC) [DCM/EA 85:15]

0.24

#### 4.3.3.3 Synthesis of 1,3-diundec-10-en-1-ylurea (Urea-M-9) (5)



Scheme 15: Synthesis of 1,3-diundec-10-en-1-ylurea (Urea-M-9, 5).

The synthesis was carried out according to literature.<sup>270,304</sup> Undec-10-en-1-amine (4.99 mmol, 0.78 mg), ethylene carbonate (2.50 mmol, 0.22 mg) and 1,5,7-triazabicyclo[4.4.0]dec-5-ene (TBD) (0.05 mmol, 6.95 mg) were placed in a one-necked round bottom flask and heated up to

130 °C for 3 h. After cooling the mixture to room temperature the crude product was purified via column chromatography (silica gel 60, DCM/EA 85:15) to yield 0.73 g of a pale yellow solid (1.99 mmol, 40 %). NMR spectra and ESI ToF MS analysis are shown in Figures A 21 and A 22.

### 5 (Urea-M-9):

#### <sup>1</sup>H-NMR (400 MHz, CDCl<sub>3</sub>)

$\delta$  = 5.88 – 5.74 (*m*, 2H, CH=CH<sub>2</sub>), 5.06 – 4.88 (*m*, 4H, CH<sub>2</sub>=CH), 4.23 (*s*, NH), 3.14 (*t*, 4H, <sup>3</sup>J<sub>H,H</sub> = 7.1 Hz, CH<sub>2</sub>), 2.12 – 1.96 (*m*, 4H, CH<sub>2</sub>), 1.48 (*t*, 4H, <sup>3</sup>J<sub>H,H</sub> = 7.0 Hz, CH<sub>2</sub>), 1.40-1.24 (*m*, 24H, CH<sub>2</sub>) ppm.

#### <sup>13</sup>C-NMR (101 MHz, CDCl<sub>3</sub>)

$\delta$  = 158.3 (C=O), 139.3 (CH=CH<sub>2</sub>), 114.3 (CH<sub>2</sub>=CH), 40.9 (CH<sub>2</sub>), 33.9 (CH<sub>2</sub>), 30.4 (CH<sub>2</sub>), 29.7 (CH<sub>2</sub>), 29.6 (CH<sub>2</sub>), 29.5 (CH<sub>2</sub>), 29.3 (CH<sub>2</sub>), 29.1 (CH<sub>2</sub>), 27.1 (CH<sub>2</sub>) ppm.

#### ESI ToF MS [m/z]

[M+H]<sup>+</sup> C<sub>23</sub>H<sub>45</sub>N<sub>2</sub>O<sub>1</sub><sup>+</sup>: calculated 365.3526 g/mol, found 365.3292 g/mol; [M+Na]<sup>+</sup> C<sub>23</sub>H<sub>44</sub>Na<sub>1</sub>N<sub>2</sub>O<sub>1</sub><sup>+</sup>: calculated 387.3346 g/mol, found 387.3089 g/mol.

#### IR (KBr) [cm<sup>-1</sup>]

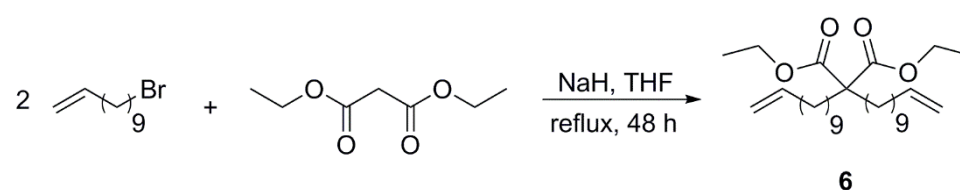
3336 (*s*), 3075 (*w*), 2927 (*s*), 2851 (*s*), 1616 (*s*), 1574 (*s*), 1461 (*m*), 1248 (*w*), 1075 (*w*), 994 (*w*), 910 (*m*), 725 (*w*), 616 (*m*).

#### R<sub>f</sub> (TLC) [DCM/EA 85:15]

0.27

## 4.3.4 Synthesis of the TEMPO containing monomer

### 4.3.4.1 Synthesis of diethyl-2,2-di(undec-10-en-1-yl)malonate (6)



**Scheme 16:** Synthesis of diethyl-2,2-di(undec-10-en-1-yl)malonate (6).

The reaction was carried out analogous to literature<sup>276,305</sup> under a dry, inert atmosphere of nitrogen. A two-necked round bottom flask, equipped with a rubber septum and a reflux condenser was filled with dry THF (30 mL) and NaH (41.59 mmol, 1.00 g). Diethyl malonate (12.49 mmol, 1.90 mL), which was distilled over CaH<sub>2</sub> (10 mbar, 76 °C) prior to use, was added to the slurry followed by the dropwise addition of 11-bromo-1-undecene (27.47 mmol, 6.03 mL). After heating the reaction mixture under reflux conditions for 48 h it was cooled to 0 °C and residual NaH was neutralized by the careful addition of H<sub>2</sub>O. The crude product was purified by column chromatography (silica gel 60, Hex/EA 99:1) to yield 4.41 g of a pale yellow liquid (9.49 mmol, 76 %). NMR spectra are shown in Figure A 23.

**6:**

$^1\text{H-NMR}$  (400 MHz,  $\text{CDCl}_3$ )

$\delta = 5.89 - 5.70$  (*m*, 2H,  $\text{CH}=\text{CH}_2$ ),  $5.07 - 4.85$  (*m*, 4H,  $\text{CH}_2=\text{CH}$ ),  $4.16$  (*q*, 4H,  $^3J_{\text{H,H}} = 7.1$  Hz,  $\text{O}-\text{CH}_2$ ),  $2.09 - 1.96$  (*m*, 4H,  $\text{CH}_2$ ),  $1.89 - 1.77$  (*m*, 4H,  $\text{CH}_2$ ),  $1.47 - 1.01$  (*m*, 28H,  $\text{CH}_2$ ),  $1.25$  (*s*, 6H,  $\text{CH}_3$ ) ppm.

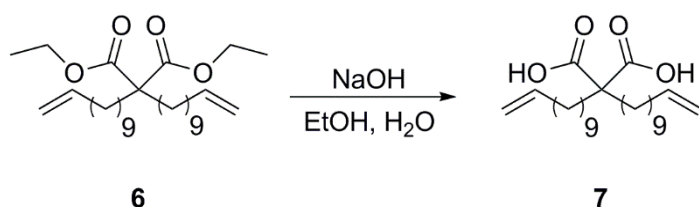
$^{13}\text{C-NMR}$  (101 MHz,  $\text{CDCl}_3$ )

$\delta = 172.1$  ( $\text{C}=\text{O}$ ),  $139.3$  ( $\text{CH}=\text{CH}_2$ ),  $114.2$  ( $\text{CH}_2=\text{CH}$ ),  $61.0$  ( $\text{CH}_2$ ),  $57.7$  ( $\text{C}_{\text{quart.}}$ ),  $33.9$  ( $\text{CH}_2$ ),  $32.3$  ( $\text{CH}_2$ ),  $30.0$  ( $\text{CH}_2$ ),  $29.6$  ( $\text{CH}_2$ ),  $29.6$  ( $\text{CH}_2$ ),  $29.4$  ( $\text{CH}_2$ ),  $29.3$  ( $\text{CH}_2$ ),  $29.1$  ( $\text{CH}_2$ ),  $24.0$  ( $\text{CH}_2$ ),  $14.3$  ( $\text{CH}_3$ ) ppm.

$R_f$  (TLC) [hexane/EA 99:1]

0.47

#### 4.3.4.2 Synthesis of 2,2-di(undec-10-en-1-yl)malonic acid (7)



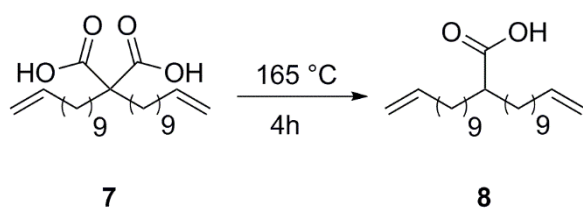
**Scheme 17:** Synthesis of 2,2-di(undec-10-en-1-yl)malonic acid (7).

The synthesis was carried out according to literature.<sup>276,305</sup> Diethyl-2,2-di(undec-10-en-1-yl)malonate (31.00 mmol, 14.41 g) and NaOH (0.16 mol, 6.2 g), dissolved in EtOH/ $\text{H}_2\text{O}$  (140 mL, 1:1), were placed in a one-necked round bottom flask and heated under reflux conditions for 24 h. After cooling the mixture to room temperature it was acidified with concentrated HCl to a pH of 1 followed by the removal of the organic solvents in vacuum at  $45^\circ\text{C}$  and extraction of the aqueous solution with  $\text{Et}_2\text{O}$ . The final product was obtained after drying the combined organic fractions over  $\text{Na}_2\text{SO}_4$  and evaporation of the solvent at  $45^\circ\text{C}$  in vacuum and was used directly without further purification.

$R_f$  (TLC) [hexane/EA 98:2]

0.44

#### 4.3.4.3 Synthesis of 2-(undec-10-en-1-yl)tridec-12-enoic acid (Acid-M-9) (8)



**Scheme 18:** Synthesis of 2-(undec-10-en-1-yl)tridec-12-enoic acid (8).

The synthesis was carried out analogous to literature.<sup>277</sup> A one-necked round bottom flask, equipped with a reflux condenser was filled with 2,2-di(undec-10-en-1-yl)malonic acid (29.76 mmol, 12.16 g) and heated up to 165 °C for 4 h. After complete decarboxylation the compound was purified via column chromatography (silica gel 60, Hex/EA 98:2) to yield 4.77 g of a pale yellow, waxy solid (13.09 mmol, 44 %). NMR spectra and ESI ToF MS analysis are shown in Figures A 24 and A 25.

### 8 (Acid-M-9):

#### <sup>1</sup>H-NMR (400 MHz, CDCl<sub>3</sub>)

$\delta$  = 5.89 – 5.74 (*m*, 2H, CH=CH<sub>2</sub>), 5.04 – 4.89 (*m*, 4H, CH<sub>2</sub>=CH), 2.40 – 2.29 (*m*, 1H, CH), 2.09 – 1.98 (*m*, 4H, CH<sub>2</sub>), 1.70 – 1.42 (*m*, 4H, CH<sub>2</sub>), 1.42 – 1.19 (*m*, 28H, CH<sub>2</sub>) ppm.

#### <sup>13</sup>C-NMR (101 MHz, CDCl<sub>3</sub>)

$\delta$  = 182.5 (C=O), 139.4 (CH=CH<sub>2</sub>), 114.2 (CH<sub>2</sub>=CH), 45.6 (CH), 34.0 (CH<sub>2</sub>), 32.3 (CH<sub>2</sub>), 29.7 (CH<sub>2</sub>), 29.7 (CH<sub>2</sub>), 29.6 (CH<sub>2</sub>), 29.6 (CH<sub>2</sub>), 29.3 (CH<sub>2</sub>), 29.1 (CH<sub>2</sub>), 27.5 (CH<sub>2</sub>) ppm.

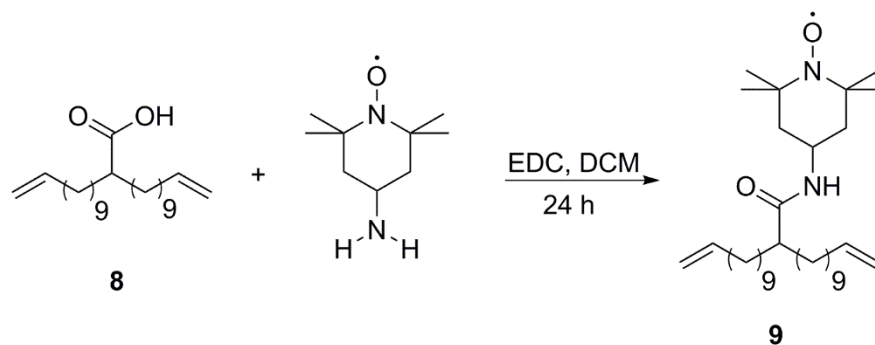
#### ESI ToF MS [m/z]

[M+Na]<sup>+</sup> C<sub>24</sub>H<sub>44</sub>Na<sub>1</sub>O<sub>2</sub><sup>+</sup>: calculated 387.3234 g/mol, found 387.3168 g/mol.

#### R<sub>f</sub> (TLC) [hexane/EA 90:10]

0.45

### 4.3.4.4 Synthesis of TEMPO-M-9 (9)



**Scheme 19:** Synthesis of TEMPO-M-9 (9).

The synthesis was carried out according to literature<sup>278,279</sup> under a dry, inert atmosphere of nitrogen. A one-necked round bottom flask was filled with 2-(undec-10-en-1-yl)tridec-12-enoic acid (19.75 mmol, 7.20 g) and 4-amino TEMPO (21.72 mmol, 3.72 g), dissolved in dry DCM (70 mL). After purging the solution with nitrogen for 30 minutes, EDC-HCl (19.75 mmol, 3.79 g) was added and the reaction mixture was allowed to stir overnight followed by washing twice with saturated NaHCO<sub>3</sub> solution and brine. The organic layer was separated and dried over MgSO<sub>4</sub> and the solvent was removed in vacuum at 45 °C. Column chromatography (silica gel 60, Hex/EA 65:35) was used for purification of the final product to yield 6.85 g of a pale orange oil (13.23 mmol, 67 %). ESI ToF MS analysis is shown in Figure 30.

## 9 (TEMPO-M-9):

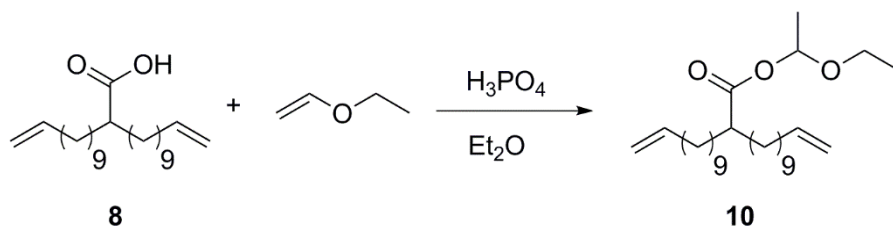
### ESI ToF MS [m/z]

$[M+H]^+$   $C_{33}H_{62}N_2O_2^+$ : calculated 517.4728 g/mol, found 517.6012 g/mol;  $[M+Na]^+$   $C_{33}H_{61}Na_1N_2O_2^+$ : calculated 540.4625 g/mol, found 540.5948 g/mol.

### $R_f$ (TLC) [hexane/EA 65:35]

0.38

## 4.3.5 Protection of Acid-M-9



Scheme 20: Synthesis of Acid-M-Ee-9 (10).

The synthesis was carried out according to literature.<sup>99</sup> A two-necked round bottom flask, equipped with a rubber septum and a gas tap was filled with ethyl vinyl ether (10.28 mmol, 1.00 mL) and phosphoric acid (cat., 1 drop), dissolved in diethyl ether (5 mL), and cooled to 0 °C. After dropwise addition of 2-(undec-10-en-1-yl)tridec-12-enoic acid (2.06 mmol, 0.75 g) in diethyl ether (10 mL) the solution was stirred for 30 minutes at 0 °C, followed by further stirring at room temperature for 3 days. Stirring the reaction mixture with basic alumina (~ 1 g) for 5 minutes was used to quench the reaction. The final product was obtained after filtration, evaporation of the solvent at 45 °C in vacuum and column chromatography (silica gel 60, Hex/EA 98:2) as a colorless oil (1.71 mmol, 0.74 g, 83 %). NMR spectra and ESI ToF MS analysis are shown in Figures A 26 and A 27.

## 10 (Acid-M-Ee-9):

### <sup>1</sup>H-NMR (400 MHz, CDCl<sub>3</sub>)

$\delta$  = 5.94 (*q*, 1H,  $^3J_{H,H}$  = 5.2 Hz, *CH*), 5.87 – 5.75 (*m*, 2H, *CH=CH*<sub>2</sub>), 5.02 – 4.90 (*m*, 4H, *CH*<sub>2</sub>=*CH*), 3.75 – 3.49 (*m*, 2H, *O-CH*<sub>2</sub>), 2.37 – 2.28 (*m*, 1H, *CH*), 2.07 – 2.00 (*m*, 4H, *CH*<sub>2</sub>), 1.64 – 1.39 (*m*, 4H, *CH*<sub>2</sub>), 1.38 – 1.17 (*m*, 34H, *CH*<sub>2</sub> + *CH*<sub>3</sub>) ppm.

### <sup>13</sup>C-NMR (101 MHz, CDCl<sub>3</sub>)

$\delta$  = 176.4 (*C=O*), 139.4 (*CH=CH*<sub>2</sub>), 114.3 (*CH*<sub>2</sub>=*CH*), 96.1 (*CH*), 64.7 (*O-CH*<sub>2</sub>), 46.3 (*CH*), 34.0 (*CH*<sub>2</sub>), 32.7 (*CH*<sub>2</sub>), 29.7 (*CH*<sub>2</sub>), 29.7 (*CH*<sub>2</sub>), 29.6 (*CH*<sub>2</sub>), 29.6 (*CH*<sub>2</sub>), 29.3 (*CH*<sub>2</sub>), 29.1 (*CH*<sub>2</sub>), 27.7 (*CH*<sub>2</sub>), 21.1 (*CH*<sub>3</sub>), 15.2 (*CH*<sub>3</sub>) ppm.

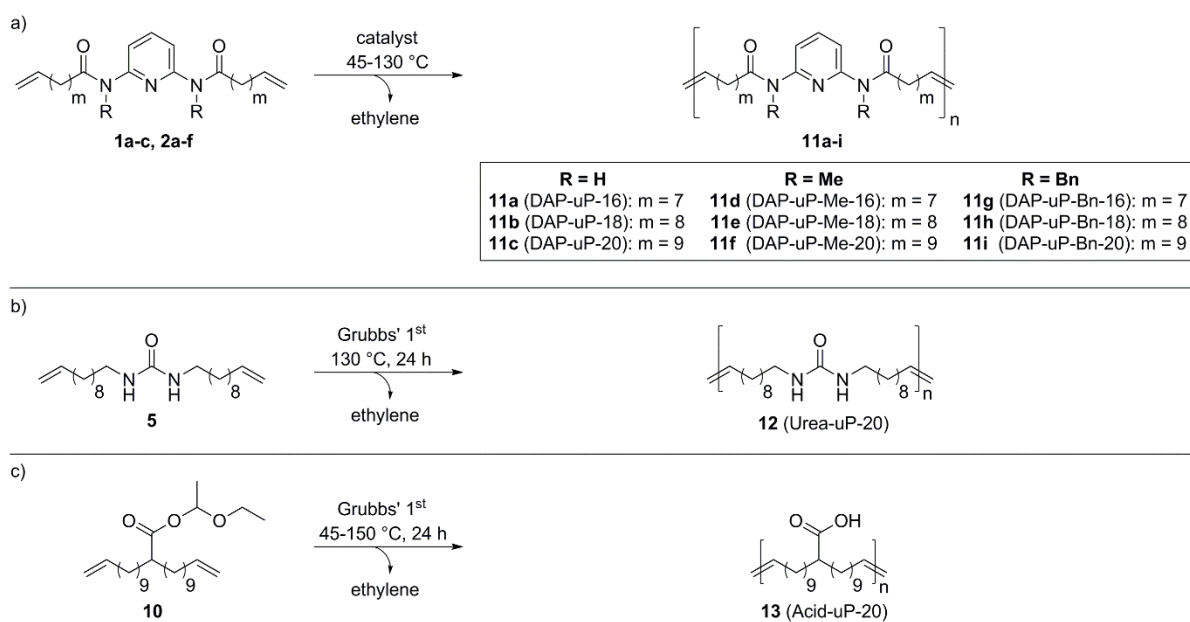
### ESI ToF MS [m/z]

$[M+Na]^+$   $C_{28}H_{52}Na_1O_3^+$ : calculated 459.3809 g/mol, found 459.3723 g/mol.

### $R_f$ (TLC) [hexane/EA 98:2]

0.43

## 4.4 ADMET-Polymerization



**Scheme 21:** ADMET-polymerization of the a) unprotected and protected DAP containing monomers (**1a-c**, **2a-f**), b) urea containing monomer (**5**) and c) acid containing monomer (**10**).

The polymerizations were carried out analogous to literature<sup>68,75,224,281</sup> and previous investigations<sup>269,270,272</sup> under a dry, inert atmosphere of nitrogen as bulk polymerization. DAP-Me-7 (**2a**) (0.11 mmol, 50.00 mg) was placed in a Schlenk tube and degassed by applying the freeze-pump-thaw technique followed by the addition of Grubbs-Hoveyda 1<sup>st</sup> generation catalyst ( $4.53 \cdot 10^{-4}$  mmol, 0.27 mg, 250:1 monomer-catalyst ratio) under a counter flow of nitrogen. Afterwards the reaction mixture was heated up to 65 °C and vacuum ( $p \sim 3$  mbar) was applied to remove the generated ethylene. To remain a consistent conversion upon increased viscosity the temperature was increased stepwise until up to 85 °C. The polymerization was quenched by opening the Schlenk tube after the evolution of ethylene stopped and the magnetic stir bar was unable to move. Complete consumption of the monomer was determined by the disappearance of the corresponding signal in TLC, wherein signal of the associated polymer was observed at the starting line of the TLC plate. The final polymer DAP-uP-Me-16 (**11d**) was obtained by dissolving the crude product in a small amount of THF and precipitation into cold methanol as white to beige solid in a yield of 98 % (49.00 mg). All other polymers **11a-c**, **11e-i**, **12** and **13** were synthesized analogously to this procedure using Grubbs 1<sup>st</sup> to 3<sup>rd</sup> generation catalyst, Grubbs-Hoveyda 1<sup>st</sup> generation catalyst or Umicore catalyst with yields ranging from 3-97 %. Polymerizations of the monomers **1a-c** and **9** were carried out at 130 °C as these compounds are present in the molten state at this temperature. The experimental details as well as the characterization data are shown in Table 7-Table 11. Selected NMR and IR spectra as well as MALDI ToF MS analyses are shown in Figures A 28-A 35.

**11a (DAP-uP-16):**IR (KBr) [cm<sup>-1</sup>]

3309 (s), 2922 (s), 2849 (s), 1670 (s), 1588 (s), 1524 (s), 1469 (s), 1412 (m), 1303 (m), 1242 (w), 1179 (w), 994 (w), 964 (w), 910 (m), 724 (w), 636 (m).

**11b (DAP-uP-18):**IR (KBr) [cm<sup>-1</sup>]

3314 (s), 2921 (s), 2849 (s), 1671 (s), 1589 (s), 1524 (s), 1470 (s), 1412 (m), 1303 (m), 1242 (w), 1179 (w), 991 (w), 963 (w), 910 (m), 723 (w), 637 (m).

**11c (DAP-uP-20):**IR (KBr) [cm<sup>-1</sup>]

3422 (s), 3318 (s), 2922 (s), 2850 (s), 1671 (s), 1588 (s), 1524 (s), 1467 (s), 1414 (m), 1300 (m), 1242 (w), 1177 (w), 992 (w), 964 (w), 911 (m), 722 (w), 652 (m).

**11d (DAP-uP-Me-16):**<sup>1</sup>H-NMR (400 MHz, CDCl<sub>3</sub>)

$\delta = 7.75$  (*t*, 1H, <sup>3</sup>*J*<sub>H,H</sub> = 7.9 Hz, *CH*),  $7.25$  (*d*, 2H, <sup>3</sup>*J*<sub>H,H</sub> = 9.0 Hz, *CH*),  $5.87 - 5.70$  (*m*, 2H, *CH=CH*<sub>2</sub>),  $5.44 - 5.23$  (*m*, 2H, =*CH*),  $5.03 - 4.84$  (*m*, 4H, *CH*<sub>2</sub>=*CH*),  $3.36$  (*s*, 6H, *CH*<sub>3</sub>),  $2.36$  (*t*, 4H, <sup>3</sup>*J*<sub>H,H</sub> = 7.5 Hz, *CH*<sub>2</sub>),  $2.09 - 1.84$  (*m*, 8H, *CH*<sub>2</sub>),  $1.78 - 1.51$  (*m*, 4H, *CH*<sub>2</sub>),  $1.50 - 1.05$  (*m*, 28H, *CH*<sub>2</sub>) ppm.

<sup>13</sup>C-NMR (101 MHz, CDCl<sub>3</sub>)

$\delta = 173.7$  (*C=O*),  $154.9$  (*C*<sub>quart.</sub>),  $139.8$  (*Ar-C*),  $130.4$  (=CH),  $130.0$  (=CH),  $117.7$  (*Ar-C*),  $35.4$  (*CH*<sub>3</sub>),  $35.3$  (*CH*<sub>2</sub>),  $32.7$  (*CH*<sub>2</sub>),  $29.9$  (*CH*<sub>2</sub>),  $29.8$  (*CH*<sub>2</sub>),  $29.5$  (*CH*<sub>2</sub>),  $29.5$  (*CH*<sub>2</sub>),  $29.3$  (*CH*<sub>2</sub>),  $29.2$  (*CH*<sub>2</sub>),  $27.4$  (*CH*<sub>2</sub>),  $25.5$  (*CH*<sub>2</sub>) ppm.

MALDI ToF MS [DCTB, LiTFA, 25:5:1] [m/z]

[M+Li]<sup>+</sup> C<sub>202</sub>H<sub>316</sub>Li<sub>1</sub>N<sub>24</sub>O<sub>16</sub><sup>+</sup>: calculated 3340.480 g/mol, found 3340.368 g/mol.

**11e (DAP-uP-Me-18):**<sup>1</sup>H-NMR (400 MHz, CDCl<sub>3</sub>)

$\delta = 7.75$  (*t*, 1H, <sup>3</sup>*J*<sub>H,H</sub> = 7.9 Hz, *CH*),  $7.24$  (*d*, 2H, <sup>3</sup>*J*<sub>H,H</sub> = 7.3 Hz, *CH*),  $5.88 - 5.70$  (*m*, 2H, *CH=CH*<sub>2</sub>),  $5.44 - 5.24$  (*m*, 2H, =*CH*),  $5.04 - 4.85$  (*m*, 4H, *CH*<sub>2</sub>=*CH*),  $3.36$  (*s*, 6H, *CH*<sub>3</sub>),  $2.36$  (*t*, 4H, <sup>3</sup>*J*<sub>H,H</sub> = 7.5 Hz, *CH*<sub>2</sub>),  $2.08 - 1.85$  (*m*, 8H, *CH*<sub>2</sub>),  $1.76 - 1.52$  (*m*, 4H, *CH*<sub>2</sub>),  $1.48 - 1.00$  (*m*, 28H, *CH*<sub>2</sub>) ppm.

<sup>13</sup>C-NMR (101 MHz, CDCl<sub>3</sub>)

$\delta = 173.7$  (*C=O*),  $155.0$  (*C*<sub>quart.</sub>),  $139.8$  (*Ar-C*),  $139.3$  (*CH=CH*<sub>2</sub>),  $130.5$  (=CH),  $130.0$  (=CH),  $117.7$  (*Ar-C*),  $35.4$  (*CH*<sub>3</sub>),  $35.3$  (*CH*<sub>2</sub>),  $32.8$  (*CH*<sub>2</sub>),  $29.9$  (*CH*<sub>2</sub>),  $29.8$  (*CH*<sub>2</sub>),  $29.6$  (*CH*<sub>2</sub>),  $29.5$  (*CH*<sub>2</sub>),  $29.3$  (*CH*<sub>2</sub>),  $25.5$  (*CH*<sub>2</sub>) ppm.

MALDI ToF MS [DCTB, LiTFA, 25:5:1] [m/z]

[M+Li]<sup>+</sup> C<sub>164</sub>H<sub>262</sub>Li<sub>1</sub>N<sub>18</sub>O<sub>12</sub><sup>+</sup>: calculated 2682.059 g/mol, found 2681.017 g/mol.

**11f (DAP-uP-Me-20):**<sup>1</sup>H-NMR (500 MHz, CDCl<sub>3</sub>)

$\delta$  = 7.75 (*t*, 1H,  $^3J_{\text{H,H}} = 7.9$  Hz, *CH*), 7.24 (*d*, 2H,  $^3J_{\text{H,H}} = 3.9$  Hz, *CH*), 5.88 – 5.64 (*m*, 2H, *CH=CH*<sub>2</sub>), 5.47 – 5.12 (*m*, 2H, =*CH*), 5.07 – 4.78 (*m*, 4H, *CH*<sub>2</sub>=*CH*), 3.36 (*s*, 6H, *CH*<sub>3</sub>), 2.36 (*t*, 4H,  $^3J_{\text{H,H}} = 7.5$  Hz, *CH*<sub>2</sub>), 2.08 – 1.84 (*m*, 8H, *CH*<sub>2</sub>), 1.71 – 1.48 (*m*, 4H, *CH*<sub>2</sub>), 1.40 – 1.04 (*m*, 32H, *CH*<sub>2</sub>) ppm.

<sup>13</sup>C-NMR (126 MHz, CDCl<sub>3</sub>)

$\delta$  = 173.7 (*C=O*), 155.0 (*C*<sub>quart.</sub>), 139.8 (*Ar-C*), 139.3 (*CH=CH*<sub>2</sub>), 130.5 (=CH), 117.7 (*Ar-C*), 114.3 (*CH*<sub>2</sub>=*CH*), 35.4 (*CH*<sub>3</sub>), 35.3 (*CH*<sub>2</sub>), 33.9 (*CH*<sub>2</sub>), 32.8 (*CH*<sub>2</sub>), 29.9 (*CH*<sub>2</sub>), 29.8 (*CH*<sub>2</sub>), 29.6 (*CH*<sub>2</sub>), 29.6 (*CH*<sub>2</sub>), 29.6 (*CH*<sub>2</sub>), 29.5 (*CH*<sub>2</sub>), 29.5 (*CH*<sub>2</sub>), 29.3 (*CH*<sub>2</sub>), 25.5 (*CH*<sub>2</sub>) ppm.

MALDI ToF MS [DCTB, LiTFA, 25:5:1] [m/z]

[*M*+*Li*]<sup>+</sup> C<sub>176</sub>H<sub>286</sub>Li<sub>1</sub>N<sub>18</sub>O<sub>12</sub><sup>+</sup>: calculated 2850.247 g/mol, found 2850.383 g/mol.

**11g (DAP-uP-Bn-16):**<sup>1</sup>H-NMR (400 MHz, CDCl<sub>3</sub>)

$\delta$  = 7.60 (*t*, 1H,  $^3J_{\text{H,H}} = 7.9$  Hz, *CH*), 7.24 – 7.14 (*m*, 10H, *CH*), 7.14-6.99 (*m*, 2H, *CH*), 5.89 – 5.71 (*m*, 2H, *CH=CH*<sub>2</sub>), 5.41 – 5.26 (*m*, 2H, =*CH*), 5.01 (*s*, 4H, *CH*<sub>2</sub>) 4.98 – 4.85 (*m*, 4H, *CH*<sub>2</sub>=*CH*), 2.35-2.15 (*m*, 4H, *CH*<sub>2</sub>), 2.06 – 1.86 (*m*, 8H, *CH*<sub>2</sub>), 1.69 – 1.51 (*m*, 4H, *CH*<sub>2</sub>), 1.38 – 1.12 (*m*, 28H, *CH*<sub>2</sub>) ppm.

<sup>13</sup>C-NMR (126 MHz, CDCl<sub>3</sub>)

$\delta$  = 173.6 (*C=O*), 154.1 (*C*<sub>quart.</sub>), 139.7 (*CH=CH*<sub>2</sub>), 137.7 (*Ar-C*), 130.4 (=CH), 130.0 (=CH), 128.6 (*Ar-C*), 127.7 (*Ar-C*), 127.3 (*Ar-C*), 119.0 (*Ar-C*), 114.3 (*CH*<sub>2</sub>=*CH*), 51.0 (*CH*<sub>2</sub>), 35.3 (*CH*<sub>2</sub>), 32.7 (*CH*<sub>2</sub>), 29.9 (*CH*<sub>2</sub>), 29.8 (*CH*<sub>2</sub>), 29.5 (*CH*<sub>2</sub>), 29.4 (*CH*<sub>2</sub>), 29.4 (*CH*<sub>2</sub>), 29.3 (*CH*<sub>2</sub>), 29.2 (*CH*<sub>2</sub>), 29.1 (*CH*<sub>2</sub>), 25.5 (*CH*<sub>2</sub>) ppm.

**11h (DAP-uP-Bn-18):**<sup>1</sup>H-NMR (500 MHz, CDCl<sub>3</sub>)

$\delta$  = 7.60 (*t*, 1H,  $^3J_{\text{H,H}} = 7.9$  Hz, *CH*), 7.24 – 7.14 (*m*, 10H, *CH*), 7.10 (*d*, 2H,  $^3J_{\text{H,H}} = 6.7$  Hz, *CH*), 5.87 – 5.72 (*m*, 2H, *CH=CH*<sub>2</sub>), 5.42 – 5.27 (*m*, 2H, =*CH*), 5.08 – 4.86 (*m*, 8H, *CH*<sub>2</sub> + *CH*<sub>2</sub>=*CH*), 2.23 (*t*, 4H,  $^3J_{\text{H,H}} = 7.0$  Hz, *CH*<sub>2</sub>), 2.04 – 1.88 (*m*, 8H, *CH*<sub>2</sub>), 1.68 – 1.52 (*m*, 4H, *CH*<sub>2</sub>), 1.37 – 1.10 (*m*, 28H, *CH*<sub>2</sub>) ppm.

<sup>13</sup>C-NMR (126 MHz, CDCl<sub>3</sub>)

$\delta$  = 173.6 (*C=O*), 154.1 (*C*<sub>quart.</sub>), 139.8 (*CH=CH*<sub>2</sub>), 137.7 (*Ar-C*), 130.5 (=CH), 130.0 (*Ar-C*), 128.6 (*Ar-C*), 127.3 (*Ar-C*), 119.0 (*Ar-C*), 50.9 (*CH*<sub>3</sub>), 35.3 (*CH*<sub>2</sub>), 32.8 (*CH*<sub>2</sub>), 29.9 (*CH*<sub>2</sub>), 29.8 (*CH*<sub>2</sub>), 29.6 (*CH*<sub>2</sub>), 29.5 (*CH*<sub>2</sub>), 29.5 (*CH*<sub>2</sub>), 29.5 (*CH*<sub>2</sub>), 29.5 (*CH*<sub>2</sub>), 29.3 (*CH*<sub>2</sub>), 29.2 (*CH*<sub>2</sub>), 27.4 (*CH*<sub>2</sub>) ppm.



**11i (DAP-uP-Bn-20):**<sup>1</sup>H-NMR (500 MHz, CDCl<sub>3</sub>)

$\delta$  = 7.60 (*t*, 1H, <sup>3</sup>J<sub>H,H</sub> = 7.9 Hz, *CH*), 7.24 – 7.16 (*m*, 10H, *CH*), 7.10 (*d*, 2H, <sup>3</sup>J<sub>H,H</sub> = 6.5 Hz, *CH*), 5.91 – 5.68 (*m*, 2H, *CH=CH*<sub>2</sub>), 5.46 – 5.21 (*m*, 2H, =*CH*), 5.10 – 4.79 (*m*, 4H, *CH*<sub>2</sub>=*CH*), 2.23 (*t*, 4H, <sup>3</sup>J<sub>H,H</sub> = 7.0 Hz, *CH*<sub>2</sub>), 2.07 – 1.88 (*m*, 8H, *CH*<sub>2</sub>), 1.70 – 1.43 (*m*, 4H, *CH*<sub>2</sub>), 1.38 – 1.11 (*m*, 32H, *CH*<sub>2</sub>) ppm.

<sup>13</sup>C-NMR (126 MHz, CDCl<sub>3</sub>)

$\delta$  = 173.6 (*C=O*), 154.1 (*C*<sub>quart.</sub>), 139.7 (*CH=CH*<sub>2</sub>), 137.7 (*Ar-C*), 130.5 (=CH), 130.0 (=CH), 128.6 (*Ar-C*), 127.7 (*Ar-C*), 127.3 (*Ar-C*), 119.0 (*Ar-C*), 51.0 (*CH*<sub>2</sub>), 35.3 (*CH*<sub>2</sub>), 33.9 (*CH*<sub>2</sub>), 32.8 (*CH*<sub>2</sub>), 29.9 (*CH*<sub>2</sub>), 29.8 (*CH*<sub>2</sub>), 29.6 (*CH*<sub>2</sub>), 29.6 (*CH*<sub>2</sub>), 29.6 (*CH*<sub>2</sub>), 29.5 (*CH*<sub>2</sub>), 29.4 (*CH*<sub>2</sub>), 29.4 (*CH*<sub>2</sub>), 25.5 (*CH*<sub>2</sub>) ppm.

**12 (Urea-uP-20):**IR (KBr) [cm<sup>-1</sup>]

3342 (*s*), 3136 (*w*), 2926 (*s*), 2852 (*s*), 1624 (*s*), 1578 (*s*), 1463 (*m*), 1255 (*w*), 1073 (*w*), 965 (*m*), 723 (*w*), 647 (*m*).

**13 (Acid-uP-20):**<sup>1</sup>H-NMR (400 MHz, CDCl<sub>3</sub>)

$\delta$  = 5.44 – 5.28 (*m*, 2H, =*CH*), 2.30 – 2.18 (*m*, 1H, *CH*), 2.08 – 1.91 (*m*, 4H, *CH*<sub>2</sub>), 1.64 – 1.39 (*m*, 4H, *CH*<sub>2</sub>), 1.40 – 1.20 (*m*, 28H, *CH*<sub>2</sub>) ppm.

<sup>13</sup>C-NMR (101 MHz, CDCl<sub>3</sub>)

$\delta$  = 177.3 (*C=O*), 131.3 (=CH), 130.7 (=CH), 46.4 (*CH*), 33.7 (*CH*<sub>2</sub>), 30.8 (*CH*<sub>2</sub>), 30.8 (*CH*<sub>2</sub>), 30.7 (*CH*<sub>2</sub>), 30.7 (*CH*<sub>2</sub>), 30.3 (*CH*<sub>2</sub>), 28.6 (*CH*<sub>2</sub>), 28.2 (*CH*<sub>2</sub>), 26.0 (*CH*<sub>2</sub>) ppm.

The monomers **1a-c** and **9** were polymerized using Grubbs' 1<sup>st</sup> generation catalyst, which was added in a monomer-catalyst ratio of 250:1. The polymerizations were carried out at 130 °C for 24 h and yielded polymers (**11a-c**, **12**), which were insoluble in any tested solvent ( $\eta$  = 41-64 %).

**Table 7:** Experimental details for the synthesis of DAP-uP-Me-16 (**11d**) and corresponding molecular weight data.

| entry | catalyst          | M:cat. | T<br>[°C] | time<br>[h] | M <sub>n</sub> <sup>e)</sup> (GPC)<br>[g/mol] | PDI | M <sub>n</sub> <sup>f)</sup> (NMR)<br>[g/mol] | yield <sup>g)</sup><br>[%] |
|-------|-------------------|--------|-----------|-------------|---|-----|---|----------------------------|
| 1     | G1 <sup>a)</sup>  | 250:1  | 50        | 144         | 13980   | 1.6 | -   | 22                         |
| 2     | G1 <sup>b)</sup>  | 250:1  | 50        | 144         | 15380   | 1.6 | -   | 14                         |
| 3     | G1 <sup>c)</sup>  | 250:1  | 50        | 144         | 21060   | 1.8 | -   | 30                         |
| 4     | G1 <sup>c)</sup>  | 250:1  | 100       | 24          | 41340   | 1.8 | -   | 7                          |
| 5     | G1 <sup>d)</sup>  | 250:1  | 100       | 24          | 76220   | 1.3 | -   | 12                         |
| 6     | G2 <sup>d)</sup>  | 250:1  | 65        | 24          | 1670  | 2.1 | -   | 75                         |
| 7     | G3 <sup>d)</sup>  | 250:1  | 65        | 24          | 680   | 1.7 | 15040   | 3                          |
| 8     | GH1 <sup>d)</sup> | 250:1  | 65        | 24          | 5770  | 1.9 | 16780   | 93                         |
| 9     | U1 <sup>d)</sup>  | 250:1  | 65        | 24          | 2330  | 2.0 | 11950   | 83                         |
| 10    | GH1 <sup>d)</sup> | 370:1  | 65        | 48          | 3360  | 1.7 | 5114  | 92                         |
| 11    | GH1 <sup>d)</sup> | 250:1  | 65        | 48          | 4250  | 1.6 | 20520   | 98                         |
| 12    | GH1 <sup>d)</sup> | 250:1  | 65-85     | 24          | 4570  | 2.4 | 41070   | 75                         |
| 13    | GH1 <sup>d)</sup> | 250:1  | 65-85     | 24          | 14930   | 1.4 | 43051   | 85                         |
| 14    | G1                | 250:1  | 65-85     | 24          | 8940  | 1.4 | 7821  | 63                         |

<sup>a)</sup>catalyst was added as stock solution in THF/HCl(0.1M) 50/50; <sup>b)</sup>catalyst was added as stock solution in toluene/HCl(0.1M) 50/50; <sup>c)</sup>catalyst was added as stock solution in dry toluene; <sup>d)</sup>catalyst was added as stock solution in dry DCM; <sup>e)</sup>determined by GPC analysis in HPLC-grade THF using polystyrene calibration; <sup>f)</sup>calculated from the ratio of signals assigned to the terminal olefins at 5.91-5.64 ppm as well as 5.10-4.78 ppm and the signals of the newly formed internal double bond at 5.47-5.12 ppm in the <sup>1</sup>H-NMR spectrum; <sup>g)</sup>isolated yields after purification.

**Table 8:** Experimental details for the synthesis of DAP-uP-Me-18 (**11e**) and corresponding molecular weight data.

| entry           | catalyst          | M:cat. | T<br>[°C] | time<br>[h] | M <sub>n</sub> <sup>f)</sup> (GPC)<br>[g/mol] | PDI | M <sub>n</sub> <sup>g)</sup> (NMR)<br>[g/mol] | yield <sup>h)</sup><br>[%] |
|-----------------|-------------------|--------|-----------|-------------|---|-----|---|----------------------------|
| 1               | GH1 <sup>e)</sup> | 250:1  | 65-85     | 48          | 3090  | 2.3 | 3902  | 61                         |
| 2               | GH1 <sup>e)</sup> | 250:1  | 65-85     | 24          | 3640  | 1.6 | 5222  | 97                         |
| 3 <sup>a)</sup> | GH1 <sup>e)</sup> | 250:1  | 40-50     | 24          | -   | -   | -   | -                          |
| 4 <sup>b)</sup> | GH1 <sup>e)</sup> | 250:1  | 40-50     | 24          | -   | -   | -   | -                          |
| 5 <sup>c)</sup> | GH1 <sup>e)</sup> | 250:1  | 40        | 24          | -   | -   | -   | -                          |
| 6 <sup>d)</sup> | GH1 <sup>e)</sup> | 250:1  | 60        | 24          | 3640  | 1.5 | 4606  | 93                         |
| 7               | G1                | 250:1  | 65-85     | 24          | 4720  | 1.4 | 4354  | 58                         |

<sup>a)</sup>addition of SnCl<sub>2</sub> (20 eq.)<sup>91</sup>; <sup>b)</sup>addition of SnBr<sub>2</sub> (20 eq.)<sup>91</sup>; <sup>c)</sup>addition of 2,6-dichloro-1,4-benzoquinone (1 eq.)<sup>92</sup>; <sup>d)</sup>addition of phenylphosphoric acid (5mol%)<sup>93</sup>; <sup>e)</sup>catalyst was added as stock solution in dry DCM; <sup>f)</sup>determined by GPC analysis in HPLC-grade THF using polystyrene calibration; <sup>g)</sup>calculated from the ratio of signals assigned to the terminal olefins at 5.91-5.64 ppm as well as 5.10-4.78 ppm and the signals of the newly formed internal double bond at 5.47-5.12 ppm in the <sup>1</sup>H-NMR spectrum; <sup>h)</sup>isolated yields after purification.

**Table 9:** Experimental details for the synthesis of DAP-uP-Me-20 (**11f**) and corresponding molecular weight data.

| entry    | catalyst         | M:cat. | T<br>[°C] | time<br>[h] | M <sub>n</sub> <sup>b</sup> (GPC)<br>[g/mol] | PDI | M <sub>n</sub> <sup>c</sup> (NMR)<br>[g/mol] | yield <sup>d</sup><br>[%] |
|----------|------------------|--------|-----------|-------------|--|-----|--|---------------------------|
| <b>1</b> | GH1 <sup>a</sup> | 250:1  | 65-85     | 24          | 19270  | 1.8 | 12670  | 70                        |
| <b>2</b> | GH1 <sup>a</sup> | 250:1  | 65-85     | 24          | 8980   | 1.8 | 8661   | 83                        |
| <b>3</b> | GH1 <sup>a</sup> | 50:1   | 65-85     | 24          | 16280  | 1.6 | -  | 64                        |
| <b>4</b> | GH1 <sup>a</sup> | 100:1  | 65-85     | 24          | 17000  | 1.9 | -  | 75                        |
| <b>5</b> | GH1 <sup>a</sup> | 250:1  | 65-85     | 24          | 13140  | 1.8 | -  | 90                        |
| <b>6</b> | GH1 <sup>a</sup> | 500:1  | 65-85     | 24          | 9460   | 2.1 | -  | 87                        |
| <b>7</b> | GH1 <sup>a</sup> | 1000:1 | 65-85     | 24          | 8050   | 2.1 | -  | 72                        |
| <b>8</b> | G1               | 250:1  | 65-85     | 24          | 6170   | 1.5 | 11134  | 83                        |

<sup>a</sup>catalyst was added as stock solution in dry DCM; <sup>b</sup>determined by GPC analysis in HPLC-grade THF using polystyrene calibration; <sup>c</sup>calculated from the ratio of signals assigned to the terminal olefins at 5.91-5.64 ppm as well as 5.10-4.78 ppm and the signals of the newly formed internal double bond at 5.47-5.12 ppm in the <sup>1</sup>H-NMR spectrum; <sup>d</sup>isolated yields after purification.

**Table 10:** Experimental details for the synthesis of the *N*-benzyl protected DAP containing polymers (**11g-i**) and corresponding molecular weight data.

| M         | entry | catalyst <sup>a</sup> | M:cat. | T<br>[°C] | time<br>[h] | M <sub>n</sub> <sup>b</sup> (GPC)<br>[g/mol] | PDI | M <sub>n</sub> <sup>c</sup> (NMR)<br>[g/mol] | yield <sup>d</sup><br>[%] |
|-----------|-------|-----------------------|--------|-----------|-------------|--|-----|--|---------------------------|
| <b>2d</b> | 1     | GH1                   | 250:1  | 65-85     | 24          | 3210   | 1.6 | 6645   | 98                        |
|           | 2     | GH1                   | 250:1  | 65-85     | 24          | 2720   | 2.2 | 7211   | 85                        |
| <b>2e</b> | 1     | GH1                   | 250:1  | 65-85     | 24          | 6410   | 1.6 | -  | 95                        |
|           | 2     | GH1                   | 250:1  | 65-85     | 24          | 4370   | 2.1 | 32225  | 65                        |
| <b>2f</b> | 1     | GH1                   | 250:1  | 65-85     | 24          | 8720   | 1.8 | 28915  | 87                        |
|           | 2     | GH1                   | 250:1  | 65-85     | 24          | 9890   | 2.1 | 20305  | 62                        |

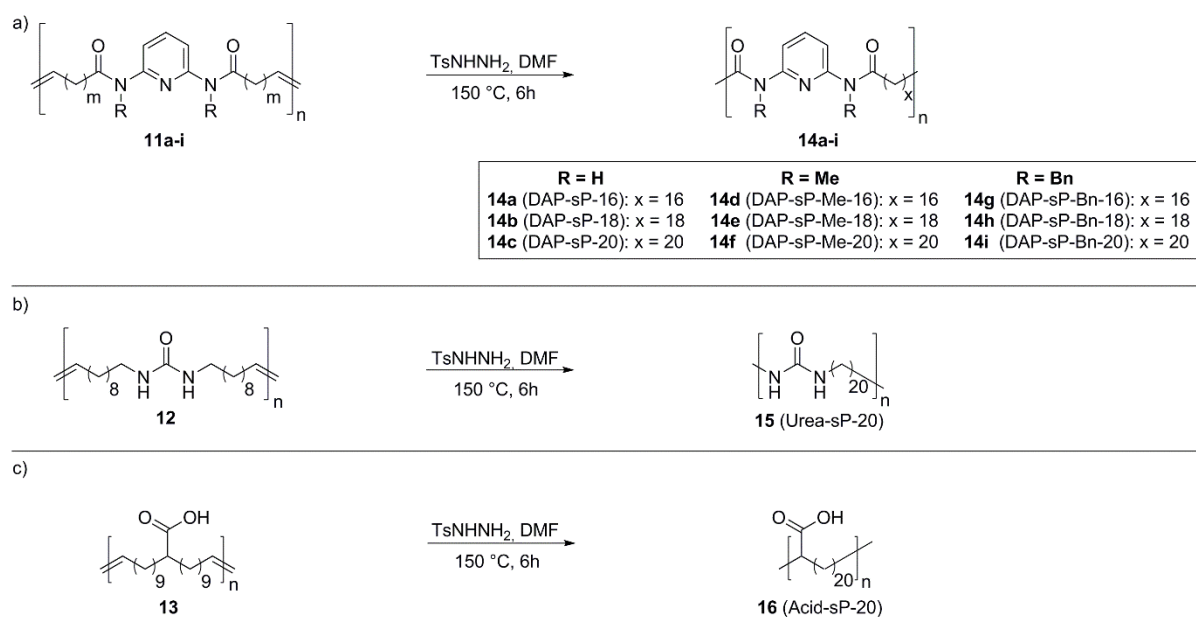
<sup>a</sup>catalyst was added as stock solution in dry DCM; <sup>b</sup>determined by GPC analysis in HPLC-grade THF using polystyrene calibration; <sup>c</sup>calculated from the ratio of signals assigned to the terminal olefins at 5.91-5.64 ppm as well as 5.10-4.78 ppm and the signals of the newly formed internal double bond at 5.47-5.12 ppm in the <sup>1</sup>H-NMR spectrum; <sup>d</sup>isolated yields after purification.

**Table 11:** Experimental details for the synthesis of Acid-uP-20 (**13**) and corresponding molecular weight data.

| entry    | catalyst | M:cat. | T<br>[°C] | time<br>[h] | M <sub>n</sub> <sup>a</sup> (GPC)<br>[g/mol] | PDI | M <sub>n</sub> <sup>b</sup> (NMR)<br>[g/mol] | yield <sup>c</sup><br>[%] |
|----------|----------|--------|-----------|-------------|--|-----|--|---------------------------|
| <b>1</b> | G1       | 250:1  | 65-85     | 24          | 16270  | 2.1 | 76681  | 96                        |

<sup>a</sup>determined by GPC analysis in HPLC-grade THF using polystyrene calibration; <sup>b</sup>calculated from the ratio of signals assigned to the terminal olefins at 5.91-5.64 ppm as well as 5.10-4.78 ppm and the signals of the newly formed internal double bond at 5.47-5.12 ppm in the <sup>1</sup>H-NMR spectrum; <sup>c</sup>isolated yields after purification

## 4.5 Hydrogenation



**Scheme 22:** Hydrogenation of the a) unprotected and protected DAP containing polymers (**11a-i**), b) urea containing polymer (**12**) and c) acid containing polymer (**13**).

The hydrogenation reactions were carried out analogous to literature<sup>217,282,285</sup> and previous investigations<sup>269,270</sup> under a dry, inert atmosphere of nitrogen. DAP-sP-Me-16 (**14d**) ( $3.35 \cdot 10^{-5}$  mol, 0.30 g), TsNHNH<sub>2</sub> (2.89 mmol, 539.88 mg, 4 eq. according to the amount of double bonds), DIPEA ( $9.05 \cdot 10^{-5}$  mol, 15.38  $\mu$ L) and DMF (10 mL) were placed in a one-necked round bottom flask. The reaction mixture was flushed with nitrogen for 30 minutes and heated to 150 °C for 6 h while stirring vigorously. After cooling to room temperature the solvent was removed in vacuum at 45 °C, followed by the addition of THF in order to dissolve the crude product. The final polymer DAP-sP-Me-16 (**14d**) was obtained by precipitation into cold methanol as beige solid in a yield of 70 % (0.21 mg). All other polymers **14a-c**, **14e-i**, **15** and **16** were synthesized analogously to this procedure with yields ranging from 33-99 %. The characterization data are shown in Table 12-Table 14. Selected NMR and IR spectra as well as MALDI ToF MS analyses are shown in Figures A 36-A 45.

### 14a (DAP-sP-16):

#### IR (KBr) [ $\text{cm}^{-1}$ ]

3313 (s), 2920 (s), 2849 (s), 1671 (s), 1589 (s), 1524 (s), 1469 (s), 1412 (m), 1301 (m), 1242 (m), 1176 (m), 996 (w), 802 (m), 723 (m), 640 (m).

### 14b (DAP-sP-18):

#### IR (KBr) [ $\text{cm}^{-1}$ ]

3312 (s), 2920 (s), 2849 (s), 1671 (s), 1589 (s), 1524 (s), 1468 (s), 1412 (m), 1304 (m), 1242 (m), 1175 (m), 801 (m), 723 (m), 641 (m).

**14c (DAP-sP-20):**IR (KBr) [cm<sup>-1</sup>]

3316 (s), 2920 (s), 2849 (s), 1672 (s), 1588 (s), 1525 (s), 1468 (s), 1412 (m), 1301 (m), 1242 (m), 1176 (m), 802 (m), 723 (m), 625 (m).

**14d (DAP-sP-Me-16):**<sup>1</sup>H-NMR (400 MHz, CDCl<sub>3</sub>)

δ = 7.75 (*t*, 1H, <sup>3</sup>J<sub>H,H</sub> = 7.9 Hz, *CH*), 7.25 (*d*, 2H, <sup>3</sup>J<sub>H,H</sub> = 4.2 Hz, *CH*), 3.36 (*s*, 6H, *CH*<sub>3</sub>), 2.36 (*t*, 4H, <sup>3</sup>J<sub>H,H</sub> = 7.6 Hz, *CH*<sub>2</sub>), 1.63 (*t*, 4H, <sup>3</sup>J<sub>H,H</sub> = 7.1 Hz, *CH*<sub>2</sub>), 1.34 – 1.10 (*m*, 36H, *CH*<sub>2</sub>), 0.86 (*t*, 6H, <sup>3</sup>J<sub>H,H</sub> = 6.7 Hz, *CH*<sub>3</sub>) ppm.

<sup>13</sup>C-NMR (126 MHz, CDCl<sub>3</sub>)

δ = 173.7 (C=O), 155.0 (C<sub>quart.</sub>), 139.8 (Ar-C), 117.6 (Ar-C), 35.4 (CH<sub>3</sub>), 35.3 (CH<sub>2</sub>), 32.0 (CH<sub>2</sub>), 29.8 (CH<sub>2</sub>), 29.8 (CH<sub>2</sub>), 29.8 (CH<sub>2</sub>), 29.7 (CH<sub>2</sub>), 29.6 (CH<sub>2</sub>), 29.5 (CH<sub>2</sub>), 25.5 (CH<sub>2</sub>), 22.8 (CH<sub>2</sub>), 14.2 (CH<sub>3</sub>) ppm.

MALDI ToF MS [DCTB, LiTFA, 25:5:1] [m/z]

[M+Li]<sup>+</sup> C<sub>152</sub>H<sub>252</sub>Li<sub>1</sub>N<sub>18</sub>O<sub>12</sub><sup>+</sup>: calculated 2527.981 g/mol, found 2527.168 g/mol.

**14e (DAP-sP-Me-18):**<sup>1</sup>H-NMR (400 MHz, CDCl<sub>3</sub>)

δ = 7.75 (*t*, 1H, <sup>3</sup>J<sub>H,H</sub> = 7.9 Hz, *CH*), 7.24 (*d*, 2H, <sup>3</sup>J<sub>H,H</sub> = 7.7 Hz, *CH*), 3.36 (*s*, 6H, *CH*<sub>3</sub>), 2.36 (*t*, 4H, <sup>3</sup>J<sub>H,H</sub> = 7.6 Hz, *CH*<sub>2</sub>), 1.64 (*t*, 4H, <sup>3</sup>J<sub>H,H</sub> = 7.6 Hz, *CH*<sub>2</sub>), 1.35 – 1.15 (*m*, 40H, *CH*<sub>2</sub>), 0.87 (*t*, 6H, <sup>3</sup>J<sub>H,H</sub> = 6.8 Hz, *CH*<sub>3</sub>) ppm.

<sup>13</sup>C-NMR (101 MHz, CDCl<sub>3</sub>)

δ = 173.7 (C=O), 155.0 (C<sub>quart.</sub>), 139.8 (Ar-C), 117.7 (Ar-C), 35.4 (CH<sub>2</sub>), 35.3 (CH<sub>2</sub>), 32.0 (CH<sub>2</sub>), 29.9 (CH<sub>2</sub>), 29.9 (CH<sub>2</sub>), 29.8 (CH<sub>2</sub>), 29.8 (CH<sub>2</sub>), 29.7 (CH<sub>2</sub>), 29.5 (CH<sub>2</sub>), 25.5 (CH<sub>2</sub>), 22.8 (CH<sub>2</sub>), 14.3 (CH<sub>3</sub>) ppm.

MALDI ToF MS [DCTB, LiTFA, 25:5:1] [m/z]

[M+Li]<sup>+</sup> C<sub>164</sub>H<sub>276</sub>Li<sub>1</sub>N<sub>18</sub>O<sub>12</sub><sup>+</sup>: calculated 2696.169 g/mol, found 2696.283 g/mol.

**14f (DAP-sP-Me-20):**<sup>1</sup>H-NMR (400 MHz, CDCl<sub>3</sub>)

δ = 7.74 (*t*, 1H, <sup>3</sup>J<sub>H,H</sub> = 7.9 Hz, *CH*), 7.23 (*d*, 2H, <sup>3</sup>J<sub>H,H</sub> = 7.7 Hz, *CH*), 3.35 (*s*, 6H, *CH*<sub>3</sub>), 2.34 (*t*, 4H, <sup>3</sup>J<sub>H,H</sub> = 7.5 Hz, *CH*<sub>2</sub>), 1.71 – 1.55 (*m*, 4H, *CH*<sub>2</sub>), 1.22 (*bs*, 48H, *CH*<sub>2</sub>), 0.86 (*t*, 6H, <sup>3</sup>J<sub>H,H</sub> = 6.8 Hz, *CH*<sub>3</sub>) ppm.

<sup>13</sup>C-NMR (126 MHz, CDCl<sub>3</sub>)

δ = 173.7 (C=O), 154.9 (C<sub>quart.</sub>), 139.8 (Ar-C), 117.6 (Ar-C), 35.3 (CH<sub>3</sub>), 35.3 (CH<sub>2</sub>), 32.0 (CH<sub>2</sub>), 29.8 (CH<sub>2</sub>), 29.8 (CH<sub>2</sub>), 29.8 (CH<sub>2</sub>), 29.8 (CH<sub>2</sub>), 29.7 (CH<sub>2</sub>), 29.6 (CH<sub>2</sub>), 29.6 (CH<sub>2</sub>), 25.4 (CH<sub>2</sub>), 22.8 (CH<sub>2</sub>), 14.2 (CH<sub>3</sub>) ppm.

MALDI ToF MS [DCTB, LiTFA, 25:5:1] [m/z]

[M+Li]<sup>+</sup> C<sub>176</sub>H<sub>300</sub>Li<sub>1</sub>N<sub>18</sub>O<sub>12</sub><sup>+</sup>: calculated 2864.356 g/mol, found 2863.460 g/mol.

**14g (DAP-sP-Bn-16):**<sup>1</sup>H-NMR (400 MHz, CDCl<sub>3</sub>)

$\delta$  = 7.60 (*t*, 1H, <sup>3</sup>*J*<sub>H,H</sub> = 7.9 Hz, *CH*), 7.24 – 7.12 (*m*, 10H, *CH*), 7.09 (*d*, 2H, <sup>3</sup>*J*<sub>H,H</sub> = 6.5 Hz, *CH*), 5.01 (*s*, 4H, *CH*<sub>2</sub>), 2.23 (*t*, 4H, <sup>3</sup>*J*<sub>H,H</sub> = 7.1 Hz, *CH*<sub>2</sub>), 1.66 – 1.49 (*m*, 4H, *CH*<sub>2</sub>), 1.21 (*bs*, 40H, *CH*<sub>2</sub>), 0.86 (*t*, 6H, <sup>3</sup>*J*<sub>H,H</sub> = 6.8 Hz, *CH*<sub>3</sub>) ppm.

<sup>13</sup>C-NMR (101 MHz, CDCl<sub>3</sub>)

$\delta$  = 173.6 (*C=O*), 154.1 (*C*<sub>quart.</sub>), 139.8 (*Ar-C*), 137.7 (*C*<sub>quart.</sub>), 128.6 (*Ar-C*), 127.7 (*Ar-C*), 127.3 (*Ar-C*), 119.0 (*Ar-C*), 51.0 (*CH*<sub>2</sub>), 35.3 (*CH*<sub>2</sub>), 29.8 (*CH*<sub>2</sub>), 29.8 (*CH*<sub>2</sub>), 29.7 (*CH*<sub>2</sub>), 29.6 (*CH*<sub>2</sub>), 29.5 (*CH*<sub>2</sub>), 25.5 (*CH*<sub>2</sub>), 21.2 (*CH*<sub>2</sub>) ppm.

**14h (DAP-sP-Bn-18):**<sup>1</sup>H-NMR (400 MHz, CDCl<sub>3</sub>)

$\delta$  = 7.60 (*t*, 1H, <sup>3</sup>*J*<sub>H,H</sub> = 7.9 Hz, *CH*), 7.24 – 7.14 (*m*, 10H, *CH*), 7.10 (*d*, 2H, <sup>3</sup>*J*<sub>H,H</sub> = 6.3 Hz, *CH*), 5.01 (*s*, 4H, *CH*<sub>2</sub>), 2.23 (*t*, 4H, <sup>3</sup>*J*<sub>H,H</sub> = 7.2 Hz, *CH*<sub>2</sub>), 1.66 – 1.50 (*m*, 4H, *CH*<sub>2</sub>), 1.44 – 1.06 (*m*, 40H, *CH*<sub>2</sub>), 0.95 – 0.77 (*m*, 6H, *CH*<sub>3</sub>) ppm.

<sup>13</sup>C-NMR (101 MHz, CDCl<sub>3</sub>)

$\delta$  = 173.6 (*C=O*), 154.1 (*C*<sub>quart.</sub>), 139.7 (*Ar-C*), 137.7 (*C*<sub>quart.</sub>), 128.6 (*Ar-C*), 127.7 (*Ar-C*), 127.3 (*Ar-C*), 119.0 (*Ar-C*), 51.0 (*CH*<sub>2</sub>), 35.3 (*CH*<sub>2</sub>), 29.9 (*CH*<sub>2</sub>), 29.9 (*CH*<sub>2</sub>), 29.8 (*CH*<sub>2</sub>), 29.7 (*CH*<sub>2</sub>), 29.6 (*CH*<sub>2</sub>), 29.5 (*CH*<sub>2</sub>), 25.5 (*CH*<sub>2</sub>) ppm.

**14i (DAP-sP-Bn-20):**<sup>1</sup>H-NMR (500 MHz, CDCl<sub>3</sub>)

$\delta$  = 7.60 (*t*, 1H, <sup>3</sup>*J*<sub>H,H</sub> = 7.9 Hz, *CH*), 7.25 – 7.15 (*m*, 10H, *CH*), 7.14 – 6.98 (*m*, 2H, *CH*), 5.01 (*s*, 4H, *CH*<sub>2</sub>), 2.23 (*t*, 4H, <sup>3</sup>*J*<sub>H,H</sub> = 7.2 Hz, *CH*<sub>2</sub>), 1.64 – 1.49 (*m*, 4H, *CH*<sub>2</sub>), 1.34 – 1.09 (*m*, 48H, *CH*<sub>2</sub>), 0.92 – 0.76 (*m*, 6H, *CH*<sub>3</sub>) ppm.

<sup>13</sup>C-NMR (126 MHz, CDCl<sub>3</sub>)

$\delta$  = 173.6 (*C=O*), 154.1 (*C*<sub>quart.</sub>), 139.7 (*Ar-C*), 137.7 (*Ar-C*), 128.6 (*Ar-C*), 127.7 (*Ar-C*), 127.3 (*Ar-C*), 119.0 (*Ar-C*), 51.0 (*CH*<sub>2</sub>), 35.3 (*CH*<sub>2</sub>), 29.9 (*CH*<sub>2</sub>), 29.9 (*CH*<sub>2</sub>), 29.9 (*CH*<sub>2</sub>), 29.8 (*CH*<sub>2</sub>), 29.7 (*CH*<sub>2</sub>), 29.6 (*CH*<sub>2</sub>), 29.5 (*CH*<sub>2</sub>), 29.4 (*CH*<sub>2</sub>), 25.5 (*CH*<sub>2</sub>), 21.0 (*CH*<sub>2</sub>), 14.3 (*CH*<sub>3</sub>) ppm.

**15 (Urea-sP-20):**IR (KBr) [cm<sup>-1</sup>]

3344 (*s*), 3051 (*w*), 2921 (*s*), 2850 (*s*), 1617 (*s*), 1574 (*s*), 1468 (*m*), 1237 (*w*), 809 (*w*), 721 (*w*), 618 (*m*).

**16 (Acid-sP-20):**<sup>1</sup>H-NMR (400 MHz, THF-d<sub>8</sub>)

$\delta$  = 2.26 – 2.15 (*m*, 1H, *CH*), 1.62 – 1.32 (*m*, 4H, *CH*<sub>2</sub>), 1.33 – 1.05 (*m*, 36H, *CH*<sub>2</sub>), 0.82 (*t*, 6H, <sup>3</sup>*J*<sub>H,H</sub> = 6.6 Hz, *CH*<sub>3</sub>) ppm.

<sup>13</sup>C-NMR (126 MHz, CDCl<sub>3</sub>)

$\delta$  = 178.0 (*C=O*), 46.4 (*CH*), 35.6 (*CH*<sub>2</sub>), 33.5 (*CH*<sub>2</sub>), 30.7 (*CH*<sub>2</sub>), 28.5 (*CH*<sub>2</sub>), 19.3 (*CH*<sub>3</sub>) ppm.

**Table 12:** Molecular weight data of the *N*-methyl protected DAP containing polymers (**14d-f**).

| precursor             | entry | $M_n^a$ (GPC)<br>[g/mol] | PDI | $M_n^b$ (NMR)<br>[g/mol] | yield <sup>c)</sup><br>[%] |
|-----------------------|-------|--------------------------|-----|--------------------------|----------------------------|
| <b>11d</b> (entry 11) | 1     | 3880                     | 1.4 | 2909                     | 73                         |
| (entry 13)            | 2     | 6090                     | 2.2 | 2493                     | 76                         |
| (entry 14)            | 3     | 8730                     | 1.4 | 6234                     | 70                         |
| <b>11e</b> (entry2)   | 1     | 3140                     | 1.6 | 3407                     | 92                         |
| (entry6)              | 2     | 4320                     | 1.3 | 2497                     | 98                         |
| (entry 7)             | 3     | 4940                     | 1.4 | 3997                     | 86                         |
| <b>11f</b> (entry1)   | 1     | 2170                     | 1.4 | -                        | 74                         |
| (entry 2)             | 2     | 6380                     | 1.8 | 8344                     | 99                         |
| (entry 3)             | 3     | 2070                     | 1.4 | -                        | 83                         |
| (entry 4)             | 4     | 1120                     | 1.6 | -                        | 68                         |
| (entry 5)             | 5     | 7120                     | 1.8 | -                        | 77                         |
| (entry 6)             | 6     | 6720                     | 2.0 | -                        | 79                         |
| (entry 7)             | 7     | 6760                     | 1.9 | -                        | 85                         |
| (entry 8)             | 8     | 4720                     | 1.4 | 6042                     | 61                         |

<sup>a)</sup> determined by GPC analysis in HPLC-grade THF using polystyrene calibration; <sup>b)</sup>calculated from the ratio of signals assigned to the terminal methyl groups at 0.95-0.76 ppm and the signal of the aromatic unit at 7.75-7.60 ppm in the <sup>1</sup>H-NMR spectrum; <sup>c)</sup>isolated yields after purification.

**Table 13:** Molecular weight data of the *N*-benzyl protected DAP containing polymers (**14g-i**).

| precursor            | entry | $M_n^a$ (GPC)<br>[g/mol] | PDI | $M_n^b$ (NMR)<br>[g/mol] | yield <sup>c)</sup><br>[%] |
|----------------------|-------|--------------------------|-----|--------------------------|----------------------------|
| <b>11g</b> (entry 2) | 1     | 4430                     | 1.6 | 8204                     | 68                         |
| <b>11h</b> (entry2)  | 1     | 7460                     | 1.4 | 8634                     | 33                         |
| <b>11i</b> (entry2)  | 1     | 10000                    | 1.9 | 5278                     | 53                         |

<sup>a)</sup> determined by GPC analysis in HPLC-grade THF using polystyrene calibration; <sup>b)</sup>calculated from the ratio of signals assigned to the terminal methyl groups at 0.95-0.76 ppm and the signal of the aromatic unit at 7.75-7.60 ppm in the <sup>1</sup>H-NMR spectrum; <sup>c)</sup>isolated yields after purification.

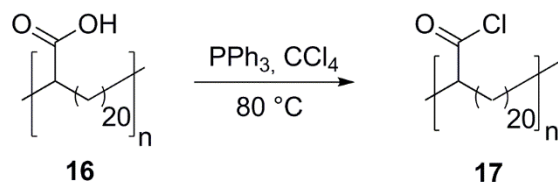
**Table 14:** Molecular weight data of Acid-sP-20 (**16**).

| precursor | entry | $M_n^a$ (GPC)<br>[g/mol] | PDI | $M_n^b$ (NMR)<br>[g/mol] | yield <sup>c)</sup><br>[%] |
|-----------|-------|--------------------------|-----|--------------------------|----------------------------|
| <b>13</b> | 1     | 18250                    | 1.9 | 5606                     | 48                         |

<sup>a)</sup> determined by GPC analysis in HPLC-grade THF using polystyrene calibration; <sup>b)</sup>calculated from the ratio of signals assigned to the terminal methyl groups at 0.95-0.76 ppm and the signal assigned to the proton next to the carboxylic acid functionality at 2.26-2.15 ppm in the <sup>1</sup>H-NMR spectrum; <sup>c)</sup>isolated yields after purification.

## 4.6 Post-functionalization of Acid-sP-20

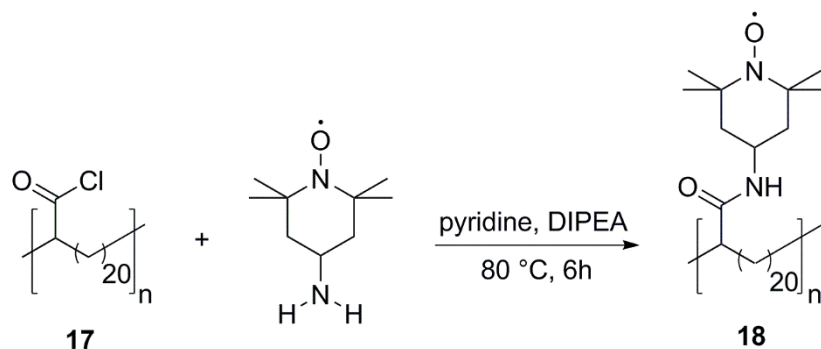
### 4.6.1 Chlorination of Acid-sP-20



**Scheme 23:** Synthesis of Acid-Cl-sP-20 (17).

The reaction was carried out analogous to literature<sup>227</sup> under a dry, inert atmosphere of nitrogen. A one-necked round bottom flask, equipped with a reflux condenser was filled with Acid-sP-20 (0.02 mmol, 0.30 g) and  $\text{PPh}_3$  (0.02 mmol, 6.47 mg), dissolved in  $\text{CCl}_4$  (5 mL). The reaction mixture was heated to  $80\text{ }^\circ\text{C}$  and was allowed to stir overnight, followed by the removal of the solvent in vacuum at  $45\text{ }^\circ\text{C}$ . After the addition of hexane, the mixture was filtered and the filtrate was concentrated in vacuum at  $45\text{ }^\circ\text{C}$  to yield Acid-Cl-sP-20 (17), which was directly used without further purification.

### 4.6.2 Synthesis of TEMPO-sP-20 (18)



**Scheme 24:** Synthesis of TEMPO-sP-20 (18).

The synthesis was carried out analogous to literature.<sup>277</sup> A one-necked round bottom flask was filled with Acid-Cl-sP-20 (0.02 mmol, 0.29 g), 4-amino-2,2,6,6-tetramethylpiperidine 1-oxyl (0.02 mmol, 3.10 mg) and DIPEA (100  $\mu\text{L}$ ), dissolved in pyridine (5 mL). The reaction mixture was stirred at  $80\text{ }^\circ\text{C}$  for 6 h, followed by pouring the mixture into an HCl-solution (10% in  $\text{H}_2\text{O}$ ). After the addition of ethyl acetate (30 mL) the organic phase was separated and washed twice with saturated sodium bicarbonate solution and dried over  $\text{MgSO}_4$ . The final product was obtained after passing the mixture through a neutral alumina column using DCM and removing the solvent in vacuum at  $45\text{ }^\circ\text{C}$  as orange solid. (0.01 mmol, 0.17 g, 59 %). Determination of the molecular weight via GPC was not possible as the compound gave no signal during the measurement. The MALDI ToF MS analysis is shown in Figure 34.

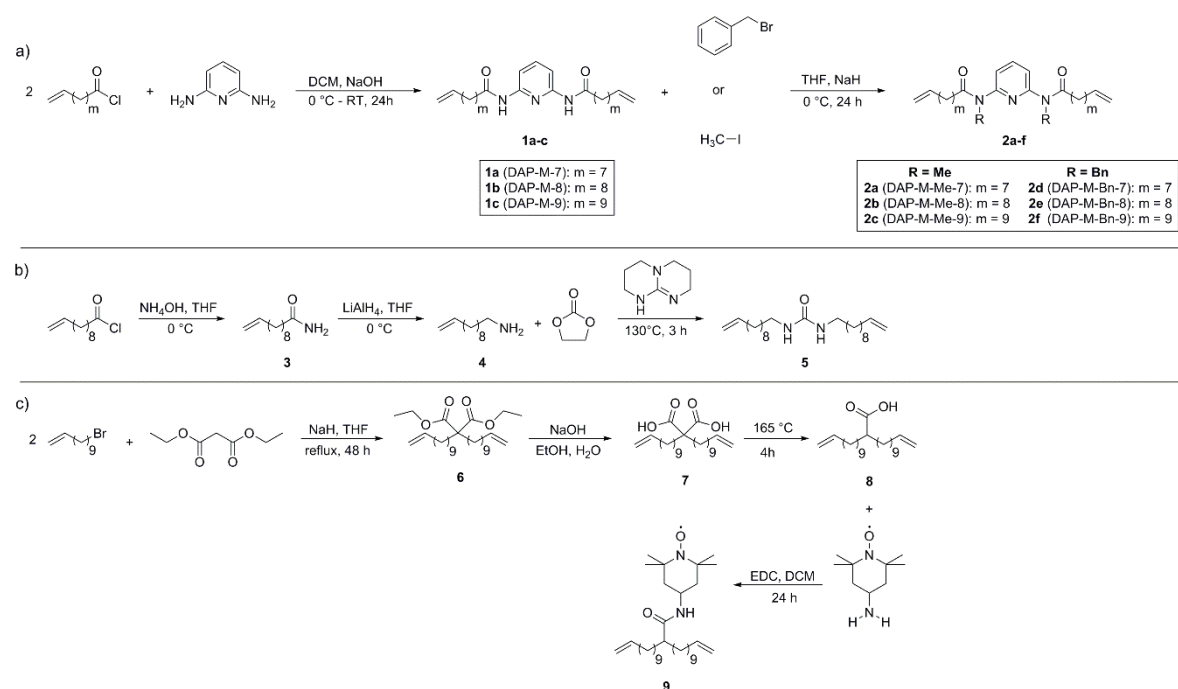


## 5. Summary

The aim of this thesis was the synthesis of precision polymers bearing different supramolecular groups via ADMET polymerization and their crystallographic characterization to determine the influence of various constraints on the crystallization of polyethylene analogues. 2,6-Diaminopyridine (DAP) and urea were chosen as supramolecular moieties as they are able to interact via hydrogen bonding and/or  $\pi$ - $\pi$ -stacking. Furthermore, these groups exert a conformational constraint on the polymer chain as they are planar and thus display hindered rotation.

The designed, symmetric monomers were synthesized via multiple step syntheses. Starting from 2,6-diaminopyridine and alkenoic acid chlorides with variable methylene spacer length ( $m = 7, 8$  and  $9$ ), the DAP containing monomers were synthesized using a Schotten-Baumann reaction. Protection of the amide moieties was achieved using methyl iodide or benzyl bromide respectively to sustain the solubility of the products after polymerization.

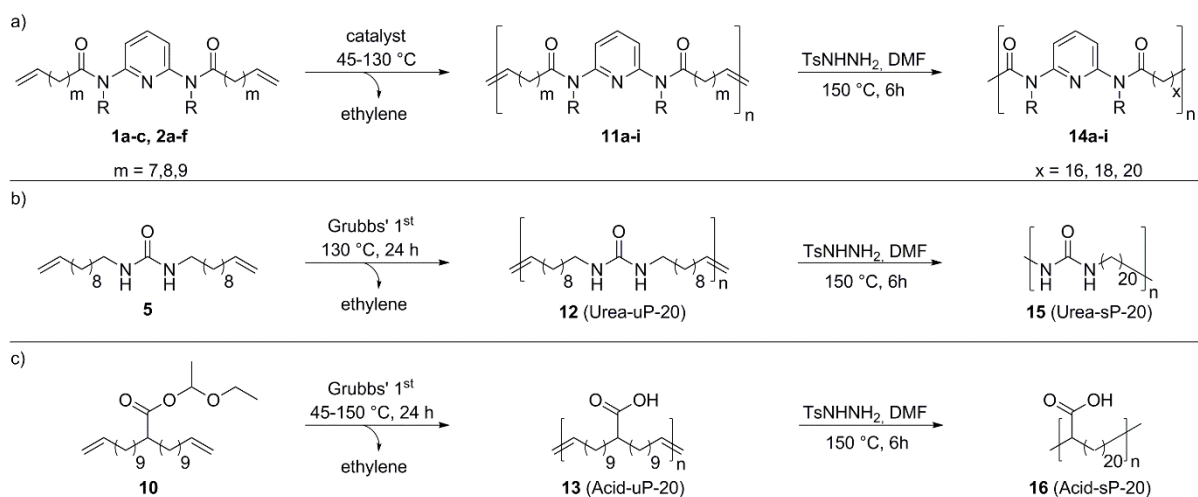
The synthesis of the urea containing polymer was accomplished by the reaction of undec-9-enoyl chloride with ammonium hydroxide, followed by the reduction with  $\text{LiAlH}_4$  and subsequent conversion with ethylene carbonate under use of TBD to yield the final product. Similarly, a monomer bearing a TEMPO moiety was synthesized via reaction of 11-bromo-1-undecene with diethyl malonate, followed by hydrolysis and decarboxylation. Further conversion with 4-amino-TEMPO led to the desired product, planned for investigation of the final polymer via EPR spectroscopy. The reaction schemes for all of the above mentioned syntheses are shown in Scheme 25.



**Scheme 25:** Synthetic route for a) the preparation of the unprotected and protected DAP containing monomers (**1a-c**, **2a-f**), b) the preparation of the urea containing monomer (**5**) and c) the preparation of the TEMPO containing monomer (**9**).

Successful conversions and the purity of the resulting compounds was proven via NMR and IR spectroscopy as well as ESI ToF MS.

All polymerizations were carried out as bulk polymerizations as the used monomers (**1a-c**, **2a-f**, **5** and **9**) were either viscous liquids or present in the molten state at the chosen polymerization temperature. Different Grubbs' type and Umicore catalysts as well as various temperatures and reaction times were tested, whereby the reaction with Grubbs' 1<sup>st</sup> generation catalyst at 65-85 °C (for monomers **2a-f** and **9**) or at 130 °C (for monomers **1a-c** and **5**) for 24 h turned out as the best method, yielding polymers (**11a-i**, **12** and **13**) with molecular weights ranging from 1700 g/mol to 76000 g/mol and polydispersity indices between 1.3 and 2.4. Attempts to polymerize the TEMPO containing monomer (**9**) using Grubbs' 1<sup>st</sup>, Grubbs' 3<sup>rd</sup> or Grubbs' Hoveyda 1<sup>st</sup> generation catalyst did not produce any polymer, wherefore the preparation via post functionalization of Acid-sP-20 (**16**) was chosen. Subsequent hydrogenation was achieved by the reaction with TsNHNH<sub>2</sub> and DIPEA in DMF at 150 °C for 6h and yielded the fully saturated polymers (**14a-i**, **15** and **16**). All polymers were characterized via NMR and IR spectroscopy, GPC and MALDI ToF MS and the corresponding reaction schemes are shown in Scheme 26.



**Scheme 26:** Polymerization and hydrogenation of a) unprotected and protected DAP containing polymers (**11a-i**), b) urea containing polymer (**12**) and c) acid containing polymer (**13**).

The thermal properties of all polymers (**11a-i**, **12**, **14a-i** and **15**) were investigated via DSC analysis whereby all benzyl protected polymers (**11g-i** and **14g-h**), except **14i**, are amorphous, showing no melting point but only a glass transition in the range of -10 to -2 °C. In these polymers the crystallization is hindered due to the sterically demanding benzyl protection group, which can be only compensated in the hydrogenated polymer with a methylene spacer length of  $x = 20$  (**14i**). Exchanging the benzyl with a methyl protection group leads to semi-crystalline polymers ( $X_c = 17-33\%$ ), which exhibit melting temperatures ranging from 60 to 96 °C. The unprotected DAP containing polymers (**14a-c**) show melting temperatures, that are above the  $T_m$  of pure ADMET polyethylene ( $T_m = 134$  °C),<sup>220</sup> explainable by enhanced thermal stability due to hydrogen bonds. Similar melting temperatures are observed for the saturated urea containing polymer (**15**) also caused by hydrogen bonding.

Furthermore, the crystallization behavior was examined via WAXS analysis, whereby a lamellar morphology was determined for all precision polymers (**14a-f**, **15** and **16**).

Investigations on the saturated DAP containing polymers with methyl protection group (**14d-f**) indicate the formation of a mixture of orthorhombic and triclinic crystal structures. Based on the DSC results and the calculated lamellar crystal thicknesses the at least partial incorporation of the functional groups into the crystalline lamella and their parallel arrangement herein was proposed. The unprotected DAP (**14c**) and urea containing (**15**) polymers are assumed to exhibit triclinic crystal structures and the estimated unit cell structures are visualized in Figure 47.

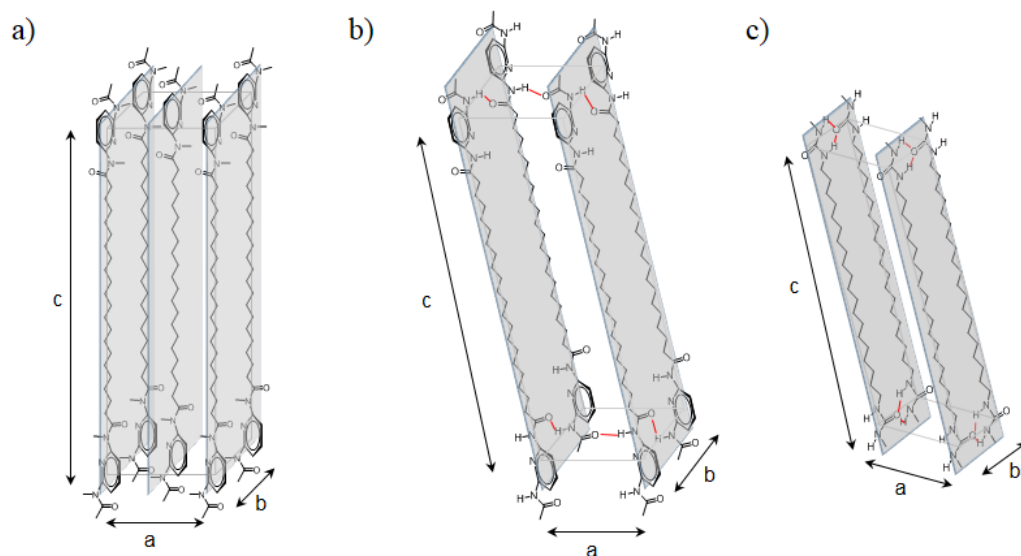


**Figure 47:** Estimated unit cell structures of the a) *N*-methyl protected DAP containing polymer (**14f**), b) the unprotected DAP containing polymer (**14c**) and c) the urea containing polymer (**15**).

That means, despite the introduction of the DAP or urea moieties, the precision polymer is able to form crystallites, whereby the defects are partially incorporated into the crystalline lamella. In the case of the *N*-methyl protected DAP containing polymers the orthorhombic crystal structure is retained but due to the increased space requirement of the defect an expansion of the unit cell compared to pure ADMET PE can be observed. Due to the supramolecular interactions between adjacent DAP units ( $\pi$ - $\pi$ -stacking) they adopt a parallel arrangement forming an ordered substructure within the crystal. Changing the supramolecular interactions from  $\pi$ - $\pi$ -stacking to hydrogen bonding by using unprotected DAP or urea moieties leads to the change from the orthorhombic to a triclinic crystal structure, wherein the defects adopt a ladder-like arrangement.

Moreover, the behavior of the saturated, *N*-methyl protected DAP containing polymers (**14d-f**) in solution was analyzed via DLS measurements. The formation of single-chain polymer nanoparticles and bigger aggregates with sizes ranging from 2-4 nm or 40-60 nm, respectively, which are not changing significantly with time, also confirmed via TEM measurements. The methylene spacer lengths as well as the choice of solvent does seem to have no influence on the particle size. Decreasing the polarity by addition of hexane leads to the unfolding of the polymer chain due to the good solubility of the oligoethylene segments. The addition of methanol and thus an increase in polarity resulted in the precipitation of the precision polymers.

Finally, the influence of the polydispersity on the melting and crystallization behavior was determined by separating the saturated *N*-methyl protected DAP containing polymer with a

methylene spacer length of  $x = 20$  (**14f**) via preparative GPC. The fractionation yielded 14 different fractions with molecular weights ranging from 19500 g/mol to 960 g/mol, which exhibit melting points ranging from 51 °C to 56 °C. WAXS measurements of three chosen fractions yielded diffraction patterns that resemble the pattern of the precursor polymer. Although, the signals become broader with decreasing molecular weight due to the elevation of the amorphous fraction, an orthorhombic crystal structure was assumed.

## 6. References

- [1] Lutz, J.-F.; Ouchi, M.; Liu, D. R.; Sawamoto, M. Sequence-Controlled Polymers. *Science* **2013**, *341*.
- [2] Lutz, J.-F. Sequence-controlled polymerizations: the next Holy Grail in polymer science? *Polym. Chem.* **2010**, *1*, 55-62.
- [3] Lutz, J. F. Defining the Field of Sequence-Controlled Polymers. *Macromol. Rapid Commun.* **2017**, *38*, 1700582.
- [4] Cole, J. P.; Hanlon, A. M.; Rodriguez, K. J.; Berda, E. B. Protein-like structure and activity in synthetic polymers. *J. Polym. Sci. Part A: Polym. Chem.* **2017**, *55*, 191-206.
- [5] Berg, J. M.; Tymoczko, J. L.; Gatto, G. J.; Stryer, L.: *Biochemie*; Springer-Verlag GmbH: Berlin-Heidelberg, 2018; Vol. 8., ISBN 978-3-662-54619-2
- [6] Chagin, V. O.; Stear, J. H.; Cardoso, M. C. Organization of DNA Replication. *Cold Spring Harb. Perspect. Biol.* **2010**, *2*.
- [7] Edward, B. R. Replication, Transcription, and Translation. *Am. Biol. Teach.* **1984**, *46*, 470-472.
- [8] Szymański, J. K.; Abul-Haija, Y. M.; Cronin, L. Exploring Strategies To Bias Sequence in Natural and Synthetic Oligomers and Polymers. *Acc. Chem. Res.* **2018**, *51*, 649-658.
- [9] ten Brummelhuis, N. Controlling monomer-sequence using supramolecular templates. *Polym. Chem.* **2015**, *6*, 654-667.
- [10] Orgel, L. E. Molecular replication. *Nature* **1992**, *358*, 203.
- [11] Li, T.; Nicolaou, K. C. Chemical self-replication of palindromic duplex DNA. *Nature* **1994**, *369*, 218.
- [12] Sievers, D.; von Kiedrowski, G. Self-replication of complementary nucleotide-based oligomers. *Nature* **1994**, *369*, 221.
- [13] Edwardson, T. G. W.; Carneiro, K. M. M.; Serpell, C. J.; Sleiman, H. F. An Efficient and Modular Route to Sequence-Defined Polymers Appended to DNA. *Angew. Chem. Int. Ed.* **2014**, *53*, 4567-4571.
- [14] Milnes, P. J.; McKee, M. L.; Bath, J.; Song, L.; Stulz, E.; Turberfield, A. J.; O'Reilly, R. K. Sequence-specific synthesis of macromolecules using DNA-templated chemistry. *Chem. Commun.* **2012**, *48*, 5614-5616.
- [15] Brix, J.; Koch, H.-G.; Heinrich, P. C.: Transkription und Prozessierung der RNA. In *Löffler/Petrides Biochemie und Pathobiochemie*; Heinrich, P. C., Müller, M., Graeve, L., Eds.; Springer Berlin Heidelberg: Berlin, Heidelberg, 2014; pp 567-587., ISBN 978-3-642-17971-6
- [16] Kozlov, I. A.; Politis, P. K.; Van Aerschot, A.; Busson, R.; Herdewijn, P.; Orgel, L. E. Nonenzymatic Synthesis of RNA and DNA Oligomers on Hexitol Nucleic Acid Templates: The Importance of the A Structure. *J. Am. Chem. Soc.* **1999**, *121*, 2653-2656.

- [17] Kozlov, I. A.; Zielinski, M.; Allart, B.; Kerremans, L.; Van Aerschot, A.; Busson, R.; Herdewijn, P.; Orgel, L. E. Nonenzymatic Template-Directed Reactions on Altritol Oligomers, Preorganized Analogues of Oligonucleotides. *Chem. Eur. J.* **2000**, *6*, 151-155.
- [18] Saiki, R.; Gelfand, D.; Stoffel, S.; Scharf, S.; Higuchi, R.; Horn, G.; Mullis, K.; Erlich, H. Primer-directed enzymatic amplification of DNA with a thermostable DNA polymerase. *Science* **1988**, *239*, 487-491.
- [19] Badi, N.; Lutz, J.-F. Sequence control in polymer synthesis. *Chem. Soc. Rev.* **2009**, *38*, 3383-3390.
- [20] Piccirilli, J. A.; Benner, S. A.; Krauch, T.; Moroney, S. E.; Benner, S. A. Enzymatic incorporation of a new base pair into DNA and RNA extends the genetic alphabet. *Nature* **1990**, *343*, 33.
- [21] Kool, E. T. Replacing the Nucleobases in DNA with Designer Molecules. *Acc. Chem. Res.* **2002**, *35*, 936-943.
- [22] Safak, M.; Alemdaroglu, F. E.; Li, Y.; Ergen, E.; Herrmann, A. Polymerase Chain Reaction as an Efficient Tool for the Preparation of Block Copolymers. *Adv. Mater.* **2007**, *19*, 1499-1505.
- [23] van Hest, J. C. M.; Tirrell, D. A. Protein-based materials, toward a new level of structural control. *Chem. Commun.* **2001**, 1897-1904.
- [24] McGrath, K. P.; Fournier, M. J.; Mason, T. L.; Tirrell, D. A. Genetically directed syntheses of new polymeric materials. Expression of artificial genes encoding proteins with repeating -(AlaGly)<sub>3</sub>ProGluGly- elements. *J. Am. Chem. Soc.* **1992**, *114*, 727-733.
- [25] Lei, W.; G., S. P. Expanding the Genetic Code. *Angew. Chem. Int. Ed.* **2005**, *44*, 34-66.
- [26] L., K. K.; M., v. H. J. C.; A., T. D. Expanding the Scope of Protein Biosynthesis by Altering the Methionyl-tRNA Synthetase Activity of a Bacterial Expression Host. *Angew. Chem. Int. Ed.* **2000**, *39*, 2148-2152.
- [27] Merrifield, R. B. Solid Phase Peptide Synthesis. I. The Synthesis of a Tetrapeptide. *J. Am. Chem. Soc.* **1963**, *85*, 2149-2154.
- [28] Merrifield, R. B. Solid Phase Synthesis (Nobel Lecture). *Angew. Chem. Int. Ed.* **1985**, *24*, 799-810.
- [29] Lutz, J.-F. Coding Macromolecules: Inputting Information in Polymers Using Monomer-Based Alphabets. *Macromolecules* **2015**, *48*, 4759-4767.
- [30] De Bo, G.; Kuschel, S.; Leigh, D. A.; Lewandowski, B.; Pappmeyer, M.; Ward, J. W. Efficient Assembly of Threaded Molecular Machines for Sequence-Specific Synthesis. *J. Am. Chem. Soc.* **2014**, *136*, 5811-5814.
- [31] Lewandowski, B.; De Bo, G.; Ward, J. W.; Pappmeyer, M.; Kuschel, S.; Aldegunde, M. J.; Gramlich, P. M. E.; Heckmann, D.; Goldup, S. M.; D'Souza, D. M.; Fernandes, A. E.; Leigh, D. A. Sequence-Specific Peptide Synthesis by an Artificial Small-Molecule Machine. *Science* **2013**, *339*, 189-193.

- [32] Hartmann, L.; Börner, H. G. Precision Polymers: Monodisperse, Monomer-Sequence-Defined Segments to Target Future Demands of Polymers in Medicine. *Adv. Mater.* **2009**, *21*, 3425-3431.
- [33] Hartmann, L. Polymers for Control Freaks: Sequence-Defined Poly(amidoamine)s and Their Biomedical Applications. *Macromol. Chem. Phys.* **2011**, *212*, 8-13.
- [34] Zuckermann, R. N.; Kerr, J. M.; Kent, S. B. H.; Moos, W. H. Efficient method for the preparation of peptoids [oligo(N-substituted glycines)] by submonomer solid-phase synthesis. *J. Am. Chem. Soc.* **1992**, *114*, 10646-10647.
- [35] Statz, A. R.; Meagher, R. J.; Barron, A. E.; Messersmith, P. B. New Peptidomimetic Polymers for Antifouling Surfaces. *J. Am. Chem. Soc.* **2005**, *127*, 7972-7973.
- [36] Statz, A. R.; Barron, A. E.; Messersmith, P. B. Protein, cell and bacterial fouling resistance of polypeptoid-modified surfaces: effect of side-chain chemistry. *Soft Matter* **2008**, *4*, 131-139.
- [37] Lau, K. H. A.; Ren, C.; Sileika, T. S.; Park, S. H.; Szleifer, I.; Messersmith, P. B. Surface Grafted Polysarcosine as a Peptoid Antifouling Polymer Brush. *Langmuir : the ACS journal of surfaces and colloids* **2012**, *28*, 16099-16107.
- [38] Fetsch, C.; Grossmann, A.; Holz, L.; Nawroth, J. F.; Luxenhofer, R. Polypeptoids from N-Substituted Glycine N-Carboxyanhydrides: Hydrophilic, Hydrophobic, and Amphiphilic Polymers with Poisson Distribution. *Macromolecules* **2011**, *44*, 6746-6758.
- [39] Hadjichristidis, N.; Iatrou, H.; Pitsikalis, M.; Sakellariou, G. Synthesis of Well-Defined Polypeptide-Based Materials via the Ring-Opening Polymerization of  $\alpha$ -Amino Acid N-Carboxyanhydrides. *Chem. Rev.* **2009**, *109*, 5528-5578.
- [40] Habraken, G. J. M.; Wilsens, K. H. R. M.; Koning, C. E.; Heise, A. Optimization of N-carboxyanhydride (NCA) polymerization by variation of reaction temperature and pressure. *Polym. Chem.* **2011**, *2*, 1322-1330.
- [41] Kricheldorf, H. R. Polypeptide und 100 Jahre Chemie der  $\alpha$ -Aminosäure-N-carboxyanhydride. *Angew. Chem.* **2006**, *118*, 5884-5917.
- [42] Gangloff, N.; Fetsch, C.; Luxenhofer, R. Polypeptoids by Living Ring-Opening Polymerization of N-Substituted N-Carboxyanhydrides from Solid Supports. *Macromol. Rapid Commun.* **2013**, *34*, 997-1001.
- [43] Niu, J.; Hili, R.; Liu, D. R. Enzyme-Free Translation of DNA into Sequence-Defined Synthetic Polymers Structurally Unrelated to Nucleic Acids. *Nat. Chem.* **2013**, *5*, 282-292.
- [44] Bamford, C. H.; Block, H.; Imanishi, Y. The chain effect. Part III. Induction of secondary structure in copolymerizations. *Biopolymers* **1966**, *4*, 1067-1072.
- [45] Volpe, R. A.; Frisch, H. L. Template effect on the copolymerization of L-alanine NCA and sarcosine NCA. *Macromolecules* **1987**, *20*, 1747-1752.
- [46] Frisch, H. L.; Xu, Q. Copolymerization of styrene and methacrylic acid in the presence of poly(2-vinylpyridine) as the template. *Macromolecules* **1992**, *25*, 5145-5149.

- [47] Amir, F.; Jia, Z.; Monteiro, M. J. Sequence Control of Macromers via Iterative Sequential and Exponential Growth. *J. Am. Chem. Soc.* **2016**, *138*, 16600-16603.
- [48] Trinh, T. T.; Laure, C.; Lutz, J.-F. Synthesis of Monodisperse Sequence-Defined Polymers Using Protecting-Group-Free Iterative Strategies. *Macromol. Chem. Phys.* **2015**, *216*, 1498-1506.
- [49] Fyles, T. M.; Hu, C.-W.; Luong, H. Solid-Phase Synthesis of Oligoester Ion Channels. *J. Org. Chem.* **2006**, *71*, 8545-8551.
- [50] Kim, J.-M.; Bi, Y.; Paikoff, S. J.; Schultz, P. G. The solid phase synthesis of oligoureas. *Tetrahedron Lett.* **1996**, *37*, 5305-5308.
- [51] Cho, C.; Moran, E.; Cherry; Stephans, J.; Fodor, S.; Adams, C.; Sundaram, A.; Jacobs, J.; Schultz, P. An unnatural biopolymer. *Science* **1993**, *261*, 1303-1305.
- [52] Lutz, J.-F.; Börner, H. G. Modern trends in polymer bioconjugates design. *Prog. Polym. Sci.* **2008**, *33*, 1-39.
- [53] Rose, K.; Vizzavona, J. Stepwise Solid-Phase Synthesis of Polyamides as Linkers. *J. Am. Chem. Soc.* **1999**, *121*, 7034-7038.
- [54] Young, J. K.; Nelson, J. C.; Moore, J. S. Synthesis of Sequence Specific Phenylacetylene Oligomers on an Insoluble Solid Support. *J. Am. Chem. Soc.* **1994**, *116*, 10841-10842.
- [55] Rieger, E.; Alkan, A.; Manhart, A.; Wagner, M.; Wurm, F. R. Sequence-Controlled Polymers via Simultaneous Living Anionic Copolymerization of Competing Monomers. *Macromol. Rapid Commun.* **2016**, *37*, 833-839.
- [56] Aerts, A.; Lewis, R. W.; Zhou, Y.; Malic, N.; Moad, G.; Postma, A. Light-Induced RAFT Single Unit Monomer Insertion in Aqueous Solution - Toward Sequence-Controlled Polymers. *Macromol. Rapid Commun.*, **2018**, *39*, 1800240.
- [57] Klumperman, B. Mechanistic considerations on styrene-maleic anhydride copolymerization reactions. *Polym. Chem.* **2010**, *1*, 558-562.
- [58] Lutz, J.-F.; Schmidt, B. V. K. J.; Pfeifer, S. Tailored Polymer Microstructures Prepared by Atom Transfer Radical Copolymerization of Styrene and N-substituted Maleimides. *Macromol. Rapid Commun.* **2011**, *32*, 127-135.
- [59] Pfeifer, S.; Lutz, J.-F. Development of a Library of N-Substituted Maleimides for the Local Functionalization of Linear Polymer Chains. *Chem. Eur. J.* **2008**, *14*, 10949-10957.
- [60] Zamfir, M.; Lutz, J.-F. Ultra-precise insertion of functional monomers in chain-growth polymerizations. *Nat. Commun.* **2012**, *3*, 1138.
- [61] Chan-Seng, D.; Zamfir, M.; Lutz, J.-F. Polymer-Chain Encoding: Synthesis of Highly Complex Monomer Sequence Patterns by Using Automated Protocols. *Angew. Chem. Int. Ed.* **2012**, *51*, 12254-12257.
- [62] Moatsou, D.; Hansell, C. F.; O'Reilly, R. K. Precision polymers: a kinetic approach for functional poly(norbornenes). *Chem. Sci.* **2014**, *5*, 2246-2250.



- [63] Yoon, K.-H.; Kim, K. O.; Schaefer, M.; Yoon, D. Y. Synthesis and characterization of hydrogenated poly(norbornene endo-dicarboximide)s prepared by ring opening metathesis polymerization. *Polymer* **2012**, *53*, 2290-2297.
- [64] Kanazawa, A.; Aoshima, S. Exclusive One-Way Cycle Sequence Control in Cationic Terpolymerization of General-Purpose Monomers via Concurrent Vinyl-Addition, Ring-Opening, and Carbonyl-Addition Mechanisms. *ACS Macro Lett.* **2015**, *4*, 783-787.
- [65] Minoda, M.; Sawamoto, M.; Higashimura, T. Sequence-regulated oligomers and polymers by living cationic polymerization. *Polym. Bull.* **1990**, *23*, 133-139.
- [66] Minoda, M.; Sawamoto, M.; Higashimura, T. Sequence-regulated oligomers and polymers by living cationic polymerization. 2. Principle of sequence regulation and synthesis of sequence-regulated oligomers of functional vinyl ethers and styrene derivatives. *Macromolecules* **1990**, *23*, 4889-4895.
- [67] Wagener, K. B.; Boncella, J. M.; Nel, J. G. Acyclic diene metathesis (ADMET) polymerization. *Macromolecules* **1991**, *24*, 2649-2657.
- [68] Sauty, N. F.; da Silva, L. C.; Schulz, M. D.; Few, C. S.; Wagener, K. B. Acyclic diene metathesis polymerization and precision polymers. *Appl. Petrochem. Res.* **2014**, *4*, 225-233.
- [69] Opper, K. L.; Wagener, K. B. ADMET: Metathesis polycondensation. *J. Polym. Sci., Part A: Polym. Chem.* **2011**, *49*, 821-831.
- [70] Grubbs, R. H.: *Handbook of Metathesis*; Grubbs, R. H.; Khosravi, E., Eds.; Wiley-VCH Verlag GmbH & Co. KGaA: Weinheim, 2015; Vol. 2. pp. 283-294., ISBN 978-3-527-33950-1
- [71] Berda, E. B.; Wagener, K. B.: Precision Polyolefins. In *Complex Macromolecular Architectures: Synthesis, Characterization and Self-Assembly*; Hadjichristidis, N., Hirao, A., Tezuka, Y., Du Prez, F., Eds.; John Wiley & Sons: Singapore, 2011; pp 317-347., ISBN 978-0-470-82513-6
- [72] Carothers, W. H. Polymers and polyfunctionality. *Trans. Faraday Soc.* **1936**, *32*, 39-49.
- [73] Bachler, P. R.; Wagener, K. B. Functional precision polymers via ADMET polymerization. *Monatsh. Chem.* **2015**, *146*, 1053-1061.
- [74] Odian, G.: *Principles of Polymerization, Fourth Edition*; John Wiley & Sons, Inc.: Hoboken: New Jersey, 2004., ISBN 978-0-471-27400-1
- [75] Caire da Silva, L.; Rojas, G.; Schulz, M. D.; Wagener, K. B. Acyclic diene metathesis polymerization: History, methods and applications. *Prog. Polym. Sci.* **2017**, *69*, 79-107.
- [76] Schrock, R. R. High-oxidation-state molybdenum and tungsten alkylidyne complexes. *Acc. Chem. Res.* **1986**, *19*, 342-348.
- [77] Schrock, R. R.; Murdzek, J. S.; Bazan, G. C.; Robbins, J.; DiMare, M.; O'Regan, M. Synthesis of molybdenum imido alkylidene complexes and some reactions involving acyclic olefins. *J. Am. Chem. Soc.* **1990**, *112*, 3875-3886.
- [78] Murdzek, J. S.; Schrock, R. R. Well-characterized olefin metathesis catalysts that contain molybdenum. *Organometallics* **1987**, *6*, 1373-1374.

- [79] Schaverien, C. J.; Dewan, J. C.; Schrock, R. R. Multiple metal-carbon bonds. 43. Well-characterized, highly active, Lewis acid free olefin metathesis catalysts. *J. Am. Chem. Soc.* **1986**, *108*, 2771-2773.
- [80] Huang, J.; Stevens, E. D.; Nolan, S. P.; Petersen, J. L. Olefin Metathesis-Active Ruthenium Complexes Bearing a Nucleophilic Carbene Ligand. *J. Am. Chem. Soc.* **1999**, *121*, 2674-2678.
- [81] Weskamp, T.; Schattenmann, W. C.; Spiegle, R. M.; Herrmann, W. A. A Novel Class of Ruthenium Catalysts for Olefin Metathesis. *Angew. Chem. Int. Ed.* **1998**, *37*, 2490-2493.
- [82] Scholl, M.; Trnka, T. M.; Morgan, J. P.; Grubbs, R. H. Increased ring closing metathesis activity of ruthenium-based olefin metathesis catalysts coordinated with imidazolin-2-ylidene ligands. *Tetrahedron Lett.* **1999**, *40*, 2247-2250.
- [83] Dias, E. L.; Nguyen, S. T.; Grubbs, R. H. Well-Defined Ruthenium Olefin Metathesis Catalysts: Mechanism and Activity. *J. Am. Chem. Soc.* **1997**, *119*, 3887-3897.
- [84] Tallarico, J. A.; Bonitatebus, P. J.; Snapper, M. L. Ring-Opening Metathesis. A Ruthenium Catalyst Caught in the Act. *J. Am. Chem. Soc.* **1997**, *119*, 7157-7158.
- [85] Adlhart, C.; Chen, P. Mechanism and Activity of Ruthenium Olefin Metathesis Catalysts: The Role of Ligands and Substrates from a Theoretical Perspective. *J. Am. Chem. Soc.* **2004**, *126*, 3496-3510.
- [86] Kingsbury, J. S.; Harrity, J. P. A.; Bonitatebus, P. J.; Hoveyda, A. H. A Recyclable Ru-Based Metathesis Catalyst. *J. Am. Chem. Soc.* **1999**, *121*, 791-799.
- [87] Schulz, M. D.; Wagener, K. B. Precision Polymers through ADMET Polymerization. *Macromol. Chem. Phys.* **2014**, *215*, 1936-1945.
- [88] Herrison, J. L.; Chauvin, Y. N. Catalysis of olefin transformations by tungsten complexes. II. Telomerization of cyclic olefins in the presence of acyclic olefins. *Makromol. Chem.* **1971**, *141*, 161-176.
- [89] Schulz, M. D.; Sauty, N. F.; Wagener, K. B. Morphology control in precision polyolefins. *Appl. Petrochem. Res.* **2015**, *5*, 3-8.
- [90] Lehman, S. E.; Schwendeman, J. E.; O'Donnell, P. M.; Wagener, K. B. Olefin isomerization promoted by olefin metathesis catalysts. *Inorg. Chim. Acta* **2003**, *345*, 190-198.
- [91] Meyer, W. H.; McConnell, A. E.; Forman, G. S.; Dwyer, C. L.; Kirk, M. M.; Ngidi, E. L.; Blignaut, A.; Saku, D.; Slawin, A. M. Z. Tin and iron halogenides as additives in ruthenium-catalyzed olefin metathesis. *Inorg. Chim. Acta* **2006**, *359*, 2910-2917.
- [92] Hong, S. H.; Sanders, D. P.; Lee, C. W.; Grubbs, R. H. Prevention of Undesirable Isomerization during Olefin Metathesis. *J. Am. Chem. Soc.* **2005**, *127*, 17160-17161.
- [93] Gimeno, N.; Formentín, P.; Steinke, J. H. G.; Vilar, R. Phenylphosphoric Acid as a New Additive to Inhibit Olefin Isomerisation in Ruthenium-Catalysed Metathesis Reactions. *Eur. J. Org. Chem.* **2007**, *2007*, 918-924.
- [94] Wagener, K. B.; Brzezinska, K. Acyclic diene metathesis (ADMET) polymerization: synthesis of unsaturated polyethers. *Macromolecules* **1991**, *24*, 5273-5277.

- [95] Thorn-Csányi, E.; Pflug, K. P. Synthesis of copolymers with a controllable sequence length of p-phenylenevinylene units. *Macromol. Rapid Commun.* **1993**, *14*, 619-624.
- [96] Qin, Y.; Hillmyer, M. A. Poly(3-hexyl-2,5-thienylene vinylene) by ADMET Polymerization of a Dipropenyl Monomer. *Macromolecules* **2009**, *42*, 6429-6432.
- [97] Delgado, P. A.; Liu, D. Y.; Kean, Z.; Wagener, K. B. Synthesis of Poly(3-dodecyl-2,5-thienylene vinylene) by Solid-State Metathesis Polycondensation. *Macromolecules* **2011**, *44*, 9529-9532.
- [98] Watson, M. D.; Wagener, K. B. Ethylene/Vinyl Acetate Copolymers via Acyclic Diene Metathesis Polymerization. Examining the Effect of “Long” Precise Ethylene Run Lengths. *Macromolecules* **2000**, *33*, 5411-5417.
- [99] Baughman, T. W.; Chan, C. D.; Winey, K. I.; Wagener, K. B. Synthesis and Morphology of Well-Defined Poly(ethylene-co-acrylic acid) Copolymers. *Macromolecules* **2007**, *40*, 6564-6571.
- [100] Opper, K. L.; Fassbender, B.; Brunklaus, G.; Spiess, H. W.; Wagener, K. B. Polyethylene Functionalized with Precisely Spaced Phosphonic Acid Groups. *Macromolecules* **2009**, *42*, 4407-4409.
- [101] Berda, E. B.; Baughman, T. W.; Wagener, K. B. Precision branching in ethylene copolymers: Synthesis and thermal behavior. *J. Polym. Sci., Part A: Polym. Chem.* **2006**, *44*, 4981-4989.
- [102] Rojas, G.; Berda, E. B.; Wagener, K. B. Precision polyolefin structure: Modeling polyethylene containing alkyl branches. *Polymer* **2008**, *49*, 2985-2995.
- [103] O'Gara, J. E.; Portmess, J. D.; Wagener, K. B. Acyclic diene metathesis (ADMET) polymerization. Synthesis of unsaturated polythioethers. *Macromolecules* **1993**, *26*, 2837-2841.
- [104] Wagener, K. B.; Smith, D. W. Acyclic diene metathesis polymerization: synthesis and characterization of unsaturated poly[carbo(dimethyl)silanes]. *Macromolecules* **1991**, *24*, 6073-6078.
- [105] Patton, J. T.; Boncella, J. M.; Wagener, K. B. Acyclic diene metathesis (ADMET) polymerization: the synthesis of unsaturated polyesters. *Macromolecules* **1992**, *25*, 3862-3867.
- [106] Tindall, D.; Wagener, K. B. Acyclic Diene Metathesis (ADMET) Segmented Copolymers. *Macromolecules* **2004**, *37*, 3328-3336.
- [107] Gutekunst, W. R.; Hawker, C. J. A General Approach to Sequence-Controlled Polymers Using Macrocyclic Ring Opening Metathesis Polymerization. *J. Am. Chem. Soc.* **2015**, *137*, 8038-8041.
- [108] Park, H.; Lee, H.-K.; Choi, T.-L. Tandem Ring-Opening/Ring-Closing Metathesis Polymerization: Relationship between Monomer Structure and Reactivity. *J. Am. Chem. Soc.* **2013**, *135*, 10769-10775.
- [109] Weiss, R. M.; Short, A. L.; Meyer, T. Y. Sequence-Controlled Copolymers Prepared via Entropy-Driven Ring-Opening Metathesis Polymerization. *ACS Macro Lett.* **2015**, *4*, 1039-1043.

- [110] Berthet, M.-A.; Zarafshani, Z.; Pfeifer, S.; Lutz, J.-F. Facile Synthesis of Functional Periodic Copolymers: A Step toward Polymer-Based Molecular Arrays. *Macromolecules* **2010**, *43*, 44-50.
- [111] König, N. F.; Al Ouahabi, A.; Poyer, S.; Charles, L.; Lutz, J. F. A Simple Post-Polymerization Modification Method for Controlling Side-Chain Information in Digital Polymers. *Angew. Chem. Int. Ed.* **2017**, *56*, 7297-7301.
- [112] Martens, S.; Holloway, J. O.; Du Prez, F. E. Click and Click-Inspired Chemistry for the Design of Sequence-Controlled Polymers. *Macromol. Rapid Commun.* **2017**, *38*, 1700469.
- [113] Yu, L.; Zhang, Z.; You, Y.-Z.; Hong, C.-Y. Synthesis of sequence-controlled polymers via sequential thiol-ene and amino-yne click reactions in one pot. *Eur. Polym. J.* **2018**, *103*, 80-87.
- [114] Han, J.; Zheng, Y.; Zhao, B.; Li, S.; Zhang, Y.; Gao, C. Sequentially Hetero-functional, Topological Polymers by Step-growth Thiol-yne Approach. *Sci. Rep.* **2014**, *4*, 4387.
- [115] Solleder, S. C.; Meier, M. A. R. Sequence Control in Polymer Chemistry through the Passerini Three-Component Reaction. *Angew. Chem. Int. Ed.* **2014**, *53*, 711-714.
- [116] Kwasny, M. T.; Watkins, C. M.; Posey, N. D.; Matta, M. E.; Tew, G. N. Functional Polyethylenes with Precisely Placed Thioethers and Sulfoniums through Thiol-Ene Polymerization. *Macromolecules* **2018**, *51*, 4280-4289.
- [117] Hoyle, C. E.; Bowman, C. N. Thiol-Ene Click Chemistry. *Angew. Chem. Int. Ed.* **2010**, *49*, 1540-1573.
- [118] Reddy, S. K.; Cramer, N. B.; Bowman, C. N. Thiol-Vinyl Mechanisms. 1. Termination and Propagation Kinetics in Thiol-Ene Photopolymerizations. *Macromolecules* **2006**, *39*, 3673-3680.
- [119] Reddy, S. K.; Cramer, N. B.; Bowman, C. N. Thiol-Vinyl Mechanisms. 2. Kinetic Modeling of Ternary Thiol-Vinyl Photopolymerizations. *Macromolecules* **2006**, *39*, 3681-3687.
- [120] Reddy, S. K.; Cramer, N. B.; O'Brien, A. K.; Cross, T.; Raj, R.; Bowman, C. N. Rate mechanisms of a novel thiol-ene photopolymerization reaction. *Macromol. Symp.* **2004**, *206*, 361-374.
- [121] Cramer, N. B.; Davies, T.; O'Brien, A. K.; Bowman, C. N. Mechanism and Modeling of a Thiol-Ene Photopolymerization. *Macromolecules* **2003**, *36*, 4631-4636.
- [122] Cramer, N. B.; Reddy, S. K.; O'Brien, A. K.; Bowman, C. N. Thiol-Ene Photopolymerization Mechanism and Rate Limiting Step Changes for Various Vinyl Functional Group Chemistries. *Macromolecules* **2003**, *36*, 7964-7969.
- [123] Willenbacher, J.; Altintas, O.; Trouillet, V.; Knöfel, N.; Monteiro, M. J.; Roesky, P. W.; Barner-Kowollik, C. Pd-complex driven formation of single-chain nanoparticles. *Polym. Chem.* **2015**, *6*, 4358-4365.
- [124] Sanchez-Sanchez, A.; Arbe, A.; Colmenero, J.; Pomposo, J. A. Metallo-Folded Single-Chain Nanoparticles with Catalytic Selectivity. *ACS Macro Lett.* **2014**, *3*, 439-443.

- [125] Tooley, C. A.; Pazicni, S.; Berda, E. B. Toward a tunable synthetic [FeFe] hydrogenase mimic: single-chain nanoparticles functionalized with a single diiron cluster. *Polym. Chem.* **2015**, *6*, 7646-7651.
- [126] Nakamoto, M.; Nonaka, T.; Shea, K. J.; Miura, Y.; Hoshino, Y. Design of Synthetic Polymer Nanoparticles That Facilitate Resolubilization and Refolding of Aggregated Positively Charged Lysozyme. *J. Am. Chem. Soc.* **2016**, *138*, 4282-4285.
- [127] Wada, Y.; Lee, H.; Hoshino, Y.; Kotani, S.; Shea, K. J.; Miura, Y. Design of multi-functional linear polymers that capture and neutralize a toxic peptide: a comparison with cross-linked nanoparticles. *J. Mater. Chem. B* **2015**, *3*, 1706-1711.
- [128] Karamessini, D.; Poyer, S.; Charles, L.; Lutz, J. F. 2D Sequence-Coded Oligourethane Barcodes for Plastic Materials Labeling. *Macromol. Rapid Commun.* **2017**, *38*, 1700426.
- [129] Pfeifer, S.; Zarafshani, Z.; Badi, N.; Lutz, J.-F. Liquid-Phase Synthesis of Block Copolymers Containing Sequence-Ordered Segments. *J. Am. Chem. Soc.* **2009**, *131*, 9195-9197.
- [130] Roy, R. K.; Meszynska, A.; Laure, C.; Charles, L.; Verchin, C.; Lutz, J.-F. Design and synthesis of digitally encoded polymers that can be decoded and erased. *Nat. Commun.* **2015**, *6*, 7237.
- [131] Mutlu, H.; Lutz, J. F. Reading Polymers: Sequencing of Natural and Synthetic Macromolecules. *Angew. Chem. Int. Ed.* **2014**, *53*, 13010-13019.
- [132] Keller, A. Polymer crystals. *Rep. Prog. Phys.* **1968**, *31*, 623.
- [133] Hoffman, J. D.; Lauritzen, J. I.; Passaglia, E.; Ross, G. S.; Frolen, L. J.; Weeks, J. J. Kinetics of polymer crystallization from solution and the melt. *Kolloid Z. Z. Polym.* **1969**, *231*, 564-592.
- [134] Sanchez, I. C. Modern Theories of Polymer Crystallization. *J. Macromol. Sci. – Revs. Macromol. Chem.* **1974**, *10*, 113-148.
- [135] Pennings, A. J. Polymer crystallization. *J. Cryst. Growth* **1980**, *48*, 574-581.
- [136] Hay, J. N.: Polymer crystallization. In *Macromolecular Chemistry: Volume 3*; Jenkins, A. D., Kennedy, J. F., Eds.; The Royal Society of Chemistry, 1984; Vol. 3; pp 204-223., ISBN 0-85186-876-2
- [137] Phillips, P. J. Polymer crystals. *Rep. Prog. Phys.* **1990**, *53*, 549.
- [138] Long, Y.; Shanks, R. A.; Stachurski, Z. H. Kinetics of polymer crystallisation. *Prog. Polym. Sci.* **1995**, *20*, 651-701.
- [139] Ungar, G.; Zeng, X.-B. Learning Polymer Crystallization with the Aid of Linear, Branched and Cyclic Model Compounds. *Chem. Rev.* **2001**, *101*, 4157-4188.
- [140] Toda, A.; Androsch, R.; Schick, C. Insights into polymer crystallization and melting from fast scanning chip calorimetry. *Polymer* **2016**, *91*, 239-263.
- [141] Zhang, M.; Guo, B.-H.; Xu, J. A Review on Polymer Crystallization Theories. *Crystals* **2017**, *7*, 4.

- [142] Piorkowska, E.; Rutledge, G. C.: *Handbook of Polymer Crystallization*; Piorkowska, E.; Rutledge, G. C., Eds.; John Wiley & Sons, Inc.: Hoboken, New Jersey, 2013., ISBN 978-0470380239
- [143] Keller, A. A note on single crystals in polymers: Evidence for a folded chain configuration. *Philos. Mag.* **1957**, *2*, 1171-1175.
- [144] Fischer, E. W.: Notizen: Stufen- und spiralförmiges Kristallwachstum bei Hochpolymeren. *Z. Naturforsch. A.* **1957**, *12*, 753-754.
- [145] Till, P. H. The growth of single crystals of linear polyethylene. *J. Polym. Sci.* **1957**, *24*, 301-306.
- [146] Piccarolo, S. Morphological changes in isotactic polypropylene as a function of cooling rate. *J. Macromol. Sci. B* **1992**, *31*, 501-511.
- [147] De Rosa, C.; Auriemma, F. Structure and physical properties of syndiotactic polypropylene: A highly crystalline thermoplastic elastomer. *Prog. Polym. Sci.* **2006**, *31*, 145-237.
- [148] Standt, U. D. Crystalline Atactic Polymers. *J. Macromol. Sci. R. M. C.* **1983**, *23*, 317-336.
- [149] Hobson, R. J.; Windle, A. H. Crystalline structure of atactic polyacrylonitrile. *Macromolecules* **1993**, *26*, 6903-6907.
- [150] Lee, L.-B. W.; Register, R. A. Hydrogenated Ring-Opened Polynorbornene: A Highly Crystalline Atactic Polymer. *Macromolecules* **2005**, *38*, 1216-1222.
- [151] Hu, W.; Zha, L.: Thermodynamicity and Kinetics of Polymer Crystallization. In *Polymer Morphology: Principles, Characterization, and Processing*; Guo, Q., Ed.; John Wiley & Sons, Inc., 2016; Vol. 1; pp 242-256., ISBN 978-1-118-45215-8
- [152] Geil, P. H.; Anderson, F. R.; Wunderlich, B.; Arakawa, T. Morphology of polyethylene crystallized from the melt under pressure. *J. Polym. Sci. Part A* **1964**, *2*, 3707-3720.
- [153] Wunderlich, B.; Mielillo, L. Morphology and growth of extended chain crystals of polyethylene. *Die Makromol. Chem.* **1968**, *118*, 250-264.
- [154] Muthukumar, M.: Nucleation in Polymer Crystallization. In *Advances in Chemical Physics*; Rice, S. A., Ed.; John Wiley & Sons, Inc.: Hoboken, New Jersey, 2004; Vol. 128; pp 1-64., ISBN 978-0-471-44528-9
- [155] Ratta, V. Crystallization, Morphology, Thermal Stability and Adhesive Properties of Novel High Performance Semicrystalline Polyimides. Ph. D. Thesis, Virginia Polytechnic Institute and State University, 1999.
- [156] Nolting, W.: *Grundkurs Theoretische Physik 6*; Springer-Verlag Berlin Heidelberg, 2007; Vol. 6. pp. 280-283., ISBN 978-3-642-25393-5
- [157] Schick, C.; Androsch, R.; Schmelzer, J. W. P. Homogeneous crystal nucleation in polymers. *J. Phys.: Condens. Matter* **2017**, *29*, 453002.
- [158] Shonaike, G. O.; Advani, S. G.: *Advanced Polymeric Materials - Structure Property Relationship*; Shonaike, G. O.; Advani, S. G., Eds.; CRC Press: Boca Raton, 2003., ISBN 978-158-716047-9

- [159] J., B. D.; A., K.; J., K. A. A new self-nucleation phenomenon and its application to the growing of polymer crystals from solution. *J. Polym. Sci. Part B* **1966**, *4*, 481-486.
- [160] Wunderlich, B.: *Macromolecular Physics, Vol. 2, Crystal Nucleation, Growth, Annealing*; Academic Press: New York, 1976., ISBN 978-0-12-765602-1
- [161] Hoffman, J. D.; Lauritzen, J. I. Crystallization of Bulk Polymers with Chain Folding: Theory of Growth of Lamellar Spherulites. *J. Res. Natl. Bur. Stand A* **1961**, *65*.
- [162] Hoffman, J. D.; Weeks, J. J. Melting Process and the Equilibrium Melting Temperature of Polychlorotrifluoroethylene. *J. Res. Natl. Bur. Stand A* **1962**, *66*, 13-28.
- [163] Weeks, J. J. Melting Temperature and Change of Lamellar Thickness with Time for Bulk Polyethylene. *J. Res. Natl. Bur. Stand A* **1963**, *67*, 441-451.
- [164] Zheng, Y.-R.; Tee, H. T.; Wei, Y.; Wu, X.-L.; Mezger, M.; Yan, S.; Landfester, K.; Wagener, K.; Wurm, F. R.; Lieberwirth, I. Morphology and Thermal Properties of Precision Polymers: The Crystallization of Butyl Branched Polyethylene and Polyphosphoesters. *Macromolecules* **2016**, *49*, 1321-1330.
- [165] Herrmann, K.; Gerngross, O.; Abitz, W. Zur roentgnographischen Strukturforchung des gelatinemicells. *Z. Phys. Chem. B* **1930**, *10*, 371-394.
- [166] Herrmann, K.; Gerngross, O. Die Elastizität des Kautschuks. *Kautschuk* **1932**, *8*, 181.
- [167] Bower, D. I.: *An Introduction to Polymer Physics*; Cambridge University Press: Cambridge, 2002., ISBN 0-521-63137-8
- [168] Flory, P. J. On the Morphology of the Crystalline State in Polymers. *J. Am. Chem. Soc.* **1962**, *84*, 2857-2867.
- [169] Storks, K. H. An Electron Diffraction Examination of Some Linear High Polymers. *J. Am. Chem. Soc.* **1938**, *60*, 1753-1761.
- [170] Keller, A.; O'Connor, A. Large Periods in Polyethylene: the Origin of Low-Angle X-ray Scattering. *Nature* **1957**, *180*, 1289.
- [171] Spells, S. J.; Sadler, D. M.; Keller, A. Chain trajectory in solution grown polyethylene crystals: correlation between infra-red spectroscopy and small-angle neutron scattering. *Polymer* **1980**, *21*, 1121-1128.
- [172] Ortmann, P.; Trzaskowski, J.; Krumova, M.; Mecking, S. Precise Microstructure Self-Stabilized Polymer Nanocrystals. *ACS Macro Lett.* **2013**, 125-127.
- [173] Weber, C. H. M.; Chiche, A.; Krausch, G.; Rosenfeldt, S.; Ballauff, M.; Harnau, L.; Göttker-Schnetmann, I.; Tong, Q.; Mecking, S. Single Lamella Nanoparticles of Polyethylene. *Nano Lett.* **2007**, *7*, 2024-2029.
- [174] Rochette, C. N.; Rosenfeldt, S.; Henzler, K.; Polzer, F.; Ballauff, M.; Tong, Q.; Mecking, S.; Drechsler, M.; Narayanan, T.; Harnau, L. Annealing of Single Lamella Nanoparticles of Polyethylene. *Macromolecules* **2011**, *44*, 4845-4851.
- [175] Hong, Y.-I.; Koga, T.; Miyoshi, T. Chain Trajectory and Crystallization Mechanism of a Semicrystalline Polymer in Melt- and Solution-Grown Crystals As Studied Using <sup>13</sup>C-<sup>13</sup>C Double-Quantum NMR. *Macromolecules* **2015**, *48*, 3282-3293.

- [176] Hong, Y.-l.; Yuan, S.; Li, Z.; Ke, Y.; Nozaki, K.; Miyoshi, T. Three-Dimensional Conformation of Folded Polymers in Single Crystals. *Phys. Rev. Lett.* **2015**, *115*, 168301.
- [177] Hong, Y.-l.; Chen, W.; Yuan, S.; Kang, J.; Miyoshi, T. Chain Trajectory of Semicrystalline Polymers As Revealed by Solid-State NMR Spectroscopy. *ACS Macro Lett.* **2016**, *5*, 355-358.
- [178] Rouse, P. E. J. A Theory of the Linear Viscoelastic Properties of Dilute Solutions of Coiling Polymers. *J. Chem. Phys.* **1953**, *21*, 1272-1280.
- [179] Stepanow, S. Kinetic mechanism of chain folding in polymer crystallization. *Phys. Rev. E* **2014**, *90*, 032601.
- [180] Edwards, S. F. The theory of polymer solutions at intermediate concentration. *Proc. Phys. Soc.* **1966**, *88*, 265.
- [181] Hoffman, J. D.; Guttman, C. M.; DiMarzio, E. A. On the problem of crystallization of polymers from the melt with chain folding. *Faraday Discuss. Chem. Soc.* **1979**, *68*, 177-197.
- [182] Mandelkern, L.: *Crystallization of Polymers*; Cambridge University Press: Cambridge, 2004; Vol. 2., ISBN 0-521-81682-3
- [183] Hu, W.; Frenkel, D.; Mathot, V. B. F. Intramolecular Nucleation Model for Polymer Crystallization. *Macromolecules* **2003**, *36*, 8178-8183.
- [184] Lauritzen, J. I.; Hoffman, J. D. Theory of formation of polymer crystals with folded chains in dilute solution. *J. Res. Natl. Bur. Stand A* **1960**, *64*, 73-102.
- [185] Lauritzen, J. I. J.; Hoffman, J. D. Extension of theory of growth of chain-folded polymer crystals to large undercoolings. *J. Appl. Phys.* **1973**, *44*, 4340-4352.
- [186] Cheng, S. Z. D.; Lotz, B. Enthalpic and entropic origins of nucleation barriers during polymer crystallization: the Hoffman–Lauritzen theory and beyond. *Polymer* **2005**, *46*, 8662-8681.
- [187] Hoffman, J. D.; Frolen, L. J.; Ross, G. S.; Lauritzen, J. I. On the Growth Rate of Spherulites and Axialites from the Melt in Polyethylene Fractions: Regime I and Regime II Crystallization. *J. Res. Natl. Bur. Stand A* **1975**, *79*, 671-699.
- [188] Lauritzen, J. I.; Passaglia, E. Kinetics of Crystallization in Multicomponent Systems: II. Chain-Folded Polymer Crystals. *J. Res. Natl. Bur. Stand A* **1967**, *71*, 261-275.
- [189] Sanchez, I. C.; DiMarzio, E. A. Dilute Solution Theory of Polymer Crystal Growth: A Kinetic Theory of Chain Folding. *J. Chem. Phys.* **1971**, *55*, 893-908.
- [190] Hoffman, J. D. Regime III crystallization in melt-crystallized polymers: The variable cluster model of chain folding. *Polymer* **1983**, *24*, 3-26.
- [191] Frank, F.; Tosi, M. On the theory of polymer crystallization. *Proc. R. Soc. Lond. A* **1961**, *263*, 323-339.
- [192] Point, J. J. A New Theoretical Approach of the Secondary Nucleation at High Supercooling. *Macromolecules* **1979**, *12*, 770-775.
- [193] Point, J.-J. Reconsideration of kinetic theories of polymer crystal growth with chain folding. *Faraday Discuss. Chem. Soc.* **1979**, *68*, 167-176.



- [194] Michell, R. M.; Müller, A. J. Confined crystallization of polymeric materials. *Prog. Polym. Sci.* **2016**, *54–55*, 183-213.
- [195] Massa, M. V.; Dalnoki-Veress, K. Homogeneous Crystallization of Poly[Ethylene Oxide] Confined to Droplets: The Dependence of the Crystal Nucleation Rate on Length Scale and Temperature. *Phys. Rev. Lett.* **2004**, *92*, 255509.
- [196] Carvalho, J. L.; Dalnoki-Veress, K. Homogeneous Bulk, Surface, and Edge Nucleation in Crystalline Nanodroplets. *Phys. Rev. Lett.* **2010**, *105*, 237801.
- [197] Kailas, L.; Vasilev, C.; Audinot, J.-N.; Migeon, H.-N.; Hobbs, J. K. A Real-Time Study of Homogeneous Nucleation, Growth, and Phase Transformations in Nanodroplets of Low Molecular Weight Isotactic Polypropylene Using AFM. *Macromolecules* **2007**, *40*, 7223-7230.
- [198] Sanandaji, N.; Oko, A.; Haviland, D. B.; Tholén, E. A.; Hedenqvist, M. S.; Gedde, U. W. Inkjet printing as a possible route to study confined crystal structures. *Eur. Polym. J.* **2013**, *49*, 203-208.
- [199] Tongcher, O.; Sigel, R.; Landfester, K. Liquid Crystal Nanoparticles Prepared as Miniemulsions. *Langmuir* **2006**, *22*, 4504-4511.
- [200] Montenegro, R.; Landfester, K. Metastable and Stable Morphologies during Crystallization of Alkanes in Miniemulsion Droplets. *Langmuir* **2003**, *19*, 5996-6003.
- [201] Liu, Y.-X.; Chen, E.-Q. Polymer crystallization of ultrathin films on solid substrates. *Coordin. Chem. Rev.* **2010**, *254*, 1011-1037.
- [202] Osichow, A.; Rabe, C.; Vogtt, K.; Narayanan, T.; Harnau, L.; Drechsler, M.; Ballauff, M.; Mecking, S. Ideal Polyethylene Nanocrystals. *J. Am. Chem. Soc.* **2013**, *135*, 11645-11650.
- [203] Michell, R. M.; Blaszczyk-Lezak, I.; Mijangos, C.; Müller, A. J. Confinement effects on polymer crystallization: From droplets to alumina nanopores. *Polymer* **2013**, *54*, 4059-4077.
- [204] Michell, R. M.; Blaszczyk-Lezak, I.; Mijangos, C.; Müller, A. J. Confined crystallization of polymers within anodic aluminum oxide templates. *J. Polym. Sci. Part B: Polym. Phys.* **2014**, *52*, 1179-1194.
- [205] Müller, A. J.; Balsamo, V.; Arnal, M. L.: Nucleation and Crystallization in Diblock and Triblock Copolymers. In *Block Copolymers II*; Abetz, V., Ed.; Springer Berlin Heidelberg: Berlin, Heidelberg, 2005; pp 1-63., ISBN 354-026902-1
- [206] Hamley, I. W.: Crystallization in Block Copolymers. In *Interfaces Crystallization Viscoelasticity. Adv. Polym. Sci.*, Vol. 148, Springer Berlin Heidelberg: Berlin, Heidelberg, 1999; pp 113-137., ISBN 978-3-540-65934-1
- [207] Few, C. S.; Wagener, K. B.; Thompson, D. L. Systematic Studies of Morphological Changes of Precision Polyethylene. *Macromol. Rapid Commun.* **2014**, *35*, 123-132.
- [208] Baughman, T. W.; Sworen, J. C.; Wagener, K. B. Sequenced Ethylene–Propylene Copolymers: Effects of Short Ethylene Run Lengths. *Macromolecules* **2006**, *39*, 5028-5036.

- [209] Sworen, J. C.; Smith, J. A.; Wagener, K. B.; Baugh, L. S.; Rucker, S. P. Modeling Random Methyl Branching in Ethylene/ Propylene Copolymers Using Metathesis Chemistry: Synthesis and Thermal Behavior. *J. Am. Chem. Soc.* **2003**, *125*, 2228-2240.
- [210] Rastogi, S.; Hikosaka, M.; Kawabata, H.; Keller, A. Role of mobile phases in the crystallization of polyethylene. Part 1. Metastability and lateral growth. *Macromolecules* **1991**, *24*, 6384-6391.
- [211] Sirota, E. B. Polymer Crystallization: Metastable Mesophases and Morphology. *Macromolecules* **2007**, *40*, 1043-1048.
- [212] Matsui, K.; Seno, S.; Nozue, Y.; Shinohara, Y.; Amemiya, Y.; Berda, E. B.; Rojas, G.; Wagener, K. B. Influence of Branch Incorporation into the Lamella Crystal on the Crystallization Behavior of Polyethylene with Precisely Spaced Branches. *Macromolecules* **2013**, *46*, 4438-4446.
- [213] Lieser, G.; Wegner, G.; Smith, J. A.; Wagener, K. B. Morphology and packing behavior of model ethylene/propylene copolymers with precise methyl branch placement. *Colloid Polym. Sci.* **2004**, *282*, 773-781.
- [214] Qiu, W.; Sworen, J.; Pyda, M.; Nowak-Pyda, E.; Habenschuss, A.; Wagener, K. B.; Wunderlich, B. Effect of the Precise Branching of Polyethylene at Each 21st CH<sub>2</sub> Group on Its Phase Transitions, Crystal Structure, and Morphology. *Macromolecules* **2006**, *39*, 204-217.
- [215] Sworen, J. C.; Smith, J. A.; Berg, J. M.; Wagener, K. B. Modeling Branched Polyethylene: Copolymers Possessing Precisely Placed Ethyl Branches. *J. Am. Chem. Soc.* **2004**, *126*, 11238-11246.
- [216] Hosoda, S.; Nozue, Y.; Kawashima, Y.; Utsumi, S.; Nagamatsu, T.; Wagener, K.; Berda, E.; Rojas, G.; Baughman, T.; Leonard, J. Perfectly Controlled Lamella Thickness and Thickness Distribution: A Morphological Study on ADMET Polyolefins. *Macromol. Symp.* **2009**, *282*, 50-64.
- [217] Berda, E. B.; Wagener, K. B. Inducing Pendant Group Interactions in Precision Polyolefins: Synthesis and Thermal Behavior. *Macromolecules* **2008**, *41*, 5116-5122.
- [218] Nozue, Y.; Kawashima, Y.; Seno, S.; Nagamatsu, T.; Hosoda, S.; Berda, E. B.; Rojas, G.; Baughman, T. W.; Wagener, K. B. Unusual Crystallization Behavior of Polyethylene Having Precisely Spaced Branches. *Macromolecules* **2011**, *44*, 4030-4034.
- [219] Rojas, G.; Inci, B.; Wei, Y.; Wagener, K. B. Precision Polyethylene: Changes in Morphology as a Function of Alkyl Branch Size. *J. Am. Chem. Soc.* **2009**, *131*, 17376-17386.
- [220] Inci, B.; Lieberwirth, I.; Steffen, W.; Mezger, M.; Graf, R.; Landfester, K.; Wagener, K. B. Decreasing the Alkyl Branch Frequency in Precision Polyethylene: Effect of Alkyl Branch Size on Nanoscale Morphology. *Macromolecules* **2012**, *45*, 3367-3376.
- [221] Hu, W.; Sirota, E. B. Monoclinic Crystallites in Ethylene Copolymers Detected by Solid-State NMR and X-ray Diffraction. *Macromolecules* **2003**, *36*, 5144-5149.

- [222] Inci, B.; Wagener, K. B. Decreasing the Alkyl Branch Frequency in Precision Polyethylene: Pushing the Limits toward Longer Run Lengths. *J. Am. Chem. Soc.* **2011**, *133*, 11872-11875.
- [223] Matsui, K.; Li, H.; Nozue, Y.; Rojas, G.; Bell, M.; Shinohara, Y.; Amemiya, Y.; Wagener, K. B. A study of ADMET polyethylene with 21-carbon branches on every 15th compared to every 19th carbon: What a difference four extra backbone methylenes make. *J. Polym. Sci Part A: Polym. Chem.* **2017**, *55*, 3090-3096.
- [224] Li, H.; Rojas, G.; Wagener, K. B. Precision Long-Chain Branched Polyethylene via Acyclic Diene Metathesis Polymerization. *ACS Macro Lett.* **2015**, *4*, 1225-1228.
- [225] Zhang, X.; Santonja-Blasco, L.; Wagener, K. B.; Boz, E.; Tasaki, M.; Tashiro, K.; Alamo, R. G. Infrared Spectroscopy and X-ray Diffraction Characterization of Dimorphic Crystalline Structures of Polyethylenes with Halogens Placed at Equal Distance along the Backbone. *J. Phys. Chem. B* **2017**, *121*, 10166-10179.
- [226] Boz, E.; Wagener, K. B.; Ghosal, A.; Fu, R.; Alamo, R. G. Synthesis and Crystallization of Precision ADMET Polyolefins Containing Halogens. *Macromolecules* **2006**, *39*, 4437-4447.
- [227] Boz, E.; Nemeth, A. J.; Ghiviriga, I.; Jeon, K.; Alamo, R. G.; Wagener, K. B. Precision Ethylene/Vinyl Chloride Polymers via Condensation Polymerization. *Macromolecules* **2007**, *40*, 6545-6551.
- [228] Boz, E.; Nemeth, A. J.; Wagener, K. B.; Jeon, K.; Smith, R.; Nazirov, F.; Bockstaller, M. R.; Alamo, R. G. Well-Defined Precision Ethylene/Vinyl Fluoride Polymers: Synthesis and Crystalline Properties. *Macromolecules* **2008**, *41*, 1647-1653.
- [229] Alamo, R. G.; Jeon, K.; Smith, R. L.; Boz, E.; Wagener, K. B.; Bockstaller, M. R. Crystallization of Polyethylenes Containing Chlorines: Precise vs Random Placement. *Macromolecules* **2008**, *41*, 7141-7151.
- [230] Kaner, P.; Ruiz-Orta, C.; Boz, E.; Wagener, K. B.; Tasaki, M.; Tashiro, K.; Alamo, R. G. Kinetic Control of Chlorine Packing in Crystals of a Precisely Substituted Polyethylene. Toward Advanced Polyolefin Materials. *Macromolecules* **2013**, *47*, 236-245.
- [231] Tasaki, M.; Yamamoto, H.; Hanesaka, M.; Tashiro, K.; Boz, E.; Wagener, K. B.; Ruiz-Orta, C.; Alamo, R. G. Polymorphism and Phase Transitions of Precisely Halogen-Substituted Polyethylene. (1) Crystal Structures of Various Crystalline Modifications of Bromine-Substituted Polyethylene on Every 21st Backbone Carbon. *Macromolecules* **2014**, *47*, 4738-4749.
- [232] Thompson, D. L.; Wagener, K. B.; Schulze, U.; Voit, B.; Jehnichen, D.; Malanin, M. Spectroscopic Examinations of Hydrogen Bonding in Hydroxy-Functionalized ADMET Chemistry. *Macromol. Rapid Commun.* **2015**, *36*, 60-64.
- [233] Trigg, E. B.; Tiegs, B. J.; Coates, G. W.; Winey, K. I. High Morphological Order in a Nearly Precise Acid-Containing Polymer and Ionomer. *ACS Macro Lett.* **2017**, *6*, 947-951.

- [234] Seitz, M. E.; Chan, C. D.; Opper, K. L.; Baughman, T. W.; Wagener, K. B.; Winey, K. I. Nanoscale Morphology in Precisely Sequenced Poly(ethylene-co-acrylic acid) Zinc Ionomers. *J. Am. Chem. Soc.* **2010**, *132*, 8165-8174.
- [235] Buitrago, C. F.; Alam, T. M.; Opper, K. L.; Aitken, B. S.; Wagener, K. B.; Winey, K. I. Morphological Trends in Precise Acid- and Ion-Containing Polyethylenes at Elevated Temperature. *Macromolecules* **2013**.
- [236] Buitrago, C. F.; Jenkins, J. E.; Opper, K. L.; Aitken, B. S.; Wagener, K. B.; Alam, T. M.; Winey, K. I. Room Temperature Morphologies of Precise Acid- and Ion-Containing Polyethylenes. *Macromolecules* **2013**.
- [237] Aitken, B. S.; Buitrago, C. F.; Heffley, J. D.; Lee, M.; Gibson, H. W.; Winey, K. I.; Wagener, K. B. Precision Ionomers: Synthesis and Thermal/Mechanical Characterization. *Macromolecules* **2012**, *45*, 681-687.
- [238] Markova, D.; Opper, K. L.; Wagner, M.; Klapper, M.; Wagener, K. B.; Mullen, K. Synthesis of proton conducting phosphonic acid-functionalized polyolefins by the combination of ATRP and ADMET. *Polym. Chem.* **2013**, *4*, 1351-1363.
- [239] Opper, K. L.; Markova, D.; Klapper, M.; Müllen, K.; Wagener, K. B. Precision Phosphonic Acid Functionalized Polyolefin Architectures. *Macromolecules* **2010**, *43*, 3690-3698.
- [240] Opper, K. L.; Wagener, K. B. Precision Sulfonic Acid Ester Copolymers. *Macromol. Rapid Commun.* **2009**, *30*, 915-919.
- [241] Gaines, T. W.; Bell, M. H.; Trigg, E. B.; Winey, K. I.; Wagener, K. B. Precision Sulfonic Acid Polyolefins via Heterogenous to Homogenous Deprotection. *Macromol. Chem. Phys.* **2018**, *219*, 1700634.
- [242] Simocko, C.; Young, T. C.; Wagener, K. B. ADMET Polymers Containing Precisely Spaced Pendant Boronic Acids and Esters. *Macromolecules* **2015**, *48*, 5470-5473.
- [243] Watson, M. D.; Wagener, K. B. Functionalized Polyethylene via Acyclic Diene Metathesis Polymerization: Effect of Precise Placement of Functional Groups. *Macromolecules* **2000**, *33*, 8963-8970.
- [244] Ortmann, P.; Mecking, S. Long-Spaced Aliphatic Polyesters. *Macromolecules* **2013**, *46*, 7213-7218.
- [245] Ortmann, P.; Wimmer, F. P.; Mecking, S. Long-Spaced Polyketones from ADMET Copolymerizations as Ideal Models for Ethylene/CO Copolymers. *ACS Macro Lett.* **2015**, *4*, 704-707.
- [246] Ortmann, P.; Heckler, I.; Mecking, S. Physical properties and hydrolytic degradability of polyethylene-like polyacetals and polycarbonates. *Green Chem.* **2014**, *16*, 1816-1827.
- [247] Watson, M. D.; Wagener, K. B. Tandem Homogeneous Metathesis/Heterogeneous Hydrogenation: Preparing Model Ethylene/CO<sub>2</sub> and Ethylene/CO Copolymers. *Macromolecules* **2000**, *33*, 3196-3201.
- [248] Marsico, F.; Wagner, M.; Landfester, K.; Wurm, F. R. Unsaturated Polyphosphoesters via Acyclic Diene Metathesis Polymerization. *Macromolecules* **2012**, *45*, 8511-8518.

- [249] Busch, H.; Majumder, S.; Reiter, G.; Mecking, S. Semicrystalline Long-Chain Polyphosphoesters from Polyesterification. *Macromolecules* **2017**, *50*, 2706-2713.
- [250] Bauer, K. N.; Tee, H. T.; Lieberwirth, I.; Wurm, F. R. In-Chain Poly[phosphonate]s via Acyclic Diene Metathesis Polycondensation. *Macromolecules* **2016**, *49*, 3761-3768.
- [251] Steinbach, T.; Alexandrino, E. M.; Wahlen, C.; Landfester, K.; Wurm, F. R. Poly[phosphonate]s via Olefin Metathesis: Adjusting Hydrophobicity and Morphology. *Macromolecules* **2014**, *47*, 4884-4893.
- [252] Busch, H.; Schiebel, E.; Sickinger, A.; Mecking, S. Ultralong-Chain-Spaced Crystalline Poly(H-phosphonate)s and Poly(phenylphosphonate)s. *Macromolecules* **2017**, *50*, 7901-7910.
- [253] Cankaya, A.; Steinmann, M.; Bülbül, Y.; Lieberwirth, I.; Wurm, F. R. Side-chain poly(phosphoramidate)s via acyclic diene metathesis polycondensation. *Polym. Chem.* **2016**, *7*, 5004-5010.
- [254] Steinmann, M.; Wagner, M.; Wurm, F. R. Poly[phosphorodiamidate]s by Olefin Metathesis Polymerization with Precise Degradation. *Chem. Eur. J.* **2016**, *22*, 17329-17338.
- [255] Gaines, T. W.; Nakano, T.; Chujo, Y.; Trigg, E. B.; Winey, K. I.; Wagener, K. B. Precise Sulfite Functionalization of Polyolefins via ADMET Polymerization. *ACS Macro Lett.* **2015**, *4*, 624-627.
- [256] Parkhurst, R. R.; Balog, S.; Weder, C.; Simon, Y. C. Synthesis of poly(sulfonate ester)s by ADMET polymerization. *RSC Adv.* **2014**, *4*, 53967-53974.
- [257] Gaines, T. W.; Trigg, E. B.; Winey, K. I.; Wagener, K. B. High Melting Precision Sulfone Polyethylenes Synthesized by ADMET Chemistry. *Macromol. Chem. Phys.* **2016**, *217*, 2351-2359.
- [258] Ortmann, P.; Lemke, T. A.; Mecking, S. Long-Spaced Polyamides: Elucidating the Gap between Polyethylene Crystallinity and Hydrogen Bonding. *Macromolecules* **2015**, *48*, 1463-1472.
- [259] Freudenberg, J.; Poppe, S.; Binder, W. H. Precision polymers containing main-chain-amino acids: ADMET polymerization and crystallization. *RSC Adv.* **2017**, *7*, 47507-47519.
- [260] Song, S.; Guo, W.; Zou, S.; Fu, Z.; Xu, J.; Fan, Z. Polyethylene containing aliphatic ring and aromatic ring defects in the main chain: Synthesis via ADMET and comparisons of thermal properties and crystalline structure. *Polymer* **2016**, *107*, 113-121.
- [261] da Silva, L. C.; Wagener, K. B. Synthesis and Thermal Characterization of Precision Poly(p-cyclohexylene alkylene)s via Acyclic Diene Metathesis Polycondensation. *Macromol. Chem. Phys.* **2016**, *217*, 850-855.
- [262] Sauty, N. F.; Caire da Silva, L.; Gallagher, C.; Graf, R.; Wagener, K. B. Unveiling the hyperbolic thermal behaviour of poly(p-phenylene alkylene)s. *Polym. Chem.* **2015**, *6*, 6073-6082.

- [263] Song, S.-F.; Guo, Y.-T.; Wang, R.-Y.; Fu, Z.-S.; Xu, J.-T.; Fan, Z.-Q. Synthesis and Crystallization Behavior of Equisquential ADMET Polyethylene Containing Arylene Ether Defects: Remarkable Effects of Substitution Position and Arylene Size. *Macromolecules* **2016**, *49*, 6001-6011.
- [264] Song, S.; Miao, W.; Wang, Z.; Gong, D.; Chen, Z.-R. Synthesis and characterization of precisely-defined ethylene-co-aryl ether polymers via ADMET polymerization. *Polymer* **2015**, *64*, 76-83.
- [265] Müller, A.; Michell, R. M.; Pérez, R.; Lorenzo, A. Successive Self-nucleation and Annealing (SSA): Correct design of thermal protocol and applications. *Eur. Polym. J.* **2015**, *65*, 132-154.
- [266] Cavallo, D.; Lorenzo, A. T.; Müller, A. J. Probing the early stages of thermal fractionation by successive self-nucleation and annealing performed with fast scanning chip-calorimetry. *J. Polym. Sci. Part B: Polym. Phys.* **2016**, *54*, 2200-2209.
- [267] Müller, A.; Arnal, M. Thermal fractionation of polymers. *Prog. Polym. Sci.* **2005**, *30*, 559-603.
- [268] Arandia, I.; Mugica, A.; Zubitur, M.; Iturrospe, A.; Arbe, A.; Liu, G.; Wang, D.; Mincheva, R.; Dubois, P.; Müller, A. J. Application of SSA thermal fractionation and X-ray diffraction to elucidate comonomer inclusion or exclusion from the crystalline phases in poly(butylene succinate-*ran*-butylene azelate) random copolymers. *J. Polym. Sci. Pol. Phys.* **2016**, *54*, 2346-2358.
- [269] Reimann, S.; Baumeister, U.; Binder, W. H. Synthesis and Crystallization of Precision Polymers with Repetitive Folding Elements. *Macromol. Chem. Phys.* **2014**, *215*, 1963-1972.
- [270] Reimann, S.; Danke, V.; Beiner, M.; Binder, W. H. Synthesis of supramolecular precision polymers: Crystallization under conformational constraints. *J. Polym. Sci., Part A: Polym. Chem.* **2017**, *55*, 3736-3748.
- [271] Danke, V.; Gupta, G.; Reimann, S.; Binder, W. H.; Beiner, M. Structure formation in nanophase-separated systems with lamellar morphology: Comb-like vs. linear precision polymers. *Eur. Polym. J.* **2018**, *103*, 116-123.
- [272] Reimann, S. Synthesis of Crystallizable Foldamer Polymers via ADMET-Polymerization. M. Sc. Thesis, Martin Luther University Halle-Wittenberg, 2013.
- [273] Jakubczyk, D.; Merle, C.; Brenner-Weiss, G.; Luy, B.; Bräse, S. Deuterium and Tritium Labelling of N-Acyl-L-homoserine Lactones (AHLs) by Catalytic Reduction of a Double Bond in the Layer-by-Layer Method. *Eur. J. Org. Chem.* **2013**, *2013*, 5323-5330.
- [274] Fang, X.; Liu, K.; Li, C. Efficient Regio- and Stereoselective Formation of Azocan-2-ones via 8-Endo Cyclization of  $\alpha$ -Carbamoyl Radicals. *J. Am. Chem. Soc.* **2010**, *132*, 2274-2283.

- [275] Macleod, C.; McKiernan, G. J.; Guthrie, E. J.; Farrugia, L. J.; Hamprecht, D. W.; Macritchie, J.; Hartley, R. C. Synthesis of 2-Substituted Benzofurans and Indoles Using Functionalized Titanium Benzylidene Reagents on Solid Phase. *J. Org. Chem.* **2002**, *68*, 387-401.
- [276] van Hensbergen, J. A.; Gaines, T. W.; Wagener, K. B.; Burford, R. P.; Lowe, A. B. Functional  $\alpha,\omega$ -dienes via thiol-Michael chemistry: synthesis, oxidative protection, acyclic diene metathesis (ADMET) polymerization and radical thiol-ene modification. *Polym. Chem.* **2014**, *5*, 6225-6235.
- [277] Becker, H. G. O.; Berger, W.; Domschke, G.; Fanghänel, E.; Habicher, W. D.; Metz, P.; Pavel, D.; Schwetlick, K.: *Organikum - Organisch-chemisches Grundpraktikum*; Wiley-VCH: Weinheim, 2001., ISBN 3-527-29985-8
- [278] Johnson, M. J.; Majmudar, C.; Skolimowski, J. J.; Majda, M. Critical Temperature and LE/G Phase Transitions in Monolayer Films of the Amphiphilic TEMPO Derivatives at the Air/Water Interface†. *J. Phys. Chem. B* **2001**, *105*, 9002-9010.
- [279] Kang, Y. S.; Jeong, M. H.; Shin, S. J.; Kim, Y. H.; Kim, C. W. Synthesis of amphiphilic TEMPO derivative and characterization of Langmuir monolayers of amphiphilic alkyl-TEMPOs at the Air/Water interface. *Int. J. Nanosci.* **2006**, *05*, 787-793.
- [280] B. Helavi, V.; B. Solabannavar, S.; Desai, U.; B. Mane, R. Microwave Assisted Hydrolysis of Meldrum's Acid Derivatives and Decarboxylation of Derived Malonic Acids. *J. Chem. Res.* **2003**, *2003*, 174-175.
- [281] Li, H.; Caire da Silva, L.; Schulz, M. D.; Rojas, G.; Wagener, K. B. A review of how to do an acyclic diene metathesis reaction. *Polym. Int.* **2017**, *66*, 7-12.
- [282] Li, Z.-L.; Li, L.; Deng, X.-X.; Zhang, L.-J.; Dong, B.-T.; Du, F.-S.; Li, Z.-C. Periodic Vinyl Copolymers Containing  $\gamma$ -Butyrolactone via ADMET Polymerization of Designed Diene Monomers with Built-in Sequence. *Macromolecules* **2012**, *45*, 4590-4598.
- [283] Petkovska, V. I.; Hopkins, T. E.; Powell, D. H.; Wagener, K. B. MALDI-TOF Detection of Olefin Structural Isomerization in Metathesis Chemistry. *Macromolecules* **2005**, *38*, 5878-5885.
- [284] Petkovska, V. I.; Hopkins, T. E.; Powell, D. H.; Wagener, K. B. Functionality Dependent Olefin Activity in Acyclic Diene Metathesis Polymerization: Mass Spectrometry Characterization of Amino Acid Functionalized Olefins. *Anal. Chem.* **2006**, *78*, 3624-3631.
- [285] Kobayashi, S.; Pitet, L. M.; Hillmyer, M. A. Regio- and Stereoselective Ring-Opening Metathesis Polymerization of 3-Substituted Cyclooctenes. *J. Am. Chem. Soc.* **2011**, *133*, 5794-5797.
- [286] Huang, D.; Simon, S. L.; McKenna, G. B. Chain length dependence of the thermodynamic properties of linear and cyclic alkanes and polymers. *J. Chem. Phys.* **2005**, *122*, 084907.

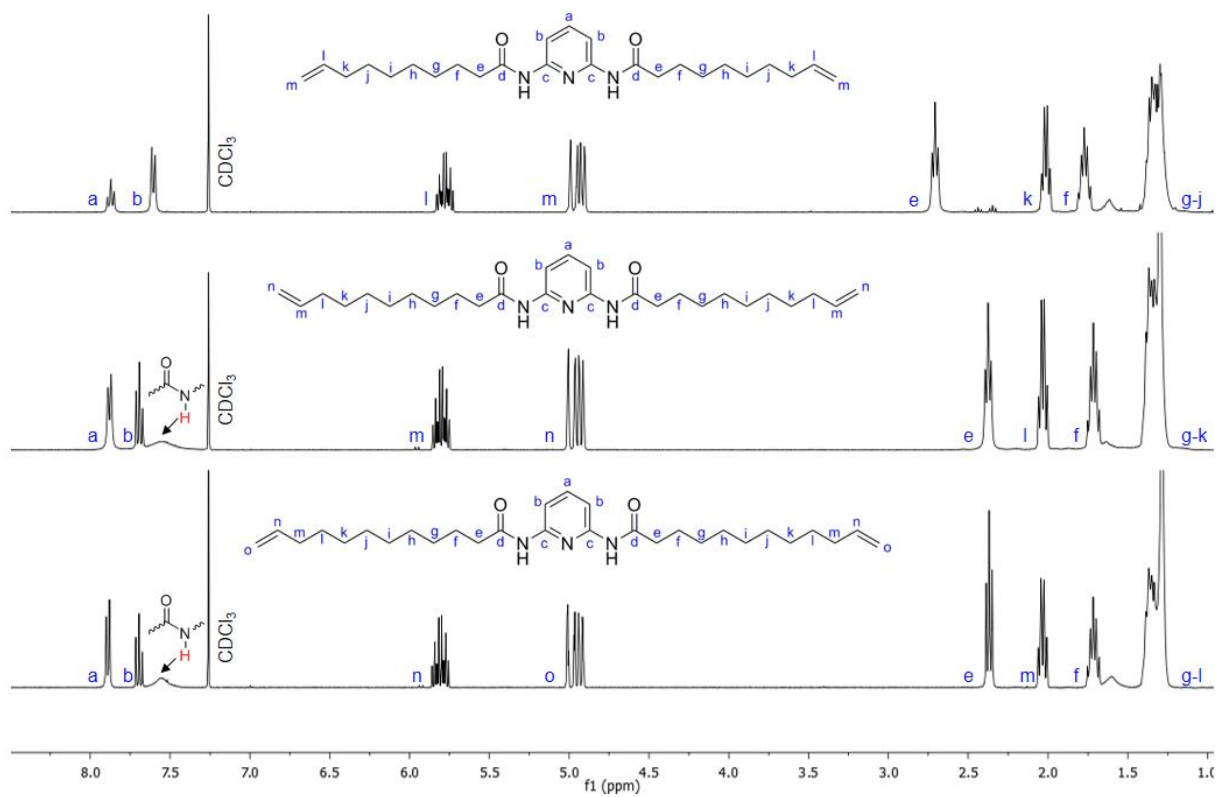
- [287] Rösler, F. Modellierung und Simulation der Phasenwechselforgänge in makroverkapselten latenten thermischen Speichern. Ph. D. Thesis, Universität Bayreuth, 2014.
- [288] Qiu, W.; Sworen, J.; Pyda, M.; Nowak-Pyda, E.; Habenschuss, A.; Wagener, K. B.; Wunderlich, B. Effect of the Precise Branching of Polyethylene at Each 21st CH<sub>2</sub> Group on Its Phase Transitions, Crystal Structure, and Morphology. *Macromolecules* **2005**, *39*, 204-217.
- [289] Terada, K.; Berda, E. B.; Wagener, K. B.; Sanda, F.; Masuda, T. ADMET Polycondensation of Diketopiperazine-Based Dienes. Polymerization Behavior and Effect of Diketopiperazine on the Properties of the Formed Polymers. *Macromolecules* **2008**, *41*, 6041-6046.
- [290] Janiak, C. A critical account on  $\pi$ - $\pi$  stacking in metal complexes with aromatic nitrogen-containing ligands. *J. Chem. Soc., Dalton Trans.* **2000**, 3885-3896.
- [291] Hanwell, M. D.; Curtis, D. E.; Lonie, D. C.; Vandermeersch, T.; Zurek, E.; Hutchison, G. R. Avogadro: an advanced semantic chemical editor, visualization, and analysis platform. *J. Cheminformatics* **2012**, *4*, 17.
- [292] Kobayashi, M. Equations of state for orthorhombic and triclinic lattices of polyethylene. *J. Chem. Phys.* **1979**, *70*, 509-518.
- [293] Mahapatra, A. K.; Sahoo, P.; Goswami, S.; Chantrapromma, S.; Fun, H.-K. Fluorescence sensing of theobromine by simple 2,6-diamino-pyridine and the novel cyclic chair-like hydrogen-bonded tetramer of its diacetyl derivative. *Tetrahedron Lett.* **2009**, *50*, 89-92.
- [294] George, M.; Tan, G.; John, V. T.; Weiss, R. G. Urea and Thiourea Derivatives as Low Molecular-Mass Organogelators. *Chem. Eur. J.* **2005**, *11*, 3243-3254.
- [295] Altintas, O.; Barner-Kowollik, C. Single Chain Folding of Synthetic Polymers by Covalent and Non-Covalent Interactions: Current Status and Future Perspectives. *Macromol. Rapid Commun.* **2012**, *33*, 958-971.
- [296] Altintas, O.; Gerstel, P.; Dingenouts, N.; Barner-Kowollik, C. Single chain self-assembly: preparation of  $\alpha,\omega$ -donor-acceptor chains via living radical polymerization and orthogonal conjugation. *Chem. Comm.* **2010**, *46*, 6291-6293.
- [297] Ozcan, A.; Christopher, B. K. Single-Chain Folding of Synthetic Polymers: A Critical Update. *Macromol. Rapid Commun.* **2016**, *37*, 29-46.
- [298] Ouchi, M.; Badi, N.; Lutz, J.-F.; Sawamoto, M. Single-chain technology using discrete synthetic macromolecules. *Nature Chem.* **2011**, *3*, 917.
- [299] Lyon, C. K.; Prasher, A.; Hanlon, A. M.; Tuten, B. T.; Tooley, C. A.; Frank, P. G.; Berda, E. B. A brief user's guide to single-chain nanoparticles. *Polym. Chem.* **2015**, *6*, 181-197.
- [300] Pomposo, J. A. Bioinspired single-chain polymer nanoparticles. *Polym. Int.* **2014**, *63*, 589-592.



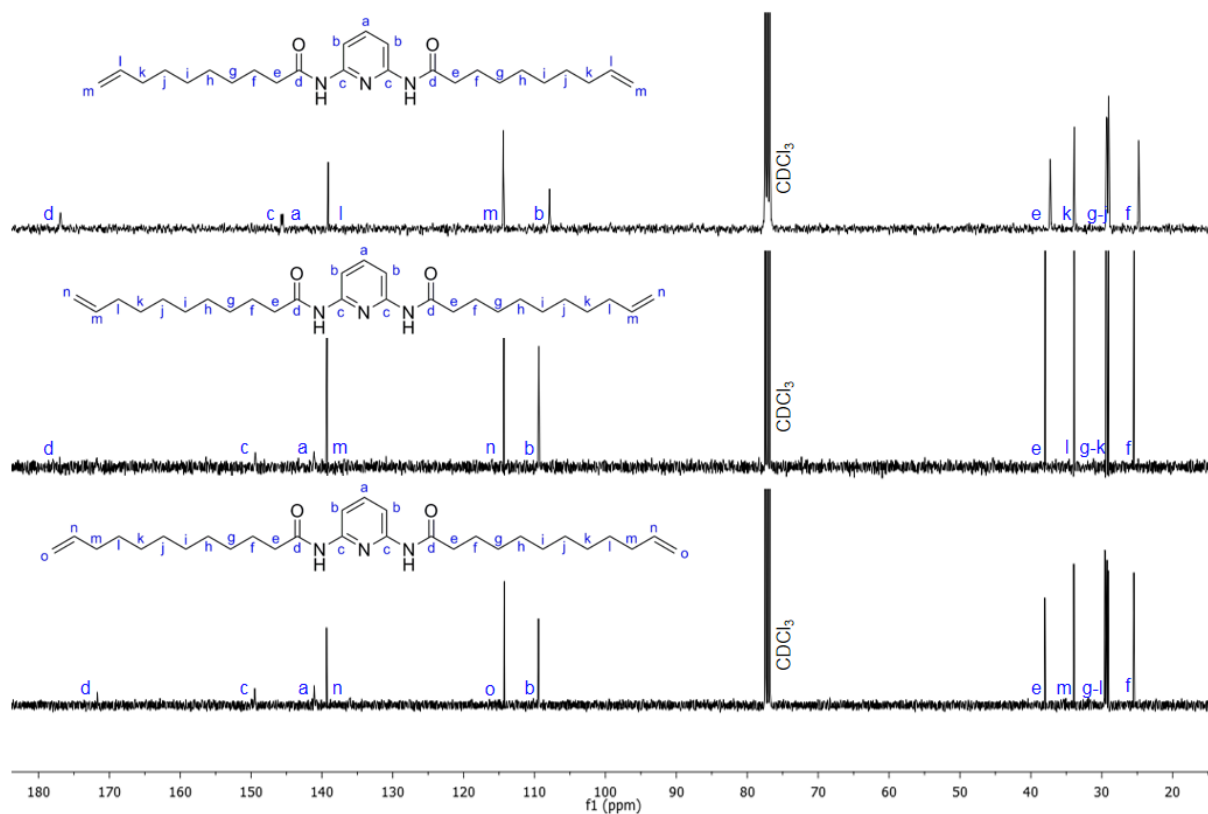
- [301] Ilhan, F.; Gray, M.; Blanchette, K.; Rotello, V. M. Control of Polymer Solution Structure via Intra- and Intermolecular Aromatic Stacking. *Macromolecules* **1999**, *32*, 6159-6162.
- [302] Lu, J.; ten Brummelhuis, N.; Weck, M. Intramolecular folding of triblock copolymers via quadrupole interactions between poly(styrene) and poly(pentafluorostyrene) blocks. *Chem. Commun.* **2014**, *50*, 6225-6227.
- [303] de Luzuriaga, A. R.; Ormategui, N.; Grande, H. J.; Odriozola, I.; Pomposo, J. A.; Loinaz, I. Intramolecular Click Cycloaddition: An Efficient Room-Temperature Route towards Bioconjugable Polymeric Nanoparticles. *Macromol. Rapid Commun.* **2008**, *29*, 1156-1160.
- [304] Saliu, F.; Rindone, B. Organocatalyzed synthesis of ureas from amines and ethylene carbonate. *Tetrahedron Lett.* **2010**, *51*, 6301-6304.
- [305] Hopkins, T. E.; Wagener, K. B. ADMET Synthesis of Polyolefins Targeted for Biological Applications. *Macromolecules* **2004**, *37*, 1180-1189.

## 7. Appendix

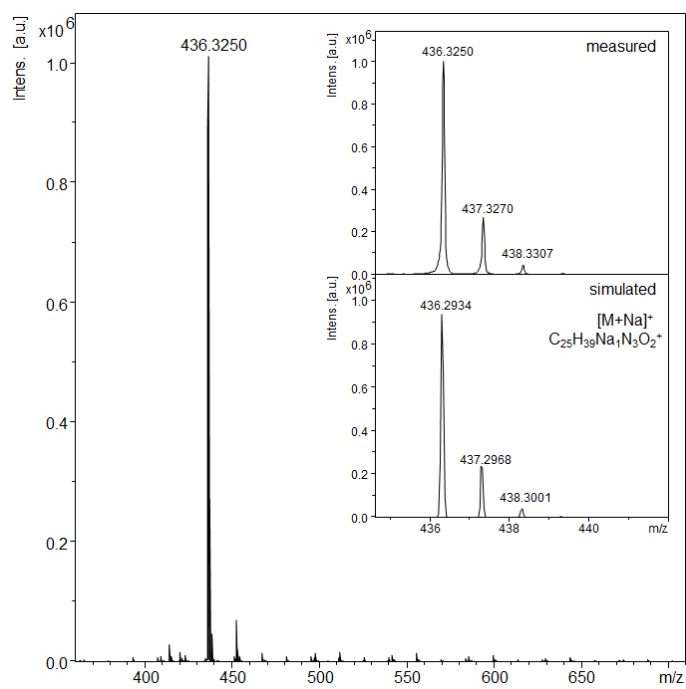
### 7.1 IR- and NMR spectra and ESI ToF MS of the DAP containing monomers (1a-c)



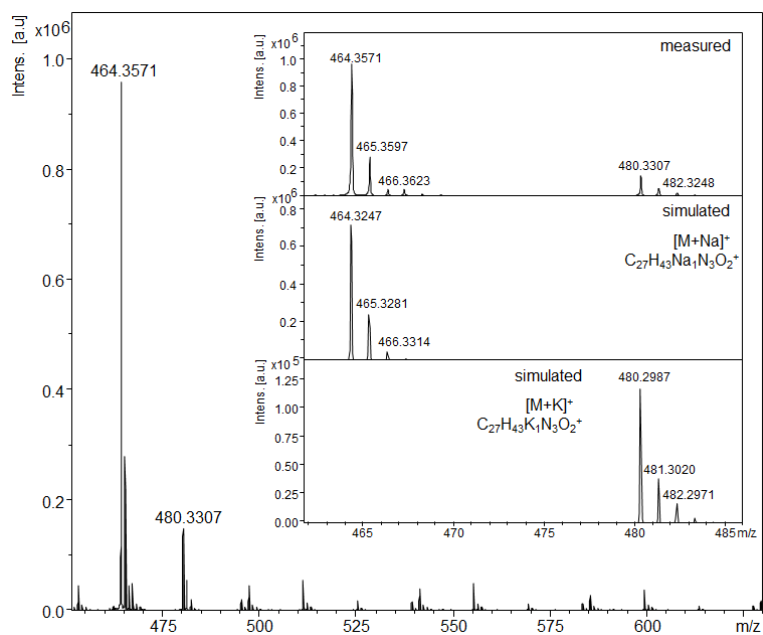
**A 1:**  $^1\text{H-NMR}$  spectra of the DAP containing monomers (1a-c).



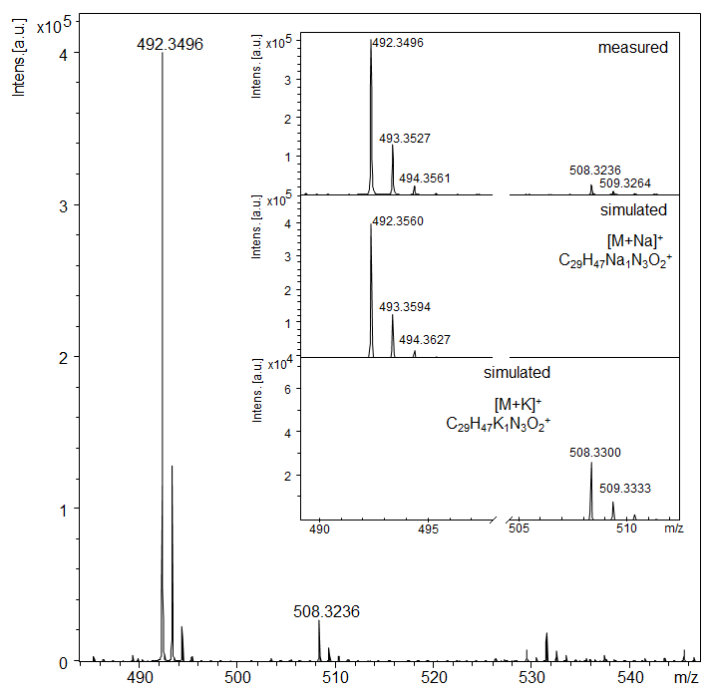
**A 2:**  $^{13}\text{C}$ -NMR spectra of the DAP containing monomers (**1a-c**).



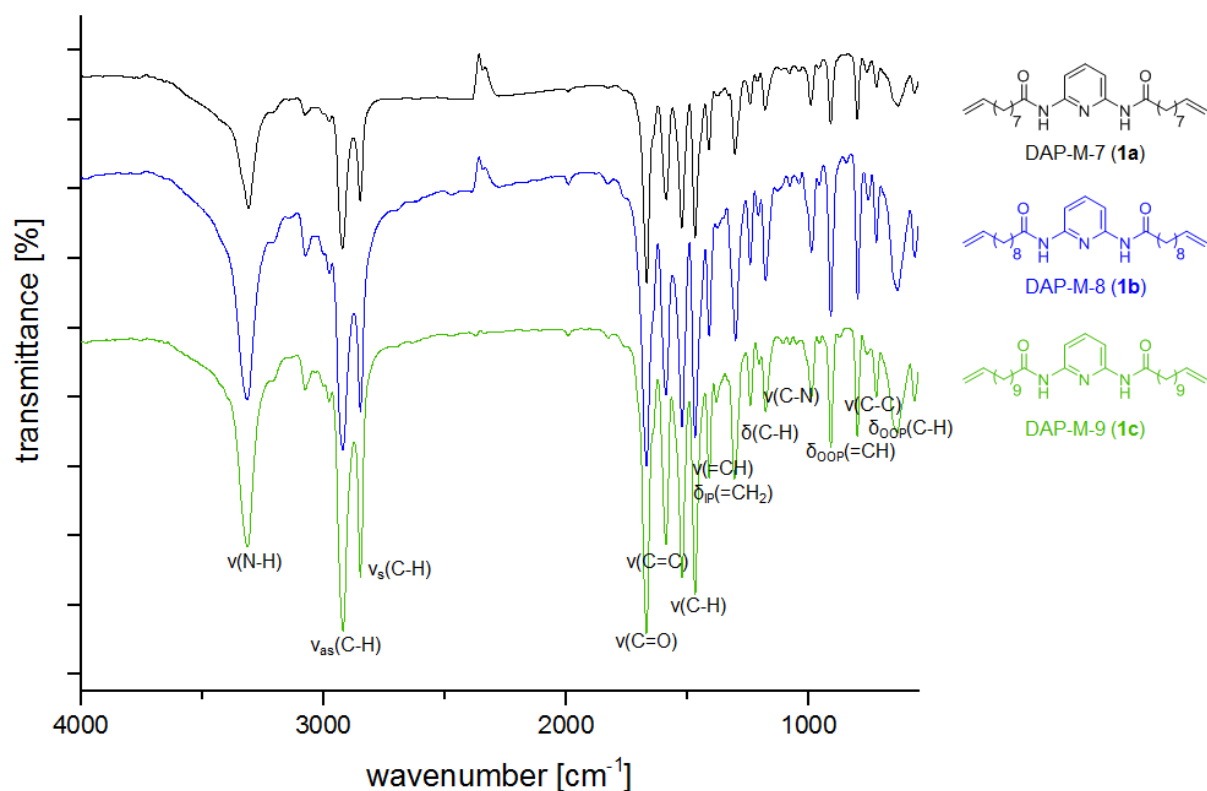
**A 3:** ESI ToF MS analysis of DAP-M-7 (**1a**).



**A 4:** ESI ToF MS analysis of DAP-M-8 (**1b**).

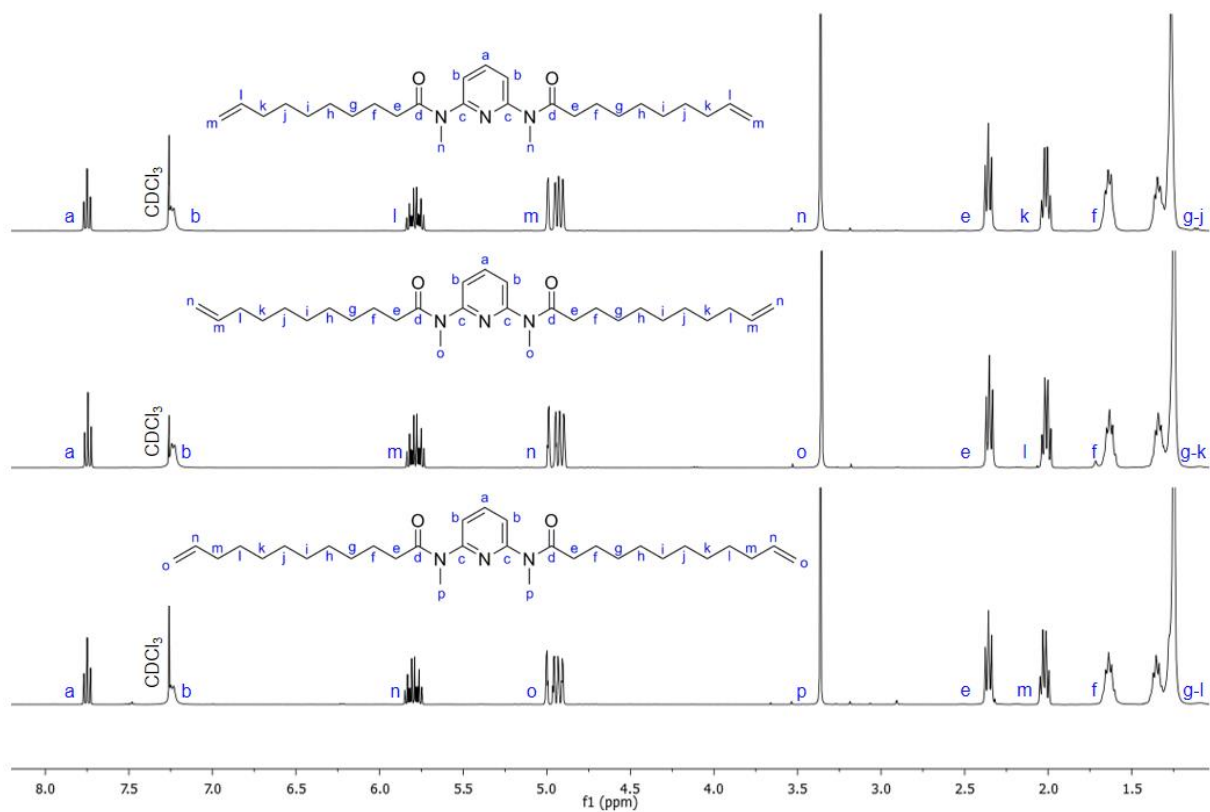


**A 5:** ESI ToF MS analysis of DAP-M-9 (**1c**).

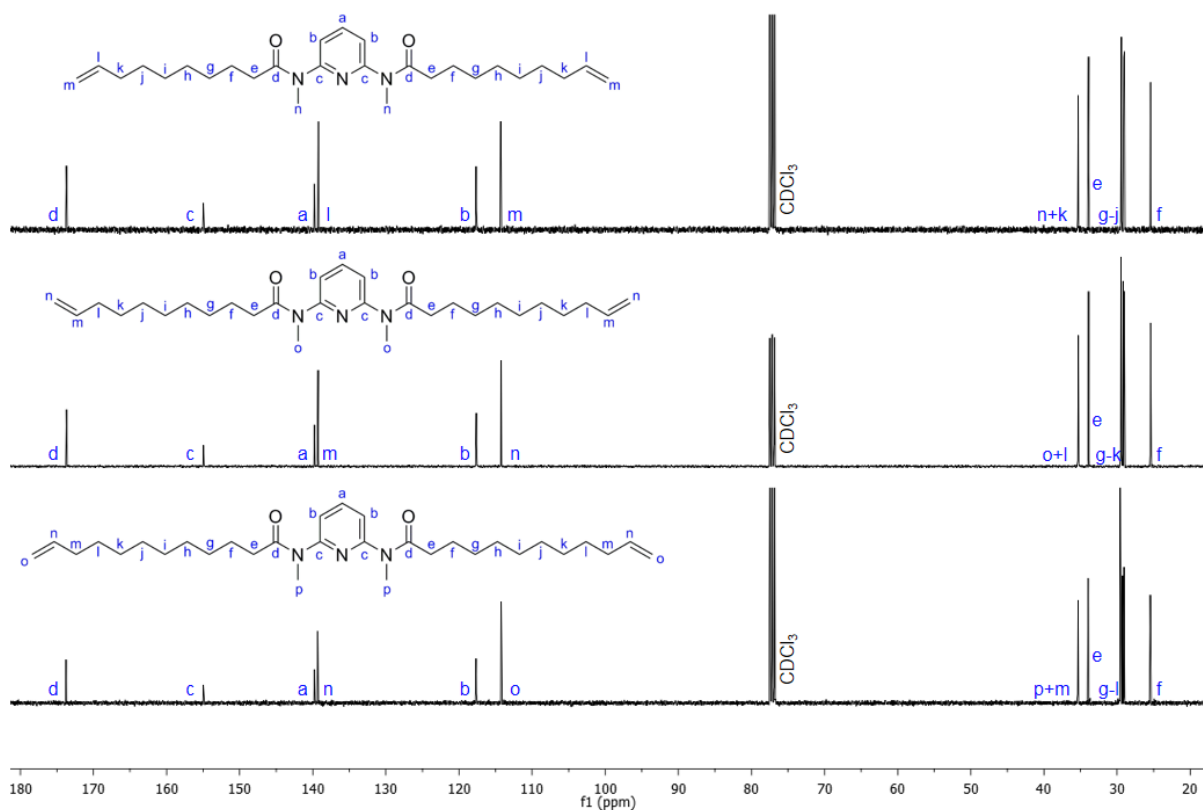


A 6: IR spectra of the DAP containing monomers (1a-c).

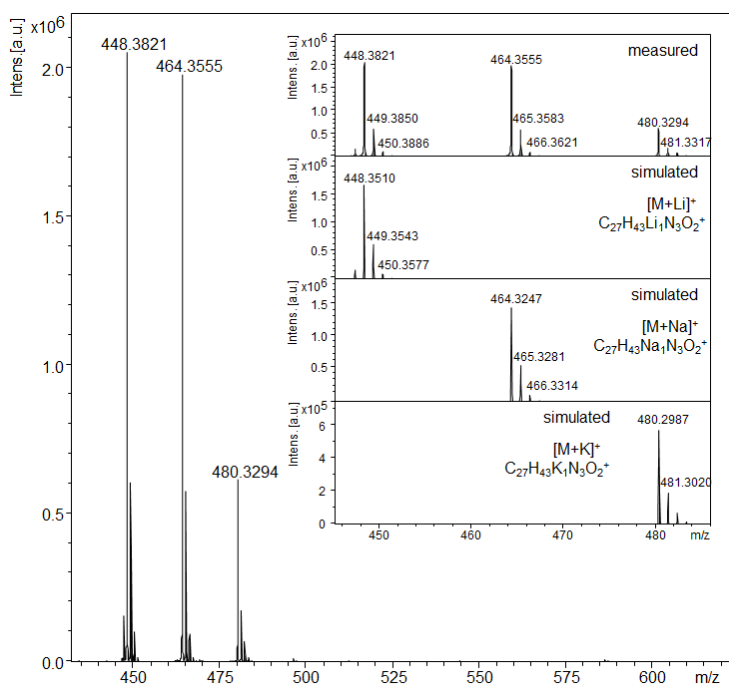
## 7.2 NMR spectra and ESI ToF MS of the *N*-methyl protected DAP containing monomers (2a-c)



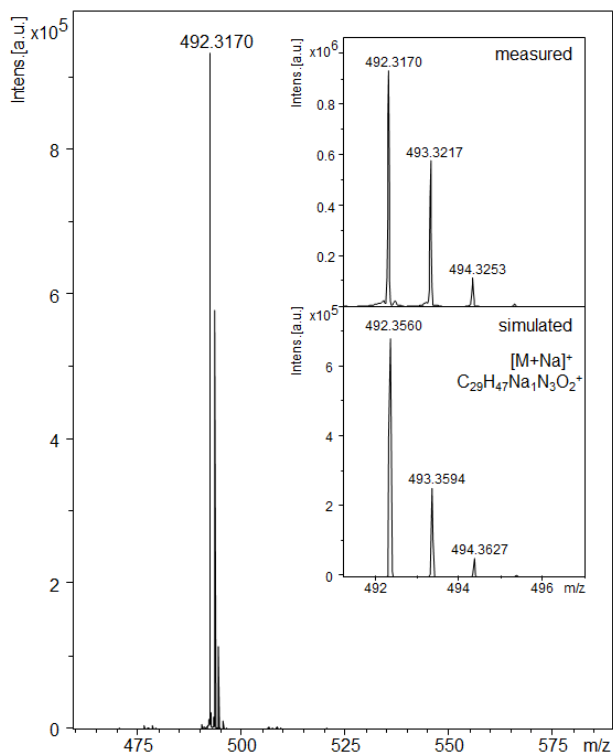
A 7:  $^1\text{H-NMR}$  spectra of the *N*-methyl protected DAP containing monomers (2a-c).



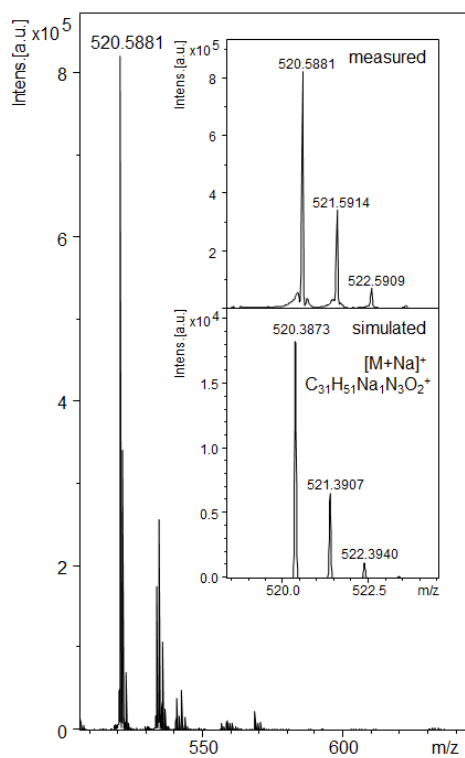
**A 8:**  $^{13}\text{C}$ -NMR spectra of the *N*-methyl protected DAP containing monomers (2a-c).



**A 9:** ESI ToF MS analysis of DAP-M-Me-7 (2a).

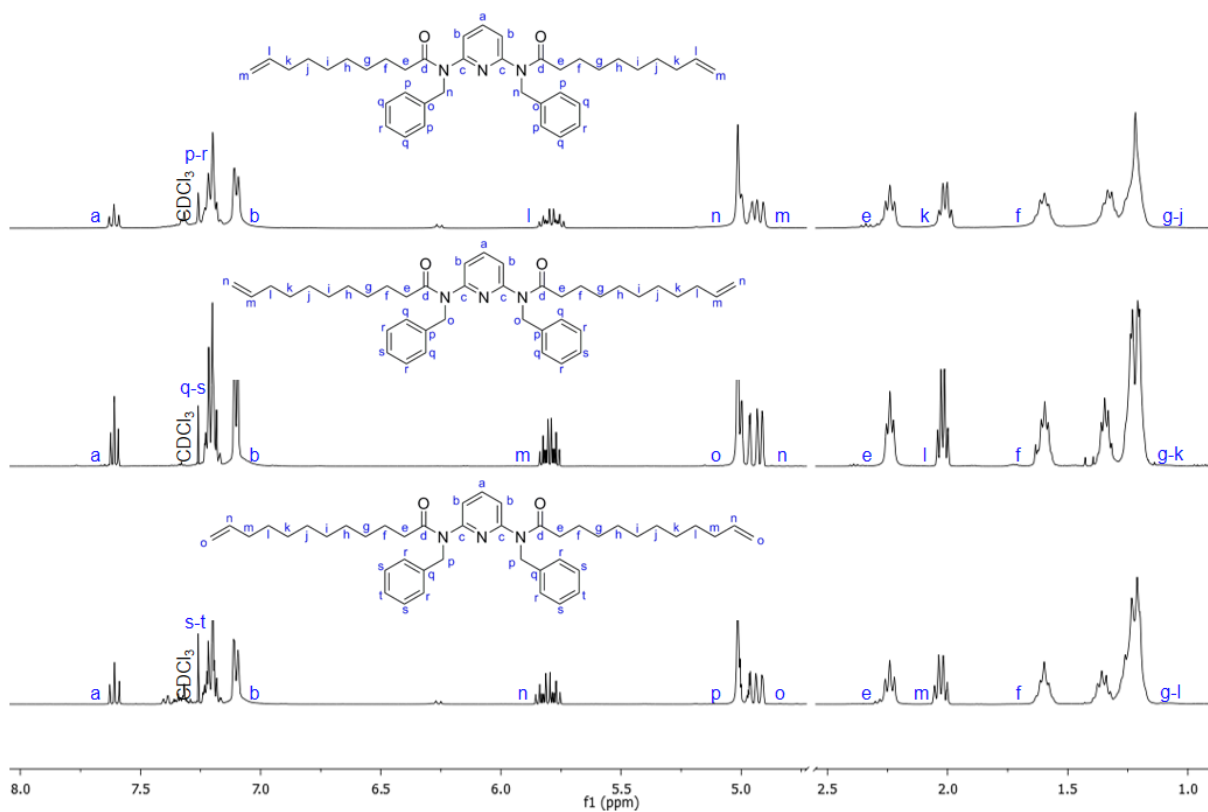


**A 10:** ESI ToF MS analysis of DAP-M-Me-8 (**2b**).

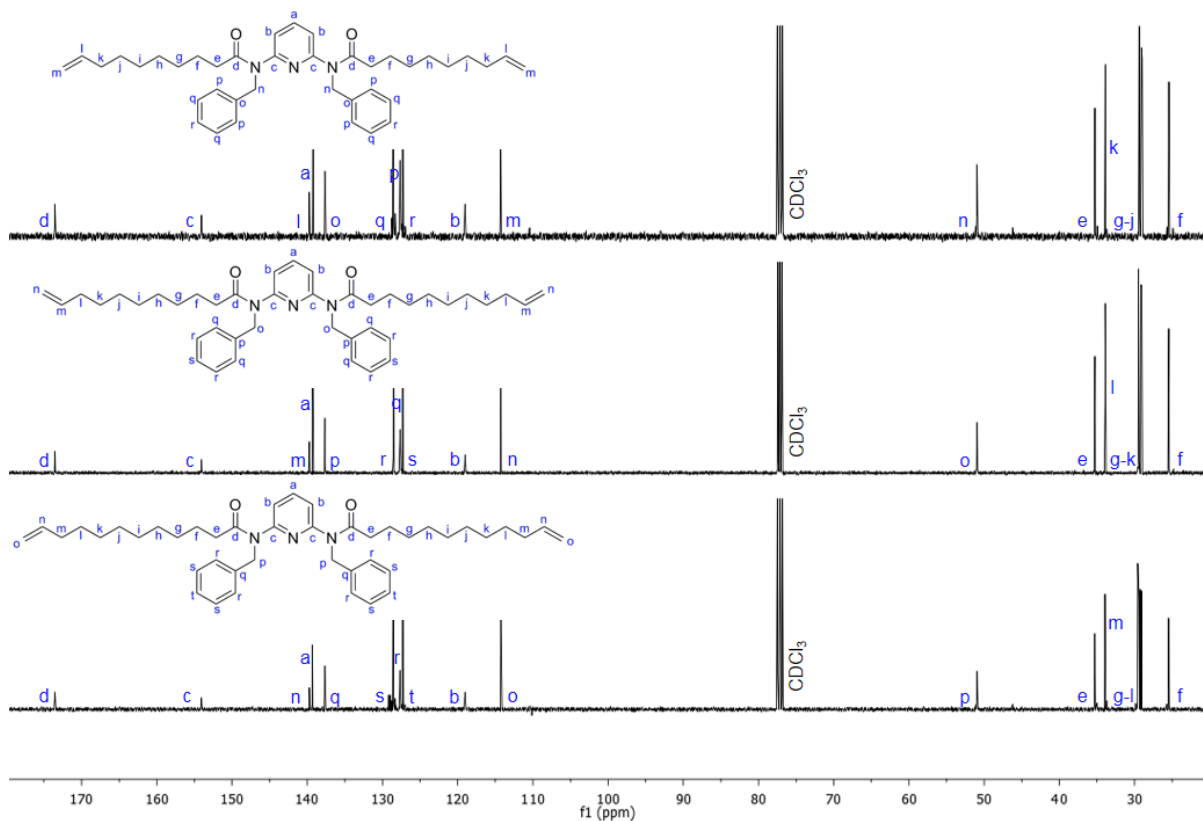


**A 11:** ESI ToF MS analysis of DAP-M-Me-9 (**2c**).

### 7.3 NMR spectra and ESI ToF MS of the *N*-benzyl protected DAP containing monomers (2d-f)

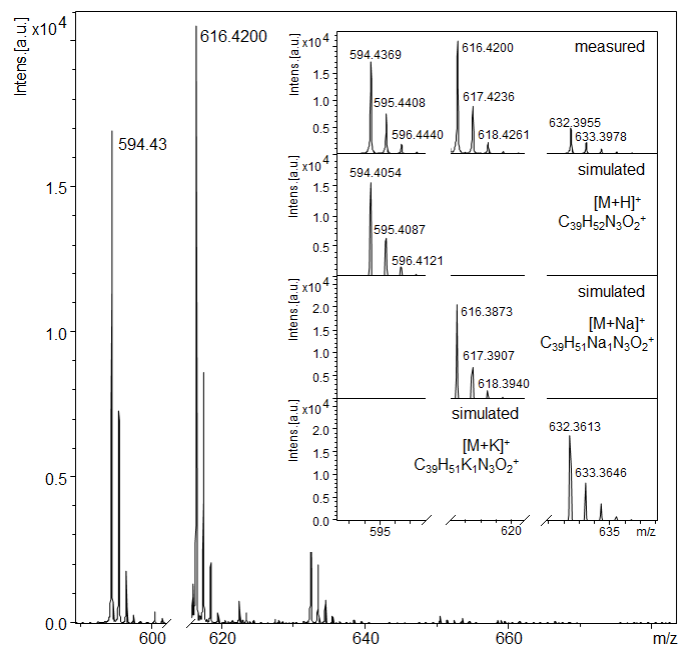


A 12:  $^1\text{H-NMR}$  spectra of the *N*-benzyl protected DAP containing monomers (2d-f).

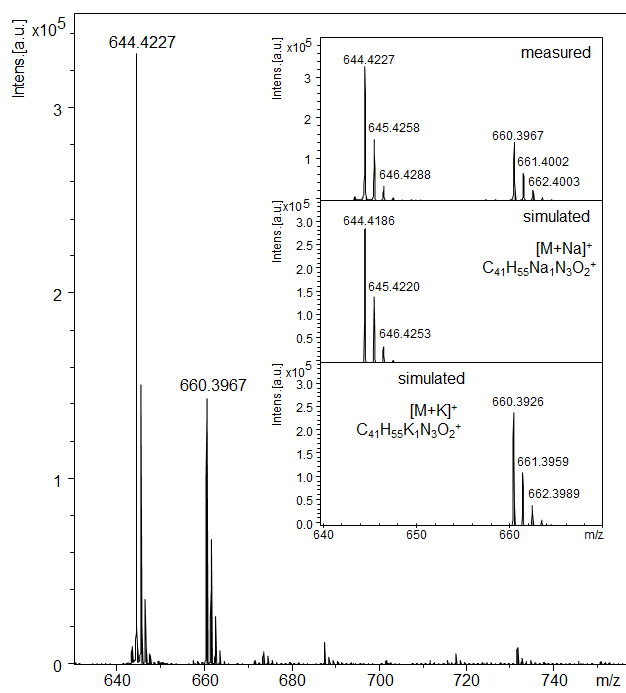


A 13:  $^{13}\text{C-NMR}$  spectra of the *N*-benzyl protected DAP containing monomers (2d-f).

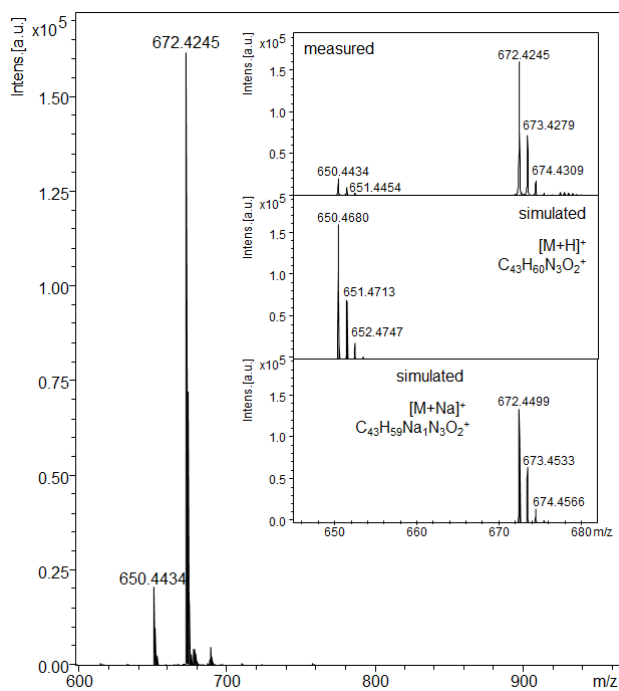




**A 14:** ESI ToF MS analysis of DAP-M-Bn-7 (**2d**).

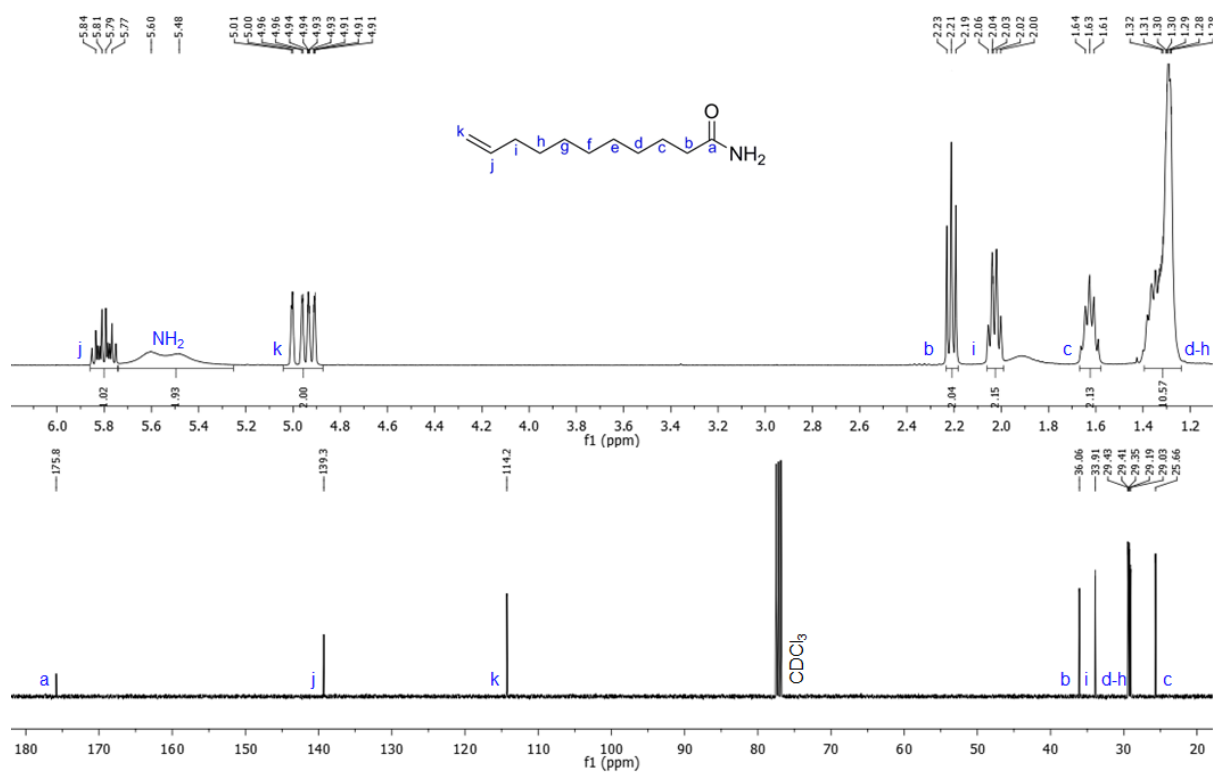


**A 15:** ESI ToF MS analysis of DAP-M-Bn-8 (**2e**).

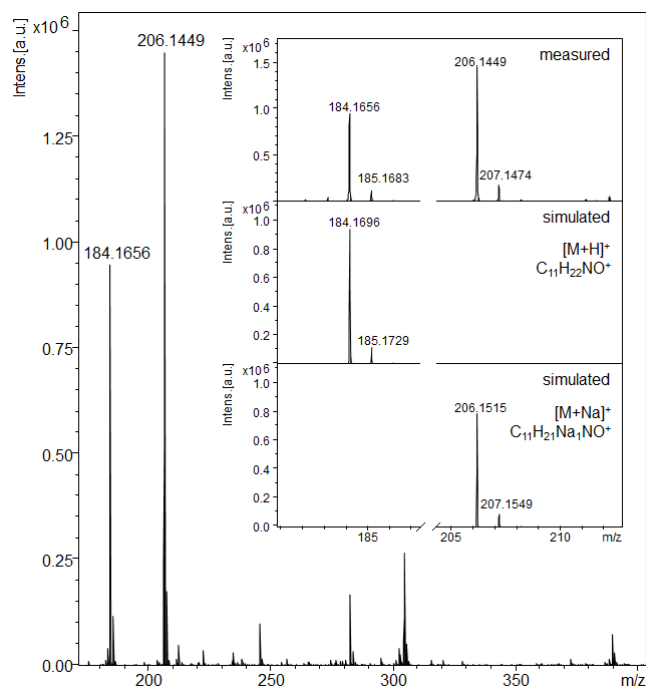


A 16: ESI ToF MS analysis of DAP-M-Bn-9 (**2f**).

## 7.4 NMR spectra and ESI ToF MS of undec-10-enamide (**3**)

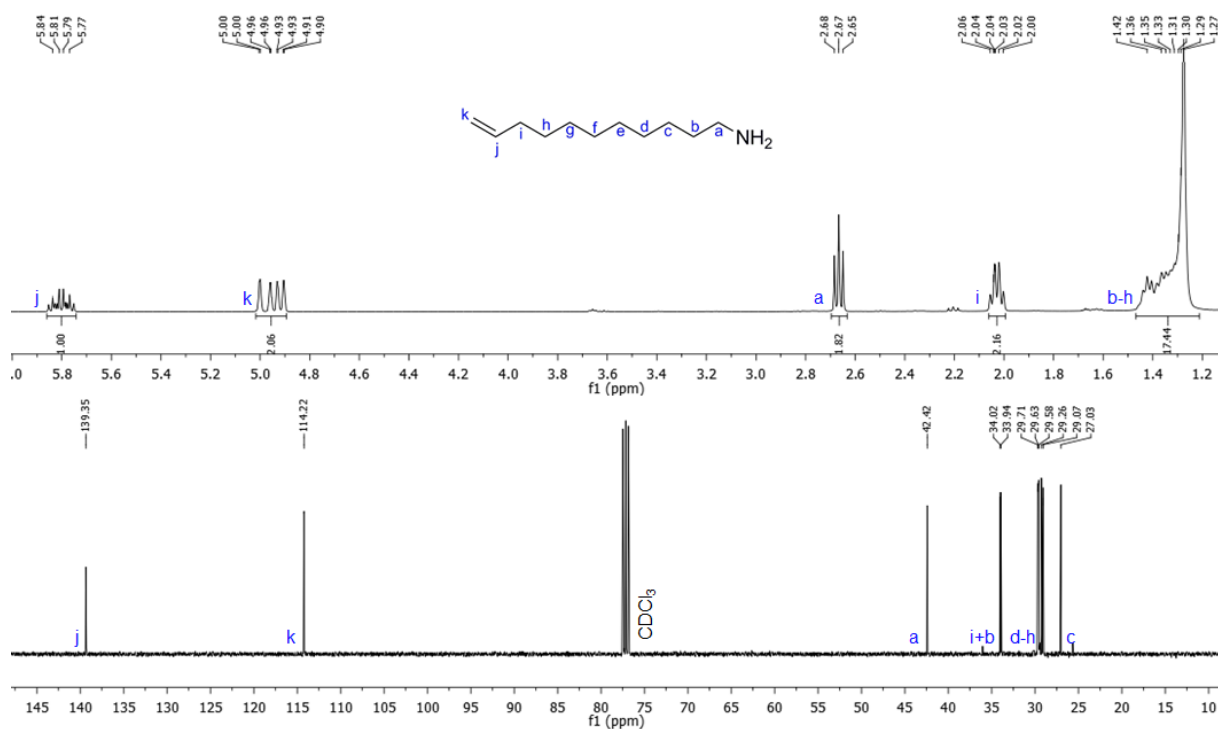


A 17:  $^1\text{H}$ - and  $^{13}\text{C}$ -NMR spectrum of undec-10-enamide (**3**).

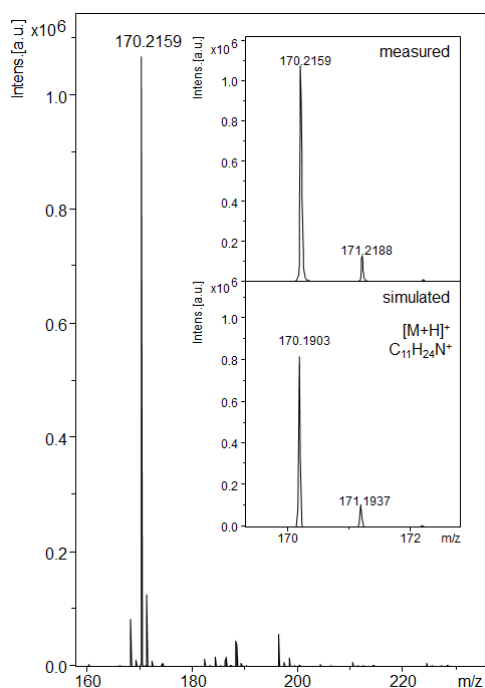


A 18: ESI ToF MS analysis of undec-10-enamide (3).

### 7.5 NMR spectra and ESI ToF MS of undec-10-en-1-amine (4)

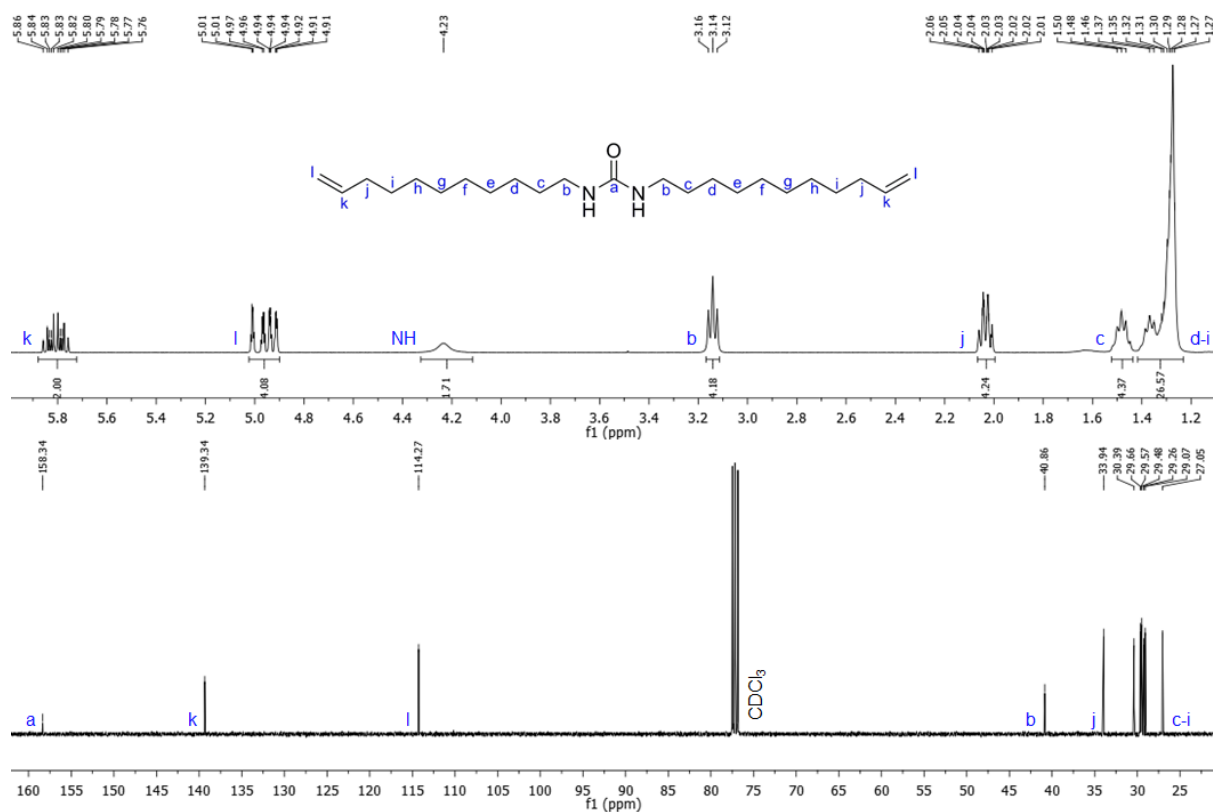


A 19: <sup>1</sup>H- and <sup>13</sup>C-NMR spectrum of undec-10-en-1-amine (4).

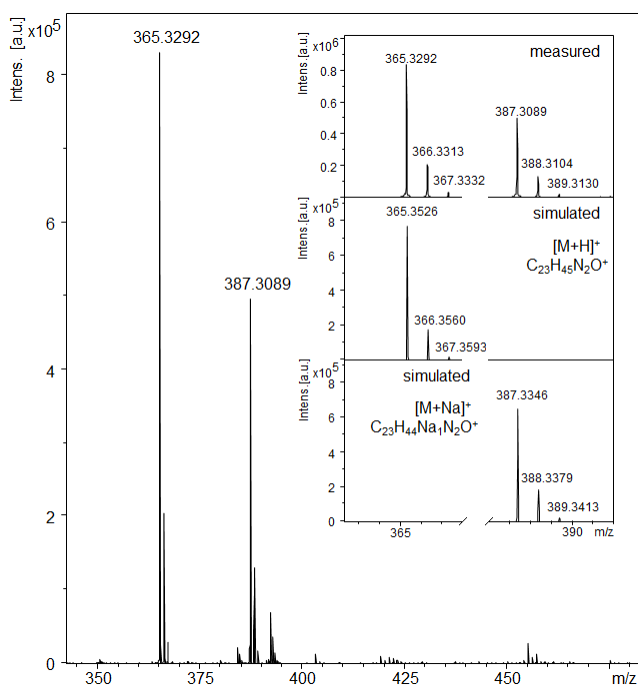


A 20: ESI ToF MS analysis of undec-10-en-1-amine (4).

## 7.6 NMR spectra and ESI ToF MS of 1,3-diundec-10-en-1-ylurea (Urea-M-9) (5)

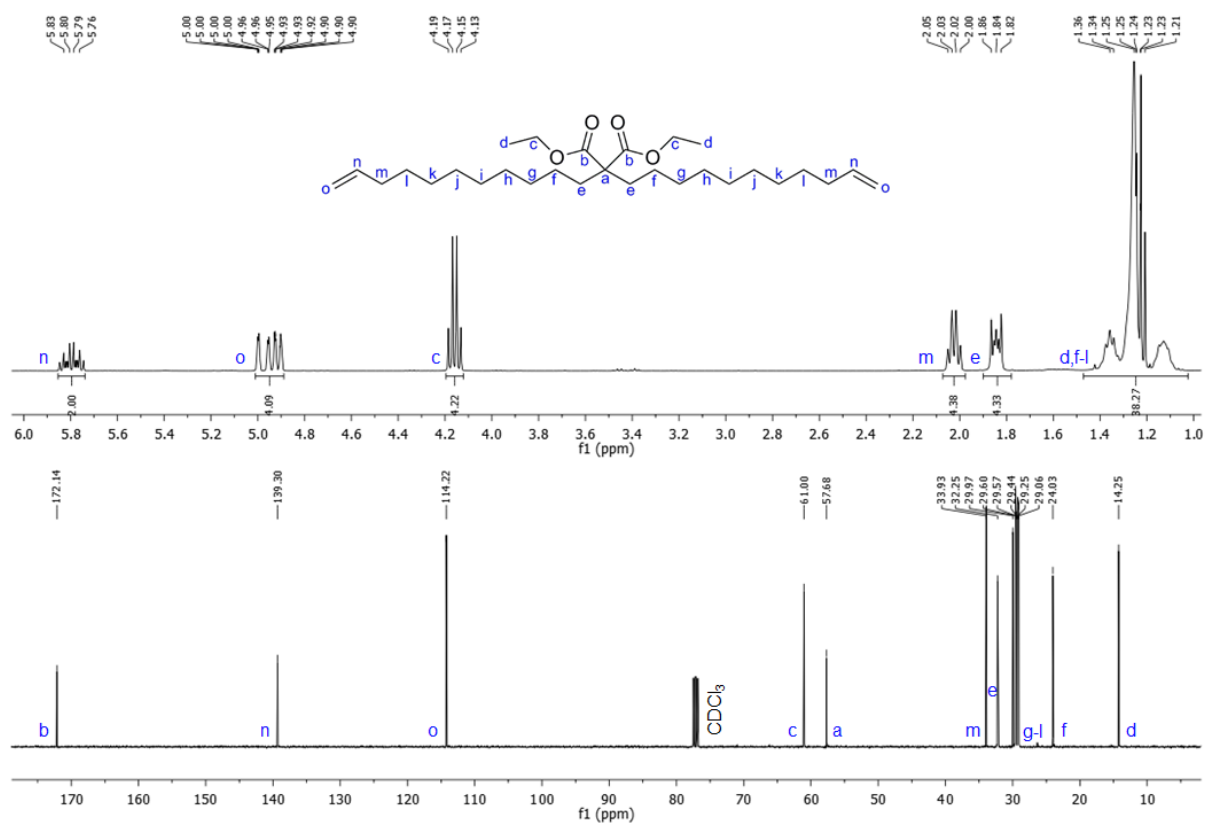


A 21:  $^1\text{H}$ - and  $^{13}\text{C}$ -NMR spectrum of Urea-M-9 (5).



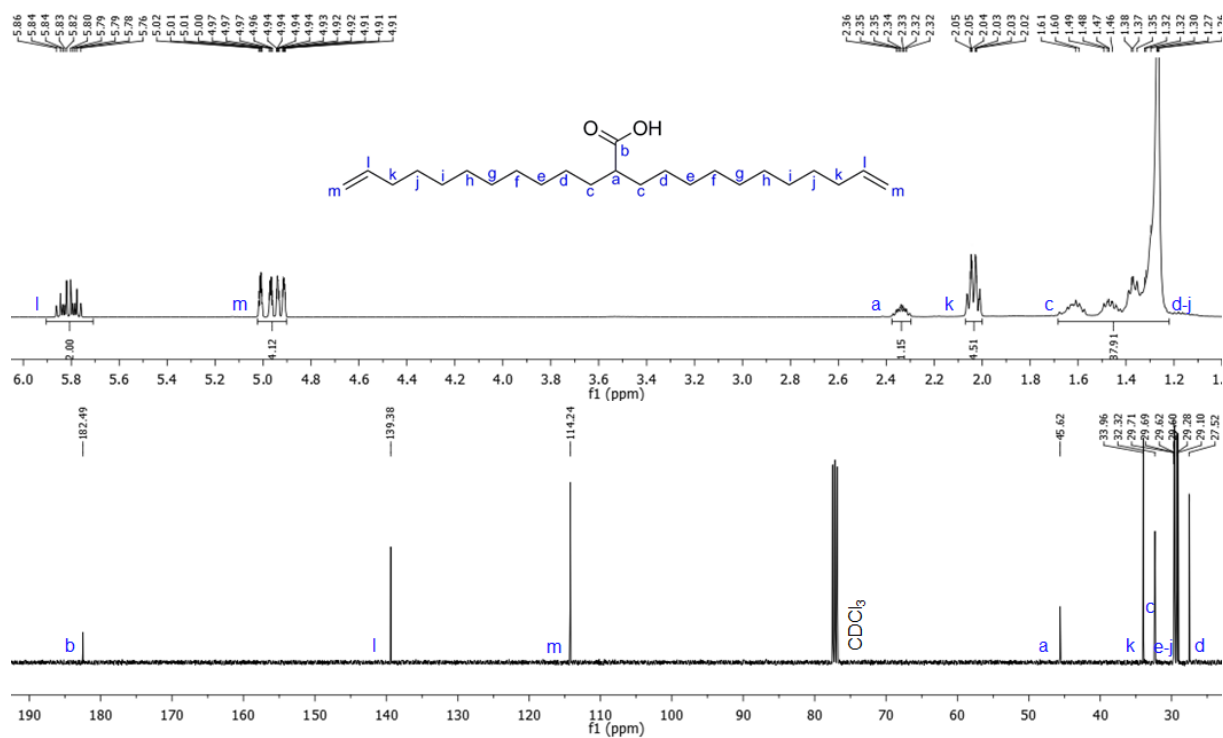
A 22: ESI ToF MS analysis of Urea-M-9 (5).

### 7.7 NMR spectra of diethyl-2,2-di(undec-10-en-1-yl)malonate (6)

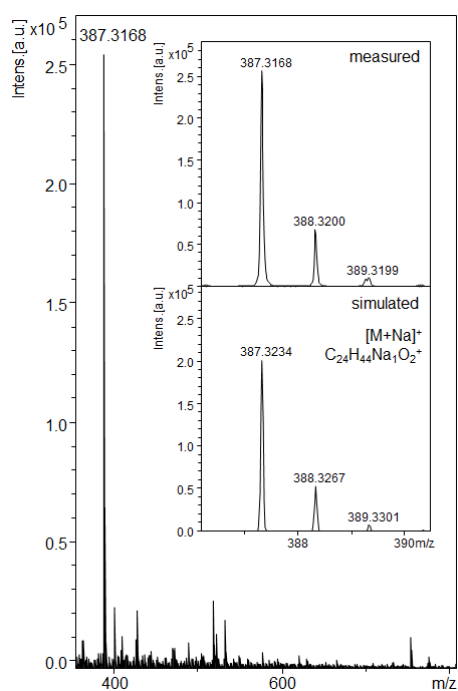


A 23: <sup>1</sup>H- and <sup>13</sup>C-NMR spectrum of diethyl-2,2-di(undec-10-en-1-yl)malonate (6).

## 7.8 NMR spectra and ESI ToF MS of 2-(undec-10-en-1-yl)tridec-12-enoic acid (Acid-M-9) (8)

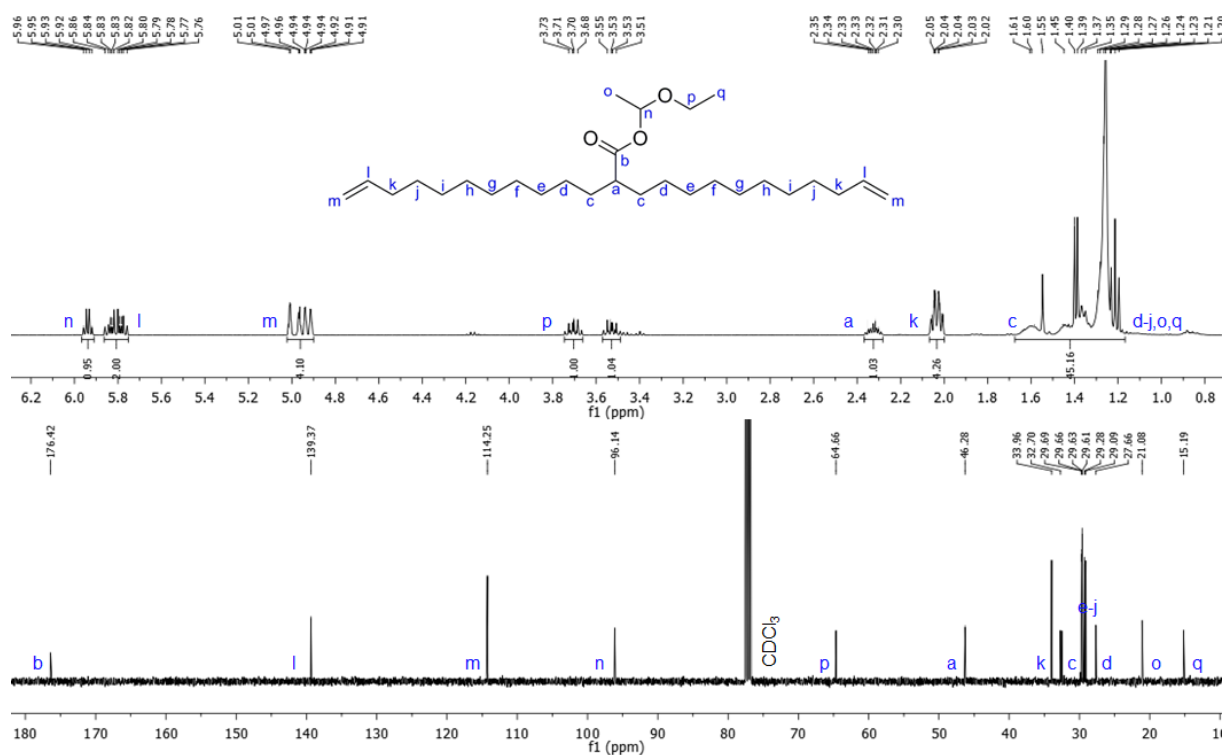


A 24:  $^1\text{H}$ - and  $^{13}\text{C}$ -NMR spectrum of Acid-M-9 (8).

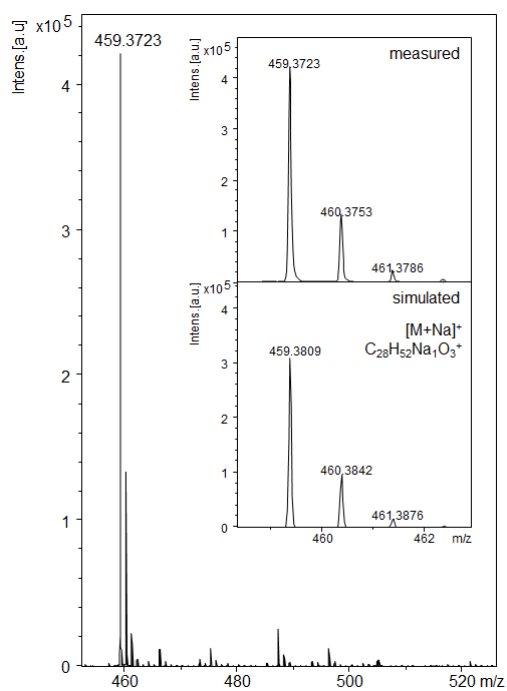


A 25: ESI ToF MS analysis of Acid-M-9 (8).

## 7.9 NMR spectra and ESI ToF MS of Acid-M-Ee-9 (10)

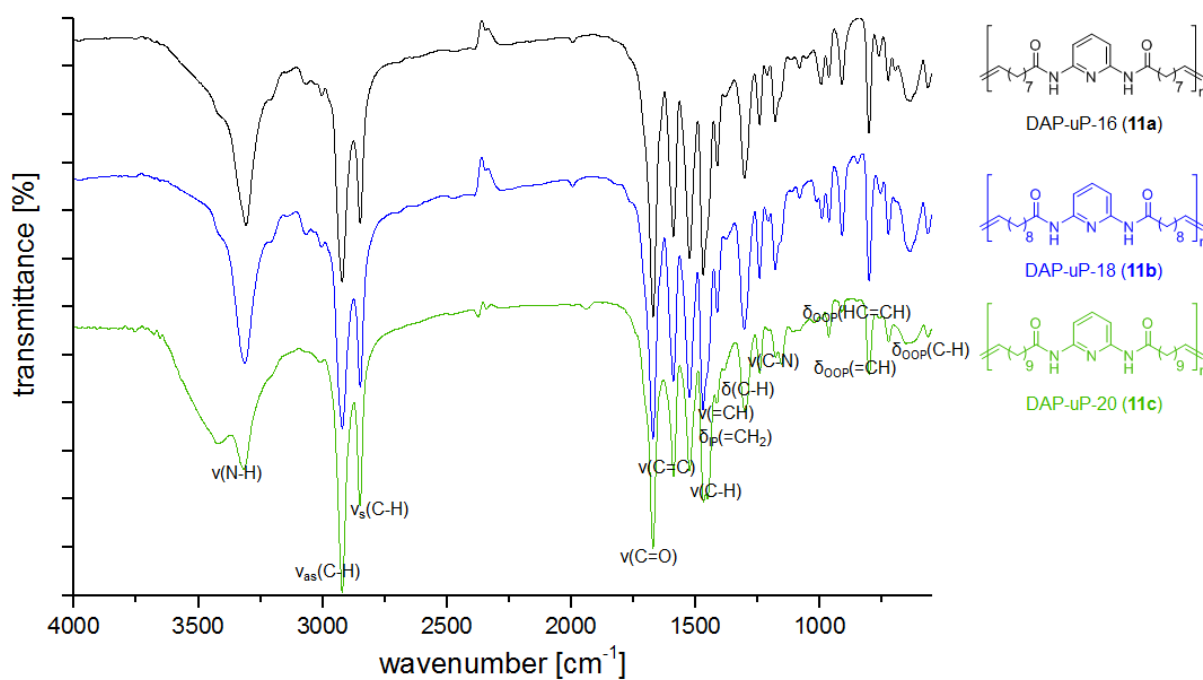


A 26: <sup>1</sup>H- and <sup>13</sup>C-NMR spectrum of Acid-M-Ee-9 (10).



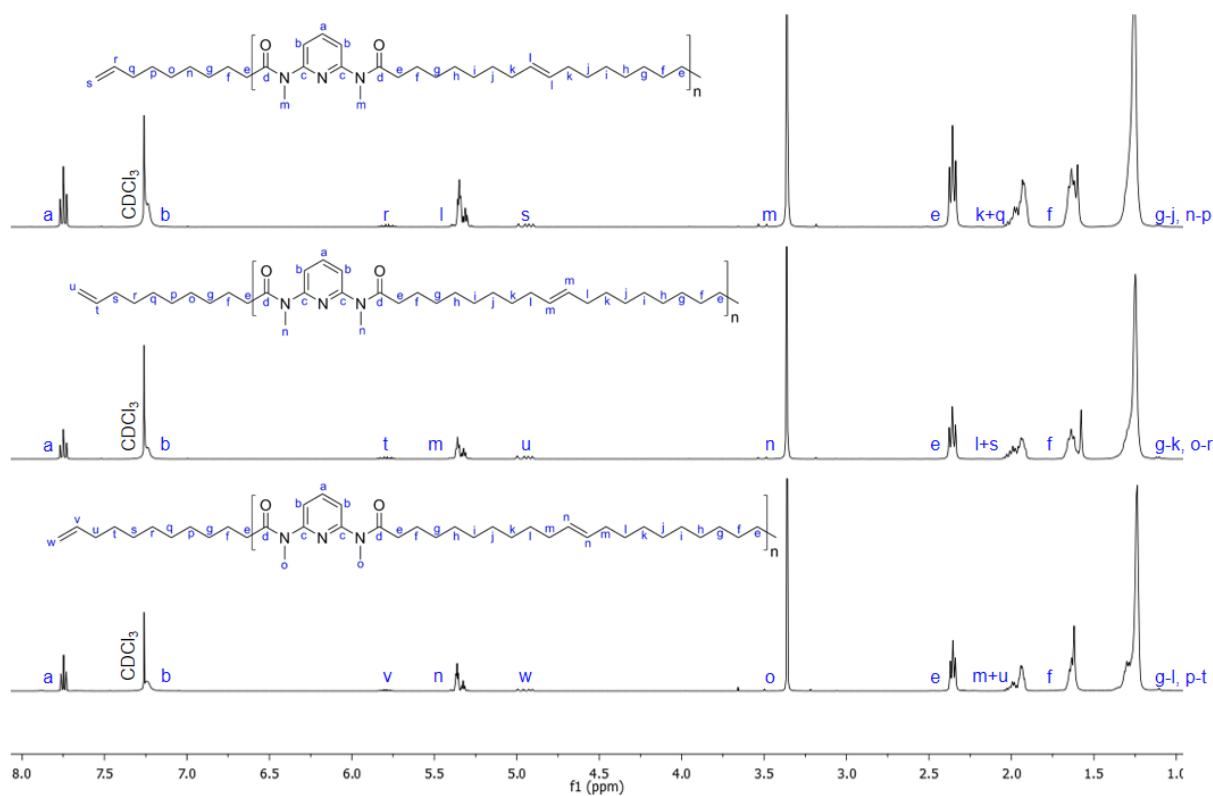
A 27: ESI ToF MS analysis of Acid-M-Ee-9 (10).

## 7.10 IR spectra of the unsaturated DAP containing polymers (11a-c)



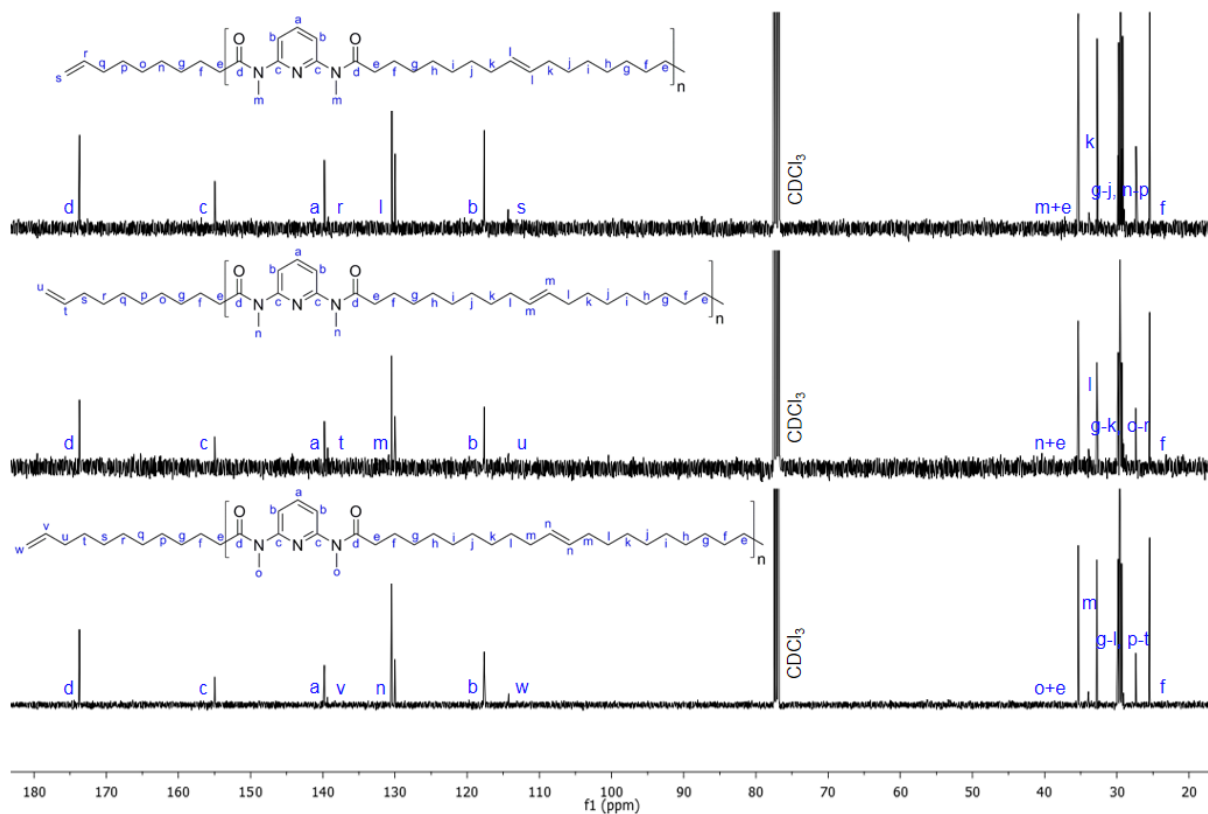
A 28: IR spectra of the unsaturated DAP containing polymers (11a-c).

## 7.11 NMR spectra and MALDI ToF MS of the unsaturated *N*-methyl protected DAP containing polymers (11d-f)

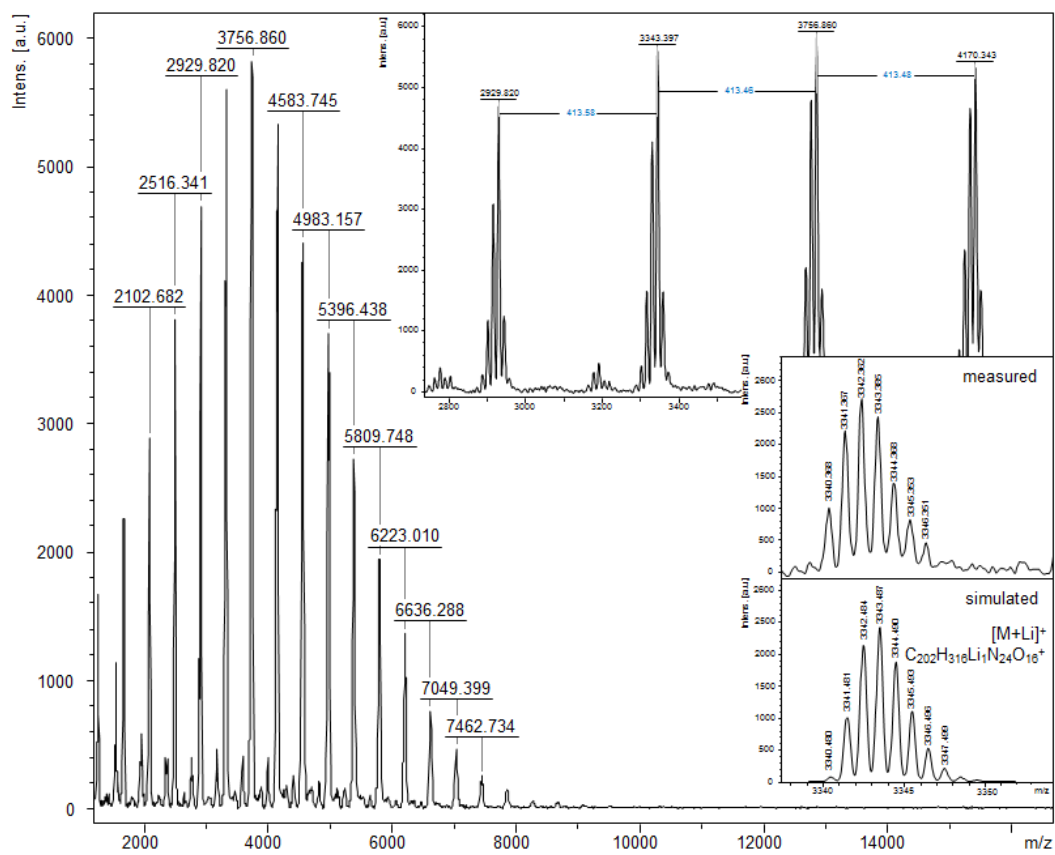


A 29: <sup>1</sup>H-NMR spectra of the unsaturated *N*-methyl protected DAP containing polymers (11d-f).

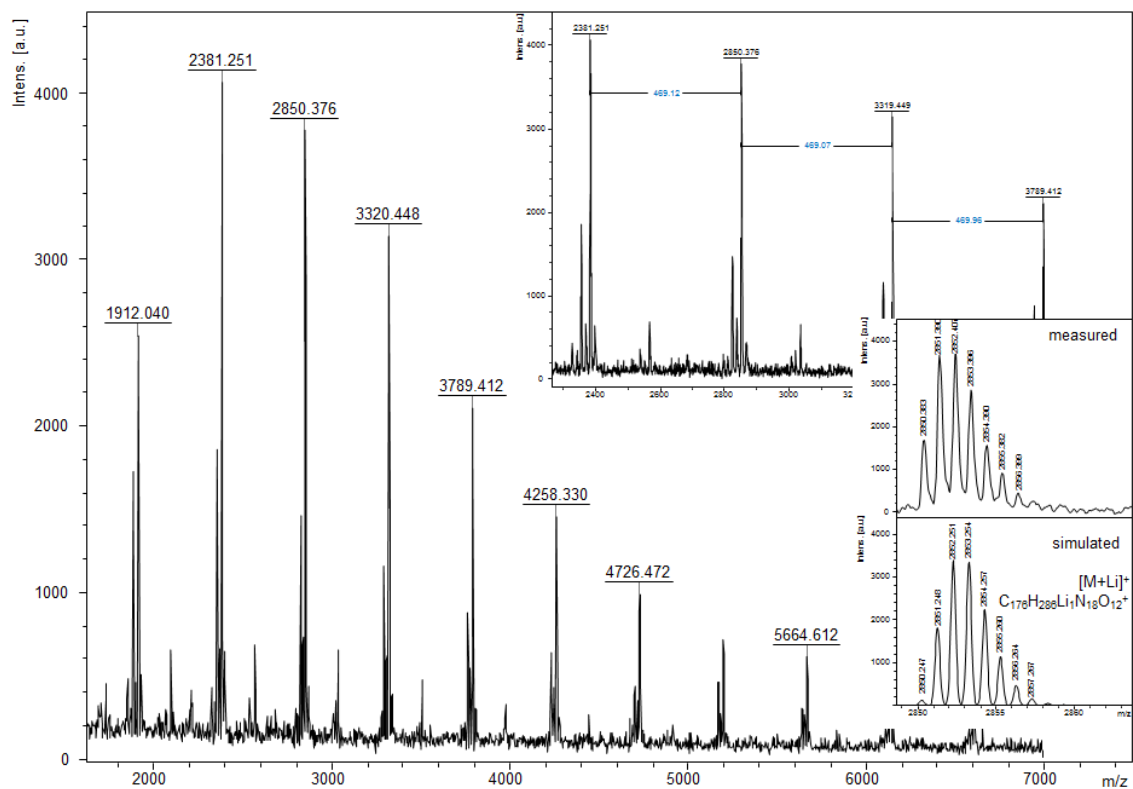




A 30:  $^{13}\text{C}$ -NMR spectra of the unsaturated *N*-methyl protected DAP containing polymers (11d-f).

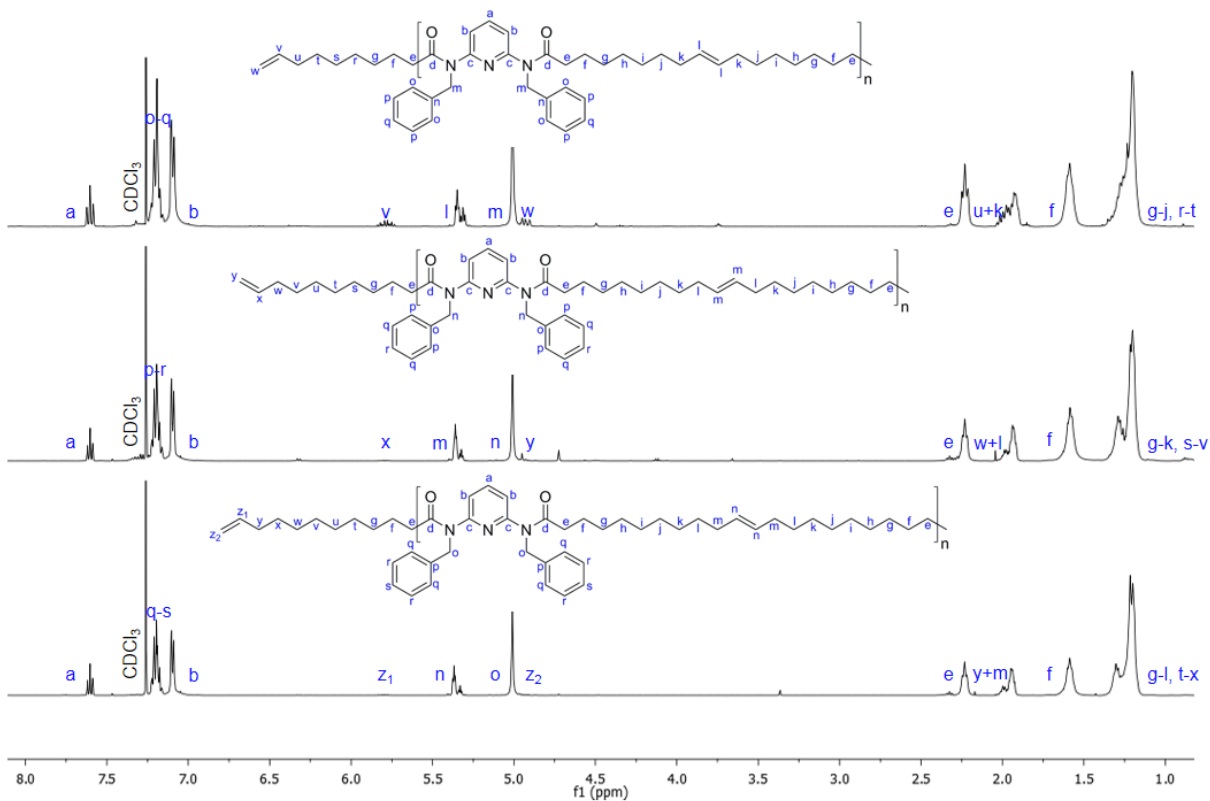


A 31: MALDI ToF MS analysis of DAP-uP-Me-16 (11d).

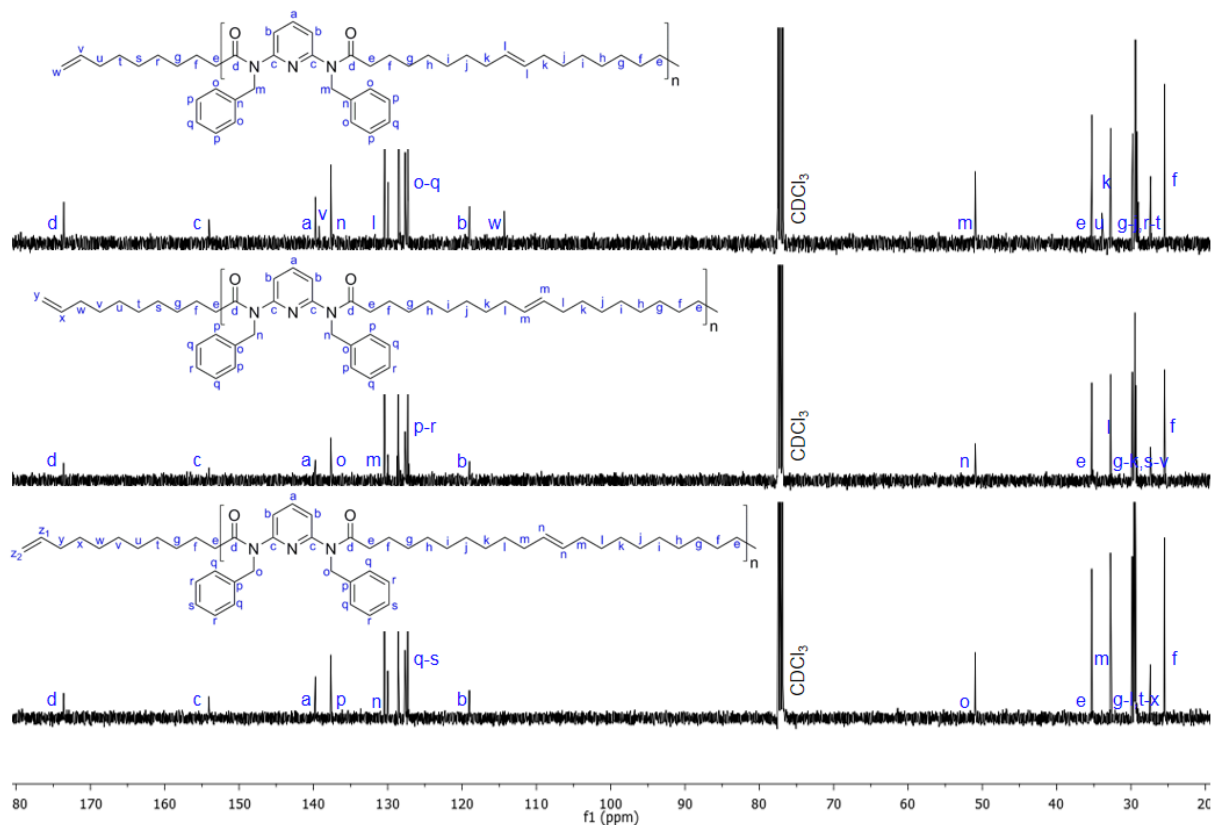


A 32: MALDI ToF MS analysis of DAP-uP-Me-20 (**11f**).

## 7.12 NMR spectra of the unsaturated *N*-benzyl protected DAP containing polymers (**11g-i**)

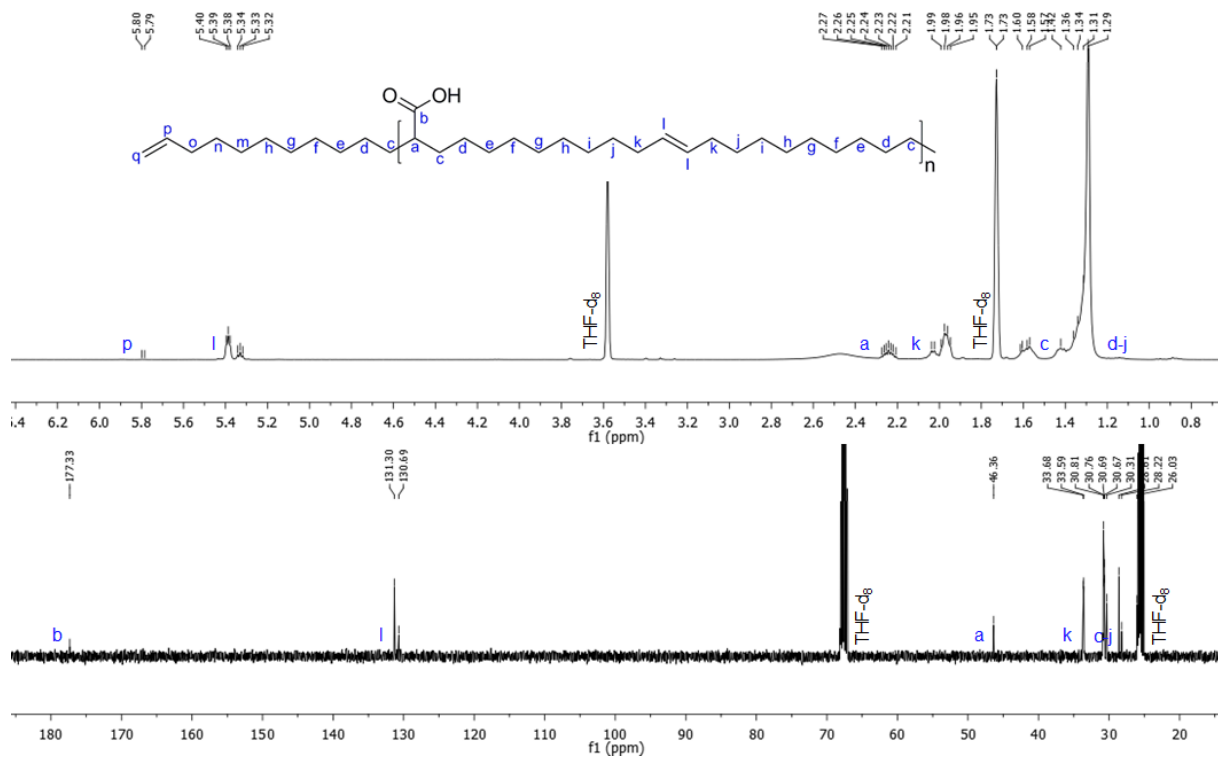


A 33: <sup>1</sup>H-NMR spectra of the unsaturated *N*-benzyl protected DAP containing polymers (**11g-i**).



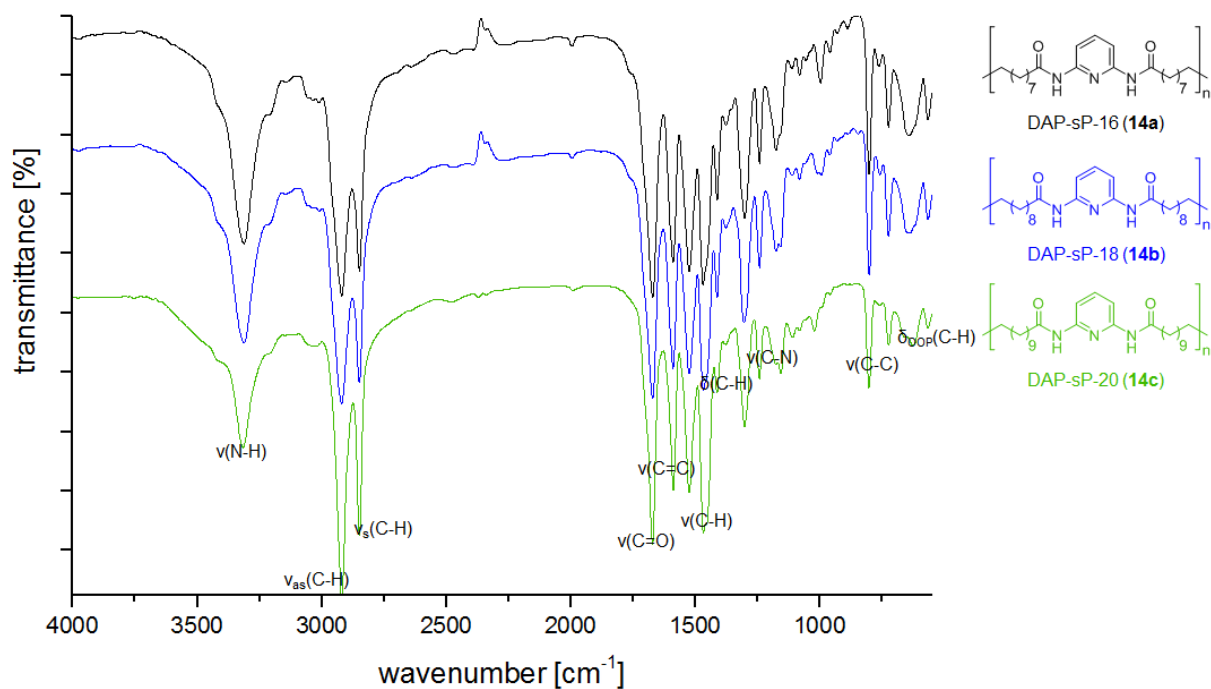
**A 34:**  $^{13}\text{C}$ -NMR spectra of the unsaturated *N*-benzyl protected DAP containing polymers (**11g-i**).

### 7.13 NMR spectra of Acid-uP-20 (**13**)



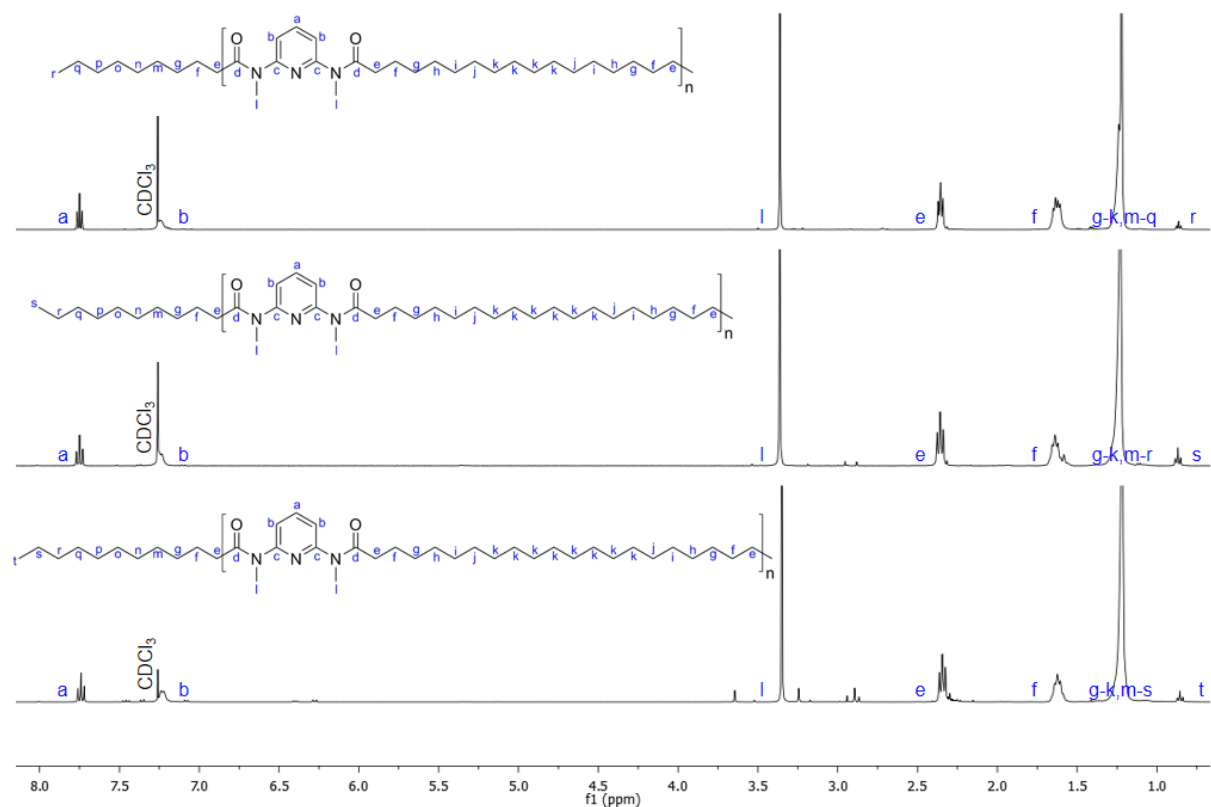
**A 35:**  $^1\text{H}$ - and  $^{13}\text{C}$ -NMR spectra of Acid-uP-20 (**13**).

### 7.14 IR spectra of the saturated DAP containing polymers (14a-c)

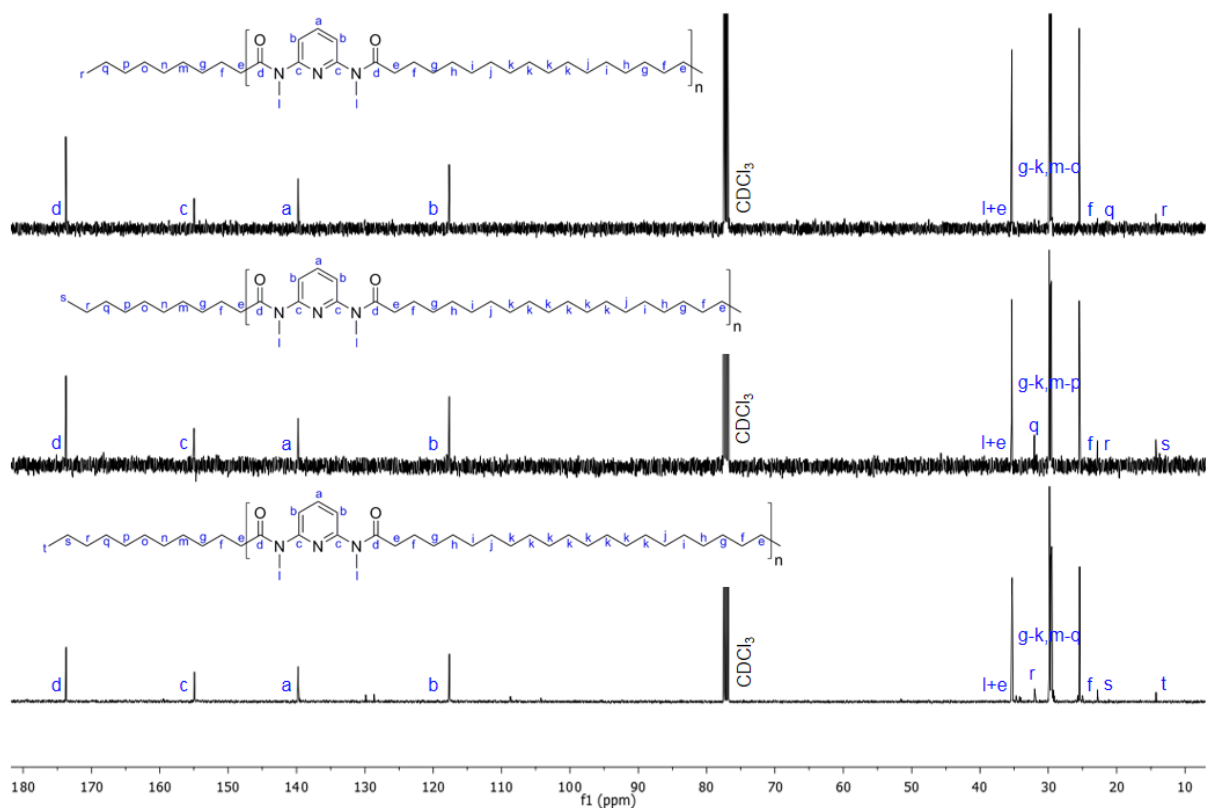


A 36: IR spectra of the saturated DAP containing polymers (14a-c).

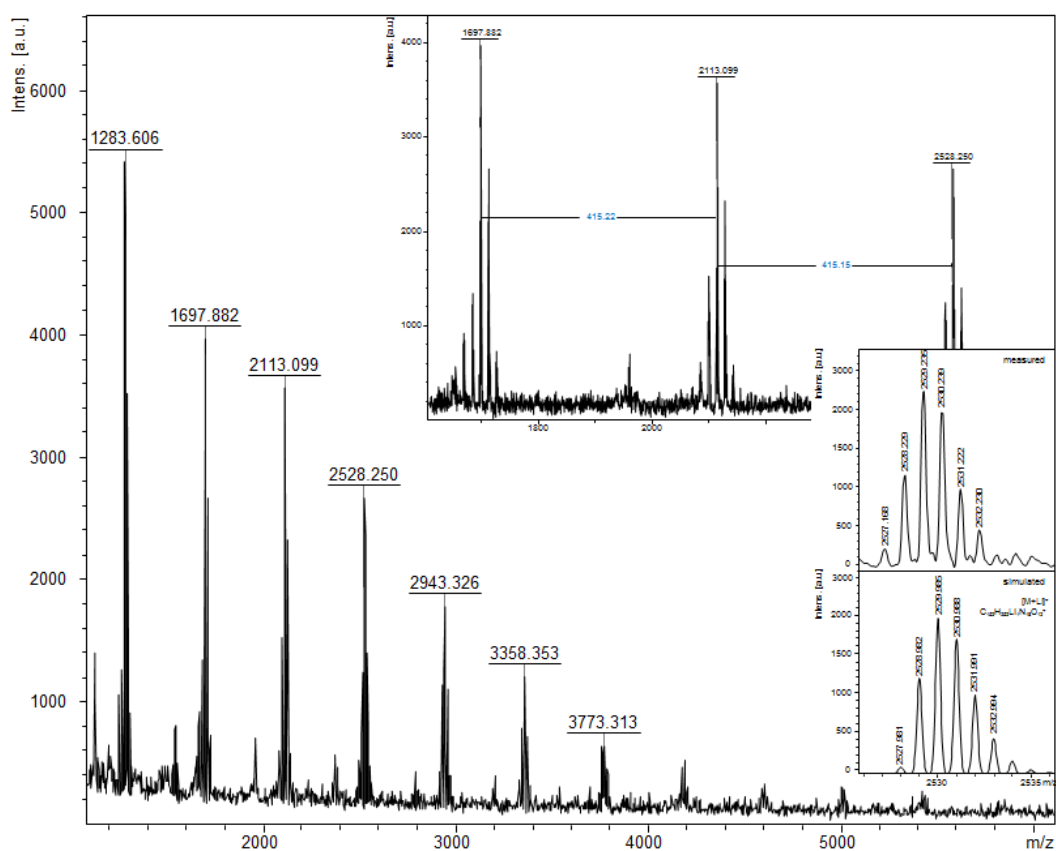
### 7.15 NMR spectra and MALDI ToF MS of the saturated *N*-methyl protected DAP containing polymers (14d-f)



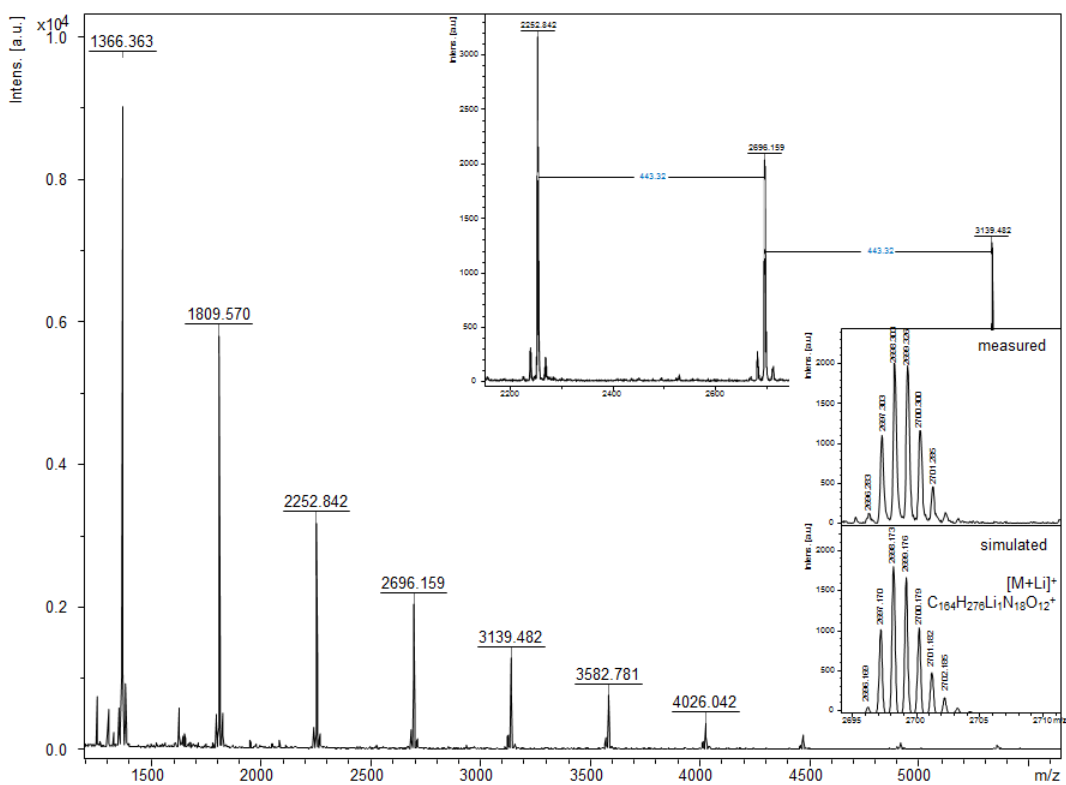
A 37: <sup>1</sup>H-NMR spectra of the saturated *N*-methyl protected DAP containing polymers (14d-f).



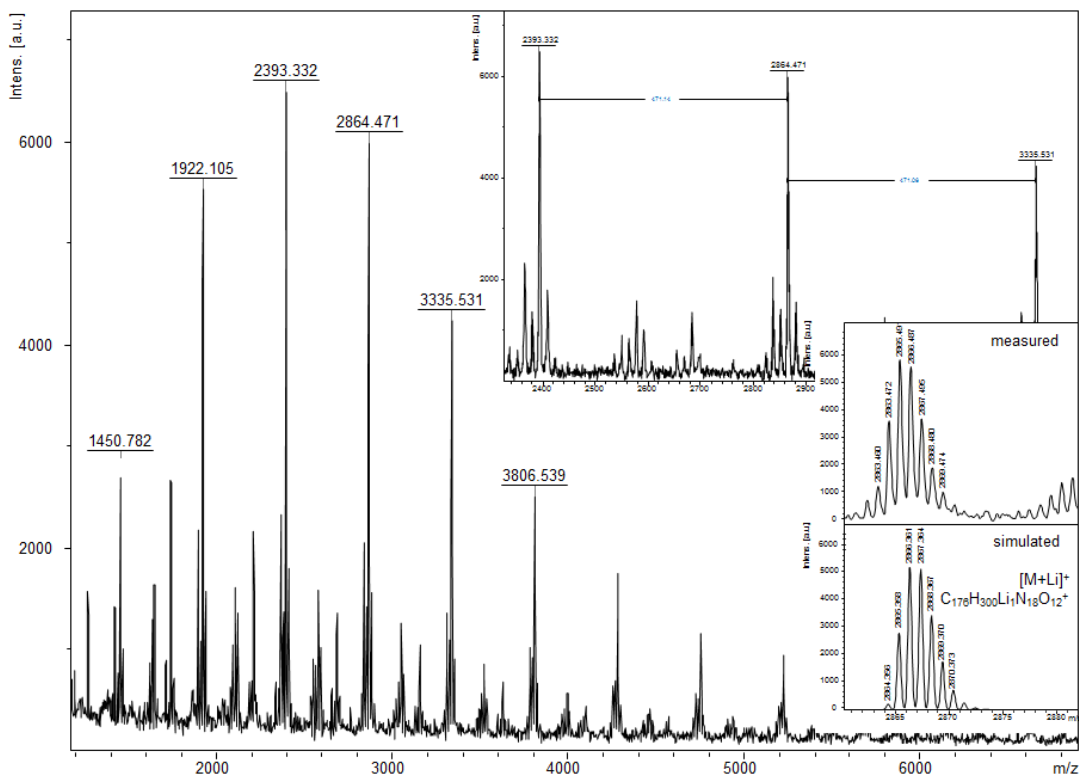
**A 38:**  $^{13}\text{C}$ -NMR spectra of the saturated *N*-methyl protected DAP containing polymers (14d-f).



**A 39:** MALDI ToF MS analysis of DAP-sP-Me-16 (14d).

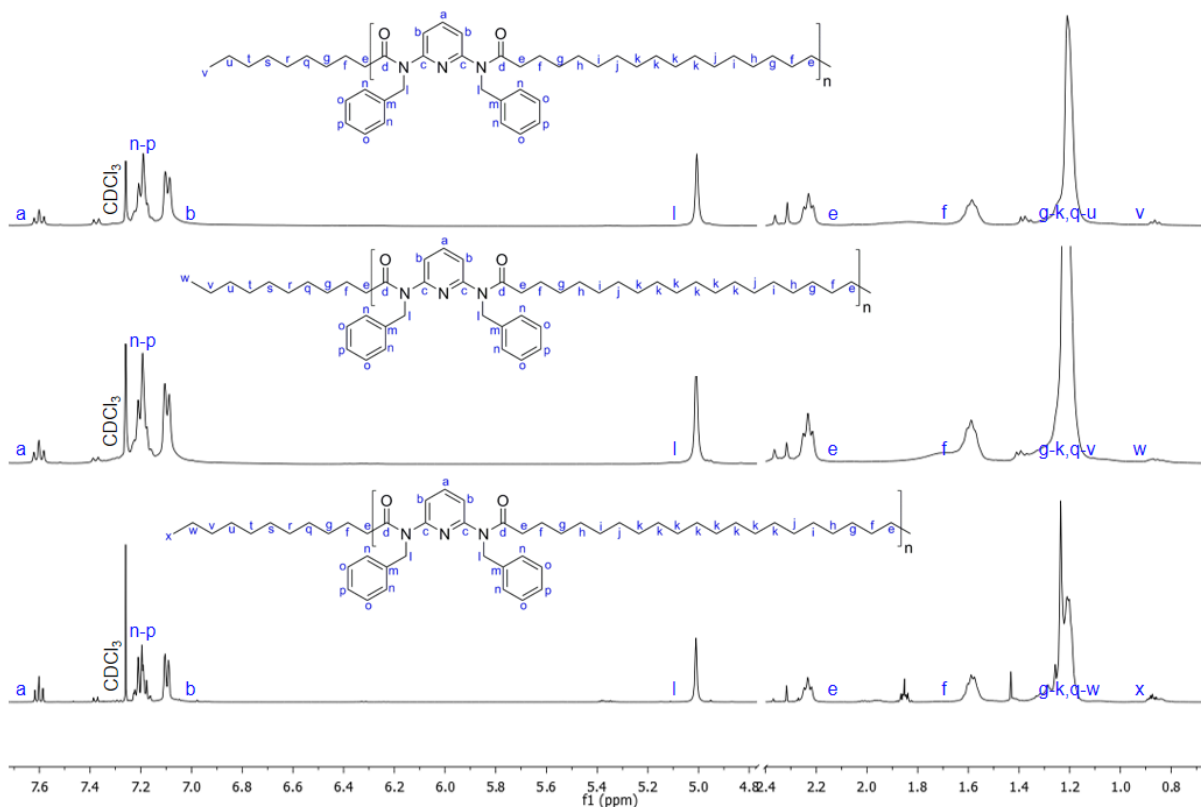


**A 40:** MALDI ToF MS analysis of DAP-sP-Me-18 (**14e**).

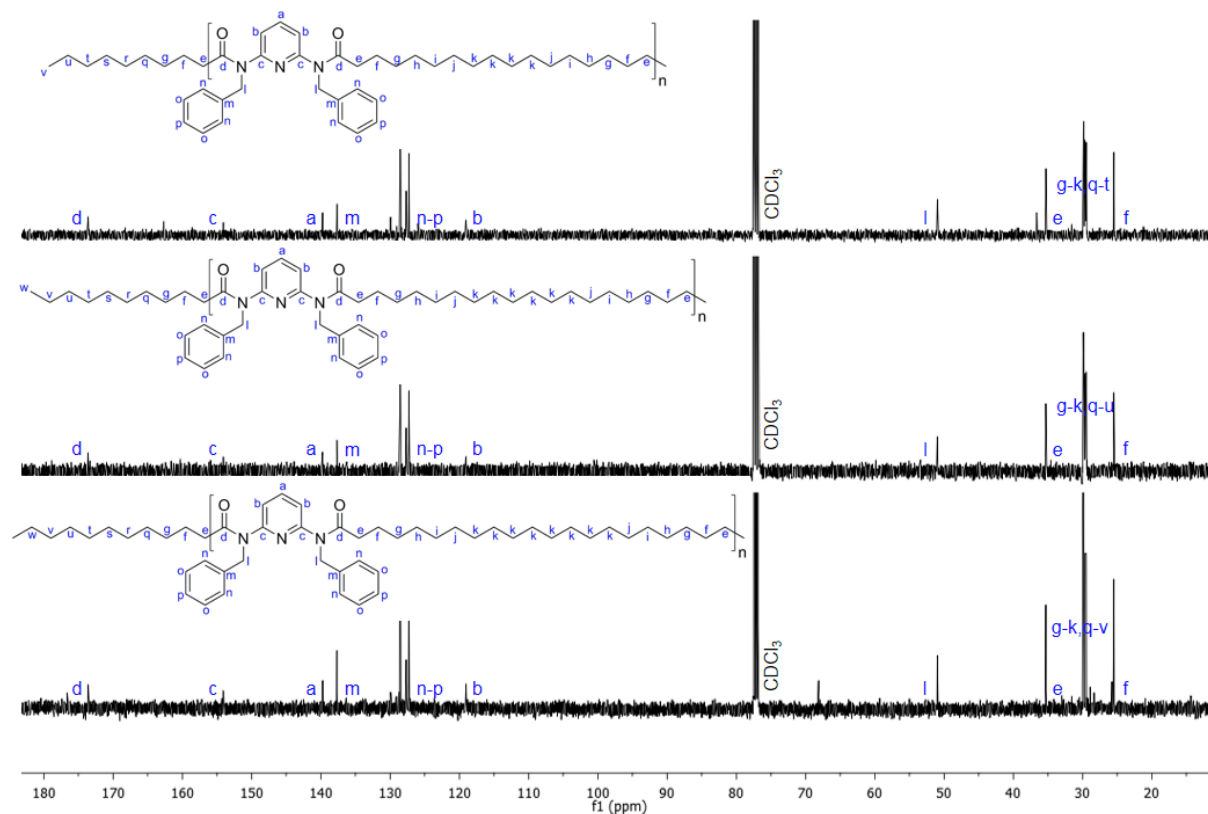


**A 41:** MALDI ToF MS analysis of DAP-sP-Me-20 (**14f**).

**7.16 NMR spectra and MALDI ToF MS of the saturated *N*-benzyl protected DAP containing polymers (14g-i)**

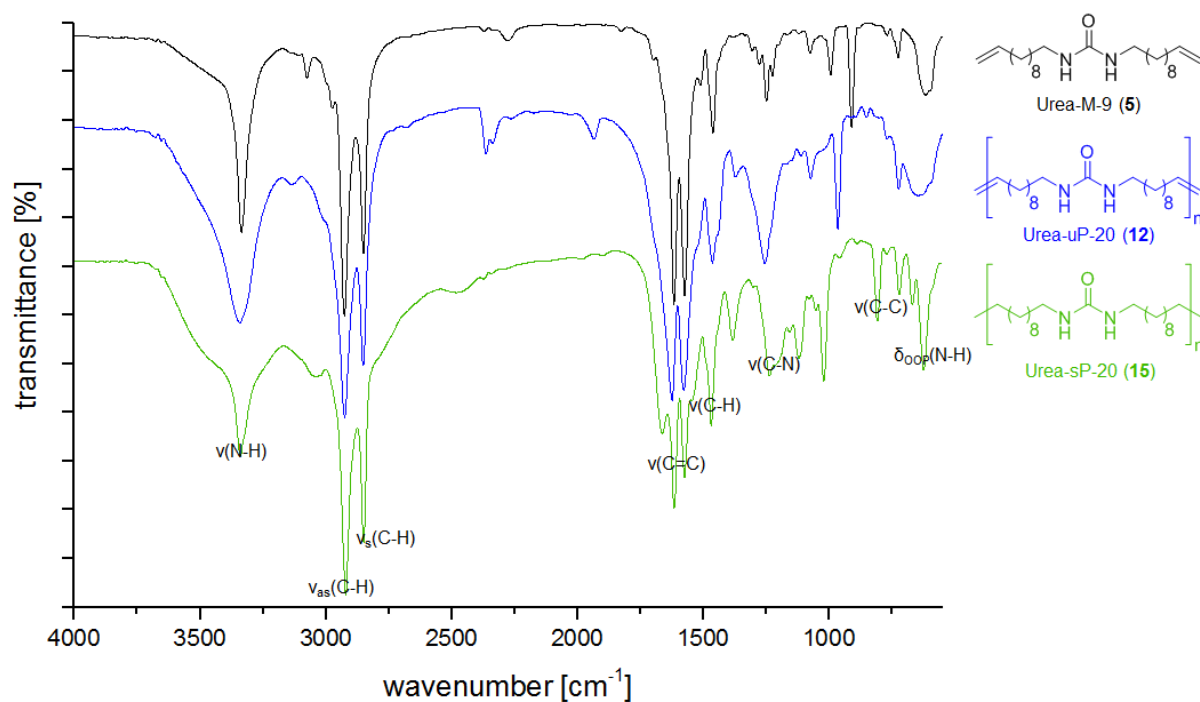


**A 42:** <sup>1</sup>H-NMR spectra of the saturated *N*-benzyl protected DAP containing polymers (14g-i).



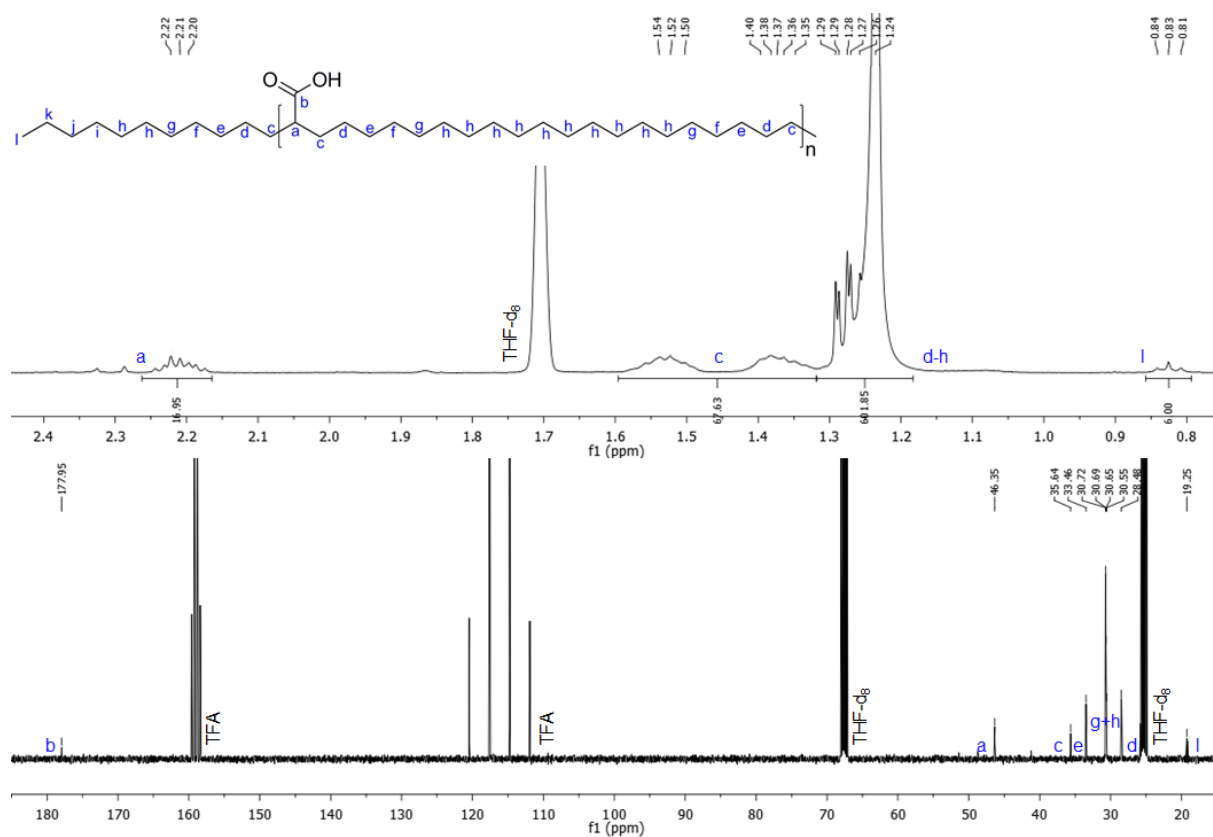
**A 43:** <sup>13</sup>C-NMR spectra of the saturated *N*-benzyl protected DAP containing polymers (14g-i).

### 7.17 IR spectra of Urea-M-9 (5), Urea-uP-20 (12) and Urea-sP-20 (15)



A 44: Comparison of the IR spectra of Urea-M-9 (5), Urea-uP-20 (12) and Urea-sP-20 (15).

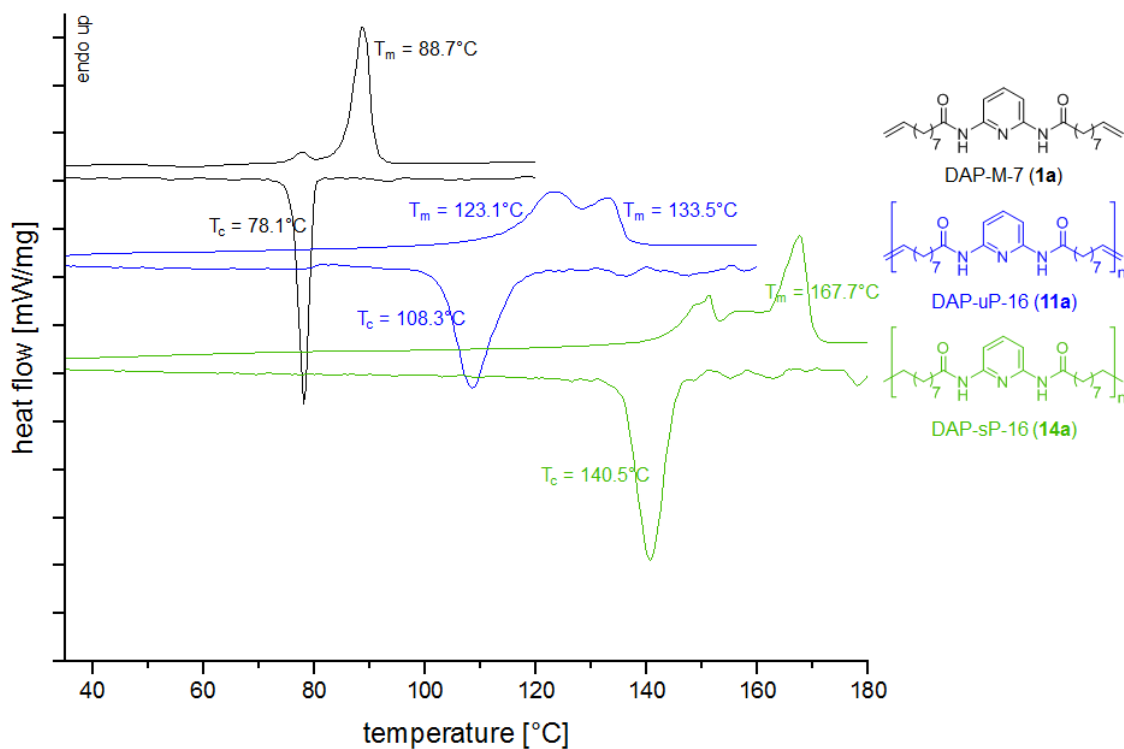
### 7.18 NMR spectra of Acid-sP-20 (16)



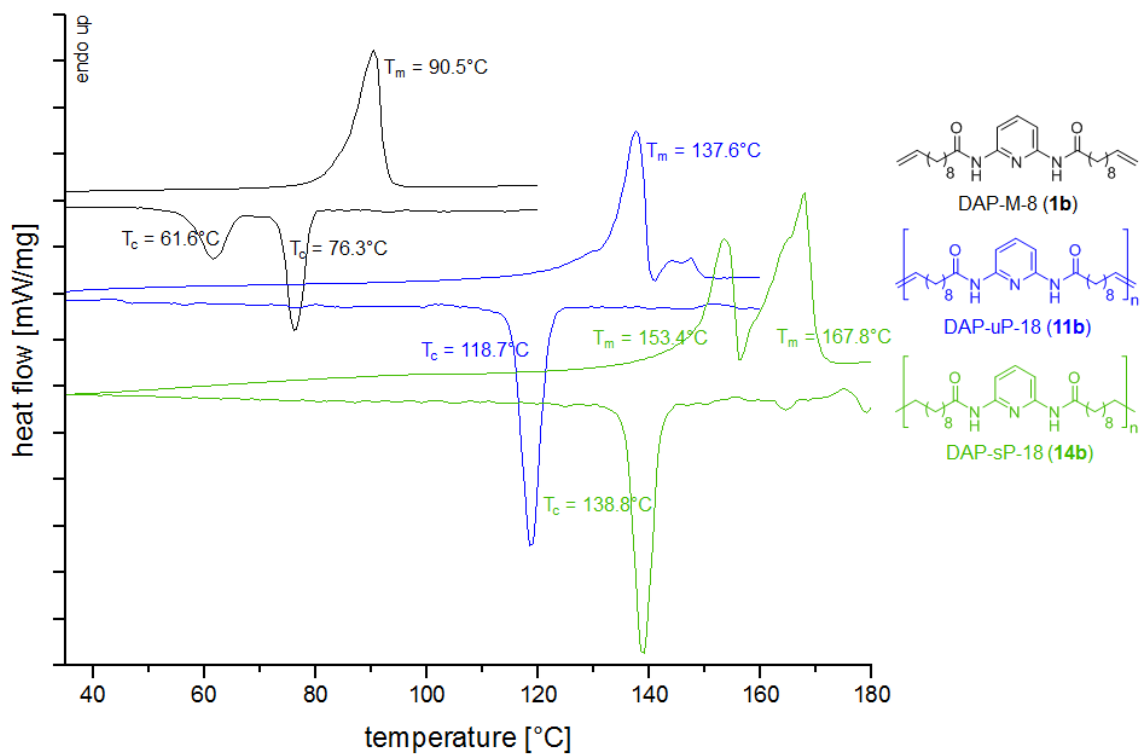
A 45: <sup>1</sup>H- and <sup>13</sup>C-NMR spectra of Acid-sP-20 (16).



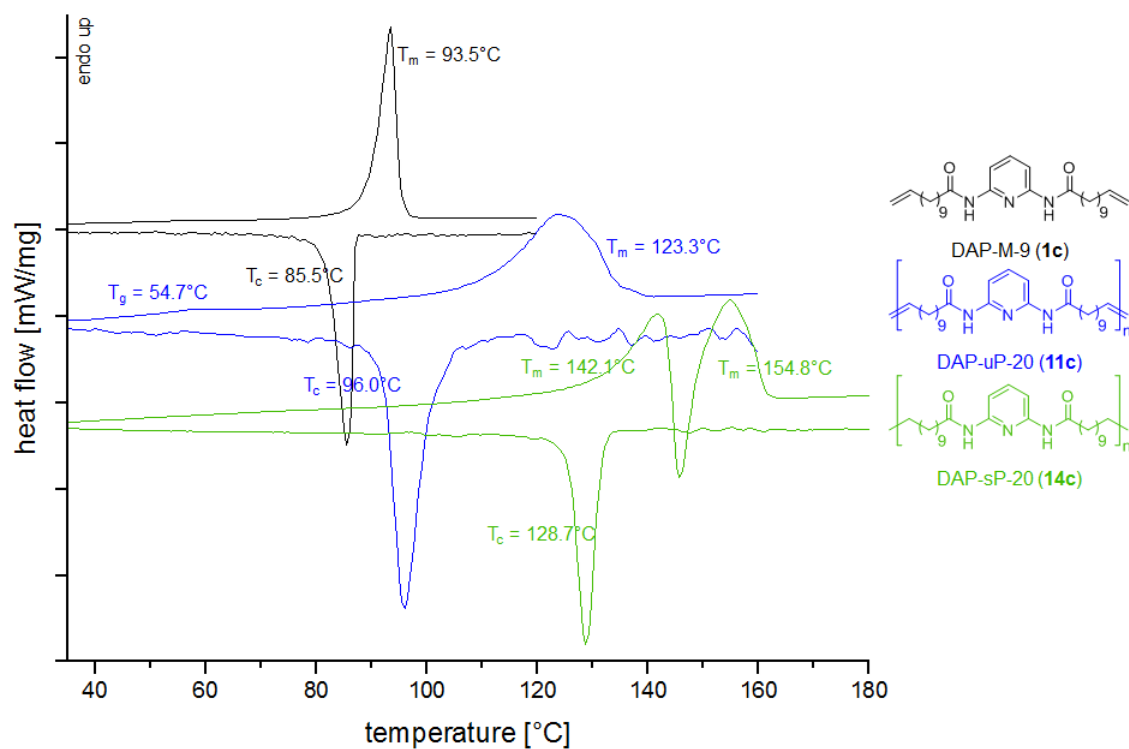
### 7.19 DSC analysis of the *N*-unprotected DAP containing monomers and polymers (1a-c, 11a-c and 14a-c)



A 46: DSC thermograms of DAP-M-7 (**1a**), DAP-uP-16 (**11a**) and DAP-sP-16 (**14a**).

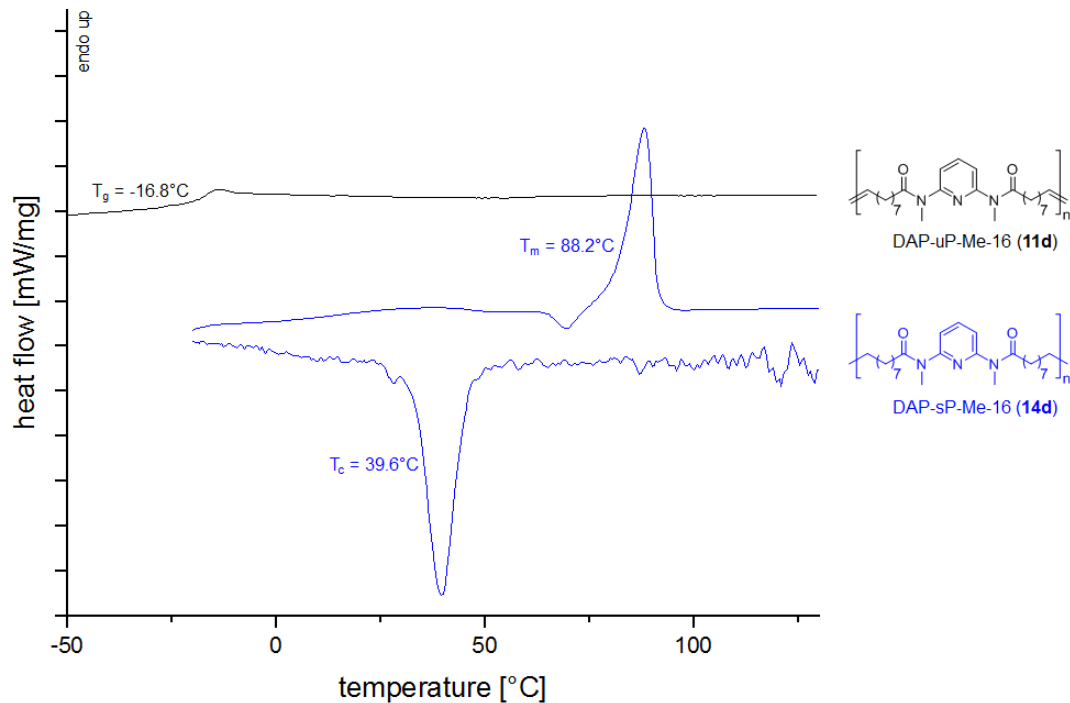


A 47: DSC thermograms of DAP-M-8 (**1b**), DAP-uP-18 (**11b**) and DAP-sP-18 (**14b**).

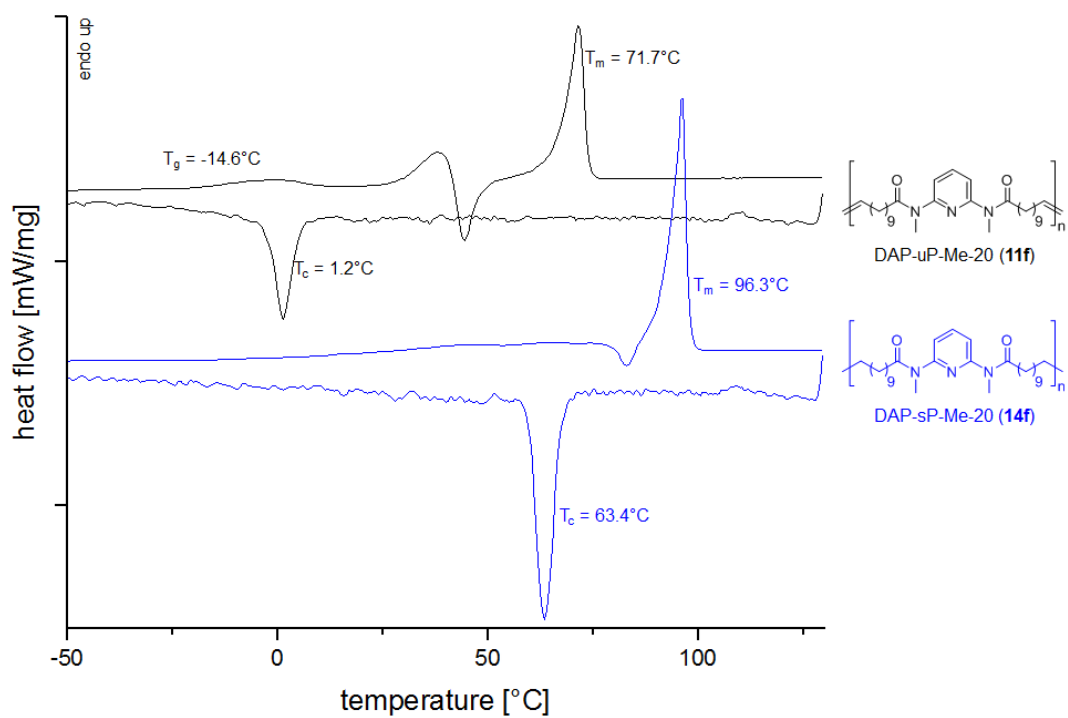


A 48: DSC thermograms of DAP-M-9 (**1c**), DAP-uP-20 (**11c**) and DAP-sP-20 (**14c**).

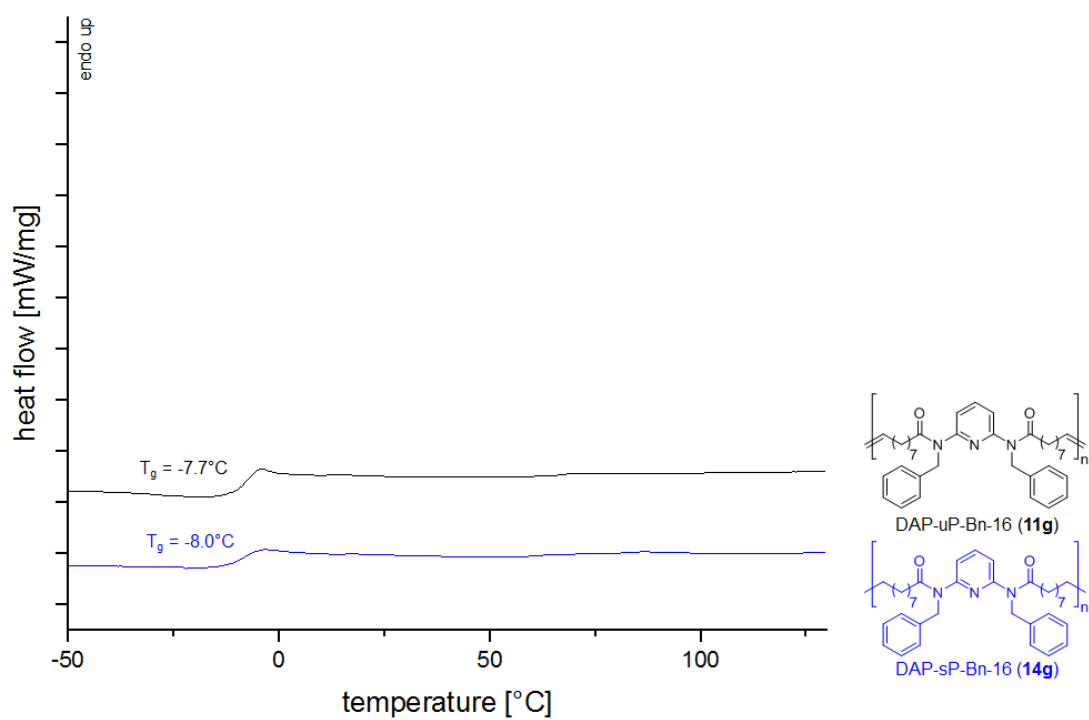
## 7.20 DSC analysis of the *N*-protected DAP containing polymers (**11d-i** and **14d-i**)



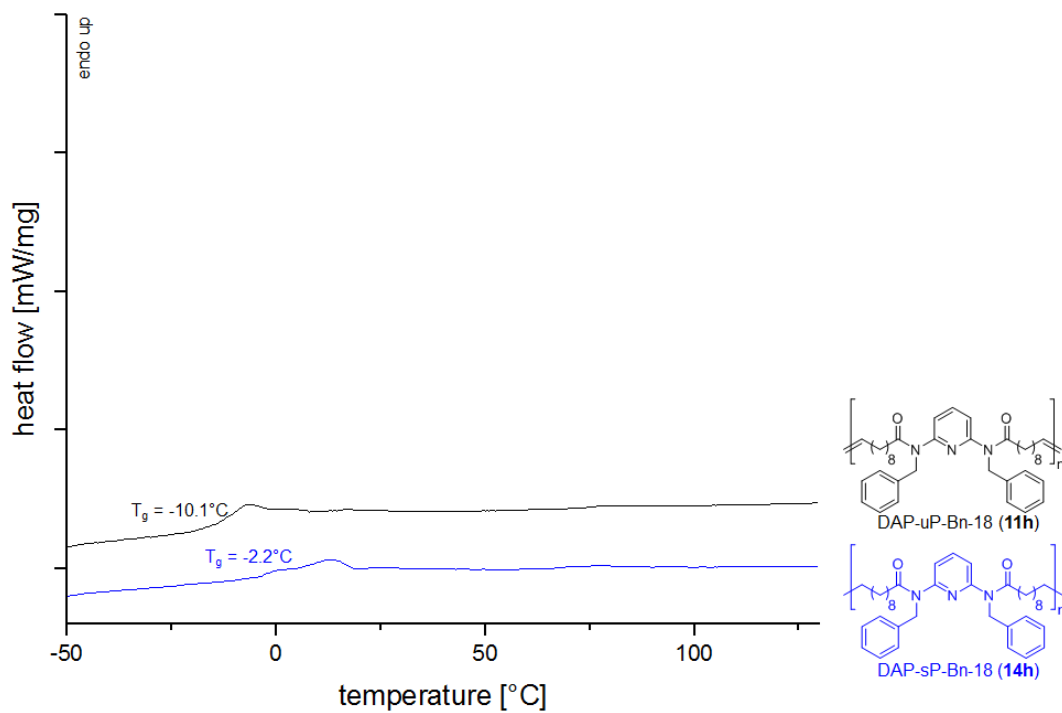
A 49: DSC thermograms of DAP-uP-Me-16 (**11d**) and DAP-sP-Me-16 (**14d**).



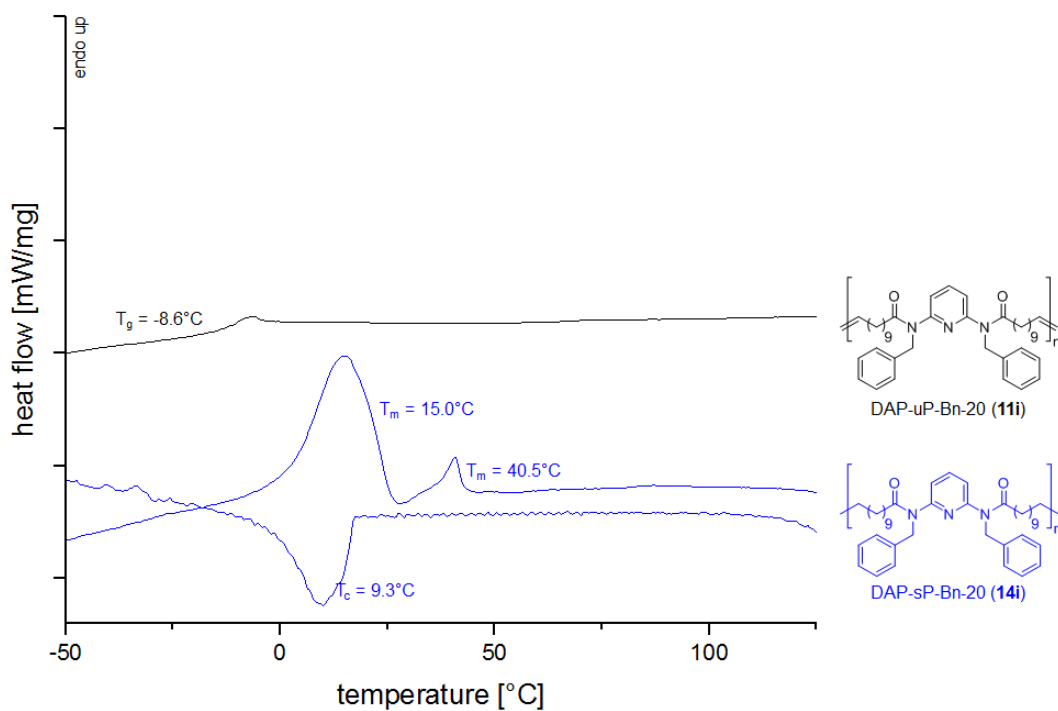
**A 50:** DSC thermograms of DAP-uP-Me-20 (**11f**) and DAP-sP-Me-20 (**14f**).



**A 51:** DSC thermograms of DAP-uP-Bn-16 (**11g**) and DAP-sP-Bn-16 (**14g**).

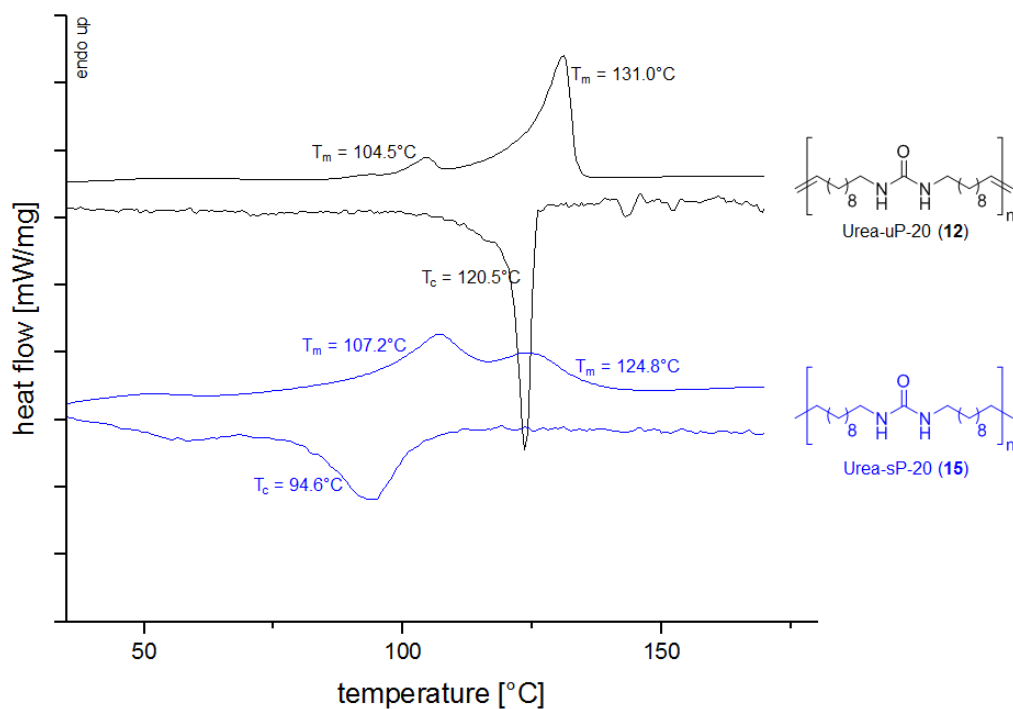


A 52: DSC thermograms of DAP-uP-Bn-18 (**11h**) and DAP-sP-Bn-18 (**14h**).

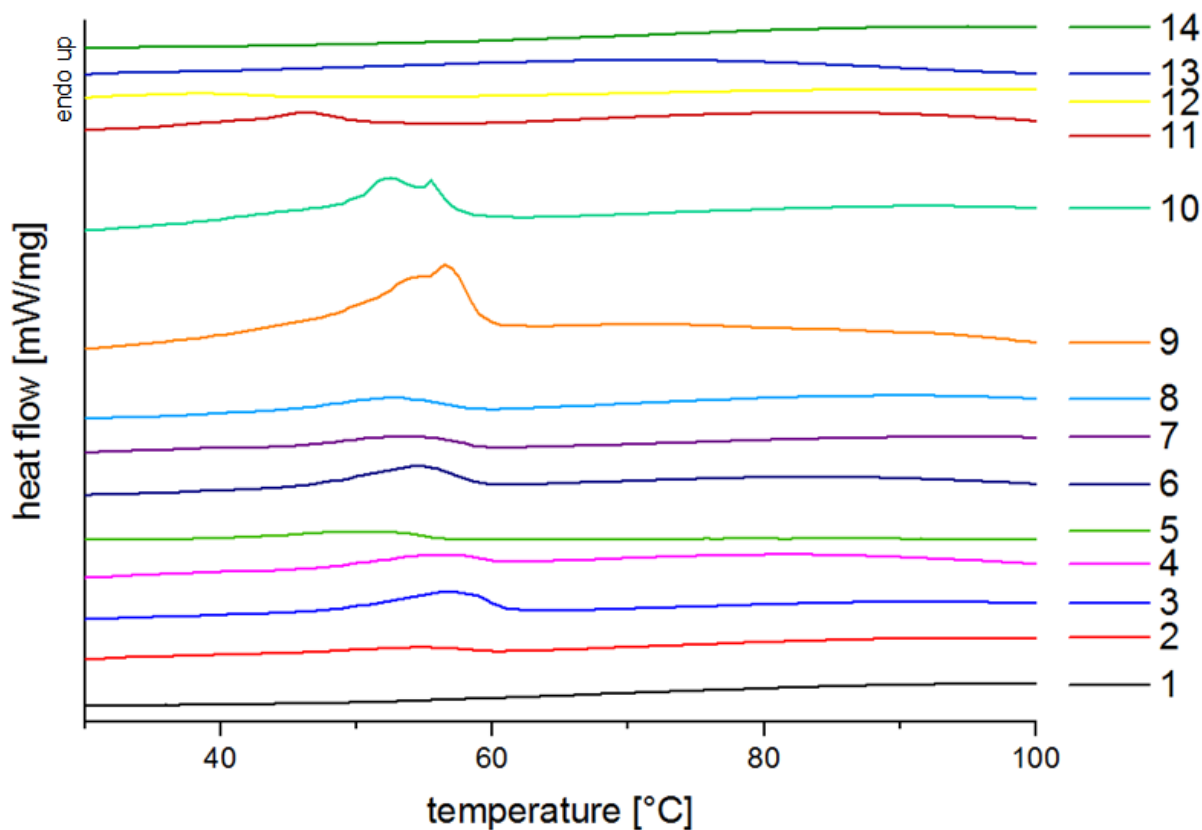


A 53: DSC thermograms of DAP-uP-Bn-20 (**11i**) and DAP-sP-Bn-20 (**14i**).

## 7.21 DSC analysis of the urea containing polymers (12 and 15)



A 54: DSC thermograms of Urea-uP-20 (12) and Urea-sP--20 (15).



A 55: DSC thermograms of the individual fractions of DAP-sP-Me-20 (14f).

## 8. Curriculum Vitae

Sophie Reimann (M. Sc.)

Anschrift: Elsbethstraße 14  
D-04155 Leipzig

Geburtsdatum: 05.06.1989

Geburtsort: Luckau

Staatsangehörigkeit: deutsch

### Werdegang

seit 03.2018

***Island Polymer Industries GmbH***

Stellvertretende Abteilungsleitung Forschung und Entwicklung

10.2013 – 12.2017

***Martin-Luther-Universität Halle-Wittenberg***

Wissenschaftliche Mitarbeiterin in der Arbeitsgruppe von Prof. W. H. Binder (Makromolekulare Chemie);  
Promotion auf dem Gebiet der supramolekularen Präzisionspolymere

### Studium

10.2011 – 09.2013

***Masterstudium***

Martin-Luther-Universität Halle-Wittenberg  
Thema: „Synthesis of Crystallizable Foldamer Polymers via ADMET-Polymerization“  
Abschluss: Master of Science (Note: 1.8)

10.2008 – 09.2011

***Bachelorstudium***

Martin-Luther-Universität Halle-Wittenberg  
Thema: „Synthese von antitumoraktiven Aminosäurederivaten der Oleanolsäure“  
Abschluss: Bachelor of Science (Note: 2.4)

### Schule

08.2001 – 07.2008

***Sängerstadt-Gymnasium Finsterwalde***

Abschluss: Abitur (Note: 1.7)

08.1995 – 07.2001

***Grundschule Crinitz***

## Publikationen

Reimann, S.; Baumeister, U.; Binder, W. H.; Synthesis and Crystallization of Precision Polymers with Repetitive Folding Elements; *Macromol. Chem. Phys.* **2014**, *215*, 1963.

Reimann, S.; Danke, V.; Beiner, M.; Binder, W. H.; Synthesis of supramolecular precision polymers: Crystallization under conformational constraints; *J. Polym. Sci.* **2017**, *55*, 3736.

Danke, V.; Gupta, G.; Reimann, S.; Binder, W. H.; Beiner, M.: Structure formation in nanophase-separated systems with lamellar morphology: Comb-like vs. linear precision polymers; *Eur. Polym. J.* **2018**, *103*, 116.

## Präsentation auf Konferenzen

Ajay Kasegaonkar, Clement Appiah, Sophie Reimann, Elena Ostas, Wolfgang H. Binder; Crystallization in Dynamic Supramolecular Polymers; Meeting of SFB-TRR 102 “Polymers under multiple constraints: restricted and controlled molecular order and mobility”, 8. November 2013, Schkeuditz, Deutschland; Poster Präsentation.

Clement Appiah, Ajay Kasegaonkar, Sophie Reimann, Wolfgang H. Binder; Crystallization of Polymers under Supramolecular & Topological constraints; Meeting of SFB-TRR 102 “Polymers under multiple constraints: restricted and controlled molecular order and mobility”, 17.-19. März 2014, Wittenberg, Deutschland; Poster Präsentation.

Ajay Kasegaonkar, Clement Appiah, Sophie Reimann, Wolfgang H. Binder; Crystallization of Polymers under Supramolecular & Topological constraints; Meeting of SFB-TRR 102 “Polymers under multiple constraints: restricted and controlled molecular order and mobility”, 16.-17. September 2014, Jena, Deutschland, Poster Präsentation.

Sophie Reimann, Ute Baumeister, Wolfgang H. Binder; Synthesis and crystallization of precision polymers with repetitive folding elements; European Polymer Federation Congress 2015, 22.-26. Juni 2015, Dresden, Deutschland; Poster Präsentation.

Sophie Reimann, Wolfgang H. Binder; Synthesis and aggregation of precision polymers with repetitive folding elements; Meeting of SFB-TRR 102 “Polymers under multiple constraints: restricted and controlled molecular order and mobility”, 02. Oktober 2015, Halle (Saale), Deutschland; Poster Präsentation.

Sophie Reimann, Wolfgang H. Binder; Synthesis, aggregation and crystallization of precision polymers with repetitive folding elements; Makro 2016: “Polymers: from Structure to Function”, 11.-13. September 2016, Halle (Saale), Deutschland; Poster Präsentation.

Clement Appiah, Merve B. Canalp, Sonu Kumar, Sophie Reimann, Yuuki Sugawara, Wolfgang H. Binder; Crystallization in dynamic and geometrically constrained supramolecular polymers; Meeting of SFB-TRR 102 “Polymers under multiple constraints: restricted and controlled

molecular order and mobility”, 28.-30. September 2016, Rathen, Deutschland; Poster Präsentation.

Clement Appiah, Sophie Reimann, Wolfgang H. Binder; Crystallization in dynamic and geometrically constrained supramolecular polymers; Meeting of SFB-TRR 102 “Polymers under multiple constraints: restricted and controlled molecular order and mobility”, 12. Mai 2017, Leipzig, Deutschland; Poster Präsentation.

Merve B. Canalp, Jan Freudenberg, Sophie Reimann, Wolfgang H. Binder; Synthesis, aggregation and crystallization of precision polymers with repetitive folding elements; Internation Discussion Meeting on Polymer Crystallization 2017: “From Classical Systems to Functional Materials and Biopolymers”, 17.-20. September 2017, Wittenberg, Deutschland; Poster Präsentation.

Halle (Saale), den 25.10.2018

---

Sophie Reimann



## **9. Eigenständigkeitserklärung**

Hiermit erkläre ich an Eides statt, dass ich die vorliegende Arbeit selbstständig und ohne fremde Hilfe verfasst habe. Andere als die angegebenen Quellen und Hilfsmittel wurden nicht benutzt und die den benutzten Werken wörtlich oder inhaltlich entnommenen Stellen wurden als solche kenntlich gemacht.

Außerdem erkläre ich, dass ich die vorliegende Dissertation an keiner anderen wissenschaftlichen Einrichtung zur Erlangung eines akademischen Grades eingereicht habe.

Halle (Saale), den 25.10.2018

---

Sophie Reimann